TO GAIN INSIGHTS INTO THE FUNCTION OF YEAST DNM1 IN MITOCHONDRIAL DYNAMICS

A Thesis

submitted in partial fulfilment of the requirements for the degree of

Doctorate of Philosophy

by

RIDDHI BANERJEE

(166106009)

Under the supervision of

Dr. Shirisha Nagotu

Department of Biosciences and Bioengineering
Indian Institute of Technology Guwahati
Guwahati-781039, Assam, India

September 2023

Dedicated to

Mother Nature

INDIAN INSTITUTE OF TECHNOLOGY GUWAHATI

Department of Biosciences and Bioengineering

Assam, Guwahati-781039

DECLARATION

I do hereby declare that the research findings in this thesis is the result of research work carried out by me in the Department of Biosciences and Bioengineering, Indian Institute of Technology Guwahati, India, under the supervision of **Dr. Shirisha Nagotu.**

I also declare that the contents of this thesis have not been the basis for award of any other degree, diploma, fellowship or any other similar title of any other University or Institution.

As per general norms of reporting research findings, due acknowledgments have been made, whenever findings of other researchers have been cited in this thesis.

Date: 27-09-2023

Place: IIT Guwahati

Riddhi Banerjee

Riddhi Banerjee

INDIAN INSTITUTE OF TECHNOLOGY GUWAHATI

Department of Biosciences and Bioengineering

Assam, Guwahati-781039

CERTIFICATE

This is to certify that the work described in the thesis entitled **"To gain insights into the function of yeast Dnm1 in mitochondrial dynamics**" is an authentic record of the results obtained from the research work carried out by **Riddhi Banerjee** in the Department of Biosciences and Bioengineering, Indian Institute of Technology Guwahati, Assam, India, under my supervision and this work in part or as a whole has not been submitted elsewhere for the award of any other degree.

Date: 27-09-2023

Place: IIT Guwahati

Dr. Shirisha Nagotu
(Supervisor)

ACKNOWLEDGMENTS

Pursuing a PhD is often an insightful and transformative journey with endless challenges, abundant opportunities for personal growth, and the exhilarating prospect of uncovering new knowledge. It requires unwavering dedication, resilience, perseverance and a relentless quest of intellectual development. This journey at IIT Guwahati has been a remarkable chapter in my life, and it would not have been possible without the support and guidance of many individuals who have played crucial roles along the way. In this section, I would like to express my sincere gratitude to those who have been instrumental in enabling and enhancing this memorable journey.

I would like to begin by conveying my sincere gratitude and respect to my PhD supervisor, ***Dr. Shirisha Nagotu****. She has been a guiding light throughout my PhD journey, providing me with scientific guidance, insightful feedback, and continuous support. I am particularly appreciative of her role in strengthening my scientific writing, communication, and critical thinking abilities. She has been a constant source of motivation, encouraging me to excel as an independent researcher. Furthermore, I am profoundly indebted to her for the necessary resources and supportive lab environment she has provided, which have fostered the exchange and exploration of a wide range of research ideas. I consider myself extremely fortunate to work under a supervisor who exhibited genuine concern for both my well-being and the quality of my work. Thank you so much for everything, Ma'am.*

I am deeply indebted to my doctoral committee members: ***Prof. Sachin Kumar, Prof. Ranjan Tamuli, and Dr. Sunanda Chatterjee.*** *Their valuable feedback and insightful suggestions not only enriched my thesis but also broadened my overall understanding of the subject. Moreover, their generosity in dedicating their time to provide constructive guidance on my work has been immensely beneficial.*

I am immensely grateful to ***Dr. Rajkumar P. Thummer*** *for his valuable input and*

feedback on my work, as well as for providing the necessary instrument facilities. Beyond our academic interactions, it was a pleasure to share some enjoyable moments on the cricket field.

I express my heartfelt gratitude to ***Prof. Ehesan Ali****,* ***Dr. Priyadarshi Satpati****,* ***Dr. Sunanda Chatterjee****,* ***Dr. Abhishek Kumar, Dr. Karabi Roy****, and* ***Dr. Shikha Sharma****, for their expertise, dedication, and collaborative spirit, which were instrumental in the success of this research.*

I would like to express my sincere gratitude to the former and current heads of the Department of Biosciences and Bioengineering, ***Prof. V. Venkata Dasu, Prof. Kannan Pakshirajan, Prof. Latha Rangan, and Prof. Rakhi Chaturvedi*** *for their unwavering support and provision of all necessary departmental facilities during their respective tenures. I am also deeply indebted to the* ***Department of Biosciences and Bioengineering, IIT Guwahati****, and the institute as a whole for providing the essential infrastructure that enabled me to conduct my research. Furthermore, I extend my gratitude to the dedicated* ***office staff members of BSBE*** *for their invaluable technical assistance, which has greatly facilitated my work.*

I would like to express my gratitude to the ***Ministry of Human Resource Development (MHRD), India*** *and the* ***Indian Institute of Technology Guwahati*** *for the generous financial assistance throughout my doctoral studies.*

I would like to extend my sincere appreciation to all former and current members of the ***Organelle Biology and Cellular Ageing Lab (OBCAL)*** *for their integral role in the progress and achievements of this research. I am deeply grateful to all of you for teaching me so much in so many area****s.*** *Our enjoyable conversations during daily tea breaks provided a refreshing respite for me. I would like to thank my seniors* ***Dr. Rachayeeta Deb*** *and* ***Dr. Nayan Moni Deori****, with whom I embarked on this journey from the inception of OBCAL and shared a significant portion of my PhD experience. I thank former OBCAL members* ***Neha*** *and* ***Suchetana*** *for their extensive support and valuable contributions to this endeavour. Additionally, I wish to express my appreciation to my junior colleagues* ***Isha, Tanveera****, and* ***Ankita****, for their graceful support,*

encouragement and assistance throughout this journey. I also appreciate the thoughtful wishes from our newly joined OBCAL members, ***Soham*** *and* ***Darshani****. I would like to express my appreciation to* ***Agradeep*** *for his invaluable contributions to this project and his support during challenging times. I also thank* ***Rishi****,* ***Sahaya****,* ***Jyoti****,* ***Terence****,* ***Atchaya****,* ***Ganesh****,* ***Abhigna****, and* ***Ishita*** *for their support in creating a vibrant and enjoyable work environment within the lab. I am grateful to all the members of* ***Stem Cell Engineering and Regenerative Medicine (SCERM) lab*** *for their support and cooperation.*

Throughout my tenure at IIT Guwahati, I was fortunate to develop profound friendships that offered priceless support in every circumstance. My heartfelt thanks go to my friends, colleagues, and seniors – ***Rajib, Chandrima, Gloria, Saddam, Gaurav, Uttariya, Manish, Jibon, Nitin, Mahesh, Debojit Da****, and* ***Arunabha Da*** *– who helped me in various ways throughout this remarkable journey.*

I owe a lot of gratitude to ***Satakshi*** *and* ***her parents*** *for their persistent support and encouragement throughout my PhD journey. She has been a constant pillar of strength and a source of inspiration, and I am truly grateful to have her by my side.*

I also want to express my deep appreciation for ***Luchui****, who taught me the importance of unconditional love, sound sleep, and playfulness during the tough times of this journey.*

Last but not least, I am profoundly grateful to my family members especially ***Maa****,* ***Baba****,* ***Dadu****,* ***Dida*** *and my younger sister* ***Tintin*** *for their steady support and sacrifices throughout my PhD journey. This accomplishment would not have been possible without their selfless dedication and belief in my aspirations. I am forever thankful for their presence in my life and their invaluable contributions to every aspect of it.*

Finally, I thank the infinite beauty and wonder of nature for inspiring my scientific journey.

Date: 27-09-2023
Place: IIT Guwahati

Riddhi Banerjee

Riddhi Banerjee

TABLE OF CONTENTS

ABSTRACT

Mitochondria, often referred to as the powerhouse of the cell, are captivating organelles that play a multifaceted role in the physiology and metabolism of eukaryotic cells. Mitochondria act as the central hub of cellular metabolism, providing sites for ATP synthesis, oxidative phosphorylation (OXPHOS), nucleotide, amino acid, and fatty acid biosynthesis, reactive oxygen species (ROS) generation, thermogenesis, and calcium homeostasis. Mitochondria are also highly dynamic organelles that constantly change shape, size, and number through fission and fusion events. This process, known as mitochondrial dynamics, is essential for maintaining their vital physiological functions. Mitochondrial fission is particularly crucial for mitochondrial biogenesis and homeostasis. As akin to many membrane-bound organelles, mitochondria cannot be created *de novo* but instead grow, divide, and are passed on to daughter cells during cell division. Mitochondrial fission is an evolutionarily conserved process dependent on the homologs of the dynamin-related proteins known as Dnm1 in yeast. Dnm1 is a large GTPase (85 kDa) with 757 residues and four domains: an N-terminal GTP-binding domain, a middle domain, a variable domain containing the B-insert, and a C-terminal GTPase effector domain. Dnm1 undergoes a repeated cycle of assembly and disassembly on the target membrane, involving the binding and hydrolysis of GTP, which leads to the remodeling of the membrane, thereby facilitating mitochondrial fission. Throughout this process, Dnm1 also interacts with various membrane-bound partners. The human homolog of Dnm1, DRP1, undergoes several post-translational modifications (PTMs) that regulate its functions, such as specific membrane recruitment, self-assembly to form oligomers, GTPase activity, and interaction with different proteins. While a detailed investigation of the structure, function, and interacting partners of Dnm1 has improved our understanding of its mechanism of action, several crucial aspects of mitochondrial fission involving Dnm1 remain poorly understood. This includes the regulation of various oligomeric forms of the protein, their role in the dynamic spatio-temporal distribution of

the protein, and the potential influence of PTMs on higher-order structure formation. Furthermore, any disruption in the intricate relationship between mitochondrial function and dynamics can give rise to a multitude of human diseases, some of which are linked to specific mutations in DRP1, leading to diverse pathological conditions. Many of these mutations are present in the middle domain of DRP1, essential for self-assembly and higher-order structure formation. Earlier studies have investigated the effect of some of these mutations on organelle morphology, albeit their impact on the protein's localization, distribution, function, and structure remains unexplored.

In this study, we aimed to investigate specific residues that are likely to undergo modifications or are mutated in disease conditions on the structure, localization, and function of Dnm1. Addressing these questions can reveal the molecular basis of mitochondrial fission, its regulation, and its relevance to human health and diseases. To achieve this, Dnm1 fusion proteins were constructed. The structural and functional properties of Dnm1 fusion proteins were investigated using molecular, biochemical, and biophysical techniques. The C-terminal GFP fusion construct of full length (FL) Dnm1 was created to visualize intracellular localization, dynamic behaviour, and to assess the *in vivo* function. FL-Dnm1-GFP was expressed as distinct green puncta, some of which exhibited dynamic behavior visualized as rapid movements during time-lapse image analysis. Moreover, FL-Dnm1-GFP was functional *in vivo*, restoring wild type (WT) reticular mitochondrial morphology in *dnm1* cells without affecting cell growth and colocalized with preCOX4-mCherry-labeled mitochondria. Furthermore, for a comprehensive *in vitr*o structural and functional evaluation, another construct (C-terminal His-HA-tagged Dnm1) was utilized, expressing WT Dnm1-His-HA. Dnm1 was expressed in its natural host and subsequently purified to obtain the protein in its native conformation. We identified and validated the purified Dnm1 sequence using mass spectrometry analysis. Additionally, circular dichroism spectroscopy confirmed that the purified protein retained its characteristic α-helical secondary structure. Like FL-Dnm1-GFP, WT-Dnm1-HisHA was also functional *in vivo*, as confirmed by

the complementation of *dnm1* cells. Therefore, both fusion proteins, FL-Dnm1-GFP and WT-Dnm1-His-HA, were appropriate for further exploring the relationship between the structure and function of Dnm1.

To decipher the potential influence of PTMs on Dnm1, we analyzed five putative phosphorylation sites (T62, S277, S575, S624, and S629) using site-directed mutagenesis (SDM) and generated nonphosphorylatable alanine (A) and phosphomimetic aspartic acid (D) variants. Dnm1 S624 corresponds to the DRP1 S616, a widely recognized phosphorylation-dependent regulatory site that influences both protein activity and mitochondrial fission in higher eukaryotes. Surprisingly, both S624A/D variants exhibited expression and localization similar to FL. No significant effect on the protein function was observed through mitochondrial morphology assessment, suggesting that Dnm1 S624, unlike DRP1 S616, may not be regulated via phosphorylation and thereby does not affect the protein's function. However, both the A/D variants of T62 in the G2 motif and S277 in the G5 motif were non-functional, as observed through *in vivo* mitochondrial morphology and *in vitro* GTPase activity assays. Interestingly, despite being non-functional in a dominant-negative manner, both the T62A/D and the S277A/D variants exhibited differences in protein localization and puncta dynamics *in vivo*. T62A/D GFP puncta were unusually large and did not localize to mitochondria, while S277A/D exhibited a mitochondrial localization and puncta distribution pattern similar to that of FL. The underlying reasons for these differences may be rooted in their structural alterations. To investigate this, we further analyzed the secondary and higher-order structures of WT, T62A/D and S277A/D. Remarkably, the overall secondary structure of the protein was unaffected in the mutants, as indicated by far-UV CD spectroscopy. Furthermore, both WT and mutant Dnm1 variants exhibited higher-order structures, as demonstrated by size exclusion chromatography and native polyacrylamide gel electrophoresis. However, the nature and functional significance of these structures need to be determined. Computational analysis and molecular dynamics (MD) simulations identified local conformational changes around the mutation site and altered

atomistic motion in distant residues, potentially explaining the observed phenotypic differences in T62A/D and S277A/D mutant *in vivo*. Overall, our findings highlight the importance of two residues in the G2 and G5 motifs of the GTPase domain, which affect Dnm1 function both *in vivo* and *in vitro*.

We extended our investigation to study four disease-causing mutations (A395D, G362D, R403C, C446F) of DRP1 by mimicking them in Dnm1 at equivalent residues (A430, G397, R438, C481). We observed that cells expressing the A430D and G397D mutations significantly impacted the structure and function of the protein. A430D displayed a complete loss of Dnm1 function in a dominant-negative manner, failing to restore normal mitochondrial morphology in *dnm1* cells. Additionally, A430D disrupted the typical Dnm1 punctate phenotype, causing most cells to exhibit cytosolic fluorescence indicative of defective oligomerization. MD simulations showed that the A430D mutation induced a major conformational change in a helix-loop region and significantly altered local flexibility compared to WT Dnm1, supporting the experimental findings. In contrast, G397D mutants exhibited fewer, larger, and less dynamic Dnm1 puncta compared to FL. Impaired growth on glycerol and highly fragmented mitochondria were observed in these cells. The mutation did not affect protein localization but most likely impedes its disassociation from the organelle. MD simulations revealed a striking change in a loop orientation of the mutated protein that might alter the formation of a higher-order structure. In essence, our results emphasize that distinct mutations within Dnm1 can yield diverse functional outcomes, and investigating each mutation in detail is crucial for gaining insights into their respective roles in disease-associated alterations of mitochondrial dynamics.

In conclusion, our study offers new insights into the molecular basis of Dnm1 function and its regulation. This will help us understand the mechanistic details of the conserved mitochondrial fission process and further develop targeted therapies for diseases where mitochondrial fission-fusion regulation is perturbed.

LIST OF ABBREVIATIONS

Abbreviations

aa	Amino Acids
Aβ	Amyloid β
AD	Alzheimer's Disease
ANOVA	Analysis of Variance
ATP	Adenosine triphosphate
$CaCl_2$	Calcium Chloride
CD	Circular Dichroism
CDK	Cyclin Dependent Kinase
CIAP	Calf Intestinal Alkaline Phosphatase
COX	Cytochrome C Oxidase
DRP	Dynamin-related protein
EM	Electron Microscope
ER	Endoplasmic Reticulum
FL	Full Length
GAPDH	Glyceraldehyde 3-phosphate dehydrogenase
GED	GTPase effector domain
HD	Huntington's Disease
IMAC	Immobilized Metal Ion Affinity Chromatography
IMM	Inner Mitochondrial Membrane
LB	Luria Bertani
LiOAc	Lithium Acetate
MMP (Ψm)	Mitochondrial Membrane Potential
MD	Molecular Dynamics
MS	Mass spectrometry
mtDNA	Mitochondrial DNA
OCR	Oxygen Consumption Rate
OMM	Outer Mitochondrial Membrane
OXPHOS	Oxidative Phosphorylation

PBS	Phosphate Buffered Saline
PCR	Polymerase Chain Reaction
PD	Parkinson's Disease
PEP	Phosphoenol pyruvate
PTM	Post Translational Modification
ROS	Reactive Oxygen Species
SDS-PAGE	Sodium Dodecyl Sulphate – Polyacrylamide Gel Electrophoresis
SEC	Size exclusion chromatography
SDM	Site-Directed Mutagenesis
SGD	Saccharomyces Genome Database
SSB	SDS-Sample Buffer
TAE	Tris-acetate-EDTA
TBS	Tris-buffered saline
TCA	Trichloro Acetic acid
VD	Variable Domain
WT	Wild Type
YPD	Yeast extract-Peptone-Dextrose
YPGal	Yeast extract-Peptone-Galactose

LIST OF FIGURES

LIST OF TABLES

Chapter 1

Introduction
&
Review of Literature

Abstract

Mitochondria are essential eukaryotic organelles that orchestrate a myriad of vital functions necessary for cellular survival and development. An intricate link between mitochondrial structure and function is now unequivocally accepted. Mitochondrial fission takes the spotlight due to its involvement in mitochondrial quality control, cellular energy distribution, and programmed cell death. Several molecular players have been identified, which are important in maintaining the structure of the organelle. Dynamin-related GTPase Dnm1 is one such conserved protein in budding yeast that is a vital regulator of mitochondrial dynamics. Multidisciplinary studies have contributed to a comprehensive understanding of the structure and mechanism of action of Dnm1 and its mammalian ortholog DRP1 in great detail. Interestingly, mutations in various domains of DRP1 have been identified that are associated with debilitating conditions in patients. The involvement of the protein in disease-conditions such as neurodegeneration, cancer, and cardiovascular disorders is also gaining attention. However, the underlying molecular mechanism is still under investigation. This chapter provides a comprehensive overview of mitochondrial dynamics and its regulation, mainly focusing on the role of *S. cerevisiae* Dnm1 in mitochondrial fission.

This chapter is a part of

Banerjee R, Mukherjee A, Nagotu S. Mitochondrial dynamics and its impact on human health and diseases: inside the DRP1 blackbox. Journal of Molecular Medicine. 2022 Jan 1:1-21.
DOI: 10.1007/s00109-021-02150-7

1.1 Introduction

The survival and development of most eukaryotic life rely on one unique and extraordinary organelle called mitochondria. Carl Benda coined the term “mitochondria” in 1898, originating from the Greek words "mitos," signifying "thread," and "chondrion," representing "grain". These semi-autonomous organelles contain their own genome and protein synthesis machinery. They are double membrane-bound and occupy a substantial portion of the cytosol of eukaryotic cells [1, 2]. The repertoire of vital cellular functions performed by mitochondria include ATP synthesis through oxidative phosphorylation (OXPHOS), calcium ion buffering, assembly of iron-sulphur clusters, biosynthesis of cellular building blocks such as nucleotides, amino acids, steroid hormones, lipids, haem and vitamin co-factors [3-6]. It also contributes to the cellular redox signalling, apoptosis, and autophagy. Additionally, vital metabolic processes such as β-oxidation of fatty acids, the citric acid cycle, urea synthesis, and gluconeogenesis occur within this organelle [3-6].

As early as 1910, the Russian scientist Konstantin Mereschkowski proposed the theory of symbiogenesis, now known as the endosymbiotic theory, which suggests that mitochondria originated from a symbiotic event where a nucleated cell engulfed an aerobic prokaryote (α-proteobacterium) [7]. The engulfed cell subsequently became dependent on the protective environment of the host cell, while the host cell relied on the engulfed prokaryote for energy production. Eventually, the descendants of the engulfed prokaryote evolved into mitochondria, playing a crucial role in eukaryotic evolution by utilizing oxygen to generate energy [8-11]. The concept of energy transformation facilitated by mitochondria has profoundly influenced cellular metabolism throughout evolution, and it is widely believed that the presence of mitochondria played a crucial role in the emergence of complex multicellular organisms. Mitochondria are especially needed in eukaryotic cells that cannot utilize sunlight for energy conversion. Without mitochondria, these cells would solely rely on glycolysis, which contributes to only a small

fraction of energy from glucose oxidation [12, 13]. Mitochondria process pyruvate and oxidize it to CO_2 and H_2O, resulting in a significant increase in total ATP production. Mitochondria can also utilize fatty acids and some of the amino acids to produce ATP [14, 15]. Hence, the evolution of cellular respiration, coupled with the utilization of oxygen as the ultimate electron acceptor, enables aerobic organisms to extract substantially more energy than anaerobic metabolism permits [15, 16].

1.2 Mitochondria: an organelle with intriguing architecture

The intricate structure of mitochondria reflects the wide array of functions it can perform. As mentioned above, the widely accepted view that mitochondria originated through an endosymbiotic process involving specialized bacteria most likely resulted in its dual-membrane structure (Fig. 1.1). The outer membrane is smooth (known as the outer mitochondrial membrane or OMM) and the inner membrane is highly convoluted (referred to as inner mitochondrial membrane or IMM). This results in mitochondria being compartmentalized into four distinct regions: the OMM, the IMM, the intermembrane space (IMS, the space between the two membranes), and the matrix (the space within the inner membrane) (Fig. 1.1). While OMM and IMM exhibit distinct compositions and functions, they can be identified separately from the plasma membrane or other cellular membranes due to the presence of the mitochondria-exclusive phospholipid, cardiolipin [17-19].

The OMM serves as a hub for cell signalling pathways, where they converge, decode, and transmit information to the mitochondria. Furthermore, it establishes membrane contact sites with various subcellular compartments, especially the endoplasmic reticulum (ER), as well as lysosomes, peroxisomes, endosomes, melanosomes, lipid droplets, and the plasma membrane [20-22]. Additionally, The OMM contains a specific type of voltage-gated anion channel (VDAC) comprised of β-barrel structured transmembrane proteins called porins [23, 24]. Porins create perforations in the OMM that enable the unrestricted diffusion of molecules smaller than

5 kDa, such as sugars, nucleotides, inorganic phosphate, and ions [23, 24].

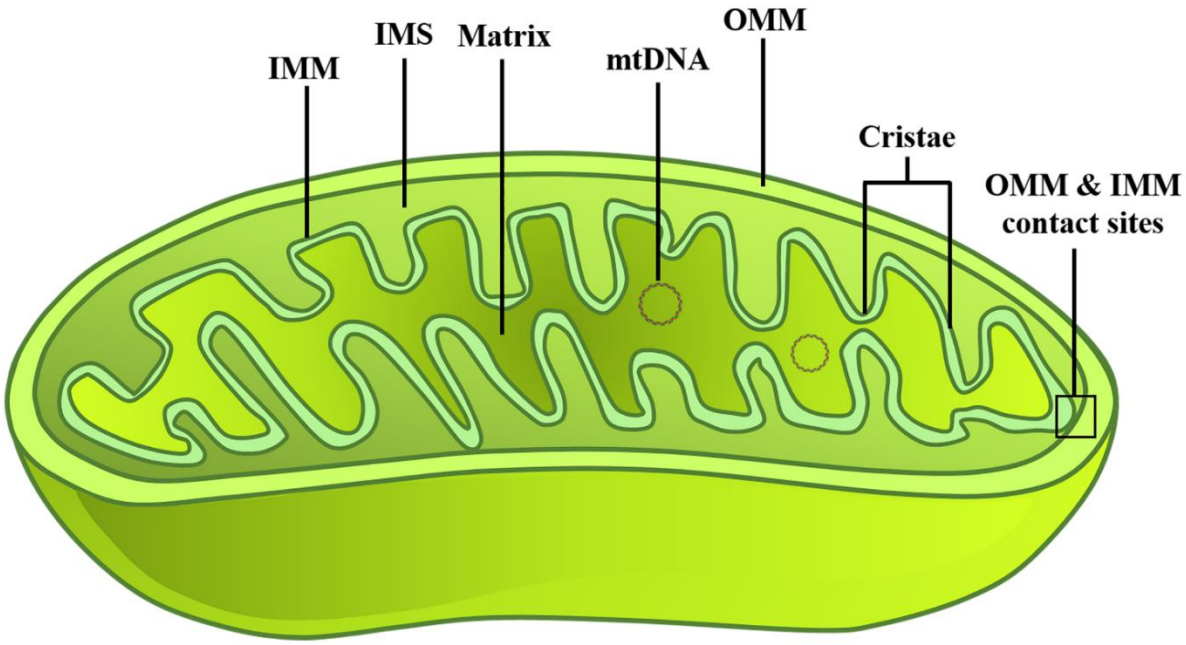

Fig. 1.1 Schematic representing the simplified architecture of a mitochondrion. Mitochondria is a double-membrane bound organelle comprising of an OMM and IMM that undergoes extensive folding and forms cristae. The space between the two membranes is called IMS and the space enclosed by the IMM is called the matrix that houses the mtDNA.

On the other hand, the IMM is a highly folded membrane that separates the mitochondrial matrix from the IMS. The IMM comprises two primary sub-compartments: the inner boundary membrane (IBM) and mitochondrial cristae [25, 26]. The IBM is situated alongside the OMM and contains several channel transporters responsible for transferring ions, ATP, ADP, and small metabolites between the cytoplasm and the mitochondrial matrix [27]. Mitochondrial cristae are deeply convoluted lamellar structures that increase the surface area of the IMM and house the respiratory chain complexes [18]. Specifically, cristae contain several transport proteins and enzymes involved in various metabolic reactions, including the electron transport chain (ETC) and ATP synthesis [18, 28]. The IMM allows water, oxygen, and CO_2 to pass through but requires specific transport machinery for other molecules and ions [29-31]. Furthermore, the OMM and the IMM also contain a translocase (translocase of the outer and inner membrane; Tom and Tim, respectively) that facilitates the movement of proteins across these membranes. This process is essential because most mitochondrial proteins are nuclear-encoded and trafficked

into the mitochondria [31, 32].

The IMS is the smallest aqueous sub-compartment found within the mitochondrion and can be categorized into two distinct parts: the intracristae space and the area between the outer and inner membranes, referred to as the "external IMS" [33]. These two sub-compartments are separated by cristae junctions, which most likely create narrow openings at the necks of the cristae [18, 33]. The components within the IMS play a pivotal role in various essential processes. This includes the exchange of proteins, lipids, or metal ions between the matrix and the cytosol, the regulated initiation of apoptotic cascades, the modulation of signalling pathways controlling respiration and metabolic functions, the mitigation of reactive oxygen species (ROS) produced by the respiratory chain, and the regulation of mitochondrial morphogenesis [34]. The IMS also functions in maintaining the balance of adenine nucleotides and serves as a processing site for proteins imported into the matrix. This compartment houses enzymes, such as adenylate kinase and creatine kinase, which utilize ATP for phosphate transfer [34].

The mitochondrial matrix is a protein-rich aqueous core containing a unique set of enzymes and molecules required for cellular respiration. It contains enzymes for pyruvate oxidation (pyruvate dehydrogenase complex), the citric acid cycle (also known as the Krebs cycle), and fatty acid oxidation [16, 35, 36]. The matrix is also a hub of important metabolites such as ATP, ADP, NAD, and $NADH^{+}$. Additionally, it possesses the mitochondrial DNA (mtDNA), which encodes subunits I, II, and III of cytochrome c oxidase (COX1, COX2, and COX3), apocytochrome b (COB), subunits 6, 8 and 9 of ATPase (ATP6, ATP8 and ATP9) and a ribosome-associated protein (VAR1) [16, 37].

1.3 Mitochondrial architecture: dynamic processes that regulate it

The complex structure of mitochondria is interlinked with the diverse functions performed by the organelle. Interestingly, mitochondria in most eukaryotes are not "pill-like" or “solitary bean-like” structures, as traditionally described [38]. Instead, they are incredibly

dynamic organelles. Three fundamental processes, namely fusion, fission, and mitochondrial motility, govern mitochondrial dynamics. The overall network morphology of the organelle is in response to the metabolic needs and functional state of mitochondria [39].

Mitochondrial fusion is a regulated and intricately complex process of combining two mitochondria, end-to-end or end-to-side, resulting in an interconnected mitochondrial network [40, 41]. The complexity arises due to the double membrane of these organelles that requires a sequential fusion of four membranes (two OMMs followed by two IMMs) [40]. The fusion process leads to content mixing, where matrix components, such as mtDNA, ETC constituents, and nutrient precursors, diffuse throughout the newly formed mitochondrial network [40]. Mitochondrial fission is the process through which a mitochondrion divides into two daughter mitochondria [42]. Fission is needed for generating new mitochondria, removing damaged mitochondria, and facilitating apoptosis during high levels of cellular stress [40]. Furthermore, mitochondrial motility, coupled with frequent fusion and fission, is essential for adapting mitochondrial quantity, shape, and internal positioning according to cellular necessities [43]. The precise placement of mitochondria at specific intracellular locations is essential for for energy use and calcium signalling [39, 44].

1.3.1 Mitochondrial dynamics: importance and benefits

Mitochondrial dynamics governed by the coordination of fission, fusion, and motility is a captivating phenomenon with far-reaching implications. Delving into the importance of mitochondrial dynamics unveils a fundamental aspect of cellular biology that influences energy production, cellular health, and adaptability.

1.3.1.1 Mitochondrial content exchange and mtDNA maintenance

Mitochondrial fusion primarily facilitates content mixing between mitochondria without altering morphology. Content exchange benefits mitochondria by ameliorating the effects of heteroplasmic mtDNA mutations, minimizing oxidative damage, providing sufficient energy

supply and maintaining mitochondrial membrane potential (Ψm) [45]. Mitochondrial fission and fusion are vital for maintaining mtDNA levels and mtDNA fidelity [46]. By evenly distributing mtDNA mutations throughout the mitochondrial population, fusion reduces the likelihood of severe effects on any one mitochondrion [47] (Fig. 1.2). Disruption of fusion in mammals leads to mitochondrial heterogeneity and dysfunction, linked to nucleoid loss [48]. In yeast, fusion-defective mutants lose mitochondrial genomes, affecting respiration due to organelle fragmentation [49]. A significant decrease in mtDNA content is reported when mitochondrial fusion is hampered by silencing or deleting necessary proteins [50]. Mutants often lack detectable mtDNA in many mitochondria, leading to impaired oxidative phosphorylation (OXPHOS) activity [51]. On the contrary, if fission is disturbed, mtDNA nucleoids aggregate, distorting mitochondrial tubules. This aggregation results in uneven mtDNA distribution and mosaic OXPHOS deficits [52]. Thus, while fission generates nucleoid-less organelles, fusion replenishes mitochondrial genomes and gene products, maintaining functional mitochondria.

1.3.1.2 Mitochondrial inheritance and distribution

Mitochondria proliferate through fission from a pre-existing organelle and be inherited by daughter cells through mitosis, as they cannot be formed *de novo* (Fig. 1.2). Proper mitochondrial distribution depends on fission to split the mitochondrial network into transportable units. In yeast, mitochondria are inherited in an ordered manner by cytoskeleton-dependent bud-directed transport [43]. Immediately after a new bud forms, mitochondria move into the bud to ensure that the daughter cell inherits the organelle. Increasing evidence suggests that myosin motor proteins drive bud-directed mitochondrial movement along actin cables [43, 53]. In mammalian cells, mitochondria fragment before cell division, allowing the organelles to be transported to the daughter cells in a stochastic manner [54].

1.3.1.3 Mitochondrial quality control through mitophagy

Mitochondrial fission helps to regulate the quality of mitochondria by identifying and

segregating poorly functioning organelles that have a reduced Ψm [55] (Fig. 1.2). This selective elimination of impaired mitochondria through autophagy is referred to as mitophagy [56]. It serves as an adaptive survival strategy that prevents cells from undergoing apoptosis and enables the preservation of a robust mitochondrial population for continuous energy generation [56]. Mitophagy requires that the mitochondria-targeted for degradation are smaller than the autophagosomes. Therefore, the engagement of the mitochondrial fission machinery plays an important role in accomplishing this size reduction [57, 58]. Indeed, numerous investigations have proposed a correlation between mitochondrial fission and the effectiveness of mitophagy in mammalian cells [55, 59, 60]. However, the role of mitochondrial fission in mitophagy is still controversial in yeast [61]. Two independent research groups reported reduced mitophagy in cells devoid of mitochondrial fission machinery [58, 62]. On the contrary, Mendl and colleagues reported that fission machinery is not required for rapamycin-induced mitophagy in yeast [63]. Further studies are required to elucidate the definitive role of fission in mitophagy in yeast cells.

1.3.1.4 Mitochondrial fission is crucial for apoptosis

Excessive mitochondrial fragmentation by fission is a common feature of cells undergoing apoptosis, a type of programmed cell death that is important for development and homeostasis in eukaryotic systems (Fig. 1.2). OMM permeabilization releases pro-apoptotic factors such as cytochrome c that initiates pathways leading to apoptosis [64]. A role for the mitochondrial fission proteins in regulating apoptosis in yeast and mammalian cells has been reported [65-67]. While several aspects are still subject to debate, it is proposed that mitochondrial fragmentation takes place early in the apoptotic process, occurring just before or concurrently with OMM permeabilization and preceding effector caspase activation [68]. Further investigation is needed to elucidate the specific roles of mitochondrial fission and fusion components in the process of apoptosis.

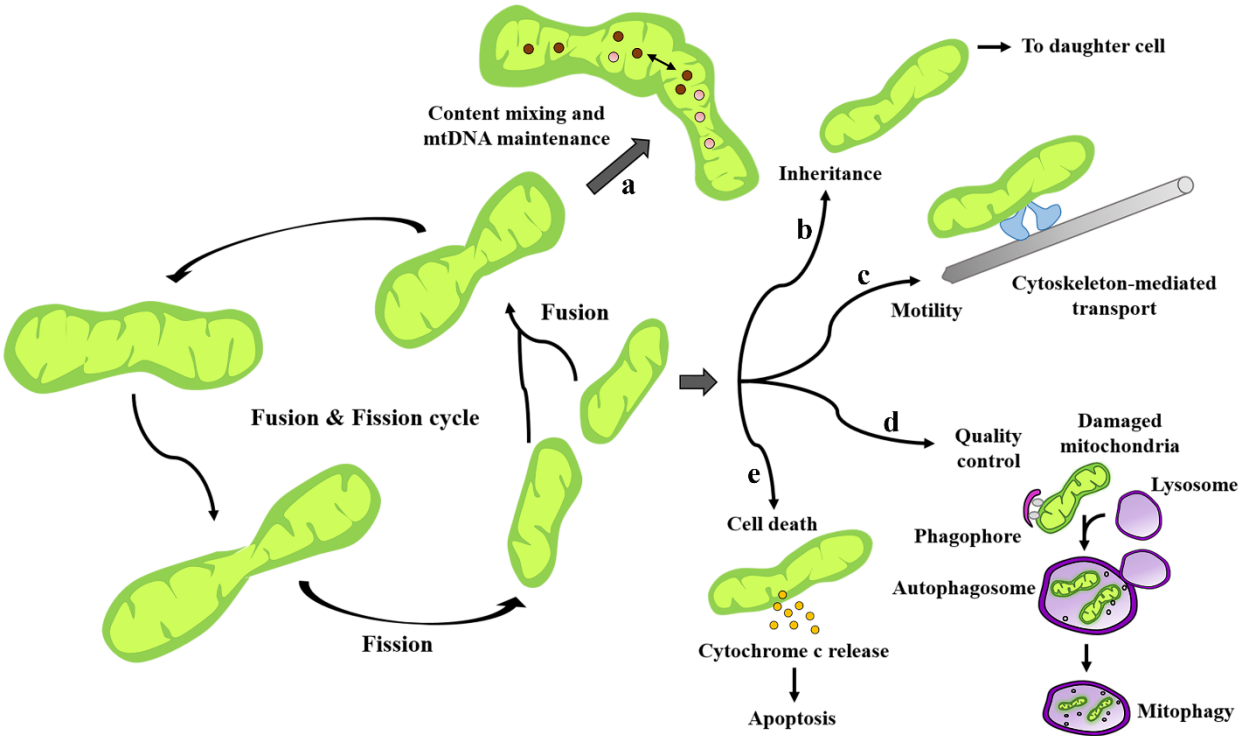

Fig. 1.2 Mitochondrial fission-fusion cycle and its implications in regulating various aspects of mitochondria. Mitochondria undergo a continuous cycle of fission and fusion that regulates their dynamic nature and is crucial to perform various functions. **(a)** Mitochondrial fusion is necessary for the content mixing and complementation of mtDNA in heteroplasmic cells. Fusion is also important for reducing oxidative damage, supplying sufficient energy and maintaining Ψm. On the contrary, mitochondrial fission is necessary for **(b)** the inheritance and distribution of organelles during cell division, **(c)** intracellular transport via the cytoskeleton **(d)** removal of damaged organelles via mitophagy and **(e)** the release of cytochrome c and other pro-apoptotic factors from the IMS required for programmed cell death.

1.4 Mitochondrial dynamics: molecular machinery required

The molecular machinery that orchestrates mitochondrial fusion and fission comprises a family of highly conserved, large, dynamin-related GTPases. Dynamins are a family of large GTPases that perform essential cellular functions such as vesicle scission, fusion and fission of organelles, vacuolar trafficking, nuclear remodelling, and microbial resistance [69-71]. Proteins belonging to the dynamin family are involved in the fission, fusion, or tubulation of specific target membranes. The dynamin superfamily can be categorized into two major groups: classical dynamin and dynamin-related proteins (DRPs) based on their domain structure [71-73]. Dynamins and DRPs share key structural features that include a large N-terminal GTPase domain, a middle domain, and a GTPase effector domain (GED) [71-73]. The GTPase domain

binds and hydrolyzes GTP, while middle and GED are crucial for forming oligomers and regulating GTPase activity [71-73]. Two additional domains, a pleckstrin homology domain (PHD) for membrane binding and a proline-rich domain (PRD) containing multiple SH3-binding sites essential for protein interactions, are present in the classical dynamin [71-73].

1.4.1 Mitochondrial fusion: core components

Mitochondrial fusion can be divided into OMM fusion and IMM fusion. In yeast, three core components of mitochondrial fusion, namely Fzo1, Ugo1, and Mgm1, are identified. Fzo1 (a large GTPase) and Ugo1 are present on the OMM, and Mgm1 is a dynamin-related GTPase present in the IMM [74-80] (Table 1.1). These proteins work together to establish a complex that facilitates mitochondrial fusion and the absence of any of these components leads to the fragmented mitochondria [68, 81]. During mitochondrial fusion, Fzo1 proteins on neighboring mitochondria form trans complexes by interacting through their C-terminal coiled-coil regions, which link the OMMs of the two mitochondria. This interaction results in the fusion of adjacent OMMs facilitated by the GTPase activity of Fzo1 [74, 75]. In a similar manner, Mgm1 forms trans complexes that bring together opposing IMMs, leading to IMM fusion through GTP hydrolysis by Mgm1 [79, 80]. Ugo1 plays a key role by physically interacting with both Fzo1 and Mgm1, forming a complex that coordinates the OMM and IMM fusion in yeast [77].

In mammals, mitochondrial fusion is dependent on three pivotal dynamin-related GTPases namely mitofusin-1 (MFN1) and mitofusin-2 (MFN2) present in the OMM and optic atrophy 1 (OPA1) localized to the IMM [82-85] (Table 1.1). MFN1 and MFN2 (orthologs of yeast Fzo1) interact, forming homo and heterodimers and utilizing their GTPase activity to fuse adjacent OMM [82]. OPA1 (ortholog of yeast Mgm1) regulates the IMM fusion together with MFN1 in an unknown manner [84]. OPA1 undergoes proteolytic processing, resulting in the formation of long and short isoforms. Interestingly, a recent study suggests that the ratio of the long form of Opa1 (l-Opa1) and short form of Opa1 (s-Opa1) levels regulates IMM fusion [85].

However, there is currently no identified mammalian equivalent of yeast Ugo1. Therefore, the coordination of fusion events between the OMMs and IMMs in mammals remains to be elucidated.

Table 1.1 Molecular machinery regulating mitochondrial dynamics in yeast and mammals

Yeast	Mammals	Function	Reference
Fzo1	MFN1 and MFN2	OMM fusion	[74, 75, 82]
Mgm1	OPA1	IMM fusion	[79, 80, 83, 84]
Ugo1	-	OMM fusion and linking of Fzo1 and Mgm1	[76-78]
Dnm1	DRP1	Mitochondrial fission	[86, 87]
Fis1	hFIS1	OMM receptor involved in fission	[88-90]
Mdv1 and Caf4	-	Adaptor for Dnm1-Fis1 interaction and nucleator for Dnm1 oligomerization	[91-94]
Num1	-	Anchors Dnm1 to the cell cortex	[95]
Mdm36	-	Adaptor for Num1-Dnm1 interaction	[96]
-	MFF	Recruits DRP1 to OMM	[97]
-	MID49/51	Recruits DRP1 to OMM	[98]

1.4.2 Dnm1 at the helm: steering the course of mitochondrial fission

The master regulator of mitochondrial fission in most eukaryotic organisms is the dynamin-related protein 1, known as Dnm1 in yeast. Dnm1 functions together with Fis1 (mitochondrial fission protein 1) and Mdv1 (mitochondrial division protein 1) or Caf4 to achieve mitochondrial fission in yeast [88, 91-94].

Dnm1 is a multidomain protein that comprises an N-terminal GTP binding domain, followed by middle domain, variable domain (VD) / B-insert and a C-terminal GED [99, 100] (Fig. 1.3A). Dnm1 was first discovered in yeast as a homolog of dynamin, a protein required for endocytosis in humans and flies [101, 102]. Later, the role of Dnm1 in mitochondrial fission was discovered during a search for yeast mutants with mitochondrial morphological defects [86]. Further investigations indicated that the loss of Dnm1 inhibited mitochondrial fission but not fusion, leading to the formation of net-like mitochondrial structure [81, 103]. Mitochondrial

fragmentation induced by a *fzo1* mutation was no longer observed in cells lacking Dnm1, indicating that Dnm1-mediated fission was the cause of mitochondrial fragmentation in *fzo1* cells [81, 103].

Dnm1 is predominantly present in the cytosol and visualized as punctate structures. Studies have reported the presence of a dimeric form of the protein in the cytosol [86, 104]. However, time-lapse imaging of immunogold or GFP-tagged Dnm1 revealed the formation of punctate structures on the potential OMM fission sites [81, 103]. The recruitment of Dnm1 from the cytosol and its assembly into punctate structures on the OMM is dependent on two proteins, Fis1 and Mdv1 in yeast (Fig. 1.3B). Fis1 is a small tail-anchored, integral membrane protein present in the OMM [88]. Its N-terminal domain faces the cytosol and forms a six-helix bundle with tandem tetratricopeptide repeat motifs (TPR) that interact with the adaptor protein Mdv1 [89]. The N-terminal extension present in Mdv1 facilitates binding with Fis1. A heptad repeat region in Mdv1 is required for the homo-oligomeric interactions and a WD40 repeat domain at the C-terminal interacts with Dnm1 [92]. Hence, Mdv1 acts as a molecular bridge between Fis1 and Dnm1 by forming the Fis1-Mdv1-Dnm1 fission complex [105]. Interestingly, a dual role for Mdv1 in functioning as a nucleator for the assembly of Dnm1 on the OMM and to serve as a functional scaffold that stabilizes oligomeric Dnm1 assemblies has been proposed [94, 105]. The Fis1–Mdv1–Dnm1 complex plays a crucial role in mitochondrial division. Fis1 can also collaborate with the Mdv1 paralog Caf4, to recruit Dnm1 to mitochondria [93]. In mutants that lack Mdv1, a role for Caf4 in regulating mitochondrial division has been reported. This suggests that Caf4 may play a role in mitochondrial division that is independent of Mdv1 [93]. Although Caf4 and Mdv1 have similar expression levels and contribute to fission, they are not functionally equivalent proteins [106]. Furthermore, Caf4 was also reported to be required for the polarized orientation of a subset of Dnm1 assemblies towards cell cortex [107].

Interestingly, yeast Dnm1 interacts with two additional proteins, Num1 (nuclear

migration 1) and Mdm36 [95, 96]. Cells lacking either Num1 or Mdm36 depict fused mitochondrial network, resembling the phenotype of *dnm1* cells (Fig. 1.3C) [95, 96]. A role for Num1, Mdm36, and Dnm1 in anchoring mitochondria to the cell cortex in coordination with actin has been proposed [68, 95, 96, 108, 109]. This, in turn, may facilitate mitochondrial division by regulating membrane tension in a mechanism similar to that described for classical dynamins [68, 95, 96, 108, 110].

Dnm1 in its GTP-bound state assembles into spirals on liposomes with a diameter of ~100 nanometers (nm) [111]. However, this diameter is inadequate to encircle a mitochondrion, which typically has an average diameter of ~300 nm. Hence, mitochondrial constriction should be the preceding step before forming Dnm1 spirals encircling the mitochondria. The constriction of the mitochondrial matrix and OMM were reported to be independent of Fis1 and Dnm1, respectively [112, 113]. Later, a role for ER in the spatial regulation of mitochondrial fission was reported [20, 114]. Friedman and colleagues showed that ER encircles mitochondria at locations where division is about to happen. This wrapping results in the constriction of the mitochondria corresponding to a diameter of ~ 100 nm, which is in line with the Dnm1 higher-order structure identified earlier [20].

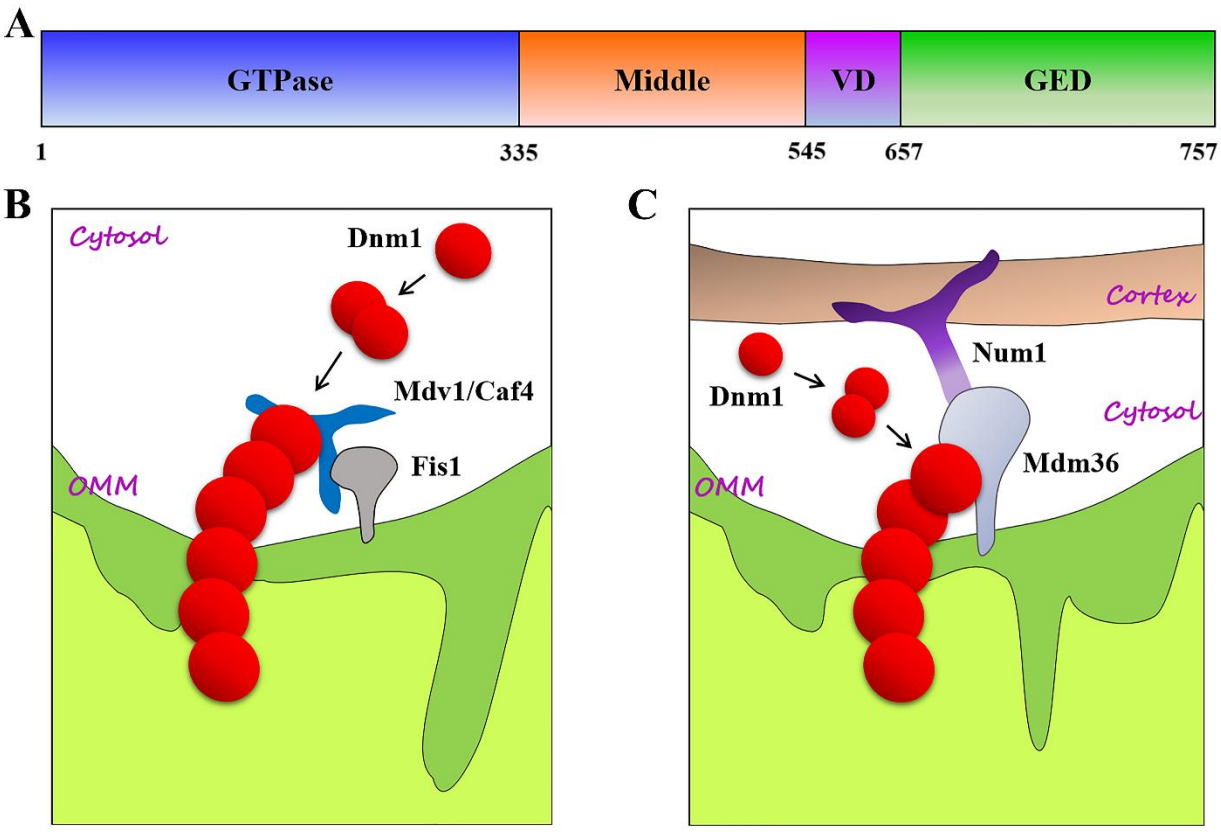

Fig. 1.3 Domain architecture of Dnm1 and its interacting partners. (A) Schematic representing various domains of Dnm1: GTPase domain (blue), middle domain (orange), V domain (purple) containing B-insert and GED (green). Dnm1 is composed of 757 aa residues. Two fission complexes constituted with Dnm1 in the core are represented. **(B)** Fis1 a C-terminal tail-anchored OMM protein interacts with the adaptor protein Mdv1 (and/or Caf4), to initiate the recruitment of Dnm1 to the OMM. **(C)** Dnm1 also interacts with Mdm36 and Num1 that aids in the anchoring of the mitochondria to the cell cortex. This subsequently creates membrane tension, facilitates the final scission of the membrane, and divides mitochondria [108].

The current model of mitochondrial division proposes that Fis1 recruits Mdv1 from the cytosol to the OMM [88, 92]. Upon its membrane association, Mdv1 helps in the nucleation and stabilization of the assembly of GTP-bound Dnm1 oligomers at the ER-mediated mitochondrial constriction sites [94, 105]. Subsequently, these Dnm1-GTP oligomers form large spirals that gradually encircle the mitochondrion. Finally, assembly-stimulated GTP hydrolysis triggers a conformational change that leads to fission [111, 115, 116]. Dnm1 mechanically severs the mitochondrion through a mechanism that closely resembles the action of classical dynamins in vesicular budding or endocytosis (Fig. 1.4). After fission, Dnm1 oligomers undergo disassembly and are recycled to the cytosol [108].

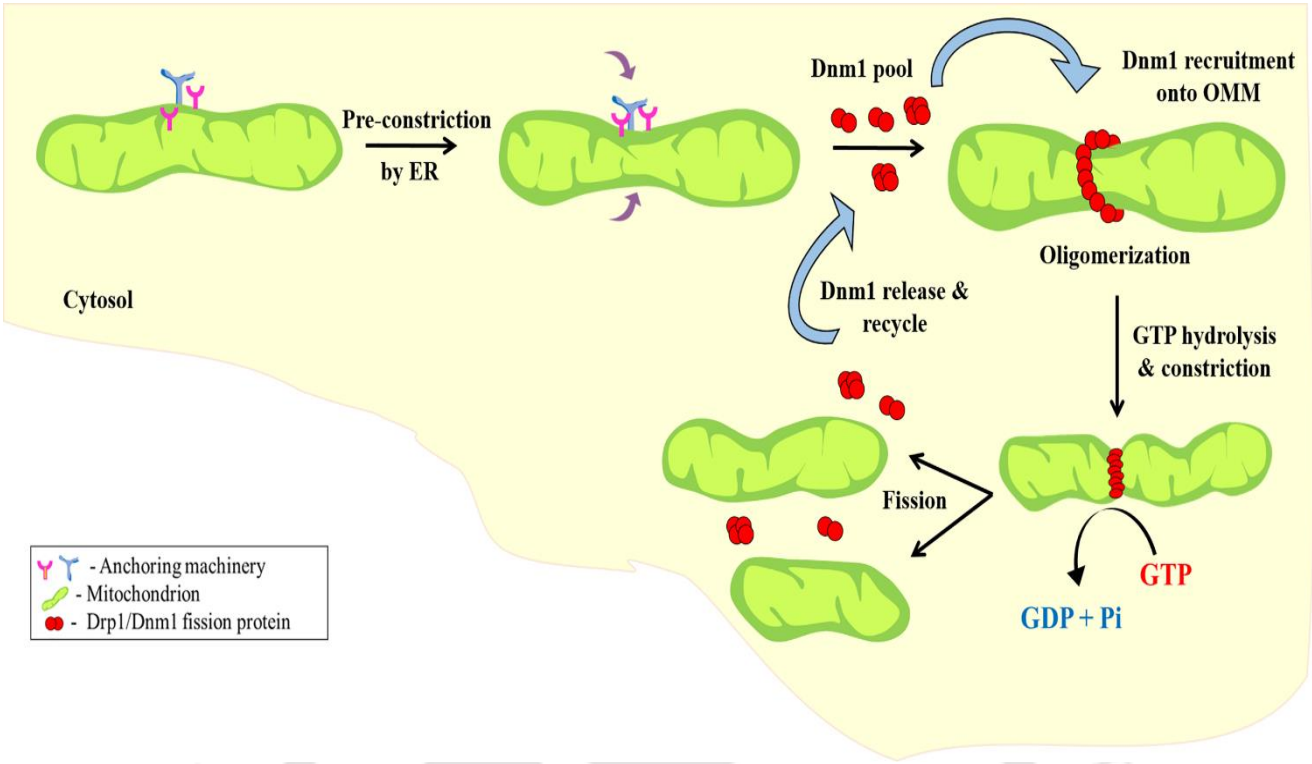

Fig. 1.4 Schematic representing Dnm1-dependent mitochondrial fission in yeast. Cytosolic Dnm1 (lower-order structures) is recruited to the pre-constricted sites on the OMM. Dnm1 anchors to the OMM with the help of its interacting partners and forms higher-order structures at the fission site. These structures further constrict the OMM and finally, GTP hydrolysis results in the division of mitochondria. Subsequently, higher-order structures of Dnm1 are disassembled and recycled back to the cytosol.

1.5 DRP1, the human homolog of Dnm1: insights into isoforms, structure and function

DRP1, the homolog of yeast Dnm1, is the central player that regulates mitochondrial fission in mammals [86, 87, 117]. These proteins are highly conserved and share similar domain architecture (Fig. 1.5A). Alternative splicing results in the formation of nine different isoforms of DRP1. DRP1L transcript that codes for DRP1 comprises of twenty-one exons, of which splicing occurs primarily in three exons (3, 16, and 17) [118] (Fig. 1.5B). Additionally, the number of amino acids (aa) in the B-insert of the VD is variable in these isoforms [118]. Isoform 1 comprises of 736 aa and lacks exon 3; isoform 2 has 710 aa and the exon 3 and 16 are spliced out; isoform 3 has 699 aa and exon 3, 16 and 17 are spliced out; and isoforms 4, 5, are comprised of 725, 710 aa respectively and lack exons 3 and 17. Isoform 6 is comprised of 749 aa and

contains all exons. Due to the absence of exons 5-8, isoform 7 has the shortest length (533 aa). It is interesting to note that translation in isoform 7 starts at exon 2 rather than exon 1. Isoform 8 has 738 aa and lacks exon 17 and isoform 9 has 712 aa and lacks exons 16 and 17. Studies of DRP1 isoforms have shown that they have expressed differently in different tissues, suggesting that they have specialized functions [118, 119].

Similar to as discussed for yeast Dnm1, recruitment of DRP1 to the OMM also requires several mitochondrial receptors such as mitochondrial fission protein 1 (FIS1), mitochondrial fission factor (MFF), mitochondrial division proteins (MID49 and MID51) [90, 97, 98, 120] (Fig. 1.5C). MFF facilitates the recruitment and assembly of DRP1 on OMM [120]. MFF is anchored to the OMM by a C-terminal transmembrane domain. A role for the N-terminal R1 and R2 motifs of MFF in the recruitment of DRP1 has been reported DRP1 [121]. On the other hand, the middle domain of DRP1 and its oligomerization status influence the interaction of DRP1 with MFF [120]. Several middle domain mutations (A395D, G350D, G363D) inhibit the interaction of DRP1 with MFF, thereby hampering its recruitment to OMM [122]. Selective recruitment of active oligomeric subpopulation of DRP1 by MFF has also been reported [120]. In line with this, increased targeting of DRP1 to the OMM upon overexpression of MFF was also reported. Knockdown of *Mff* in MEFs exhibits elongated mitochondria, most likely due to the hampered recruitment of DRP1 to the OMM. Recently, a peptide (P259) that specifically inhibits DRP1-MFF interaction was synthesized, further highlighting the importance of this interaction in mitochondrial dynamics [123].

Another important DRP1 interacting protein required for its recruitment is FIS1 (homolog of yeast Fis1). However, the role of FIS1 in DRP1 recruitment is still controversial in mammalian cells. Homologs of Mdv1 and Caf4 have not been identified in mammalian cells. The absence of FIS1 results in elongated mitochondrial morphology in HeLa cells but does not alter the mitochondrial morphology in HCT116 cells [97, 124]. Furthermore, increased or decreased

expression of FIS1 had minimal or no effect on the subcellular distribution of DRP1 between mitochondria and cytosol in mammalian cells [97, 124, 125]. FIS1-dependent recruitment of DRP1 to mitochondria in response to mitophagy and certain pathological conditions has also been reported [126-128]. The highly conserved chordate-specific mitochondrial dynamics proteins MID49 (MIEF2) and MID51 (MIEF1) also interact with DRP1 at the OMM [98]. Both proteins possess an N-terminal transmembrane domain for OMM integration and a nucleotidyltransferase domain for nucleotide diphosphate binding [129, 130]. Structural analysis using cryo-EM revealed four DRP1 interfaces that interact with MID49 and MID51 [131]. The proposed model suggests that MID49/51 recruits a nucleotide-bound specific conformation of DRP1 and initiates polymerization. Subsequently, the nucleotide exchange and hydrolysis results in the disassociation of MID49/51 receptors, followed by the curling of the DRP1 filaments into closed rings. Dissociation of MID49 or MID51 before constriction is suggested to be essential, and this might also explain the inhibition of mitochondrial fission reported upon overexpression of the MID receptors [131]. The MID49 and MID51-dependent recruitment of DRP1 onto the OMM was also reported to be independent of FIS1 or MFF [98, 125].

A recent study highlighted the importance of DRP1 interaction with mitochondrial Zn^{2+} transporter ZIP1 (Fig. 1.5c). This interaction was required to eliminate dysfunctional mitochondria through mitophagy [132]. Mitochondrial depolarization results in MFF-dependent recruitment of DRP1 from the cytosol followed by its interaction with ZIP1 on the OMM. DRP1/ZIP1 interaction facilitated the transport of Zn^{2+} into the mitochondrial matrix via mitochondrial cation uniporter. Accumulation of Zn^{2+} in the matrix resulted in further loss of MMP, leading to mitochondrial dysfunction and selective degradation of damaged mitochondria through mitophagy [132]. Recent studies also provide evidence for a direct interaction between DRP1 and a mitochondrial membrane-specific lipid called cardiolipin (CL) [133]. Zabalbeitia and colleagues showed that DRP1 had a preferential binding to CL over other anionic

phospholipids [134]. Detailed analysis revealed that several lysines in the B-insert are involved in DRP1-CL interaction. Furthermore, Cryo-EM studies confirmed that the VD domain plays an important role by targeting DRP1 to CL-enriched areas to promote mitochondrial constriction followed by fission [133]. Direct interaction of DRP1 with CL that enables the assembly of higher-order structures and stimulates GTPase activity was also reported [134]. However, further investigation is required to understand the regulation between the other interacting partners of DRP1 and cardiolipin. Furthermore, a role for actin and ER in the constriction of the membrane followed by recruitment of DRP1 and its oligomerization has been proposed [135-137]. Several actin-interacting proteins such as IFN2, SPIER1C, myosin II, cortactin, and cofilin also impact the function of DRP1 in mitochondrial fission [121, 138]. Ji and colleagues recently proposed an interesting model that depicts DRP1 maturation. The authors report the association of smaller DRP1 units to the OMM, which progressively mature into oligomers. A role for actin filaments as a signal for such a maturation process was reported by the authors (Fig. 1.5). The binding of actin filaments to purified DRP1 and reduced DRP1-dependent mitochondrial fission upon inhibition of actin polymerization was also reported [135].

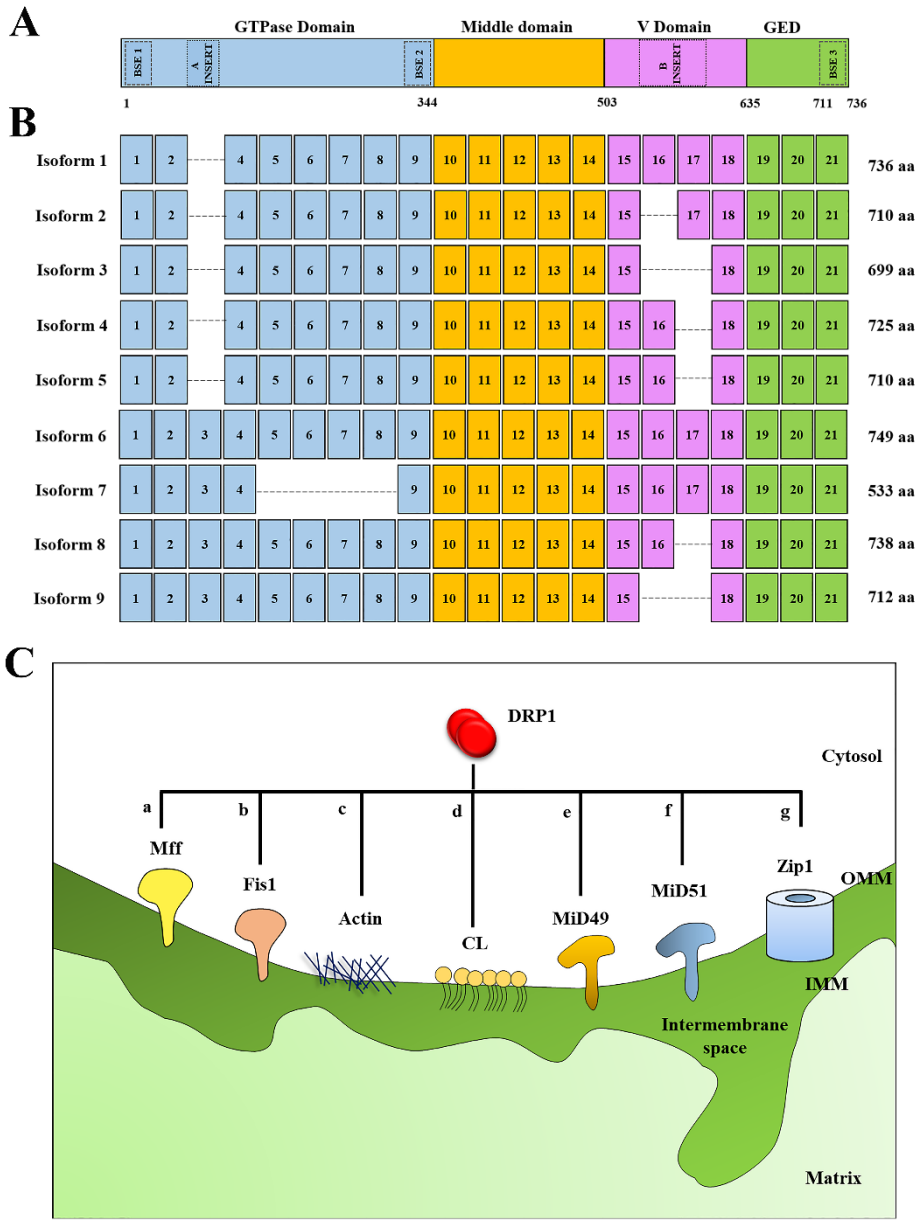

Fig. 1.5 DRP1: domain architecture, isoforms and interacting partners. A. GTPase domain (blue) containing bundle signalling elements BSE 1, BSE 2 (dashed line) and A-insert (dotted line), middle domain (yellow), V domain (purple) including B-insert (dotted line), and GED (green) comprising of BSE3 (dashed line) [118]. **B.** Cartoon representing coding region and length of different isoforms of DRP1. Exons represented by different colours indicate coding regions in various domains. GTPase domain (Blue, exon 1–9), middle domain (yellow, exon 10–14), V domain (purple, exon 15–18), and GED (green, exon 19–21). A-insert (exon 3) and B-insert (exon 16,17) are part of the GTPase and V domain, respectively [118]. **C.** Schematic representation of DRP1 interacting partners. Cytosolic DRP1 requires several macromolecules for recruitment onto OMM and subsequent execution of mitochondrial fission. (**a**) Integral membrane protein MFF is reported as a major DRP1 recruitment factor. MFF aids in the recruitment of DRP1 tetramers or higher-order structures onto OMM [120]. (**b**) Mammalian FIS1, on the other hand, is reported to recruit DRP1 under both physiological and certain induced conditions, such as during selective autophagy (mitophagy) of mitochondria [128, 139]. (**c**) Assembly of actin filaments was proposed to act as a signal for mitochondrial fission. Direct interaction between actin and DRP1 helps in the stimulation of DRP1 activity via the maturation process and thereby assists in mitochondrial fission [135, 137]. (**d**) Interaction of the mitochondria-specific cardiolipin with the V domain of Drp1 promotes its assembly and augments GTPase activity [133, 134]. Two structurally similar mitochondrial integral membrane proteins (**e**) MID49 and (**f**) MID51 are also required for the localization of DRP1 to OMM [98]. The GTP hydrolysis of DRP1 drives the dissociation of MID49 or MID51 before the constriction of the mitochondrial membrane [131]. (**g**) Interaction of DRP1 with mitochondrial Zn^{2+}

transporter ZIP1, primarily at the mitochondrial fission site, regulates membrane potential and aids in the selective removal of dysfunctional mitochondria [132].

1.6 DRP1: Regulation via post-translational modifications

Apart from the above-mentioned interacting partners of DRP1 on the OMM, a significant role for the various post-translational modifications (PTM) of the protein in regulating its activity has been reported. PTMs such as phosphorylation, dephosphorylation, ubiquitination, deubiquitination, sumoylation, desumoylation and S-nitrosylation have been reported [70, 140] (Table 1.2).

Table 1.2 Post-translational modifications of human DRP1 identified under physiological and disease conditions

Modified residue	Cell type	Enzyme involved	Phenotypic effect reported	Reference
Phosphorylation				
S637	HeLa cells	Cyclic AMP-dependent protein kinase (PKA)	•Disrupts the intramolecular interaction of GED and GTPase domain of DRP1 •Decreased DRP1 activity •Inhibitory effect on mitochondrial division	[141, 142]
S616	HeLa cells	Cyclin-dependent kinase 1(CDK1)	•Increased DRP1 activity •Promotes mitochondrial fission during mitosis	[142]
S616	HEK-TtH, HeLa, CFPac, and Panc-1	Extracellular signal-regulated kinase 2 (ERK2)	•Increased DRP1 activity •Enhanced mitochondrial fission	[143]
S616	Human Mesenchymal Stem Cells	p38 mitogen-activated protein kinase (MAPK)	•Enhanced DRP1 translocation to the OMM •Promotes mitochondrial fission	[144]
S585	HeLa cells	Cyclin-dependent kinase 1 (CDK1)/Cyclin B	•Increased DRP1 activity •Promotes mitochondrial fission during mitosis	[54]
S693	HeLa cells and HEK293 cells	Glycogen synthase kinase-3β (GSK-3β)	•Inactivates DRP1 by decreasing GTPase activity •Inhibits mitochondrial fission	[145]
Y266, Y368, Y449	HEK 293T and SH-SY5Y cells	c-Abl	•Augments DRP1 GTPase activity and mitochondrial fission	[146]

Dephosphorylation				
S637	HeLa cells	Calcineurin	•Increased translocation of DRP1 to the OMM •Increased DRP1 activity and promotes mitochondrial fission	[142]
S-nitrosylation				
C644	HEK293 cells	Nitric oxide synthase (NOS)	•Assists in dimerization of DRP1 •Increased GTPase activity •Increased mitochondrial fission	[147]
Sumoylation				
K532, K535, K558, K568, K594, K597, K606, K608	HEK293 cells	Ubc9/mitochondria associated protein ligase (MAPL)	•Locking of SUMOylated DRP1 on the mitochondrial membrane •Increased mitochondrial fission	[148]
Desumoylation				
-	HEK293T cells	SENP5L	• Desumoylation leads to ubiquitination and degradation of DRP1 •Decreased mitochondrial fission	[149]
-	HEK293 cells	SENP3	• Facilitates DRP1 localisation at OMM • Increased mitochondrial fission	[150]
Ubiquitination				
-	HeLa cells	Mitochondrially localized RING finger E3 ligase (MARCH5)	•Required for mitochondrial division and accurate sub-cellular trafficking of DRP1	[151]
-	HeLa and SH-SY5Y cells	Parkin	•Assists in the removal and degradation of DRP1 from the OMM after every round of fission •Inhibits excessive fragmentation	[152]
Deubiquitination				
-	HEK293 and HCT116 cells	OTUD6A	• Stabilizes DRP1 and increases mitochondrial fission	[153]

1.7 DRP1: involvement in various disease conditions

Altered mitochondrial dynamics can severely affect tissues and organs, such as the brain and heart, that extensively depend on energy produced by functional mitochondria [140, 154]. Hence, most mitochondria-associated diseases are linked to development, neurodegeneration, metabolic disorders, and cardiomyopathies. Mitochondrial dysfunction is one of the hallmark pathological features in many neurodegenerative disorders. Increased mitochondrial fragmentation, aberrant mitochondrial function, and apoptosis are characteristics reported in most of the above-mentioned disease conditions [155]. As discussed in earlier sections, DRP1 is an essential protein that plays a significant role in regulating mitochondrial structure and its role in various disease conditions has just begun to be explored. Studies in several model systems have resulted in understanding the effects of altered expression of DRP1 and the pathways affected in these debilitating conditions. Altered mitochondrial dynamics (mediated by DRP1) contribute to age-associated disease conditions such as neurodegeneration and cancer. Interestingly, reducing/blocking the activity of DRP1 using pharmacological inhibitors has been reported as a treatment option for these disease conditions. The role of DRP1 and mitochondrial dynamics in neurodegeneration, cancer, and cardiovascular diseases and their potential cure by targeting DRP1 for therapeutic approaches are depicted in detail in box 1 and box 2 (Fig. 1.6 and Fig. 1.7).

Interestingly, several random and rare genetic mutations in DRP1 result in altered mitochondrial dynamics and are associated with pathological conditions. Dominant and recessive mutations in the GTPase, middle, and GED that alter the protein function and result in disease conditions are reported (Fig. 1.8; Table 1.3). This section discusses the structural and functional changes of such mutant variants of DRP1 that lead to debilitating conditions.

BOX: 1

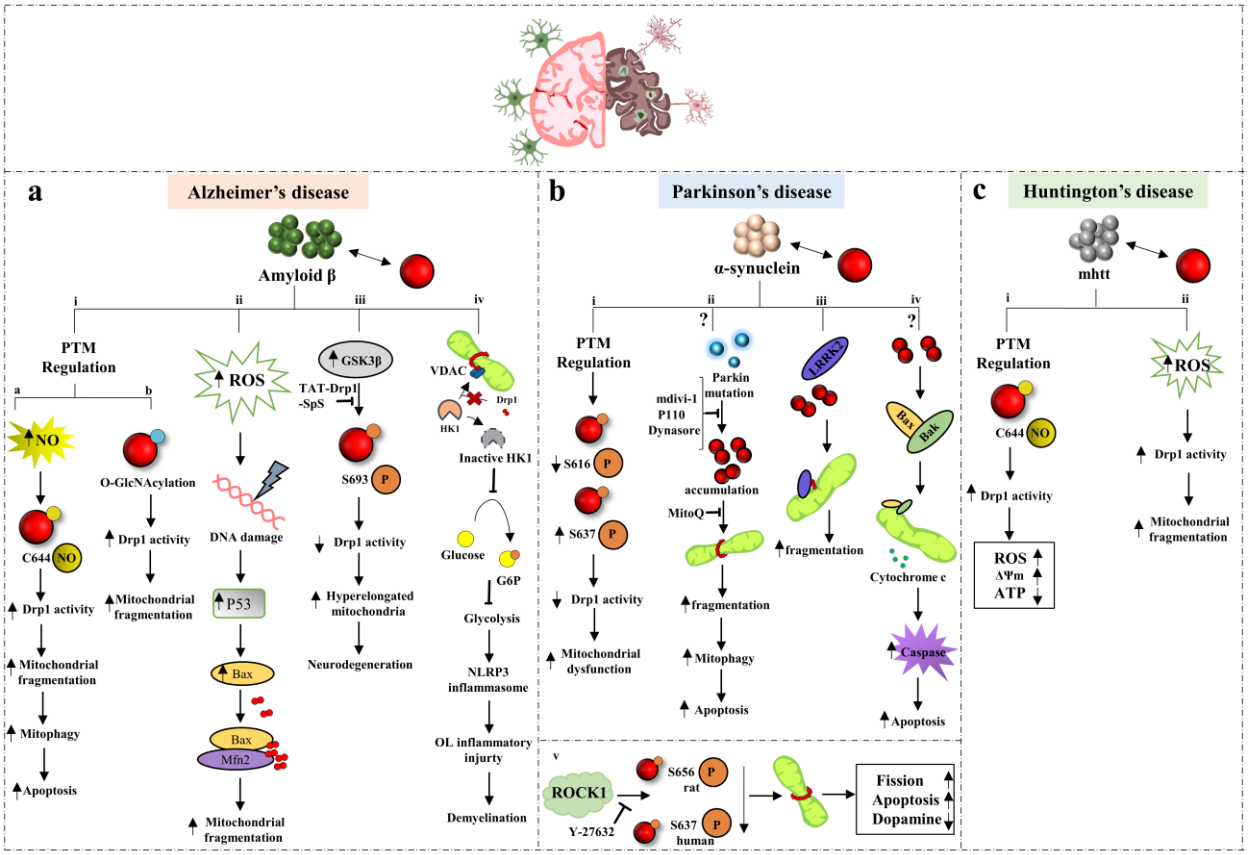

Fig. 1.6 Role of DRP1 in various neurodegenerative conditions.

a Alzheimer's disease is characterized by the accumulation of Aβ. (i) This accumulation leads to enhanced mitochondrial fission via regulating PTM dependent activity of DRP1 (red circles). Increased DRP1 activity due to either (**a**) S-nitrosylation of DRP1C644 residue or (**b**) O-GlcNAcylation leads to fragmentation of mitochondria and triggers mitophagy and apoptosis [147, 156]. (ii) DNA damage due to increased intracellular ROS is responsible for the induction of tumour suppressor P53 which subsequently mobilizes Bax, a pro-apoptotic factor. Interaction of Bax along with MFN2 and DRP1 promotes increased mitochondrial fission and subsequent neuronal injury [157]. (iii) Aβ mediated activation of serine/threonine protein kinase GSK3β results in DRP1S693 phosphorylation. This inhibits DRP1 activity resulting in hyperelongated mitochondria in AD neurons. Synthetic peptide TAT-DRP1-SPS could block GSK3β mediated DRP1 phosphorylation [145, 158]. (iv) Aβ mediated hyperactivation of DRP1 inhibits the interaction between VDAC and HK1 on OMM. Further inactive HK1 results in suppression of glycolysis and causes glycolytic stress. Destabilized VDAC causes oxidative stress due to the release of mitochondrial content into the cytosol. Stress-induced activation of NLRP3 mediated inflammasome results in inflammatory injury and white matter loss in mature oligodendrocytes [159]. **b** Accumulation of α-synuclein is a hallmark feature of Parkinson's disease: (i) α-synuclein interacts with DRP1 and regulates the PTMs. Decreased DRP1S616 phosphorylation and increased DRP1S637 phosphorylation that results in reduced DRP1 activity and mitochondrial dysfunction are reported [160]. (ii) Mutant Parkin results in DRP1 accumulation due to its inability to ubiquitinate DRP1, a prerequisite for proteasomal degradation. This leads to increased mitochondrial fission and fragmentation that further results in enhanced apoptosis mediated neuronal cell death. The detrimental effect of increased mitochondrial fission could be suppressed by inhibitors such as mdivi-1, P110, and dynasore which reduces DRP1 accumulation and MitoQ that inhibits DRP1 oligomer formation on OMM [161-165]. (iii) Direct interaction between LRRK2 and Drp1 increases DRP1 recruitment to OMM and leads to excessive mitochondrial fragmentation [166]. (iv) Accumulation of DRP1 leads to Bax/Bak activation resulting in the release of cytochrome c from mitochondria. This is followed by a series of caspase activation and subsequent neuronal cell death [167]. (v) ROCK1 dephosphorylates DRP1 (S637) that increases mitochondrial translocation of DRP1 resulting in fission, apoptosis of dopaminergic cells and loss of dopamine. Y-27632, an inhibitor that blocks ROCK1 activation, could significantly alter this process [168]. **c** mhtt accumulation is an important characteristic of Huntington's disease. This accumulation of mhtt resulted in increased DRP1 GTPase activity. (i) NO-mediated DRP1 S-nitrosylation at DRP1C644 or (ii) increased oxidative stress lead to increased activity of DRP1 [169, 170]. Increased activity of DRP1 results in fragmentation of mitochondria, increased Ψm, and decreased ATP production and neuronal damage.

BOX: 2

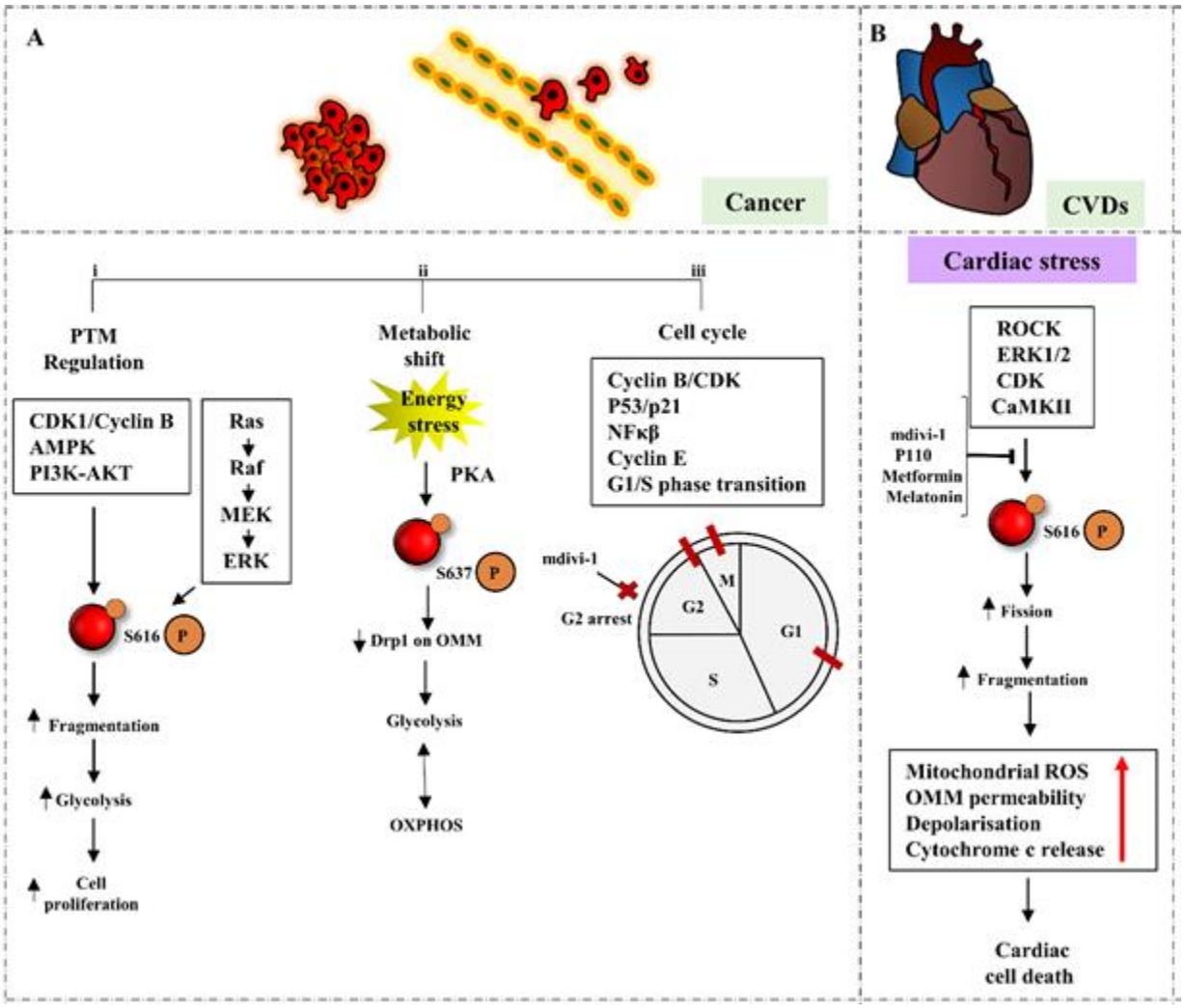

Fig. 1.7 Role of DRP1 in cellular pathways leading to cancer and cardiovascular diseases. A. Altered PTMs of DRP1 in various cancer types have been reported. (i) Kinases such as CDK1/cyclin B, AMPK, PI3K-AKT, and signalling pathways such as Ras-MAPK and ERK1/2 activate DRP1 by phosphorylation. Activation of DRP1 results in enhanced mitochondrial fission that further results in increased glycolysis. This leads to the synthesis of essential cellular building blocks required for cell growth and tumour progression [171]. (ii) Under nutrition-deprived conditions in tumour cells, altered mitochondrial morphology that compensates for this was observed. PKA mediated DRP1S637 phosphorylation retracts DRP1 from OMM, and a role for DRP1 in the metabolic shift of cancer cells from OXPHOS to glycolysis and vice versa depending upon stress conditions is proposed [171, 172]. (iii) Phosphorylation of DRP1 by cyclin B/CDK results in enhanced mitochondrial fission and activates different signalling pathways (P53/P21, NFκβ) responsible for G1 to S progression [54, 173]. Cyclin E and DRP1 association controls cell proliferation in a cell density–dependent manner [174]. Treatment with the DRP1 inhibitor mdivi-1 rescued most of the cells in the G2 phase highlighting a positive correlation between enhanced DRP1 activation and cell cycle progression [175]. **B.** Various kinases (ROCK, ERK 1/2, CDK, CamKII) phosphorylate and activate DRP1 under cardiac stress [140, 176]. A subsequent increase in mitochondrial fission and fragmentation results in increased mitochondrial ROS, OMM permeability, membrane depolarization, and cytochrome c release leading to cardiac cell death. Drugs targeting DRP1 such as mdivi-1, metformin, melatonin, and P110 can be used to block CVD progression [140, 177, 178].

1.7.1 GTPase domain

The GTPase domain of DRP1 is involved in the binding and hydrolysis of GTP and in the formation of a higher-order structure on OMM. Assembly is predominantly regulated by 80-loop, a region of 16 aa stretch that extends from the globular GTPase domain. 80-loop mediates tethering between the intermolecular GTPase domains, and mutations in this region inhibit dimer formation [72]. The GTPase domain in isoforms 6, 8, and 9 contains a 13 aa insertion called A-insert. The presence of A-insert was reported to reduce the GTPase activity of the protein [179]. Yoon and colleagues reported two compound heterozygous nonsense mutations in the coding region of the GTPase domain of *DRP1*, resulting in p.W88M (OMIM: 603850.0004) and p.D129K (OMIM: 603850.0005) that inhibited the protein activity. Patients with these mutations showed hypotonia, absent respiratory effort, and giant mitochondria in neurons [180]. Myelination of the sural nerve and reduced axon numbers were also reported in these patients [180]. Another heterozygous mutation p.S36G (OMIM: 603850.0007) in the GTPase domain, was detected in a patient with psychomotor delay [181]. Immunofluorescence staining of DRP1 in the patient fibroblast revealed localization of the protein to the cytosol. This resulted in a block in fission and the formation of elongated mitochondria in patient fibroblasts [181]. A role for S36 residue in binding GTP/GDP through the side-chain hydroxyl group has been proposed [181, 182]. In the disease condition, this interaction is lost; hence, the protein cannot bind to GTP/GDP. The yeast orthologous variant of this mutation was identified to be hypomorphic recessive, and cells expressing the mutation exhibited decreased oxygen consumption rate (OCR) and growth [181].

Gerber and colleagues reported two cases of heterozygous dominant optic atrophy due to the degeneration of retinal ganglion cells [183]. In most cases, a mutation in *OPA1* that encodes another large GTPase required for mitochondrial fusion is the cause of the disease condition [184]. However, sequencing analysis revealed that the patients had dominantly inherited

missense mutations in two highly conserved aa E2A (OMIM: 603850.0009) and A192E (OMIM: 603850.0010) in the GTPase domain of DRP1 [183]. Immunofluorescence studies showed reduced localization of DRP1 to mitochondria in patient fibroblasts [183]. Additional analysis revealed hyperfilamentous mitochondria in the patient's fibroblast, indicating severe fission defect, although mitochondrial respiration remained unaltered [183]. Retinal ganglion cells from a mouse model with a knockout in the *DRP1* allele were analyzed for further insight into the pathological mechanism. TEM images of the retina and optic nerve showed a significant increase in mitochondrial length in these cells [183].

An infant was presented with a history of profound hypotonia, developmental delay, and abnormal movement. A homozygous mutation at p.T115M in the GTPase domain was identified by panel sequencing [185]. This particular mutant variant increased the monomeric form of DRP1 up to three-fold and reduced the formation of the functional oligomers of the protein in the patient fibroblast [185]. Phenotypes such as elongated mitochondria with notably fewer branch points and lack of uniform size and distribution were observed by microscopic analysis [185]. Balanced mitochondrial fusion and fission are also required to maintain mtDNA content. mtDNA was significantly (60%) reduced in the patient cells. Additionally, loss of OCR and decreased Ψm were also observed in the patient fibroblasts. Molecular modelling of DRP1 suggested that T115 lies at the interface where GTPase head domains interact during oligomerization. Changing this threonine to methionine introduced a significant steric hindrance between adjacent head domains that disrupted oligomer formation [185, 186].

Two *DRP1* heterozygous mutations in patients affected by severe encephalopathy were reported recently [187]. One of them, a 2-year-old infant, was detected with chronic seizure and ataxia and later developed global cerebral and cerebellar atrophy. High-throughput sequencing studies identified a heterozygous *DRP1* variant c.668G > T (p.G223V) (Another mutation found in the patient was in the middle domain and is discussed in the subsequent section). Upon

culturing patient cells in a glucose-containing medium, hyperfused mitochondria that are swollen and rod-shaped were observed [187]. In galactose-containing media, a condition that requires cells to perform oxidative phosphorylation (OXPHOS) for ATP generation, the mitochondrial network of DRP1G223V mutant was more disorganized with swollen puncta, rings, and chain-like structure [187]. OCR was reported to be decreased by 60% in yeast cells expressing the orthologous disease variant DRP1G252V. In addition to this, a significant increase (50%) of petite colonies was observed compared to WT, indicative of decreased mtDNA stability [187]. G223V mutation resulted in substituting a small and flexible glycine with a hydrophobic valine, leading to a structural change in the GTPase domain near residues 215 to 221 and hampered GTPase activity [187].

A 5-year-old patient was diagnosed with severe psychomotor developmental delay, global hypotonia, and limb ataxia due to axonal sensory neuropathy. Clinical exome sequencing revealed a *de novo* heterozygous missense mutation (p.D146N) in the DRP1 GTPase domain [188]. Confocal and electron microscopy (EM) analysis showed that mitochondria in patient fibroblasts were excessively hyperfused and formed a giant balloon-like structure compared to control cells. Expression of the mutant (D146N) in WT fibroblast also resulted in hyperfused mitochondrial network morphology, suggesting a dominant-negative characteristic of the mutation. p.D146N cells also had a markedly reduced mitochondrial turnover rate compared to WT fibroblast due to decreased autophagy. Furthermore, aberrant mitochondrial turnover increased oxidative stress due to enhanced mitochondrial ROS. These cells also showed higher levels of carbonylated proteins in the mitochondrial fraction, indicating enhanced mitochondrial ROS [188]. Whitley and colleagues identified two novel *de novo* heterozygous missense variants of DRP1, G32A in the GTPase domain, and C431Y in the middle domain [189]. Both patients demonstrated hypotonia, developmental delay, and/or regression. The individual with the G32A variant exhibited significant ocular involvement, abnormally increased lactate concentration, and

very long-chain fatty acids in the brain cells. Mitochondria in G32A patient-derived fibroblasts were dramatically hyperfused and showed a highly connected network compared to same-aged control fibroblasts. When expressed in WT HCT116 cells, DRP1G32A showed a very strong dominant-negative effect. Cells expressing the mutant variant exhibited a significant increase in hyperfused mitochondria [189]. The yeast orthologue of this mutation Dnm1G35A was equally dominant-negative. WT yeast cells expressing GFP tagged DRP1G32A depicted hyperfused mitochondria, absence of DRP1 puncta on the mitochondria, and cytosolic localization of the protein [189].

Keller and colleagues recently reported a case of a 10-year-old boy with a severe neurodevelopmental disorder characterized by profound amyotrophy, dystonia, and sensory neuropathy [190]. The condition was attributed to a heterozygous *de novo* missense variant in the GTPase domain coding region of *DRP1* (NM_012062.4: c.115 A > G), resulting in the substitution of a serine residue with glycine (p.Ser39Gly) [190]. This variant affects the evolutionarily conserved serine 39 located in the G1 motif (P-Loop) of the GTPase domain [182]. The serine 39 residue in the P-Loop plays a crucial role in GTP binding, forming one of the four hydrogen bonds that stabilize the α-phosphate to the P-Loop. This interaction facilitates a conformational change, wherein the side chain of serine 39 rotates approximately 180° upon GTP binding, thus potentially stabilizing a GTP transition state. However, despite this important finding, the exact underlying pathological mechanism of DRP1 mutations, particularly those leading to impairment of peripheral sensory nerves while sparing motor neurons, has yet to be fully elucidated. Further research is needed to gain a comprehensive understanding of these mechanisms.

Another recent study from Lhuissier and colleagues revealed a heterozygous *de novo* variant in the GTPase domain coding region of *DRP1* [NM_001278464.1: c.176C>A p.(Thr59Asn)] leading to defective mitochondrial and peroxisomal fission [191]. The adult

female patient showed a complex neurological phenotype associated with developmental delay, progressive spastic quadriplegia, dystonia, dysarthria, dysphagia, axonal neuropathy, ataxia, nystagmus, optic atrophy, epilepsy, low sensitivity to pain, scoliosis, delayed menarche, and learning difficulties. Interestingly, when the skin fibroblast from the patient carrying the DRP1 p.Thr59Asn mutation was analyzed by western blotting, a strong decrease of DRP1 protein levels was observed [191]. Additionally, *in silico* analysis indicated that the "Thr" is situated in the GTPase domain, specifically within a sequence of remarkably conserved residues of the switch I region that is crucial for ligand binding, the enzyme's catalytic activity, and its interaction with other domains, including switch II [182]. Hence, the variant Thr59Asn may have a destabilizing effect on the protein. Furthermore, as compared to control fibroblasts, which possess small and abundant peroxisomes and dynamic tubular mitochondrial network, mutated fibroblasts showed a significantly elongated decreased number of peroxisomes and a hyper-connected mitochondrial network [191].

A *de novo* mutation in the DRP1 GTPase domain was identified in a 4.5-year-old male child [192]. The child displayed symptoms of developmental delay, ataxia, and peripheral neuropathy. Whole exome sequencing analysis of the patient revealed the presence of a missense mutation in *DRP1* (c.445 G>A, p.G149R) [192]. Interestingly, Gly149 is a constituent of the conserved DxxG motif located in the switch II region of DRP1, and it helps to bind the γ-phosphate of GTP through its main chain. [182]. Therefore, it is plausible that the p.G149R mutation disrupts GTP binding or hydrolysis, consequently affecting DRP1's motor function [182]. This may lead to a dominant-negative effect due to the formation of non-functional heteromers comprising both the mutated and WT DRP1 [192].

In a recent study, Nolden and colleagues examined a case involving a patient who experienced several conditions, such as chronic ataxia, mild learning difficulties, status epilepticus, epilepsy, motor axonal neuropathy with edema and flexed right knee contracture

[193]. Comparative genomic hybridization assay detected a microduplication on chromosome 19p13.3, which is a single *de novo* heterozygous c.687_689dup, p.Leu230dup *DRP1* variant. The patient exhibited elongated mitochondrial morphology, characterized by reduced branch points. Additionally, the peroxisomes appeared more fused, with a decreased number of peroxisomes overall and a diminished size distribution. These observations collectively suggest an impaired fission process. Moreover, the patient's (p.Leu230dup) fibroblasts exhibited multiple OXPHOS defects, with decreased steady-state levels of NDUFB8, UQCRC2, and COX2. Further *in silico* analysis suggested the insertion of an additional leucine at position 231 (L230dup) within the GTPase domain. This insertion is situated in a short α-helix surrounded by two disordered loops called the G4 and G5 motifs, which are essential for nucleotide binding [182, 193]. Although not experimentally tested, the authors predict that the introduction of the extra leucine has the potential to induce conformational changes in nearby regions, including the G4 and G5 motifs and the D190-containing helix, which could impair GTPase domain dimerization and negatively impact GTPase activity by disrupting the nucleotide binding.

1.7.2 Middle domain

DRP1 middle domain forms part of the stalk along with the GED. It is an intermediate region between GTPase and VD and is required for DRP1 self-assembly and the formation of higher-order structures [122]. Waterham and colleagues first reported the effect of *DRP1* mutations on human health and diseases [194]. In this study, a newborn girl was diagnosed with lethal encephalopathy characterized by microcephaly, abnormal brain development, optic atrophy, and hypoplasia, persistent lactic acidemia, and elevated plasma concentration of long-chain fatty acids. The patient survived only for the first 37 days. Sequence analysis identified a single heterozygous mutation c.1148C > A in the coding region of the *DRP1*. This resulted in the substitution of a conserved alanine at position 395 by aspartic acid (OMIM: 603850.0001). Immunofluorescence with antiserum against peroxisomal catalase suggested that patient

fibroblast had fewer peroxisomes compared to the control. In addition to this, the mitochondria in the patient's cells were also observed to be elongated. Most of the tubular mitochondria were found around the nuclear periphery in the patient's fibroblast [194]. Overexpression of the mutant variant of DRP1 in control fibroblasts induced aberrant mitochondrial phenotype. This indicates that the A395D mutation interferes with the homo-oligomerization of DRP1 in a dominant-negative manner [194].

A *de novo* variant of DRP1 was reported in a patient who presented with refractory epilepsy and global developmental delay at the age of 6 months [195]. The whole-exome sequencing of the patient identified a missense substitution in exon 10 of *DRP1* NM_012062.4:c.1085G4A; NP_036192.2:p.(G362D; OMIM: 603850.0002). Confocal imaging of the patient's primary fibroblasts revealed the presence of hyperfused mitochondria compared to control [195]. The substitution of adjacent glycine to aspartate (G363D) resulted in DRP1 tetramerization in the cytoplasm but diminished the assembly of higher-order structures and polymerization-dependent GTPase activity [122]. The hyperfused mitochondrial phenotype observed in the patient was most likely due to the inability of DRP1 to form helical structures on OMM, leading to impaired mitochondrial fission [195]. Another de novo heterozygous, dominant mutation (c.1084G > A) in the same aa, i.e., G362S (OMIM: 603850.0003) of DRP1, was identified in a patient who exhibited chronic neurological disorder, characterized by postnatal microcephaly, developmental delay, and pain insensitivity [196]. Muscle biopsy revealed decreased respiratory chain complex IV activity, ATP production, and oxygen consumption, indicating compromised mitochondria function. Mitochondria in the patient's fibroblast were aberrant and nine times longer than control cells when visualized by fluorescence microscope and TEM [196].

Diez and colleagues reported a case of infantile parkinsonism as a result of *de novo DRP1* middle domain mutation (NM_005690,c.1337G > T; p.C446F) [197]. The patient died when he

was two and a half years old due to cardiac arrest. The patient's skin fibroblasts showed a 70% decrease in the number of mitochondria (compared to control) and were observed to be significantly elongated and fused compared to control mitochondria [197]. A significant reduction in the number of peroxisomes (50% decrease compared to the control) was also observed [197]. The impaired mitochondrial fission may further disrupt mitochondrial transport in neuronal cells, leading to loss of synapse and causing neurodegeneration [198].

A novel, *de novo*, missense heterozygous mutation in *DRP1* c.1207C > T (p.R403C; OMIM: 603850.0006) was identified in two unrelated patients who presented similar problems such as refractory epilepsy, encephalopathy, and developmental regression [199]. However, unlike the previous cases of missense mutations (A395D and G362D), where the patients suffered encephalopathy and epilepsy in the early stages of life, these patients had normal development until 4–5 years of age before the sudden onset of epilepticus and subsequent developmental regression and encephalopathy [194, 195]. This variant of DRP1 also exhibited a dominant-negative phenotype and interfered with the function of WT DRP1 [199]. The change of cationic arginine into a neutral and smaller cysteine most likely altered the oligomerization of the protein in the patient cells [199].

Zaha and colleagues reported another novel *de novo DRP1* mutation (c.1217 T > C, p.L406S) where a 6-month-old infant presented with severe hypotonia, infantile spasms with suppression-burst, and a high level of lactate in cerebrospinal fluid. The patient had delayed development and eventually died at the age of eighteen months [200]. The presence of elongated mitochondria in the patient's cells was observed using fluorescence microscopy. Similar to the mutations mentioned above, the L406S variant was also reported to be heterozygous dominant-negative and interfered with the formation of helical polymers of the protein [200].

Mutations in *DRP1* were identified in two patients characterized by poor feeding, poor growth, developmental delay, and hypotonia [201]. One of them was a 14-month-old infant and

exhibited global developmental delay, hypotonia, and status epilepticus. EM of the muscle suggested mitochondrial pleomorphism along with lipid accumulation in the muscle. The patient died at the age of 5 years due to severe status epilepticus with respiratory failure. Whole exome sequencing revealed c.1048G > A, p.G350R mutation in *DRP1* (OMIM: 603850.0005) [201]. The other patient was diagnosed with persistent lactic acidosis, and the MRI of the brain showed microcephaly and the absence of corpus callosum. The patient also had diffused hypotonia, global developmental delay, and poor growth. The patient passed away at 10 months of age due to pneumonia. Whole exome sequencing revealed two *de novo* mutations in mitochondria-related genes, one in *DRP1* (c.1135G > A, p.E379K) and the other one in *PDHA1*, linked to pyruvate dehydrogenase E1 deficiency (OMIM: *300502) [201]. Both the above *DRP1* mutations were also studied in Drosophila to understand their effect on mitochondrial morphology and structure. DRP1G350R showed a dominant-negative effect on peroxisomal and mitochondrial morphology [201]. Larvae expressing the G350R mutant variant showed aberrant mitochondrial distribution and trafficking in synapse compared to cells expressing WT DRP1. DRP1E379K showed a milder effect on aberrant mitochondrial trafficking when compared to G350R [201, 202].

A 5-year-old child was presented with an abrupt manifestation of a myoclonic status epilepticus, psychomotor deterioration and long-duration seizures [187]. High throughput sequencing studies identified a heterozygous *DRP1* variant c.1109 T > G (p.F370C). Mitochondria in the patient's fibroblast were typically hyperfused and showed swollen puncta and ring-like structures [187]. F370C variant replaces the large hydrophobic phenylalanine that plays an important role in monomer stability and tetramer formation. Several hydrophobic interactions that involve F370 are disrupted due to the incorporation of cysteine. This further resulted in the formation of disulfide bonds with nearby cysteines and influenced the oligomerization of the protein. A significant increase in the protein level was observed in patient fibroblasts, most likely due to increased stability and altered degradation [187].

A novel and lethal *de novo* heterozygous missense variant C431Y was reported in a patient by Whitney and colleagues [189]. The patient had hypotonia, developmental delay, regression, and seizures. An abnormal brain MRI was reported, and the patient eventually died at the age of 10 months. However, when mitochondrial morphology was investigated in HCT116 cells and yeast that express the mutant variant, no robust dominant-negative activity was observed [189]. Structural analysis suggested that, as the mutation is situated in an assembly interface, the substitution of tyrosine in this region could damage the integrity of the interface, thereby affecting assembly [189].

An 8-month-old girl presented with an autosomal dominant, spontaneous DRP1 c. 1228G>A (p. E410K) mutation. The symptoms included septo-optic dysplasia, hypotonia, developmental delay, elevated blood lactate, and severe mitochondrial cardiomyopathy. The condition progressed to non-ischemic congestive heart failure and cardiogenic shock, ultimately leading to the unfortunate demise of the patient [203]. Earlier research has demonstrated that the location of p. E410 within the DNM1L protein domain is crucial for its tetramerization [122]. In the case of this patient, the DRP1 c. 1228G>A (p. E410K) mutation could potentially hinder cardiac differentiation by impeding protein tetramerization. This, in turn, might lead to inadequate energy supply and the consequent development of ineffective cardiomyocytes, ultimately resulting in cardiomyopathy [203].

Two heterozygous DNM1L variants, c.1085G>A (p.Gly362Asp) and c.1535T>C (p.Ile512Thr) were identified in the same patient [187]. The patient exhibited psychomotor delay, partial motor status epilepticus, refractory epilepsy and psychomotor regression, spastic tetraparesis, lack of postural control, hyperkinesis, and severe cognitive impairment. Sanger sequencing revealed that the c.1535T>C (p.Ile512Thr) was inherited from the mother while the c.1085G>A (p.Gly362Asp) represents a *de novo* event. To assess the pathogenic role of the DRP1 G362D and I512T variant *Saccharomyces cerevisiae dnm1* strains were used for

complementation studies. The amino acid residues corresponding to p.Gly362Asp and p.Ile512Thr variants are conserved between the two species (p.Gly397 and p.Ile543 in yeast, respectively). Multiple experiments, such as growth analysis on media supplemented with different carbon sources (glucose, glycerol, and ethanol), OCR, and petite frequency measurement, were conducted to evaluate the impact of the mutants on mitochondrial function. These experiments collectively indicated that the alteration at p.Ile512Thr may serve as a modifier, exacerbating the phenotype linked to the p.Gly362Asp mutation [187].

1.7.3 GTPase Effector Domain

GED is also known as the C-terminal assembly domain. It is critical for the formation of higher-order complexes. It also acts as a cooperative stimulator for the GTPase activity by interacting with the GTPase domain [204]. Mutations in the GED disrupt its intramolecular interaction with the GTPase domain, leading to decreased GTPase activity of DRP1 [204].

A 27-year-old patient was presented with static encephalopathy, a history of seizures, and nystagmus. A novel heterozygous variant in the GED of DRP1 Y691C was identified in the patient cells. Overexpression of the Y691C variant resulted in a dramatic change in muscle mitochondrial morphology and distribution in the Drosophila model. Perinuclear distribution of the mitochondrial network and scarcity of mitochondria in the muscle fibers were also reported [205].

Recently, Nolden and colleagues reported a second case of a novel, *de novo* heterozygous DRP1 mutation in the GED (c.2128A>G, p. R710G) [193]. The affected patient, a 17-year-old, passed away due to a combination of chronic inflammatory demyelinating polyneuropathy, extra-pyramidal movement disorder, epilepsy, optic atrophy, fatigue, and episodes of developmental regression triggered by infections. Upon investigation, the patient's fibroblast exhibited hyperfused mitochondria when examined using a high-resolution confocal microscope. The mutant DRP1 was predominantly found in the cytosol and showed decreased recruitment to

mitochondria. Interestingly, the expression of DRP1 R710G in the patient's fibroblast was significantly lower compared to the control, suggesting a possible dominant-negative effect of the mutated protein, overriding the function of the wild-type allele. Furthermore, the mutant showed diminished GTPase activity *in vitro* compared to the control. *In silico* analyses indicated that residue R710G, situated around the BSE region of GED, forms a salt bridge with E702. The substitution of R710G most likely resulted in the loss of this salt bridge. Moreover, the authors proposed that R710G is assembly-deficient compared to the WT variant and exists in a dynamic equilibrium between the dimeric and tetrameric states. The study suggested that the R710G variant disrupts the coupling between DRP1 assembly and assembly-stimulated GTP hydrolysis, providing valuable insights into how assembly-state information is translated to the GTPase domain [193].

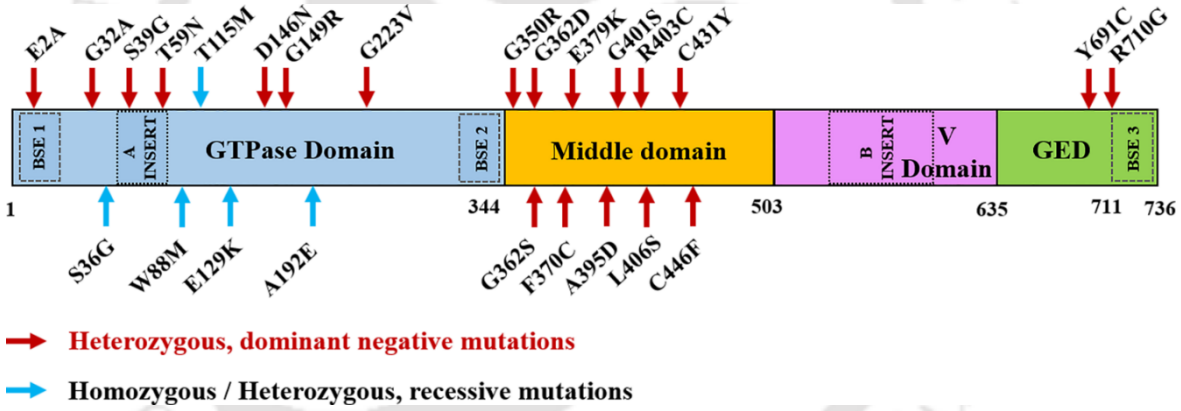

Fig. 1.8 Schematic representing the position of various DRP1 mutations associated with disease conditions. Arrows determine the position of each mutation in the encoded DRP1 protein.

Table 1.3 DRP1 mutations and associated phenotypes discussed in this chapter

Domain	Mutation	Type	Drp1 structure and function	Pathology	Pathophysiology	Reference
GTPase	E2A, A192E	Missense, dominant-negative	Loss of DRP1 activity	Dominant optic atrophy	Cytoplasmic DRP1 aggregates, elongated mitochondria	[183]
	D146N	Missense, heterozygous, dominant-negative	Loss of DRP1 GTPase function	Psychomotor developmental delay, global hypotonia, limb ataxia	Giant balloon-like mitochondria and elongated peroxisomes	[188]

	S36G	Missense, recessive, heterozygous	Loss of DRP1 GTPase function	Psychomotor delay, ocular and cerebellar involvement	Elongated mitochondria and aberrant peroxisomes	[181]
	T115M	Homozygous	Impairs oligomer formation	Developmental delay, neurological impairment	Elongated mitochondria, reduced mtDNA and OCR	[185]
	W88M, E129K	Nonsense, heterozygous	Loss of DRP1 GTPase activity	Hypotonia	Giant mitochondria	[180]
	G32A	Missense, heterozygous dominant-negative	Lack of formation of higher-order structure	Hypotonia, developmental delay, optic atrophy, ocular involvement	Hyperfused mitochondria	[189]
	G223V	Missense, heterozygous	No GTP binding	Seizure, epileptic encephalopathy	Hyperfused, swollen, mitochondria	[187]
	S39G	Missense, heterozygous	GTP hydrolysis completely abolished	severe neurodevelopmental disorder with severe amyotrophy, dystonia, and sensory neuropathy	–	[190]
	T59N	Heterozygous	Decreased level of DRP1 due to probable degradation	Axonal sensory neuropathy, spasticity, optic atrophy, ataxia, dysarthria, dysphasia	Block in mitochondrial and peroxisomal fission.	[191]
	G149R	Missense, heterozygous, dominant-negative	Likely to interfere with GTP binding/ hydrolysis	Developmental delay, ataxia, peripheral neuropathy	–	[192]
	L230dup	Heterozygous, dominant-negative	May impair GTPase domain dimerization	Chronic ataxia, Left sided chorea. Seizures, status post epilepticus and epilepsy, Motor axonal neuropathy	_	[193]
Middle	A395D	Heterozygous, dominant-negative	Defect in oligomer formation	Microcephaly, abnormal brain development, optic atrophy and hypoplasia	Fission defect of mitochondria and peroxisomes	[194]
	G362D	Missense, dominant-negative	Block in helical polymer formation	Developmental delay, refractory epilepsy	Hyperfused mitochondrial network	[195]
	C446F	Missense, heterozygous	–	Severe infantile parkinsonism	Elongated mitochondria	[197]

		dominant-negative			and peroxisomes	
	R403C	Missense, dominant-negative	Reduces DRP1 oligomer formation	Epileptic encephalopathy	Hyperfused mitochondria (mouse)	[199]
	L406S	Missense, dominant-negative	Block in helical polymer formation	Hypotonia, infantile spasms, delayed development	Neuronal necrosis, fission defect of mitochondria and peroxisomes	[200]
	C431Y	Missense, heterozygous dominant-negative	–	Hypotonia, developmental delay	–	[189]
	G362S	Heterozygous, dominant-negative	–	Postnatal microcephaly, developmental delay, pain insensitivity	Complex IV inactivity, impaired mitochondrial fission defect	[196]
	G350R, E379K	Missense	–	Infantile encephalopathy	Lactic acidosis, developmental delay, hypotonia	[201]
	F370C	Missense, heterozygous	Abnormal multimer formation	Myoclonic status epilepticus	Increased DRP1 level, hyperfused, swollen, mitochondria	[187]
	E410K	Autosomal dominant	–	Septo-optic dysplasia, hypotonia, developmental delay, elevated blood lactate, and severe mitochondrial cardiomyopathy	–	[203]
Middle & VD	I512T, G362D	Compound heterozygous, recessive	–	Psychomotor delay, Epileptic encephalopathy	Abnormally elongated mitochondria and aberrant peroxisomes	[187]
GED	Y691C	Missense, heterozygous	Proposed to disrupt GED-GTPase interactions	Static encephalopathy, nystagmus, hypotonia, epilepsy	–	[205]
	R710G	Heterozygous	Decreased level of DRP1, loss of GED-GTPase interactions, and impair assembly driven GTP hydrolysis	Chronic inflammatory demyelinating polyneuropathy, extra-pyramidal movement disorder, epilepsy, optic atrophy, fatigue	–	[193]

1.8 *S. cerevisiae* as a model organism to study mitochondrial dynamics and associated diseases

For several decades, *S. cerevisiae* has been a valuable tool for understanding basic cellular mechanisms that contribute to human physiology. In recent years, yeast has gained substantial attention as a tool for exploring the genetic and molecular foundations of human diseases. This is because of the high degree of homology between yeast and human genes and highly conserved cellular activities and metabolic pathways in all eukaryotes. Due to these reasons, *S. cerevisiae* has been popularly called an "honorary mammal" [206]. *S. cerevisiae* was the maiden eukaryotic organism to have its entire genome sequenced and published [207]. Interestingly, approximately 46% of known human proteins exhibit orthologs in yeast. This includes crucial proteins involved in DNA replication, recombination, transcription, translation, cellular trafficking, and mitochondrial biogenesis [208]. Additionally, around 40% of human genes responsible for disease-causing mutations possess orthologs in yeast [209]. Due to this, yeast has been extensively used to understand the molecular processes that underlie many diseases. Additionally, yeast is a valuable model organism for studying mitochondrial functions and dysfunctions because mitochondrial genetics and recombination were first discovered in yeast [210]. *S. cerevisiae* was chosen for mitochondrial studies for specific reasons: its metabolic regulation according to carbon and oxygen availability, metabolic shifts from glucose-induced glycolysis to respiration upon glucose depletion, and utilization of non-fermentable carbon sources like glycerol and ethanol requiring functional mitochondria. Yeast, a facultative anaerobe, can survive without mitochondrial function and mtDNA as long as fermentable carbon is present. Yeast mutants impaired in OXPHOS are respiratory deficient and form petite colonies on non-fermentable sources due to ethanol accumulation. This petite-positive feature facilitates studying mitochondrial mutations without lethality. Conserved mitochondrial genes/functions between yeast and humans enable modelling mitochondria-related pathologies, often

characterized by impaired oxidative growth, reduced respiratory activity, and rearranged cytochromes [210, 211]. Yeast can be used to study human diseases in two important ways. First, if the disease-associated gene has an ortholog in yeast, the disease-causing mutation can be introduced into the yeast gene and its effects can be studied. Furthermore, this organism's capability to exist as haploid or diploid offers flexibility in determining the dominant or recessive property of the mutation. Conversely, if the disease-related gene lacks a counterpart in yeast, the transgene can be expressed in yeast to create a "humanized yeast" strain for functional analysis [212, 213]. Moreover, several mitochondrial diseases are caused by defects in mtDNA, and the ability to introduce mutations into mtDNA in yeast allows researchers to study the effects of these mutations in a living organism. Lastly, yeast can serve to identify compounds capable of mitigating the phenotypic abnormalities triggered by mutations. This involves introducing the defective human protein into yeast and subsequently exposing the yeast to various compounds. Those compounds, which alleviate the phenotypic irregularities, can then be subjected to deeper investigation for their potential in human disease treatment.

1.9 Perspectives on future work

Mitochondria are essential organelles vital for optimal cellular function. Malfunctions in the fission machinery leading to alterations in mitochondrial dynamics are implicated in various potentially life-threatening disorders. Extensive research over the past few decades has tremendously improved our knowledge about the mechanisms of mitochondrial division, its regulation, and its relevance to cellular health. Yeast has proven to be a useful model for these studies since the initial discovery of Dnm1, the master regulator of mitochondrial fission [86, 103]. Further research into Dnm1's structure, function, and interacting partners has paved the way for a better understanding of its mechanism of action. However, several crucial aspects of mitochondrial fission involving Dnm1 are still not vividly understood. Some of these aspects are listed below.

- How is the formation of various oligomeric forms of *S. cerevisiae* Dnm1 regulated?
- How are these different oligomeric forms related to the dynamic spatio-temporal localization of the protein?
- Is the function and formation of higher-order structures regulated by PTMs?
- Can *S. cerevisiae* Dnm1 be used as a model and decipher the mechanisms of DRP1-associated disease mutations?

Addressing these questions can provide deeper insights into the molecular basis of mitochondrial fission, its regulation, and its relevance to human health and disease. Harnessing yeast as a model organism for studying mitochondrial dynamics and diseases can also be advantageous due to the ease of performing high-throughput screens to enable the discovery of potential therapeutic compounds for human diseases.

1.10 Motivation of the research work

Dnm1 is a multidomain protein. The role of these domains in the structural regulation of the protein, thereby influencing its function, are well reported. Several studies in various model organisms have identified important residues in the protein essential for maintaining the structure. DRP1, the human homolog of Dnm1, is known to be regulated via various PTMs. However, such a regulation in the case of yeast Dnm1 is not reported. Global proteome studies have identified various residues in Dnm1 that can undergo phosphorylation [214-219]. However, detailed studies of these putative sites on the structure, function and localization of the protein are not performed. Furthermore, several studies have reported that random mutations in different domains of DRP1 contribute to the pathophysiology of several debilitating disease conditions [188, 193-195, 197, 199, 220]. Several of those reported mutations are found in the middle domain of the protein that forms part of the stalk along with GED and is required for self-assembly and higher-order structure formation [194, 195, 197, 199]. Although certain mutations have been investigated regarding their influence on organelle morphology, their effects on protein localization, distribution, function, and structure have yet to be explored.

In this study, we aimed to study these two important aspects using *S. cerevisiae* Dnm1 and set out to investigate if and how certain residues (that undergo modifications or are mutated in disease conditions) affect protein's conformation, localization and function. Our study will shed light, contribute to the understanding of the structure of the protein in more detail, and associate the structural changes with the function of the protein.

1.11 Objectives of the thesis

Based on the available literature and the potential for future research in understanding the role of Dnm1 in mitochondrial dynamics, the following objectives were formulated.

- Cloning, expression and characterization of Dnm1 fusion proteins
- To analyze the role of PTMs in the function of Dnm1
- To mimic and characterize the disease-causing DRP1 mutations in yeast Dnm1

1.12 Organization of the Ph.D thesis

Chapter 1 provides an overview of mitochondrial dynamics and its regulation. The importance of mitochondrial fission is highlighted, and the role of dynamin-related protein 1, Dnm1/DRP1 in *S. cerevisiae* and humans is discussed in detail. The differences between these two proteins in structure, interacting partners, and regulation via PTMs are also highlighted. Pathological conditions resulting from an imbalance in fusion and fission, especially the severe phenotypes caused by mutations in DRP1, are enlisted. The chapter concludes by explaining the aim of the thesis, which, in a nutshell, is to understand how the function of Dnm1 is regulated in a cell and the contribution of various domains of the protein to this. In this study, yeast Dnm1 was also used to mimic disease-causing mutations of DRP1 to understand structural and functional alterations in detail.

Chapter 2 provides a description of the materials and methods used to conduct the experiments. The experimental methods are described in detail and the details of materials used, such as the manufacturers of the chemicals and components, are listed.

Chapter 3 describes the construction of fusion proteins of Dnm1. Both the C-terminal GFP and C-terminal His-HA fusion proteins were further characterized for functionality by complementation in *dnm1* cells. Using Dnm1-GFP, mitochondrial morphology, protein localization, and dynamics have been studied. Dnm1-His-HA was used for protein expression,

purification, identification by mass spectrometry and structural analysis by circular dichroism spectroscopy. The results confirmed the functionality of the fusion proteins and their suitability for further work.

Chapter 4 investigates putative phosphorylation sites of Dnm1 identified in earlier studies. Two specific residues, T62 and S277 in the GTPase domain of the protein were analyzed for the structure, function, and localization of the protein. The selected residues were mutated to either alanine (A) or aspartic acid (D) to mimic phosphorylated and non-phosphorylated conditions of the protein. Our results demonstrate that both residues are crucial for protein function, although mutant variants showed differences in protein localization and dynamics. Interestingly, the mutant variants retained their secondary structure and were able to form higher-order structures but were non-functional both *in vivo* and *in vitro*. We went ahead and obtained insights into the local structural alteration in these variants using molecular dynamics simulations.

In ***Chapter 5***, four disease-causing mutations reported in the middle domain of human DRP1 were mimicked in yeast Dnm1 and characterized using a comprehensive approach that includes fluorescence microscopy, live cell imaging, biochemistry and MD simulations. Interestingly, out of the four mutations studied, one mutation mimicked the exact loss of function phenotype as observed in patients (A430D). One mutation resulted in partial loss of function (G397D). The remaining two mutations did not show any effect when introduced in yeast Dnm1 (R438C and C481F).

Chapter 6 is the conclusion and future perspective that summarizes and highlights the significant findings from the work carried out. This chapter also emphasizes the future direction of research to elucidate the mechanism by which Dnm1 governs mitochondrial dynamics.

Chapter 2

Materials & Methods

2. 1 MATERIALS

2.1.1 Strains and plasmids

The *S. cerevisiae* strains utilized in this study are listed in Table 2.1. The deletion strains used in this study were acquired from the gene deletion library (Dharmacon) and their authenticity was verified through polymerase chain reaction (PCR). Table 2.2 gives a list of plasmids used in this study.

2.1.2 Primers

The primers used in the study are listed in Table 2.3. Primers used for cloning and site-directed mutagenesis (SDM) were constructed using the clone manager 9 software.

2.1.3 Culture media

For this study, the molecular biology-grade components of bacterial and yeast culture media were procured from HiMedia (HiMedia Laboratories Pvt. Ltd., India) or SRL (Sisco Research Laboratories Pvt. Ltd., India). The growth media for cell culture were sterilized by autoclaving at 121 °C and 15 psi for 20 min, while heat-sensitive elements such as antibiotics were sterilized through filtration using a 0.22 µ membrane filter. The composition of different media used in the study are given below.

2.1.3.1 Bacterial media

Luria Bertani (LB)

5 g/L Yeast extract, 10 g/L Tryptone and 10 g/L NaCl.

For the preparation of LB agar plates, 20 g/L agar was added to the media before autoclaving. If required, the media was supplemented with ampicillin at a concentration of 100 µg/mL. A stock solution of ampicillin at a concentration of 100 mg/mL was prepared in sterile distilled water, filter sterilized, and stored at -20 °C. The antibiotic was added to the autoclaved LB agar media, which was moderately warm, just before pouring it into the plates.

2.1.3.2 Yeast media

Yeast extract-Peptone-Dextrose (YPD) media

1% Yeast extract, 1% Peptone and 1% Glucose

To prepare YPD agar plates, the media was supplemented with 2% agar as mentioned above.

Minimal media (YND)

0.17% yeast nitrogen base (YNB) without amino acids and ammonium sulphate supplemented with 2% glucose and 0.5% ammonium sulphate as nitrogen source. pH was adjusted to 6.0 using KOH (Erdmann et al. 1989). When necessary, the media was supplemented with leucine (3 mg/mL), lysine (10 mg/mL), histidine (10 mg/mL), and uracil (3 mg/mL). To facilitate growth on plates, 2% agar was added to the media.

Minimal media (YNG)

YNG media is composed of 0.17% YNB without amino acids and ammonium sulfate, 2% glycerol and 0.5% ammonium sulfate as a nitrogen source. The pH of the media was adjusted to 6.0 using KOH (Erdmann et al.1989). When necessary, the media was supplemented with leucine (3 mg/mL), lysine (10 mg/mL), histidine (10 mg/mL), and uracil (3 mg/mL). To enable growth on plates, 2% agar was added to the media.

Raffinose-containing media (YNR)

0.17% YNB without amino acids and ammonium sulphate, 0.5% ammonium sulphate, 2% raffinose, isoleucine (30 mg/L), valine (150 mg/L), arginine (20 mg/L), histidine (20 mg/L), leucine (30 mg/L), methionine (20 mg/L), phenylalanine (50 mg/L), tryptophan (20 mg/L) and tyrosine (30 mg/L). pH of the media was adjusted to 6.0 using KOH.

Galactose-containing media (YPGal)

Yeast-extract and peptone (YP) supplemented with 6% galactose.

2.1.4 Buffers and solutions

2.1.4.1 Buffers for protein extraction

Lysis buffer

50 mM Tris-HCl (pH 7.5), 200 mM Nacl, 10 mM imidazole, 0.1% Triton X-100, 20% glycerol (v/v), 1 mM PMSF, 1X protease inhibitor cocktail without EDTA and 1X phosphatase inhibitor cocktail. The protease and phosphatase inhibitor cocktail was added just before using the buffer.

TCA buffer

50% (w/v) Tri-chloro acetic acid

Ice-cold 80% (v/v) acetone

1% (w/v) SDS in 0.1 N NaOH

2.1.4.2 Buffers for protein purification

Equilibration buffer

50 mM Tris-HCl (pH 7.5), 200 mM NaCl, 30 mM imidazole, 0.1% Triton X-100 and 20% glycerol.

Wash buffer

50 mM Tris-HCl (pH 7.5), 200 mM NaCl and imidazole at varying concentrations of 60 mM, 80 mM and 100 mM.

Elution buffer

50 mM Tris-HCl (pH 7.5), 200 mM NaCl and 500 mM imidazole.

2.1.4.3 Buffers and solutions for SDS-PAGE (sodium dodecyl sulphate-polyacrylamide gel electrophoresis)

30% Acrylamide solution

29 g acrylamide, 1 g bis-acrylamide dissolved in 100 mL water

10% Sodium Dodecyl Sulphate (SDS)

10 g SDS dissolved in 100 mL water

Resolving gel mix (10%, 10 mL)

4 mL Tris-Cl (1M, pH 8.8), 1 mL SDS (1%), 3.3 mL acrylamide: bis-acrylamide (29:1), 1.7 mL

H_2O, 100 µl ammonium persulphate (APS) (10%), 10 µl TEMED.

Stacking gel mix (4%, 5 mL)

0.6 mL Tris-Cl (1M, pH 6.8), 0.5 mL SDS (1%), 0.7 mL acrylamide: bis-acrylamide (29:1), 3.2 mL H_2O, 50 µl ammonium persulphate (APS) (10%), 5 µl TEMED.

SDS sample buffer (SSB)

0.1 M Tris-Cl (pH 6.8), 20% Glycerol (v/v), 4% SDS (w/v), 0.0002% bromophenol blue, 10% β-mercaptoethanol. The SDS sample buffer was prepared as a 2X concentrate and used at 1X final concentration.

SDS-PAGE electrophoresis buffer

0.25 M Tris-Cl (pH 8.0), 1.92 M Glycine and 1% SDS. A 10X stock solution was prepared and used at 1X final concentration.

Gel fixing solution

40% (v/v) ethanol, 10% (v/v) glacial acetic acid and 50% water

Coomassie Brilliant Blue (CBB) staining solution

0.1% Coomassie Brilliant Blue R-250, 50% (v/v) Methanol and 10% (v/v) Glacial acetic acid

Destaining solution

40% (v/v) Methanol, 10% (v/v) Glacial acetic acid, and 50% water

2.1.4.4 Buffers for western blotting

Transfer buffer (10X stock solution)

0.25 M Tris-Cl (pH 8.0), 1.92 M Glycine and 1% SDS. A 10X stock solution was prepared and used at a final concentration of 1X containing 20% methanol.

Tris-Buffered Saline (TBS)

50 mM Tris and 150 mM NaCl, final pH was adjusted to 7.4 with HCl. TBS buffer was made as a 10X concentrate and used at a final concentration of 1X.

Wash buffer (TBS-T)

TBS (1X final concentration) with 0.1% Tween-20. The required volume was mixed with water.

Blocking buffer

TBST (1X final concentration), 5% skim milk, 0.1% Tween-20

Ponceau S staining solution

0.25% (w/v) Ponceau S, 40% (v/v) Methanol and 15% (v/v) Acetic acid

2.1.4.5 GTPase activity assay buffers

Reaction buffer (RB) (20X)

25 mM HEPES, 25 mM PIPES, pH 7.0, 100 mM $MgCl_2$, 20 mM phosphoenol pyruvate (PEP) and 150 mM KCl, prepared and stored in -80 °C as aliquots.

GTPase assay reaction mixture

For each 200 µl reaction: 10 µl 20X RB, 6 µl 20 mM NADH, 12 µl 2 M NaCl, 132 µl 25 mM HEPES, 25 mM PIPES, pH 7.0, 5 µl pyruvate kinase/lactate dehydrogenase mixture, 20 µl 10X GTP stock solution, 15 µl Dnm1 (0.1 µM).

2.1.4.6 Size exclusion chromatography (SEC) buffers

Column equilibration buffer

50 mM Tris-Cl pH 7.5, 200 mM NaCl, and 5% glycerol

2.1.4.7 Native polyacrylamide gel electrophoresis (Native PAGE) buffers (8%, 10 mL)

2.5 mL Tris-Cl (1.5 M, pH 8.8), 2 mL 40% acrylamide: bis-acrylamide, 5.5 mL deionized H_2O, 100 µl APS (10%), 10 µl TEMED.

2.1.4.8 Phos-tag gel electrophoresis buffers

1.5 M Tris-Cl (pH 8.8), 1% (w/v) SDS, 30% (w/v) acrylamide: bis-acrylamide, 5 mM Phos-tag™ solution, 10 mM $MnCl_2$ solution.

2.1.4.9 Other buffers

SHP buffer (1X)

0.6 M Sorbitol, 20 mM HEPES-KOH pH, 7.4, 1 mM PMSF

Phosphate buffer (20 mM, pH 7.5)

100 mM phosphate buffer (pH 7.5) contains 16 mL 100 mM of NaH_2PO_4 and 84 mL 100 mM of Na_2HPO_4.

Phosphate-Buffered Saline (PBS), pH 7.4

137 mM NaCl, 2.7 mM KCl, 10 mM Na_2HPO_4, 2 mM KH_2PO_4. PBS buffer was made as a 10X concentrate and used at a final concentration of 1X.

Tris-acetic acid EDTA (TAE) buffer

40 mM Tris base, 0.5 M EDTA. Final pH was adjusted to 8 with glacial acetic acid. TAE buffer was prepared as a 10X concentrate and used at a final concentration of 1X.

Yeast transformation buffer

1 M Lithium acetate (LiOAc), 50% Polyethylene glycol (PEG), 100 mM Tris-Cl pH 7.5 and 10 mM EDTA.

2. 2 METHODS

2.2.1 Microbiological techniques

2.2.1.1 Bacterial growth and storage conditions

Escherichia coli DH5α cells were used for cloning purposes. The cells were cultured at 37 °C in LB medium with the addition of ampicillin (100 µg/mL) when required. The strains were preserved as stocks in glycerol (850 µl cell culture and 150 µl 87% glycerol) and stored at -80 °C. To revive the cells from glycerol stocks, they were streaked onto agar plates containing the appropriate antibiotic marker.

To isolate plasmids, bacterial cells that contain a selection marker, such as ampicillin, were grown overnight in LB medium with the appropriate antibiotic at 37 °C and 180 rpm. The overnight cultured cells were then harvested by centrifugation and subsequently used for plasmid extraction.

2.2.1.2 Bacterial transformation by calcium chloride ($CaCl_2$) method

E. coli DH5α cells were grown overnight in 5 mL LB medium at 37 °C and 180 rpm until they reached saturation. The overnight culture was then diluted to 20 mL of fresh LB medium (OD_{600} = 0.1) and allowed to grow until the OD_{600} reached 0.3-0.5. 2 mL of these cells were collected by centrifugation at 14,000 rpm for 30 sec. The resulting cell pellet was resuspended in 1 mL of ice-cold 0.1 M $CaCl_2$ and incubated on ice for 45 min. Subsequently, another round of centrifugation (14,000 rpm for 30 sec) was performed, and the cell pellet was gently resuspended in 100 µl of ice-cold 0.1 M $CaCl_2$. To introduce the plasmid DNA into the cells, the cells were mixed with the plasmid DNA and the mixture was incubated on ice for 30 min, followed by a brief heat shock at 42 °C for 105 sec. The cells were then immediately transferred back to ice for 1 min. Subsequently, 1 mL of LB medium was added to the cells and incubated at 37 °C and 180 rpm for 1 h. The cells (1%, 10%, and 89% of the total) were then plated on selective plates with ampicillin. Colonies were visible after incubation for 16-24 h at 37 °C.

2.2.1.3 Yeast strains and culture conditions

S. cerevisiae strains used in this study are derivatives of BY4742 unless mentioned otherwise and are listed in Table 2.1. The yeast strains were preserved in glycerol (600 µl cell culture and 400 µl 87% glycerol) at -80 °C. To revive the cells from glycerol stocks, they were streaked onto agar plates containing specific amino acids, nucleotide or an antibiotic marker. The wild type (WT) strain BY4742 and cells with gene deletions (*dnm1*) were streaked onto YPD plates. Whereas, the cells containing plasmids were streaked onto YND plates with suitable markers. Cells were cultured at 30 °C and at 200 rpm in selective/minimal medium (YND) (0.17% yeast nitrogen base without amino acids and ammonium sulphate, 1% glucose, and 0.5% ammonium sulphate) along with the necessary supplements. The cells grown till stationary phase were pre-cultured twice and then shifted to fresh media for further experiments. The growth of yeast cells was analyzed in the presence of different carbon sources by serial dilution on YND or YNG (glycerol) plates containing 2% agar. Plates were incubated for 2-7 days at 30 °C. The protease-deficient strain BJ2168 was used for protein expression (Table 2.1) [221].

2.2.1.4 Yeast transformation by LiOAc method

S. cerevisiae cells were transformed using the LiOAc method and recombinant clones were chosen by auxotrophy/marker selection [222]. Subsequently, when required, these cells were further transformed with pHS12-preCOX4-mCherry (presequence of cytochrome c oxidase (COX) tagged with mCherry, Addgene, plasmid 25444) for analysis of mitochondrial morphology. A loop full of freshly streaked yeast cells was suspended in 500 µl of a solution containing 40% PEG (3350) in LiOAc/TE. Subsequently, 5-6 µl of denatured herring sperm DNA and 2-3 µl of plasmid DNA or 5 µl of PCR product were added to the cell suspension. The mixture was incubated for 30 min at 30 °C with shaking. Following this, 40 µl of DMSO was added, and a heat shock was applied at 42 °C for 5 min. The cells were then collected by centrifugation at 5000 rpm for 2 min, and the resulting cell pellet was resuspended in 100 µl of

1 M sorbitol. The suspension was plated on selective plates and colonies were visible after incubation at 30 °C for 2-3 days.

2.2.1.5 Serial dilution assay/Spot assay

dnm1 cells expressing FL-Dnm1 and the mutant variants were spotted onto selective fermentable (glucose) and non-fermentable (glycerol) plates by drop serial dilution assay to study the effect on cell growth. Cells were grown initially in liquid YNG media till they reach log phase (OD_{600} = 1). Tenfold serial dilutions of log phase cultures were then plated/spotted onto either YND or YNG plates and incubated in 30 °C for 3 days and 7 days, respectively to visualize cell growth.

2.2.2 Molecular biology techniques

2.2.2.1 Yeast genomic DNA (gDNA) isolation

Yeast cells were collected from a freshly streaked plate and mixed with 30 µl of 0.2% sodium dodecyl sulfate (SDS). The mixture of cells and SDS was then vigorously mixed for 15 sec using a vortex and heated at 80 °C for 5 min. Following this, the cells were centrifuged at 13,000 g for 1 min to separate the gDNA from the cell debris. The resulting supernatant containing the gDNA was carefully separated into a new tube and stored at -20 °C.

2.2.2.2 Polymerase chain reaction (PCR) of endogenous *DNM1*

Endogenous *DNM1* was amplified for the construction of Dnm1-GFP fusion protein using specific primers (Table 2.3), Phusion DNA polymerase and 10 ng of template in a reaction volume of 50 µl. The initial denaturation step was at 95°C for 5 min before the start of the thermal cycle. Denaturation at 95 °C for 1 min, annealing temperature range of 50 °C to 62 °C for 1 min, and an extension step at 72 °C for 2.5 min. After completing 30 cycles, a final extension step was performed at 72 °C for 10 min. The amplified products were then run on an agarose gel for visualization.

2.2.2.3 Gel extraction and PCR product clean-up

The DNA from the excised gel fragments and the amplified PCR product were extracted and purified using the Macherey-Nagel (MN) Nucleospin® gel and PCR clean-up kit. All steps and protocols were executed according to the instructions provided by the manufacturer. (https://www.mn-net.com/media/pdf/02/1a/74/Instruction-NucleoSpin-Gel-and-PCR-Clean-up.pdf)

2.2.2.4 Plasmid isolation

Plasmid DNA was isolated from *E. coli* DH5α cells using the MN Nucleospin® plasmid isolation kit. The cells were first revived from glycerol stocks by streaking them on a fresh LB-agar plate containing ampicillin. A single colony from the agar plate was then inoculated in 5 mL of LB-ampicillin liquid medium and allowed to grow overnight at 37 °C and 180 rpm. The overnight culture was then centrifuged at 11,000 g for 30 sec, and the plasmid DNA was isolated according to the manufacturer's protocol. (https://www.mn-net.com/media/pdf/45/51/02/Instruction-NucleoSpin-Plasmid.pdf)

2.2.2.5 Restriction digestion and ligation

The cloning process involved digesting both the amplified product and the vector using the same set of restriction enzymes (Table 2.6). Subsequently, the digested products were purified either through a PCR purification kit or by extracting them from excised agarose gel fragments using a gel extraction kit. Following purification, the digested PCR product (insert) and the plasmids (vector) were ligated together using T4 DNA ligase. The ratio of vector to insert was determined using NEBioCalculator online tool. The ligation mixture consisting of vector, insert, ligase and reaction buffer was incubated at 16 °C for 16 h and then transformed into *E. coli* DH5α cells.

2.2.2.6 Site-directed mutagenesis (SDM)

Plasmids constructed and used in this study are listed in Table 2.2. Full length (FL) *DNM1* fused to GFP (pRBA005) was used as a template for the generation of mutant variants. To

introduce targeted mutations in *DNM1*, a two stage PCR was conducted using PfuTurbo DNA polymerase (Agilent Technologies, USA) as described by Wang and Malcom [223] (Fig. 2.1). Briefly, in stage one, two extension reactions were carried out in two tubes, one carrying the forward primer and the other containing the reverse primer (Table 2.3 and 2.4). The thermal cycler conditions were as follows: initial denaturation at 95 °C for 2 min; subsequent denaturation at 95 °C for 30 sec; primer annealing at 55 °C - 62 °C for 30 sec; and primer elongation at 68 °C for 17 min. The individual reactions were run for 9 cycles, and then they were combined (Stage 2) before amplification for an additional 19 cycles. The procedure ended with a 10 min, 72 °C terminal extension. The amplified product was then assessed using agarose gel electrophoresis, followed by *Dpn*I digestion for 1 h at 37 °C to eliminate unwanted parental DNA. *Dpn*I is a restriction enzyme that cleaves only methylated DNA at the GATC site. Since the parental DNA is methylated while the amplified product is not, *Dpn*I specifically cleaves the parental DNA, leaving the amplified product intact. The *Dpn*I-digested DNA was then externally ligated using ligase. Both the unligated and ligated products were subsequently transformed into DH5α cells. Following that, the ligated products (plasmids) containing the desired mutations were isolated from DH5α cells and were initially confirmed through digestion with unique restriction enzymes generated by specific nucleotide(s) changes in the mutant (without altering the amino acid). Confirmation was further ensured through DNA sequencing analysis. The primers and template DNA used to generate the plasmid carrying the desired mutation are specified in the Table 2.4.

A similar strategy with minor modifications was also used to introduce mutations in *DNM1* fused to His-HA in the template plasmid pRBA031. The thermal cycler conditions followed were 2 min 95 °C initial denaturation step, a 30 sec 95 °C denaturation step, a 30 sec 58 °C - 60 °C primer annealing step followed by a 22 min 68 °C primer elongation step. The resulting plasmids pRBA032, pRBA033, pRBA034 and pRBA035 harbouring mutant variants of *DNM1* were confirmed by specific restriction enzymes and sequencing analysis.

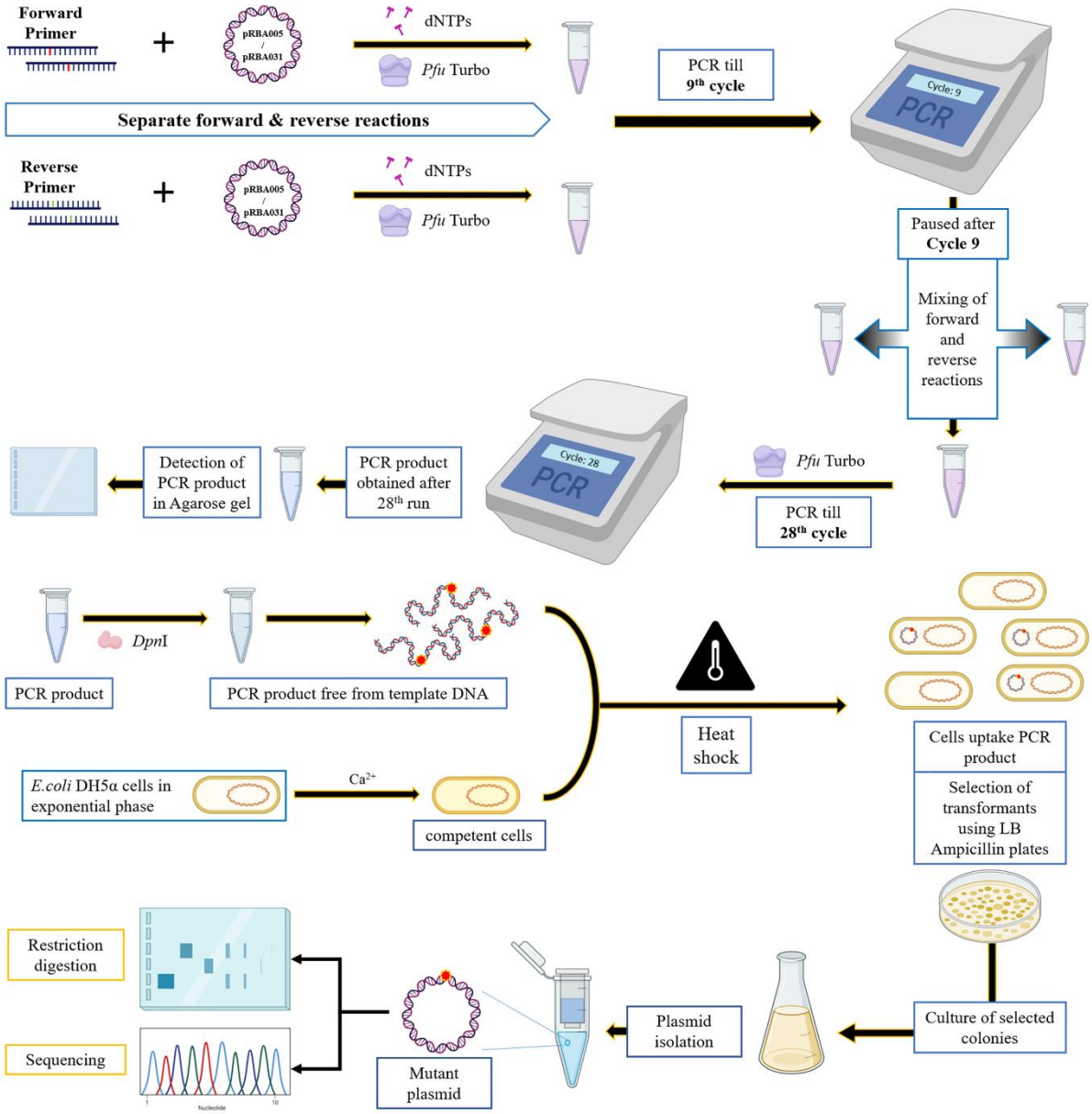

Fig. 2.1 Schematic representation of the construction of Dnm1-GFP and Dnm1-His-HA mutant variants by two-stage PCR-based SDM. In stage 1, two independent PCRs were carried out for 9 cycles with mutation-specific forward or reverse primers. The individual reactions were then combined, and PCR was continued for 28 cycles. The PCR product was detected in an agarose gel, and template DNA was removed by *Dpn*I digestion. *E. coli* DH5α competent cells were prepared using $CaCl_2$ and mutated PCR product was transformed. Positive colonies were then selected based on the antibiotic resistance and cultured to isolate mutated plasmids. Suitable restriction digestion and DNA sequencing analysis further confirmed the desired mutations. Images are created using *BioRender*.com.

2.2.3 Proteomics, biophysical and biochemical analysis

2.2.3.1 Purification of Dnm1-His-HA (Wild type, T62A/D and S277A/D)

S. cerevisiae Y258 cells expressing Dnm1-His-HA under the control of an inducible galactose promoter and BJ2168 cells expressing plasmids pRBA032, pRBA033, pRBA034,

pRBA035 that code for T62A, T62D, S277A and S277D variants respectively were grown as per the specifications of the Yeast ORF collection instruction manual (https://horizondiscovery.com/-/media/Files/Horizon/resources/Technical-manuals/yeast-orf-collection-manual.pdf) (Fig.2.2). Briefly, cells were precultured overnight at 30 °C and 200 rpm in YND medium containing the following amino acids: isoleucine (30 mg/L), valine (150 mg/L), arginine (20 mg/L), histidine (20 mg/L), leucine (30 mg/L), lysine (30 mg/L), methionine (20 mg/L), phenylalanine (50 mg/L), tryptophan (20 mg/L) and tyrosine (30 mg/L). The overnight culture was diluted to 0.1 OD_{600} in fresh medium containing 2% raffinose (YNR) and grown until it reached 1.2 OD_{600} units. Subsequently, 3x yeast extract-peptone (YP) with 6% galactose was added to the culture and cells were incubated for 8-10 h. Galactose-induced cells were harvested by centrifugation at 10000 rpm for 10 min. Subsequently, the pellet was resuspended in lysis buffer containing 50 mM Tris–HCl (pH 7.5), 200 mM NaCl, 0.1% Triton X-100, 10 mM imidazole, 20% glycerol, 1 mM PMSF, 1 × protease inhibitor cocktail without EDTA [Sigma-Aldrich] and 1 × phosphatase inhibitor cocktail [Sigma-Aldrich] [224].

Zirconia beads equivalent to one-third of the volume were added to the cell suspension and cells were disrupted by periodic vortexing for 30 sec and incubation on ice for 1 min repeated for 15–20 cycles. The obtained whole cell extract (WCE) was centrifuged at 14000 rpm, 4 °C for 15 min to remove cell debris and bead particles. The supernatant was mixed with Ni-NTA resin and incubated overnight at 4 °C. The column was stringently washed twice with increasing concentrations of imidazole (60, 80 and 100 mM). Resin-bound wild type (WT), T62A/D and S277A/D Dnm1-His-HA proteins were eluted using 500 mM imidazole. The eluate was analyzed for the extent of purification of Dnm1 by SDS-PAGE gel stained with Coomassie brilliant blue G-250 and immunoblot with polyclonal antibody against HA (1:5000; BioBharati Life Science, India).

Fig. 2.2 Schematic representation of the expression and purification of Dnm1. Cells containing plasmids pRBA031-035 were sequentially grown in YND and YNR media before being shifted to YPGal medium. After 8-10 hours, galactose-induced cells were collected by centrifugation and dissolved in lysis buffer. Cells were lysed by periodic ice-vortexing in the presence of zirconia beads. Lysis was confirmed from the morphology of the yeast cells under a microscope. The WCE obtained after lysis was checked for the presence of induced Dnm1 by SDS-PAGE. The WCE was then incubated overnight in a column containing Ni^{2+}/NTA resin. Dnm1-His-HA was finally eluted with elution buffer containing 500 mM imidazole after stringent washing of the column. Images are created with *BioRender*.com.

2.2.3.2 Circular dichroism (CD) spectroscopy analysis

After every purification experiment, purified eluates were pooled together and desalted in 20 mM phosphate buffer using PD10 columns (GE Healthcare) according to the manufacturer's protocol prior to CD spectroscopy. Far-UV CD of purified WT, T62A/D and S277A/D was recorded under continuous nitrogen purging on a J-1500 spectropolarimeter (Jasco, Japan) at 25 °C. The far-UV CD spectra were acquired from 260 to 190 nm. A continuous scan rate of 100 nm/min with 5.0 nm bandwidth and 1 sec data integration time was used. The acquired spectra are the average of five scans, and the buffer signal was subtracted from the final signal of each sample to remove the background ellipticity of the buffer components. Measurements of 0.25 mg/mL protein were recorded using a quartz cuvette with a path length of 0.1 cm. The data obtained is represented as $\Delta\varepsilon$ (M^{-1} cm^{-1}). $\Delta\varepsilon$ was calculated with the following

equation [θ × (MRW × 0.1)/(C × L)/3298], where θ = ellipticity (millidegrees), C = concentration of the sample (mg/mL), L = pathlength (cm) and MRW = mean residue weight (Da) as described in [225].

2.2.3.3 Mass spectrometry (MS) analysis

In-gel digestion

The MS analysis was performed at the Proteomic facility, Institute of Bioinformatics, Bengaluru, India. The purified Dnm1 band was excised for MS analysis. The excised gel fragment was subjected to a destaining solution of 40 mM ammonium bicarbonate (Sigma-Aldrich) and 40% (v/v) acetonitrile (Merck Millipore). Once the gel fragments were completely destained, 0.5 mL of 100% acetonitrile was added and incubated for 10–15 min until the gel slice shrunk and became opaque. After destaining, a reduction solution of 5 mM dithiothreitol (Sigma-Aldrich) in ammonium bicarbonate was added to the gel fragment and incubated at 60 °C for 30 min. This was followed by incubation of the gel fragment in an alkylation solution consisting of 20 mM iodoacetamide (Sigma-Aldrich) in 40 mM ammonium bicarbonate for 10 min at room temperature in the dark. The gel fragment was then dehydrated in 100% acetonitrile solution followed by digestion with trypsin (Promega) overnight at 37 °C. Following overnight digestion, the peptides were extracted using an extraction buffer consisting of 5% formic acid (Merck Millipore) and 40% acetonitrile. The final peptide extraction was performed in 100% acetonitrile solution, followed by subjecting the pooled extract to vacuum-dry in a SpeedVac.

LC-MS/MS analysis

Reconstitution of the dried peptides was performed in 0.1% formic acid. The reconstituted peptides were then analyzed using Orbitrap Fusion Tribrid™ (Thermo Scientific ™, Bremen, Germany) mass spectrometer coupled with Proxeon Easy nLC system (Thermo Scientific™, Bremen, Germany). Peptide enrichment was achieved by allowing the protein fragments to pass through at a flow rate of 3 µL/min on to an Acclaim™ PepMap™ trap column

(2 cm × 75 µm, Magic C_{18}AQ, 5 µm, 100 Å, Michrom Biosciences Inc.). Peptides were separated on an analytical column (10 cm × 75 µm, Magic C_{18}AQ, 3 µm, 100 Å, Mi-chrom Biosciences Inc.) at a flow rate of 350 nL/min employing a linear gradient of 5–32% acetonitrile for 40 min with a total run time of 60 min. MS and MS/MS scan acquisitions were executed in the Orbitrap mass analyzer at a mass resolution of 120,000 and 15,000 at 200 m/z, respectively. MS spectra were acquired in a data dependent manner targeting the twenty most abundant ions with charge state ≥ 2 in each survey scan in the m/z range of 350–1600. Fragmentation was carried out using higher energy collisional dissociation mode with normalized collision energy of 34. Isolation width was set to 1.6 m/z with 0.5 m/z offset. Precursor ions selected for MS/MS fragmentation were dynamically excluded for 30 s. The automatic gain control for full MS and MS/MS was set to 4×10^5 and 1×10^5 ions, respectively. The maximum ion injection time for full MS and MS/MS was set to 50 ms and 75 ms, respectively. Internal calibration was carried out by enabling lock mass option using polydimethylcyclosiloxane (m/z, 445.1200025) ions [226].

Data analysis

The mass spectrometry data were searched against Saccharomyces genome database and analyzed using Mascot (version 2.2.0, Matrix Science, London, UK) and SequestHT algorithm and Proteome Discoverer software (Version 1.4.0.288, Thermo Fisher Scientific). The analyzing criteria were set as oxidation of methionine and phosphorylation modification of serine, threonine and tyrosine as variable modifications and carbamidomethyl modification of cysteine as fixed modification. A 10 ppm of precursor mass tolerance, 0.02 Da of fragment mass tolerance and a maximum of two missed cleavages were allowed. The spectral match hits were screened with 1% false discovery rate at the peptide level.

2.2.3.4 Phosphatase treatment, Phos-tag SDS-PAGE

The WT Dnm1 protein were purified and subjected to treatment with three units of calf intestinal alkaline phosphatase (CIAP) (Promega). The mixture was then incubated at 37 °C for

a duration of 30 min. Eluate fractions of Dnm1 without CIAP treatment were taken as control. Further, these proteins were separated using a 10% SDS-PAGE containing 50 µM Phos-tag (Wako chemicals) and 100 µM $MnCl_2$ in the resolving gel [227]. Electrophoretic separation was performed at 80 volt (V) for 5 h in an ice-tank. Following electrophoresis, the gel was soaked with gentle agitation in transfer buffer (25 mM Tris, 192 mM glycine, 10% methanol, pH 8.3) containing 1 mM EDTA for a duration of 10 min, and then with transfer buffer without EDTA. Subsequently, the proteins were transferred onto a nitrocellulose membrane at 20 V for 30 min.

2.2.3.5 Continuous GTPase activity assay

GTPase activity of Dnm1 was assessed through a previously described coupled assay in which the enzyme pyruvate kinase continuously converts GDP into GTP using the substrate PEP (Fig. 2.3) [228]. The pyruvate generated in the process is reduced to lactate by the enzyme lactate dehydrogenase. Simultaneous depletion of co-substrate NADH during this process was measured at A_{340} to obtain the rate of GTP hydrolysis. This assay allows continuous GTP regeneration, maintaining the required substrate concentration until NADH is depleted (Fig. 2.3). For determination of kinetic parameters, reactions were carried out in a buffer containing 25 mM HEPES, 25 mM PIPES, pH 7.0, 7.5 mM KCl, 150 mM NaCl, 5 mM $MgCl_2$, 1 mM PEP, 20 units/mL pyruvate kinase/lactate dehydrogenase, 600 µM NADH and variable concentration of GTP (100-1500 µM). The final concentration of purified Dnm1 used in each reaction was 10 µg/mL (0.096 µM). The final volume of all assay reactions was 200 µl, of which 150 µl was aliquoted into a 96-well plate. Depletion of NADH over time was measured for a duration of 90 min at 20 sec intervals using Multiskan GO 96-well plate reader (Thermo Scientific). Spectrophotometric data was imported to Microsoft Excel and the measured depletion of NADH with time was converted into protein activity. Absorbance *vs* time was plotted for each GTP concentration using the 'add trendline' function. The slope (ΔA_{340}/min) was converted to activity (min^{-1}) with the following equation, activity = [{(ΔA_{340}/min) * (10^6 µM/M)} / (ε * d)]/[Dnm1],

where ΔA_{340} = change in absorbance of NADH at 340 nm for the steady state linear depletion, ε = molar extinction coefficient of NADH i.e. calculated as 6220 M^{-1} cm^{-1}, d = pathlength of the well which is 0.38 cm in our assay conditions, [Dnm1] = concentration of Dnm1 used in this assay [37]. Activity at each GTP concentration was plotted in GraphPad prism software. The data were fitted globally to a Michaelis-Menten model to estimate the kinetic parameters V_{max}, K_M and k_{cat} (V_{max}/[Dnm1]).

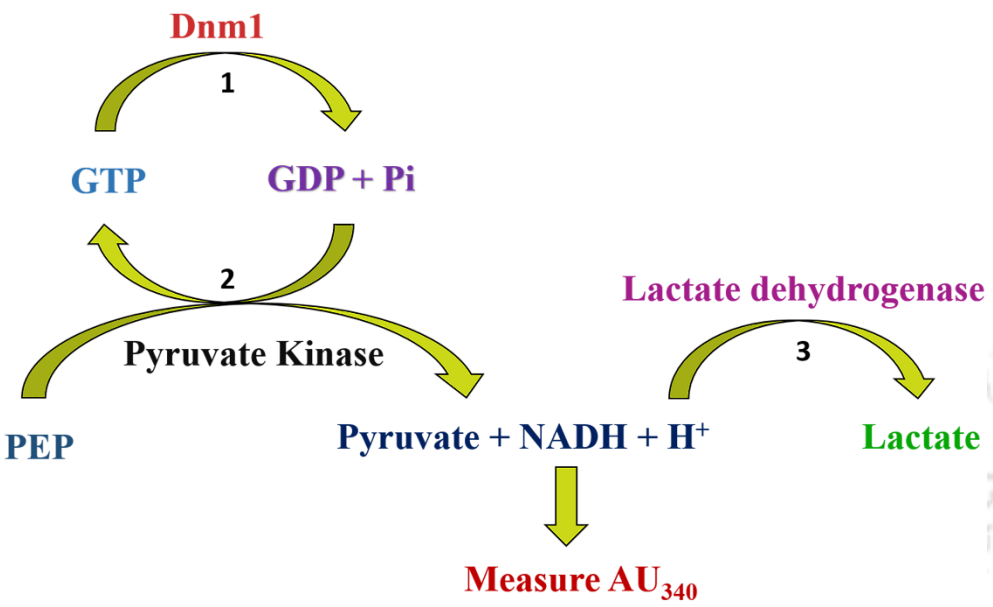

Fig. 2.3 Schematic representation of the coupled GTP hydrolysis assay for continuous GTP (substrate) regeneration. In the continuous GTP-regenerating assay, Dnm1 catalyzes the conversion of GTP into GDP and inorganic phosphate (1). GTP is regenerated from GDP and PEP through the enzymatic activity of pyruvate kinase (2). The pyruvate generated in this regenerative process is subsequently converted into lactate by the enzyme lactate dehydrogenase, utilizing NADH as a co-substrate (3). NADH depletion is measured by monitoring absorbance at 340 nm over time. The decrease in absorbance is directly proportional to GTP hydrolysis [228].

2.2.3.6 Size exclusion chromatography (SEC) analysis

SEC was carried out using HiLoad™ 16/600 Superdex™ 200 pg column (GE Healthcare #28-9893- 35) connected to a BioRad NGCTM chromatography system [229]. The column was equilibrated with a buffer comprising 50 mM Tris-Cl pH 7.5, 200 mM NaCl, and 5% glycerol. The column was calibrated at room temperature with β-amylase (200 kDa), alcohol dehydrogenase (158 kDa), albumin (66 kDa), carbonic anhydrase, (29 kDa) and cytochrome C

(12.4 kDa) (Sigma, catalog no. MWGF-200) at a flow rate of 1 mL/min. The SEC of affinity-purified WT Dnm1, Dnm1 T62A/D, and Dnm1 S277A/D was then carried out under the same operating conditions.

2.2.3.7 Isolation of mitochondrial crude extract

Mitochondrial crude extracts were isolated by yeast cell fractionation as described previously [230]. Briefly, yeast cells grown till mid log phase were harvested by centrifugation (3000×g, 5 min, 4 ◦C), washed once with water and resuspended in 1 mL ice cold 1X SHP buffer (0.6 M sorbitol, 20 mM HEPES-KOH, pH 7.4, 1 mM PMSF). Cells were lysed under ice cold conditions by brief vortexing using zirconia/ silica beads (0.5 mm diameter) (Unigenetics). Lysates were centrifuged (600×g, 5 min, 4 °C) to remove cell debris and supernatants were collected and centrifuged two times (4000×g, 5 min; 12,000×g, 30 min, 4 °C). The supernatant S_{12000} obtained later was used as cytosolic fraction whereas the pellet P_{12000} containing crude mitochondria were further dissolved in 1X SHP buffer. Protein concentrations in both the fractions were determined using Bradford protein estimation assay (Sigma Aldrich, USA). Presence of Dnm1-GFP in both cytosol and mitochondria were verified using immunoblot with rabbit polyclonal α-GFP (1:5000; BioBharati Life Science, India) and α-GAPDH (1:5000; BioBharati Life Science, India) or mouse monoclonal α-porin (1:5000; Invitrogen, Thermo Fisher Scientific, US) antibodies.

2.2.3.8 Western blotting

Trichloroacetic acid (TCA) treated cell extracts obtained from either bead lysis or trichloroacetic acid (TCA) treatment were prepared for SDS-PAGE analysis. as previously reported [231] Briefly, the culture volume corresponding to 3 OD_{600} units was spun down and the pellet obtained was resuspended in 50% TCA and incubated for 30 min at -80 °C. The cell suspension was centrifuged and the obtained pellet was washed twice with 80% acetone (ice cold) and air dried. Pellets were finally dissolved in 1% SDS/0.1 N NaOH solution. For certain

experiments cell lysate obtained by bead lysis was also analysed by SDS-PAGE.

Protein concentration was determined using Lowry's protein estimation technique or Bradford protein estimation method. Subsequently, equal amount of protein was loaded in each lane of the gel [232, 233]. The gels were run at a constant voltage of 130 V and then transferred onto nitrocellulose membrane using Bio-Rad Trans-Blot®Turbo^{TM}. The membrane was treated with a blocking solution (either 5% skimmed milk or 5% bovine serum albumin) at room temperature for a duration of 2 h. The blots were probed with antibodies as mentioned in Table 2.5. The blots were developed using the Bio-Rad ECL substrate and captured using the Bio-Rad ChemiDoc^{TM} XRS+ system.

2.2.3.9 Native polyacrymide gel electrophoresis (Native PAGE)

Purified WT and mutant Dnm1 samples were mixed with 4x native sample buffer (240 mM Tris-HCl pH 6.8, 40% glycerol, 0.04 % bromophenol blue). The different oligomeric states of the proteins were then analysed on an 8% native polyacrylamide gel after resolving for 5 h at 120 V. The resolved proteins in the native gel were stained with Coomassie and compared to known molecular weight standard protein markers (Invitrogen, catalogue no. LC0725).

2.2.4 Fluorescence microscopy analysis

Imaging was carried out using an inverted microscope (IX83, Olympus) equipped with a 100x/1.4 oil immersion objective. Samples were illuminated using pE-300^{white} CoolLED light source. GFP signal was detected using a U-FBNA filter with an excitation range 470–495 nm, dichroic 505 nm and emission 510–550 nm. mCherry was visualised with a brightline triple-bandpass filter (Semrock) operating at 378/474/575 nm and a dichroic beamsplitter operating at 409/493/596 nm (Semrock). CellSens Dimension (Olympus) and ImageJ/Fiji software were used for image analysis. Deconvolution of mitochondrial morphology images was perfomed using CellSens Dimension (Olympus) software. Final images were assembled using Adobe Photoshop. Cells expressing pHS12-preCOX4-mCherry were used for quantitative evaluation of

mitochondrial morphology. Mitochondrial morphology was classified into four types: reticular/branched, tubular, collapsed, and fragmented. Cells were fixed with 4% formaldehyde in phosphate-buffered saline, pH 7.4, for 15 min on ice for colocalization studies and for quantification of Dnm1-GFP puncta. Z-stacks were captured from top to bottom and at intervals of 0.3 µm. The same z-sections from both fluorescence channels were then extracted and merged to analyze colocalization. The ImageJ "line profile" tool was used for this analysis. Additionally, the "multi-point" tool in ImageJ was utilized to mark individual cells in the images for quantification purposes. Dnm1-GFP puncta were quantified by counting GFP spots in 50 randomly selected yeast cells from each experiment. Two independent experiments were considered for the statistical analysis.

For time lapse imaging, cells were placed on a thin layer of 2% low-melting temperature agarose and covered under a glass coverslip. A single 0.28-µm step size section was imaged and used for time lapse analysis. A total of 31 images were captured for 1 min at regular intervals of 2 sec with 2x2 binning. Tracking of Dnm1-GFP puncta was monitored using 2D/3D particle tracker under Mosaic plugin of ImageJ software.

2.2.5 Computational methods

2.2.5.1 Homology modelling

The objective of homology modelling procedure is to generate the three-dimensional (3D) structure of a protein by "fitting" its sequence into a known template structure. Greater the sequence homology (greater than 30% with the template) better the structural model. The 3D structure of yeast Dnm1 was generated by homology modelling [234-236]. Sequence alignment of the protein was performed using the program BLAST (Basic Local Alignment Search Tool), which finds regions of similarity between biological sequences. The homology model of the Dnm1 protein described in chapter 4 was derived using experimentally determined structures of the proteins with more than 90% identity. Four PDB templates (5A3F; 4BEJ; 6FGZ and 5WP9)

were used to build the Dnm1 model. Further sequence alignment of the target and template proteins was performed using the Modeller program. Of the four models generated by Modeller, the one with the highest Discrete Optimized Protein Energy (DOPE) score was selected. In chapter 5, X-ray structures (PDB 3SNH, 5A3F, and 3ZVR) were used as templates to build the 3D structure of Dnm1 [237-239]. 64 out of 757 amino acids were modelled using ab initio method (threading) for which structural template was unavailable.

2.2.5.2 Molecular dynamics (MD) simulations

Classical MD simulations were performed on the WT Dnm1 and its variants (T62A, T62D, S277A and S277D) as described in chapter 4. The structures of the variants were generated using the mutagenesis function of PyMOL by substituting the residue of WT with A/D residue [240-242]. The pKa values of the individual amino acids were calculated on the PDB2PQR server. To generate the force fields of WT Dnm1, T62A/D and S277A/D structures, AMBER FF14SB force-field was used [243]. Classical MD simulations were performed using NAMD 2.12 package [244]. The protein was explicitly solvated in a 15 Å margin TIP3P water box to perform MD simulations [245]. The system was centered in the periodic box of dimensions of 90.12x89.99x110.64 Å3 containing water molecules. Particle mesh Ewald method was used to account for the long-range interaction with a cut-off distance of 12 Å [246]. The temperature and pressure were controlled using the Langevin algorithm at 300 K and 1 atm, respectively [247]. A time step of 2 fs was used to integrate the equations of motion. Initially, the system was equilibrated for 5 ns and subsequently, 150 ns long trajectories were obtained as the production dynamics to perform statistical analysis. The simulated trajectories of all systems were analyzed to calculate various parameters such as root mean square deviation (RMSD), root mean square fluctuation (RMSF) and radius of gyration (Rg). Visual Molecular Dynamics (VMD) software was utilized for visualization and analysis of the trajectories, Bio3D package was used to perform the dynamical cross-correlations matrix (DCCM) and define secondary structure of proteins

(DSSP) for analyzing secondary structure percentages [248, 249].

A slightly modified MD simulation setup was used for the analysis of Dnm1 A430D, G397D, and C481F variants described in chapter 5. A 25 Å radii sphere, centered at the mutation site (A430D, G397D, and C481F) of the modelled Dnm1 was spherically truncated and subjected to MD simulations (Fig. 2.4). The mutants were modelled by altering the side-chain of a single amino acid residue in the homology modelled structure. The outer region of the spherically truncated MD model (buffer region, between 22 and 25 Å) was harmonically restrained by applying force constant (gradually increased from 3.0 to 5.0 kcal/mol/Å2 to the boundary) to the non-hydrogen protein atoms. The inner region (up to 22 Å radius) was fully flexible during production MD trajectory. The spherically truncated protein was overlaid with a cubic water box (edge length 80 Å, Fig. 2.4) and the waters that overlapped with the protein were deleted. The overall charge of the simulation box, including protein and waters were neutralized by adding counter ions. The simulation model consists of ~ 49000 atoms that include more than 15,000 explicit water molecules and 3–7 counter ions. MD was performed with a constant temperature (310 K), pressure (1 bar) with 2 fs time-step in the periodic boundary condition setup. Particle Mesh Ewald method [246] was used to compute long-range electrostatics. van der Waals interaction was truncated at 16 Å cut-off distance. Langevin dynamics [250] (bath coupling coefficient of 5 ps-1) and Langevin piston [251] was used for controlling the simulation temperature and pressure, respectively. Protein, waters and ions were described using standard CHARMM36 force field [252]. Explicit waters were represented using TIP3P water model [253]. CHARMM programme [254] has been used to generate input files and NAMD program [255] was used to perform MD simulation. Each simulation model was subjected to two independent MD simulations by randomizing the initial velocities. Each replica includes 325 ps equilibration followed by 50 ns production dynamics, thus total 100 ns production run was considered for structural analysis for each simulation model. In total 600 ns of production MD simulations were

considered for structural analysis of three WT regions and three of its mutant Dnm1 analogues. The simulation box was slowly heated up (upto 310 K) in the first phase of equilibration and then kept fixed during the production dynamics. During equilibration, harmonic restraint was also imposed to the heavy atoms of the inner region (within 22 Å, force constant = 4 kcal/mol/Å2) relative to the starting structure. The restraints of the inner region (within 22 Å) were completely removed at the final stage of equilibration. RMSD of the protein-heavy atoms relative to the homology modelled structure was estimated. Average RMSD was estimated by averaging over the last 40 ns of 50 ns trajectory. Estimation of RMSF and structural analysis was performed from the last 25 ns of 50 ns production MD.

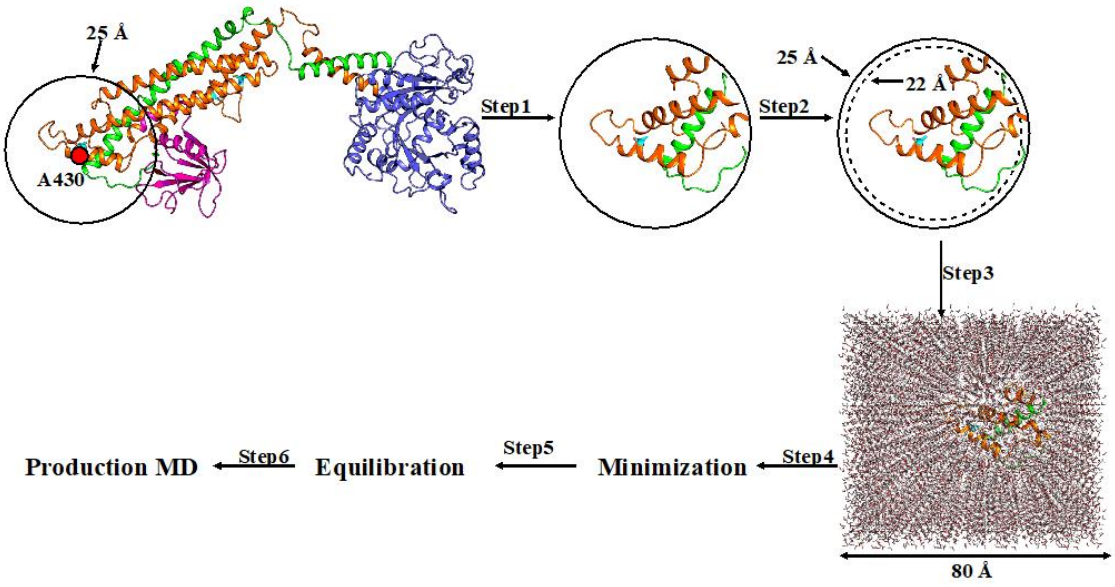

Fig. 2.4 MD setup used in this study. Step 1: Selection of 25Å radii sphere centered at mutation site (e.g, A430D site) of the homology modelled yeast Dnm1. Step 2, 3: Heavy atoms of the "buffer region" (22Å-25Å) of the spherically truncated model (25Å sphere) were harmonically restrained relative to template modelled structure. Step 4-6: Water box (~ edge length 80Å) overlaid and subjected to minimization, equilibration, and finally production MD.

2.2.6 Statistical analysis

All experiments were performed with a minimum of two or three independent biological replicates. One-way or two-way ANOVA with Dunnet's multiple comparison test as per requirement was used to determine statistical significance. The error bar indicates mean ± SEM.

For all statistical analysis *p < 0.05, **p < 0.01, ***p < 0.001, ****p < 0.0001 were considered.

GraphPad Prism 8 software was used for statistical analysis and data visualization.

Table 2.1 *S. cerevisiae* strains used in this study

Strain	Description	Source
BY4742 WT	MATα *his3*Δ *leu2*Δ *lys*Δ *ura3*Δ	Dharmacon Inc
BY4742 *dnm1*	*dnm1Δ*::kanMX4	Dharmacon Inc
BY4742 WT preCox4-mCherry	BY4742WT.*LEU2*::P_{ADH1}*PreCOX4-mCHERRY*	This study
BY4742 *dnm1* preCox4-mCherry	BY4742 *dnm1.LEU2*::P_{ADH1}*PreCOX4-mCHERRY*	This study
BY4742 *dnm1* FL-Dnm1-GFP	BY4742 *dnm1.URA3*::P_{MET25} *DNM1-GFP*	This study
BY4742 *dnm1* Dnm1^{T62A}-GFP	BY4742 *dnm1.URA3*::P_{MET25} *DNM1^{T62A}-GFP*	This study
BY4742 *dnm1* Dnm1^{T62D}-GFP	BY4742 *dnm1.URA3*::P_{MET25} *DNM1^{T62D}-GFP*	This study
BY4742 *dnm1* Dnm1^{S277A}-GFP	BY4742 *dnm1.URA3*::P_{MET25} *DNM1^{S277A}-GFP*	This study
BY4742 *dnm1* Dnm1^{S277D}-GFP	BY4742 *dnm1.URA3*::P_{MET25} *DNM1^{S277D}-GFP*	This study
BY4742 *dnm1* Dnm1^{S575A}-GFP	BY4742 *dnm1.URA3*::P_{MET25} *DNM1^{S575A}-GFP*	This study
BY4742 *dnm1* Dnm1^{S575D}-GFP	BY4742 *dnm1.URA3*::P_{MET25} *DNM1^{S575D}-GFP*	This study
BY4742 *dnm1* Dnm1^{S624A}-GFP	BY4742 *dnm1.URA3*::P_{MET25} *DNM1^{S624A}-GFP*	This study
BY4742 *dnm1* Dnm1^{S624D}-GFP	BY4742 *dnm1.URA3*::P_{MET25} *DNM1^{S624D}-GFP*	This study
BY4742 *dnm1* Dnm1^{S629A}-GFP	BY4742 *dnm1.URA3*::P_{MET25} *DNM1^{S629A}-GFP*	This study
BY4742 *dnm1* Dnm1^{S629D}-GFP	BY4742 *dnm1.URA3*::P_{MET25} *DNM1^{S629D}-GFP*	This study
BY4742 *dnm1* Dnm1^{A430D}-GFP	BY4742 *dnm1.URA3*::P_{MET25} *DNM1^{A430D}-GFP*	This study
BY4742 *dnm1* Dnm1^{G397D}-GFP	BY4742 *dnm1.URA3*::P_{MET25} *DNM1^{G397D}-GFP*	This study
BY4742 *dnm1* Dnm1^{R438C}-GFP	BY4742 *dnm1.URA3*::P_{MET25} *DNM1^{R438C}-GFP*	This study
BY4742 *dnm1* Dnm1^{C481F}-GFP	BY4742 *dnm1.URA3*::P_{MET25} *DNM1^{C481F}-GFP*	This study
BY4742 *dnm1* preCox4-mCherry Dnm1-GFP	BY4742 *dnm1.URA3*::P_{MET25} *DNM1-GFP LEU2::* P_{ADH1} *PreCOX4-mCHERRY*	This study
BY4742 *dnm1* preCox4-mCherry Dnm1^{T62A}-GFP	BY4742 *dnm1.URA3*::P_{MET25} *DNM1^{T62A}-GFP LEU2::* P_{ADH1} *PreCOX4-mCHERRY*	This study
BY4742 *dnm1* preCox4-mCherry Dnm1^{T62D}-GFP	BY4742 *dnm1.URA3*::P_{MET25} *DNM1^{T62D}-GFP LEU2::* P_{ADH1} *PreCOX4-mCHERRY*	This study

BY4742 *dnm1* preCox4-mCherry Dnm1^{S277A}-GFP	BY4742 *dnm1.URA3*::P$_{MET25}$ *DNM1^{S277A}-GFP LEU2::* P$_{ADH1}$ *PreCOX4-mCHERRY*	This study
BY4742 *dnm1* preCox4-mCherry Dnm1^{S277D}-GFP	BY4742 *dnm1.URA3*::P$_{MET25}$ *DNM1^{S277D}-GFP LEU2::* P$_{ADH1}$ *PreCOX4-mCHERRY*	This study
BY4742 *dnm1* preCox4-mCherry Dnm1^{S575A}-GFP	BY4742 *dnm1.URA3*::P$_{MET25}$ *DNM1^{S575A}-GFP LEU2::* P$_{ADH1}$ *PreCOX4-mCHERRY*	This study
BY4742 *dnm1* preCox4-mCherry Dnm1^{S575D}-GFP	BY4742 *dnm1.URA3*::P$_{MET25}$ *DNM1^{S575D}-GFP LEU2::* P$_{ADH1}$ *PreCOX4-mCHERRY*	This study
BY4742 *dnm1* preCox4-mCherry Dnm1^{S624A}-GFP	BY4742 *dnm1.URA3*::P$_{MET25}$ *DNM1^{S624A}-GFP LEU2::* P$_{ADH1}$ *PreCOX4-mCHERRY*	This study
BY4742 *dnm1* preCox4-mCherry Dnm1^{S624D}-GFP	BY4742 *dnm1.URA3*::P$_{MET25}$ *DNM1^{S624D}-GFP LEU2::* P$_{ADH1}$ *PreCOX4-mCHERRY*	This study
BY4742 *dnm1* preCox4-mCherry Dnm1^{S629A}-GFP	BY4742 *dnm1.URA3*::P$_{MET25}$ *DNM1^{S629A}-GFP LEU2::* P$_{ADH1}$ *PreCOX4-mCHERRY*	This study
BY4742 *dnm1* preCox4-mCherry Dnm1^{S629D}-GFP	BY4742 *dnm1.URA3*::P$_{MET25}$ *DNM1^{S629D}-GFP LEU2::* P$_{ADH1}$ *PreCOX4-mCHERRY*	This study
BY4742 *dnm1* preCox4-mCherry Dnm1^{A430D}-GFP	BY4742 *dnm1.URA3*::P$_{MET25}$ *DNM1^{A430D}-GFP LEU2::* P$_{ADH1}$ *PreCOX4-mCHERRY*	This study
BY4742 *dnm1* preCox4-mCherry Dnm1^{G397D}-GFP	BY4742 *dnm1.URA3*::P$_{MET25}$ *DNM1^{G397D}-GFP LEU2::* P$_{ADH1}$ *PreCOX4-mCHERRY*	This study
BY4742 *dnm1* preCox4-mCherry Dnm1^{R438C}-GFP	BY4742 *dnm1.URA3*::P$_{MET25}$ *DNM1^{R438C}-GFP LEU2::* P$_{ADH1}$ *PreCOX4-mCHERRY*	This study
BY4742 *dnm1* preCox4-mCherry Dnm1^{C481F}-GFP	BY4742 *dnm1.URA3*::P$_{MET25}$ *DNM1^{C481F}-GFP LEU2::* P$_{ADH1}$ *PreCOX4-mCHERRY*	This study
BY4742 WT preCox4-mCherry Dnm1^{T62A}-GFP	BY4742 WT.*URA3*::*P$_{MET25}$ DNM1^{T62A}-GFP LEU2::* P $_{ADH1}$ *PreCOX4-mCHERRY*	This study
BY4742 WT preCox4-mCherry Dnm1^{T62D}-GFP	BY4742 WT.*URA3*::*P$_{MET25}$ DNM1^{T62D}-GFP LEU2::* P $_{ADH1}$ *PreCOX4-mCHERRY*	This study
BY4742 WT preCox4-mCherry Dnm1^{S277A}-GFP	BY4742 WT.*URA3*::*P$_{MET25}$ DNM1^{S277A}-GFP LEU2::* P $_{ADH1}$ *PreCOX4-mCHERRY*	This study
BY4742 WT preCox4-mCherry Dnm1^{S277D}-GFP	BY4742 WT.*URA3*::*P$_{MET25}$ DNM1^{S277D}-GFP LEU2::* P $_{ADH1}$ *PreCOX4-mCHERRY*	This study
BY4742 WT preCox4-mCherry Dnm1^{S575A}-GFP	BY4742 WT.*URA3*::*P$_{MET25}$ DNM1^{S575A}-GFP LEU2::* P $_{ADH1}$ *PreCOX4-mCHERRY*	This study
BY4742 WT preCox4-mCherry Dnm1^{S575D}-GFP	BY4742 WT.*URA3*::*P$_{MET25}$ DNM1^{S575D}-GFP LEU2::* P $_{ADH1}$ *PreCOX4-mCHERRY*	This study
BY4742 WT preCox4-mCherry Dnm1^{S624A}-GFP	BY4742 WT.*URA3*::*P$_{MET25}$ DNM1^{S624A}-GFP LEU2::* P $_{ADH1}$ *PreCOX4-mCHERRY*	This study
BY4742 WT preCox4-mCherry Dnm1^{S624D}-GFP	BY4742 WT.*URA3*::*P$_{MET25}$ DNM1^{S624D}-GFP LEU2::* P $_{ADH1}$ *PreCOX4-mCHERRY*	This study
BY4742 WT preCox4-mCherry Dnm1^{S629A}-GFP	BY4742 WT.*URA3*::*P$_{MET25}$ DNM1^{S629A}-GFP LEU2::* P $_{ADH1}$ *PreCOX4-mCHERRY*	This study
BY4742 WT preCox4-mCherry Dnm1^{S629D}-GFP	BY4742 WT.*URA3*::*P$_{MET25}$ DNM1^{S629D}-GFP LEU2::* P $_{ADH1}$ *PreCOX4-mCHERRY*	This study
BY4742 WT preCox4-mCherry Dnm1^{A430D}-GFP	BY4742 WT.*URA3*::*P$_{MET25}$ DNM1^{A430D}-GFP LEU2::* P $_{ADH1}$ *PreCOX4-mCHERRY*	This study
BY4742 WT preCox4-mCherry Dnm1^{G397D}-GFP	BY4742 WT.*URA3*::*P$_{MET25}$ DNM1^{G397D}-GFP LEU2::* P $_{ADH1}$ *PreCOX4-mCHERRY*	This study
BY4742 WT preCox4-mCherry Dnm1^{R438C}-GFP	BY4742 WT.*URA3*::*P$_{MET25}$ DNM1^{R438C}-GFP LEU2::* P $_{ADH1}$ *PreCOX4-mCHERRY*	This study

BY4742 WT preCox4-mCherry Dnm1^{C481F}-GFP	BY4742 WT.*URA3*::P_{MET25} *DNM1*^{C481F}*-GFP LEU2::* P_{ADH1} *PreCOX4-mCHERRY*	This study
Y258 Dnm1-His-HA	MATα *pep4-3, his4-580, leu2-3,112, URA3::*P_{GAL} *DNM1-His-HA*	Dharmacon Inc
BJ2168	MATa,*ura3–52, trp1–289, leu2–3, 112, prb1–1122, prc1– 407, pep4 –3*	Prof. K. Mishra lab
BJ2168 Dnm1^{T62A}- His HA	BJ2168.*URA3::*P_{GAL}*DNM1*^{T62A}*-His-HA*	This study
BJ2168 Dnm1^{T62D}- His HA	BJ2168.*URA3::*P_{GAL}*DNM1*^{T62D}*-His-HA*	This study
BJ2168 Dnm1^{S277A}- His HA	BJ2168.*URA3::*P_{GAL}*DNM1*^{S277A}*-His-HA*	This study
BJ2168 Dnm1^{S277D}- His HA	BJ2168.*URA3::*P_{GAL}*DNM1*^{S277D}*-His-HA*	This study

Table 2.2 Plasmids used in this study

Plasmid	**Description**	**Source**
pUG35 GFP	P_{MET25} *GFP*; amp^R *Sc-URA*3	Prof. Johannes Hegemann lab
pUG35 DNM1-GFP (pRBA005)	P_{MET25} *DNM1-GFP*; amp^R *Sc-URA*3	This study
pHS12-mCherry	P_{ADH1} *preCOX4-mCHERRY*; amp^R *Sc-LEU2*	Addgene (25444)
pUG35-DNM1^{G397D}-GFP (pRBA017)	P_{MET25} *DNM1*^{G397D}*-GFP*; amp^R *Sc-URA*3	This study
pUG35-DNM1^{C481F}-GFP (pRBA018)	P_{MET25} *DNM1*^{C481F}*-GFP*; amp^R *Sc-URA*3	This study
pUG35-DNM1^{R438C}-GFP (pRBA019)	P_{MET25} *DNM1*^{R438C}*-GFP*; amp^R *Sc-URA*3	This study
pUG35-DNM1^{A430D}-GFP (pRBA020)	P_{MET25} *DNM1*^{A430D}*-GFP*; amp^R *Sc-URA*3	This study
pUG35-DNM1^{T62A}-GFP (pRBA021)	P_{MET25}*DNM1*^{T62A}*-GFP*; amp^R *Sc-URA*3	This study
pUG35-DNM1^{T62D}-GFP (pRBA022)	P_{MET25}*DNM1*^{T62D}*-GFP*; amp^R *Sc-URA*3	This study
pUG35-DNM1^{S277A}-GFP (pRBA023)	P_{MET25}*DNM1*^{S277A}*-GFP*; amp^R *Sc-URA*3	This study
pUG35-DNM1^{S277D}-GFP (pRBA024)	P_{MET25}*DNM1*^{S277D}*-GFP*; amp^R *Sc-URA*3	This study
pUG35-DNM1^{S575A}-GFP (pRBA025)	P_{MET25}*DNM1*^{S575A}*-GFP*; amp^R *Sc-URA*3	This study
pUG35-DNM1^{S575D}-GFP (pRBA026)	P_{MET25}*DNM1*^{S575D}*-GFP*; amp^R *Sc-URA*3	This study
pUG35-DNM1^{S624A}-GFP (pRBA027)	P_{MET25}*DNM1*^{S624A}*-GFP*; amp^R *Sc-URA*3	This study
pUG35-DNM1^{S624D}-GFP (pRBA028)	P_{MET25}*DNM1*^{S624D}*-GFP*; amp^R *Sc-URA*3	This study
pUG35-DNM1^{S629A}-GFP (pRBA029)	P_{MET25}*DNM1*^{S629A}*-GFP*; amp^R *Sc-URA*3	This study
pUG35-DNM1^{S629D}-GFP (pRBA030)	P_{MET25}*DNM1*^{S629D}*-GFP*; amp^R *Sc-URA*3	This study
BG1805-DNM1-His-HA (pRBA031)	P_{GAL} *DNM1-His-HA*; amp^R *Sc*-URA3	Dharmacon
BG1805-DNM1^{T62A}-His-HA (pRBA032)	P_{GAL} *DNM1*^{T62A}*-His-HA*; amp^R *Sc*-URA3	This study

BG1805-DNM1^{T62A}-His-HA (pRBA033)	P_{GAL} *DNM1*^{T62D}*-His-HA*; amp^{R} *Sc*-URA3	This study
BG1805-DNM1^{S277A}-His-HA (pRBA034)	P_{GAL} *DNM1*^{S277A}*-His-HA*; amp^{R} *Sc*-URA3	This study
BG1805-DNM1^{S277D}-His-HA (pRBA035)	P_{GAL} *DNM1*^{S277D}*-His-HA*; amp^{R} *Sc*-URA3	This study

Table 2.3 Primers used in this study

Primer	Sequence
pr-RBA001	5'-CGCGGATCCATGGCTAGTTTAGAAGATC-3'
pr-RBA002	5'-TCCCCCGGGCAGAATATTACTAATAAGGGT-3'
pr-RBA005	5'-GAATACGATACAGAGGAAGGCGC-3'
pr-RBA014	5'-CGAAGGAACTCTGTGATGGCGCCCGTATTTATTAC-3'
pr-RBA015	5'- GTAATAAATACGGGCGCCATCACAGAGTTCCTTCG-3'
pr-RBA016	5'-GAAAATATGCCATAAATTTGGATCCGCTGAGCTAG-3'
pr-RBA017	5'-CTAGCTCAGCGGATCCAAATTTATGGCATATTTTC-3'
pr-RBA018	5'-CAGACAAGAAAAGAGCAATTGCCGGTGATGG-3'
pr-RBA019	5'-CCATCACCGGCAATTGCTCTTTTCTTGTCTG-3'
pr-RBA020	5'-CAGACAAGAAAAGAGATATTGCAGGTGATGG-3'
pr-RBA021	5'-CCATCACCTGCAATATCTCTTTTCTTGTCTG-3'
pr-RBA026	5'-CTTGATGTTAGAACAGATATTAGGAATTCTACTGGTC-3'
pr-RBA027	5'-GACCAGTAGAATTCCTAATATCTGTTCTAACATCAAG-3'
pr-RBA028	5'-GAAATTCTACTGGGCCCTGTCCTACATTATTTGTACC-3'
pr-RBA029	5'-GGTACAAATAATGTAGGACAGGGCCCAGTAGAATTTC-3'
pr-RBA030	5'- GTATTAATGGTACCTCAGCTATCTCTTCGAATATAG-3'
pr-RBA031	5'-CTATATTCGAAGAGATAGCTGAGGTACCATTAATAC-3'
pr-RBA032	5'-GGTATTAATGGTACTTCAGATATCTCTTCGAATATAGAT-3'
pr-RBA033	5'-ATCTATATTCGAAGAGATATCTGAAGTACCATTAATACC-3'
pr-RBA038	5'-GGTACTGGTATTGTCGCGAGGAGACCGTTAGTTCTTC-3'
pr-RBA039	5'-GAAGAACTAACGGTCTCCTCGCGACAATACCAGTACC-3'
pr-RBA040	5'-GGTACTGGTATTGTCGACAGAAGGCCGTTAGTTCTTC-3'
pr-RBA041	5'-GAAGAACTAACGGCCTTCTGTCGACAATACCAGTACC-3'
pr-RBA042	5'-GGTGTAGTGAATCGCGCGCAACAGGATATTCAA-3'
pr-RBA043	5'-TTGAATATCCTGTTGCGCGCGATTCACTACACC-3'

pr-RBA044	5'-GGTGTAGTGAATCGCGATCAACAGGATATTC-3'
pr-RBA045	5'-GAATATCCTGTTGATCGCGATTCACTACACC-3'
pr-RBA046	5'-CCTGTGTTCGATGCAGCTGACAAGAAAAGATCC-3'
pr-RBA047	5'-GGATCTTTTCTTGTCAGCTGCATCGAACACAGG-3'
pr-RBA048	5'-CCTGTGTTCGATGCAGATGACAAGAAAAGATCC-3'
pr-RBA049	5'-GGATCTTTTCTTGTCATCTGCATCGAACACAGG-3'

Table 2.4 Primers and template DNA used for SDM

Plasmid	Mutation	Primer pair	Template	Effect of restriction digestion
pRBA017	G397D	pr-RBA014 pr-RBA015	pRBA005	*Sfo*I digestion; WT = 8502 bp; Mutant = 7057, 1445 bp
pRBA018	C481F	pr-RBA016 pr-RBA017	pRBA005	*Bam*HI digestion; WT = 8502 bp; Mutant = 7053, 1449 bp
pRBA019	R438C	pr-RBA028 pr-RBA029	pRBA005	*Apa*I digestion; WT = 8502 bp; Mutant = 5294, 3208 bp
pRBA020	A430D	pr-RBA026 pr-RBA027	pRBA005	*Eco*RI digestion; WT = 6579,1054,869 bp; Mutant = 6579, 998, 869, 66 bp
pRBA021	T62A	pr-RBA038 pr-RBA039	pRBA005	*Nru*I digestion; WT = No cut; Mutant = 8502 bp
pRBA022	T62D	pr-RBA040 pr-RBA041	pRBA005	*Sal*I digestion; WT = 8502 bp; Mutant = 6372, 2130 bp
pRBA023	S277A	pr-RBA042 pr-RBA043	pRBA005	*Bss*HII (*Pau*I) digestion; WT = 4725, 3777 bp; Mutant = 4725,2508,1269 bp
pRBA024	S277D	pr-RBA044 pr-RBA045	pRBA005	*Nru*I digestion; WT = No cut; Mutant = 8502 bp
pRBA025	S575A	pr-RBA030 pr-RBA031	pRBA005	*Kpn*I digestion; WT = 8502 bp; Mutant = 6915, 1587 bp
pRBA026	S575D	pr-RBA032 pr-RBA033	pRBA005	*Acu*I digestion; WT = 4017, 2994, 1012, 479 bp; Mutant = 3048, 2994, 1012, 969, 479 bp
pRBA027	S624A	pr-RBA046 pr-RBA047	pRBA005	*Pvu*II digestion; WT = 4450, 4052 bp; Mutant = 4450, 2493, 1559 bp
pRBA028	S624D	pr-RBA048 pr-RBA049	pRBA005	*Nsi*I digestion; WT = 6302, 2200 bp; Mutant = 8502 bp
pRBA029	S629A	pr-RBA018 pr-RBA019	pRBA005	*Mun*I digestion; WT = 5431, 2038, 1033 bp; Mutant = 5431, 1042, 1033, 996 bp
pRBA030	S629D	pr-RBA020 pr-RBA021	pRBA005	*KpnI+Bve*I (*Bsp*MI) digestion; WT = 8502 bp; Mutant = 6904, 5481, 1598, 1423 bp
pRBA032	T62A	pr-RBA038 pr-RBA039	pRBA031	*Nru*I digestion; WT = No cut; Mutant = 9030 bp
pRBA033	T62D	pr-RBA040 pr-RBA041	pRBA031	*Sal*I digestion; WT = No cut; Mutant = 9030 bp

pRBA034	S277A	pr-RBA042 pr-RBA043	pRBA031	*Bss*HII (*Pau*I) digestion; WT = 5514, 3473 bp; Mutant = 5514,2141,1332 bp
pRBA035	S277D	pr-RBA044 pr-RBA045	pRBA031	*Nru*I digestion; WT = No cut; Mutant = 9030 bp

Table 2.5 List of antibodies used in this study

Primary antibodies				
Name	**Dilution used**	**Source**	**Clonality**	**Company**
α-GFP	1:5000	Rabbit	Polyclonal	Biobharti Life Science
α-HA	1:5000	Rabbit	Polyclonal	Biobharti Life Science
α-GAPDH	1:5000	Rabbit	Polyclonal	Biobharti Life Science
α-β-actin	1:5000	Mouse	Monoclonal	Invitrogen
α-porin	1:5000	Mouse	Monoclonal	Invitrogen
Secondary antibodies				
α-rabbit IgG (HRP-conjugated)	1:5000	Goat		Biobharti Life Science
α-mouse IgG (HRP-conjugated)	1:5000	Goat		Invitrogen

Table 2.6 List of chemicals used in this study

Chemical	**Name**	**Manufacturer**
Enzymes	Phusion DNA polymerase	New England Biolabs (NEB)
	Pfu Turbo DNA polymerase	Agilent Technologies
	T4 DNA ligase	ThermoFisher Scientific
	Alkaline Phosphatase	Promega
	*Xba*I	ThermoFisher Scientific
	*Sma*I	ThermoFisher Scientific
	*Eco*RI	ThermoFisher Scientific
	*Bam*HI	ThermoFisher Scientific
	*Bgl*II	ThermoFisher Scientific
	*Mun*I	New England Biolabs (NEB)
	*Bss*HII (*Pau*I)	ThermoFisher Scientific
	*Bve*I(*Bsp*MI)	ThermoFisher Scientific
	*Nru*I	New England Biolabs (NEB)

	*Sfo*I	New England Biolabs (NEB)
	*Kpn*I	ThermoFisher Scientific
	*Apa*I	New England Biolabs (NEB)
	*Dpn*I	ThermoFisher Scientific
	*Acu*I	New England Biolabs (NEB)
	*Sal*I	ThermoFisher Scientific
	*Pvu*II	ThermoFisher Scientific
	*Nsi*I	ThermoFisher Scientific
Kits	Plasmid isolation Miniprep kit	Macherey-Nagel
	PCR purification kit	Macherey-Nagel
	Gel extraction kit	Macherey-Nagel
	Protein concentration estimation kit	BioRad
Other chemicals	Phos-tag	Wako chemicals
	ECL	BioRad
	Protease inhibitor cocktail without EDTA	SigmaAldrich
	1x phosphatase inhibitor cocktail	SigmaAldrich
	Pyruvate kinase/Lactate dehydrogenase	SigmaAldrich
	NADH	SigmaAldrich
	GTP	SigmaAldrich
	Phospho(enol)pyruvate	SigmaAldrich

Chapter 3

Cloning, expression and characterization of Dnm1 fusion proteins

Abstract

The dynamin-related GTPase, Dnm1, plays a pivotal role in regulating yeast mitochondrial morphology through mitochondrial fission. To study the localization, function, and structural properties of Dnm1, fusion proteins have been constructed in this study. A C-terminal GFP fusion (FL-Dnm1-GFP) and a C-terminal His-HA fusion (Dnm1-His-HA) were used to characterize the protein. Both the fusion proteins were functional *in vivo* upon complementation analysis of mitochondrial morphology in *dnm1* cells. No effect on the growth and survival of cells was observed upon expression of the fusion proteins. FL-Dnm1-GFP was expressed in cells as punctate GFP fluorescence, which partially colocalized with a mitochondrial marker. Dnm1-His-HA was expressed in yeast and was successfully purified from the native host, ensuring its suitability for *in vitro* studies. Mass spectrometry analysis confirmed the successful purification of Dnm1, validating its identity and purity. Further, analysis of the purified protein with circular dichroism spectroscopy showed that Dnm1 retained predominantly α-helical secondary structure. The fusion proteins and strains generated in this study can be instrumental in deciphering the structure-function relationship of Dnm1.

This chapter is a part of

Banerjee R, Mukherjee A, Adhikary A, Hussain S, Sharma S, Ali E, Nagotu S. Insights into the role of the conserved GTPase domain residues T62 and S277 in yeast Dnm1. **International Journal of Biological Macromolecules, 2023**.
DOI: https://doi.org/10.1016/j.ijbiomac.2023.127381

3.1 Introduction

Compartmentalizing cellular contents into functional units called organelles is an essential feature of eukaryotic cells. One such important organelle in a cell is the mitochondrion, which harbors the TCA cycle and oxidative phosphorylation machinery for energy production. Biosynthesis of cellular building blocks such as nucleotides, amino acids, and Ca^{2+} buffering also requires active mitochondria [3, 15, 256]. A role for mitochondria in regulating cellular redox balance and apoptosis has also been reported [257, 258]. Interestingly, mitochondrial shape and dynamics profoundly affect the functions mentioned above. Mitochondria are dynamic in nature, whose morphology is maintained by a continuous process of fission and fusion [259]. Several proteins involved in these processes are identified and are conserved across eukaryotic organisms [108].

Mitochondrial fission is a highly conserved process and is dependent on the homologs of the dynamin-related proteins in all organisms studied [86, 87, 260-262]. It is now widely accepted that Dnm1, a large GTPase, plays a crucial role in mitochondrial membrane fission in yeast [86, 103, 116, 263]. The protein consists of four structural domains: An N-terminal GTP-binding domain, the middle domain, the variable domain (VD) containing the B-insert, and the C-terminal GTPase effector (GED) domain [99, 100]. The life cycle of Dnm1 unfolds in the cytosol, where it most likely exists as a dimer [104]. The process of targeting this protein to the membrane is not entirely understood. In *S. cerevsiae* Dnm1 interacts with Fis1, an OMM protein, and two WD40 repeat proteins, Mdv1/Caf4, that function as adapter proteins and are part of the fission complex at the mitochondrial membrane [88, 92, 105]. However, the proteins with which Dnm1 interacts and associates for the fission of the membrane seem to be variable in different organisms [88, 89, 93, 94, 98, 120, 139]. Electron microscopy (EM) studies have reported that Dnm1 forms large oligomers/helical structures with a radius similar to that of mitochondrial girth at the OMM [20, 111]. Following its fission activity at the OMM, it is proposed that Dnm1 dislodges itself

from the membrane and is released into the cytosol [108]. Multiple localizations of the protein and variable oligomeric forms highlight the very dynamic nature of the protein. However, several facets of the life cycle of the protein are not yet deciphered. Studying yeast Dnm1 will enable us to understand these important and interesting questions. In this study, we investigated the structural and functional properties of Dnm1 using molecular, biochemical, and biophysical approaches. Our findings show that Dnm1 resides as punctate structures in the cytosol and mitochondria. These punctate structures are dynamic as assessed using live-cell imaging. Cells lacking Dnm1 have collapsed and fused mitochondria, similar to as reported in earlier studies. Purified Dnm1 retained its characteristic secondary structure, demonstrating its suitability for future *in vitro* investigations.

3.2 Results

3.2.1 FL-Dnm1-GFP is functional *in vivo* and does not affect the growth of cells

The utilization of the GFP tag to study Dnm1 offers several advantages. The GFP tag not only enables visualization of the protein *in vivo* but also allows us to identify its localization to sub-cellular compartments. It also provides insights into the spatio-temporal distribution and dynamics of the protein. To construct a C-terminal GFP fusion protein, *DNM1* was amplified from yeast genomic DNA using primers pr-RBA001 and pr-RBA002 (Fig. 3.1.A.i). The amplified gene (2289 bp) and the pUG35-GFP vector (6231 bp) were digested with restriction enzymes *Bam*HI and *Sma*I, and the resulting fragments were purified (Fig. 3.1.A.ii). The purified fragments were ligated using T4 DNA ligase, and the ligated product was transformed into *E. coli* DH5α cells. The transformed cells were plated onto selective plates and colonies were screened and confirmed for the presence of the desired plasmid pRBA005 (expressing fusion protein FL-Dnm1-GFP) by restriction digestion with *Bgl*II and *Xba*I followed by sequencing analysis (Fig. 3.1.A.iii and 3.1.A.iv). pRBA005 was subsequently transformed into *S. cerevisiae*

dnm1 cells and analyzed for expression by fluorescence microscopy and western blotting. As depicted in Fig. 3.1.B, FL-Dnm1-GFP was visualized as a distinct green puncta in contrast to the diffused GFP signal observed in cells expressing pUG35 (empty vector). Further, expression of FL-Dnm1-GFP in exponentially growing cells was determined by western blotting using α-GFP antibody. Fig. 3.1.C depicts the detection of FL-Dnm1-GFP (112 kDa) by α-GFP antibody in cells containing plasmid pRBA005, whereas no band was detected in *S. cerevisiae dnm1* (control) cells. To determine the effect of the expression of FL-Dnm1-GFP on cell growth, *dnm1* cells containing pRBA005 were spotted onto selective (YND or YNG) plates by drop serial dilution and cultured in YND or YNG liquid medium. Cells lacking Dnm1 did not exhibit a significant difference in growth compared to wild type (WT) in YND (doubling time: WT-2.33 h and *dnm1*-2.74 h; FL-2.52 h) (Fig. 3.2.A). Unlike glucose, glycerol is a non-fermentable carbon source, and glycerol utilization requires two major steps, including phosphorylation of glycerol in cytosol followed by conversion of glycerol phosphate to dihydroxyacetone in mitochondria [264, 265]. While there was no notable difference in doubling times of the WT, *dnm1*, and FL-Dnm1-GFP expressing cells when cultured on YNG (doubling time: WT-11.04 h and *dnm1*-11.39 h; FL-9.21 h), the growth of all the strains was slower compared to their growth in YND (Fig. 3.2.B).

Dnm1 is required for mitochondrial membrane fission, and WT yeast cells with a functional Dnm1 exhibit a reticular/branched mitochondrial phenotype (Fig. 3.2.C) [86]. Cells lacking Dnm1 (*dnm1*) exhibit a characteristic collapsed/fallen mitochondrial morphology (Fig. 3.2.C) [86]. To evaluate if the constructed FL-Dnm1-GFP was functional, it was expressed in *dnm1* cells containing preCOX4-mCherry that labels mitochondria. Upon expression of FL-Dnm1-GFP in these cells, the collapsed mitochondrial phenotype characteristic of *dnm1* cells was restored to reticular mitochondrial morphology corresponding to the morphology observed in WT cells, suggesting that the fusion protein was functional *in vivo* (Fig. 3.2.C).

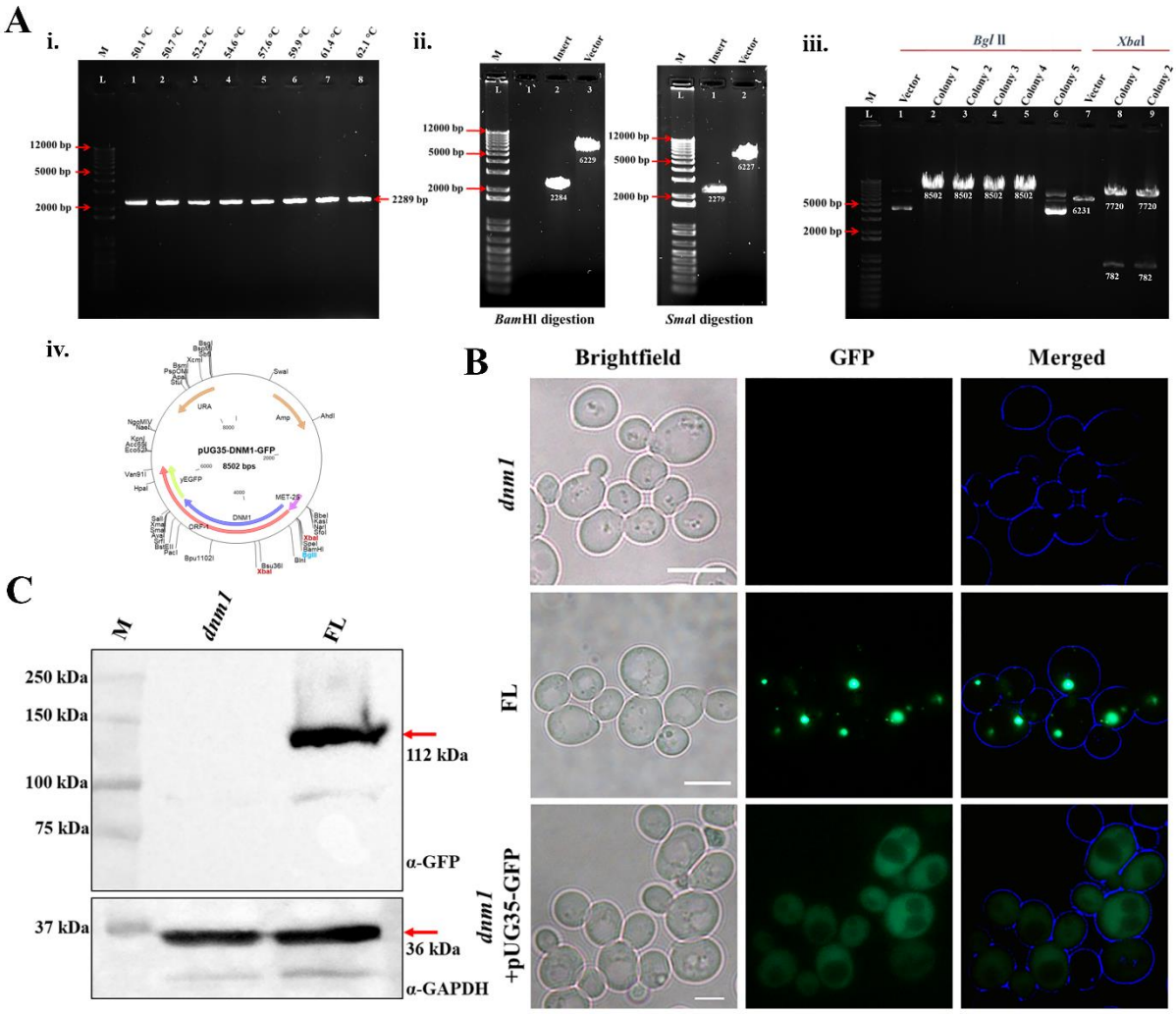

Fig. 3.1 Construction and expression of FL-Dnm1-GFP

(A) Construction of FL-Dnm1-GFP. **(i)** Gradient PCR was used to amplify *DNM1* at annealing temperatures ranging from 50 to 62°C, resulting in a 2289 bp product. **(ii)** Linear fragments of the vector (pUG35-6227 bp) and the PCR product (2279 bp) obtained by sequential digestion with *Bam*HI and then *Sma*I are represented. **(iii)** Screening of colonies by digestion of DNA with the single cutter *Bgl*II and the double cutter *Xba*I is represented. Lane 6 shows a negative colony, while all other lanes show positive colonies. **(iv)** Plasmid map represents pRBA005 (8502 bp) containing FL-Dnm1-GFP. **(B)** Fluorescence microscopy analysis of *dnm1* cells expressing FL-Dnm1-GFP or empty vector pUG35. FL-Dnm1-GFP is visualized as distinct puncta in contrast to a diffused cytosolic GFP expressed from pUG35. **(C)** represents a western blot of whole cell extracts probed with α-GFP. A band of approximately 112 kDa was observed in FL-Dnm1-GFP-expressing cells. (M.W. of Dnm1 and GFP is ≈ 85 kDa and 27 kDa, respectively). M represents the molecular weight marker.

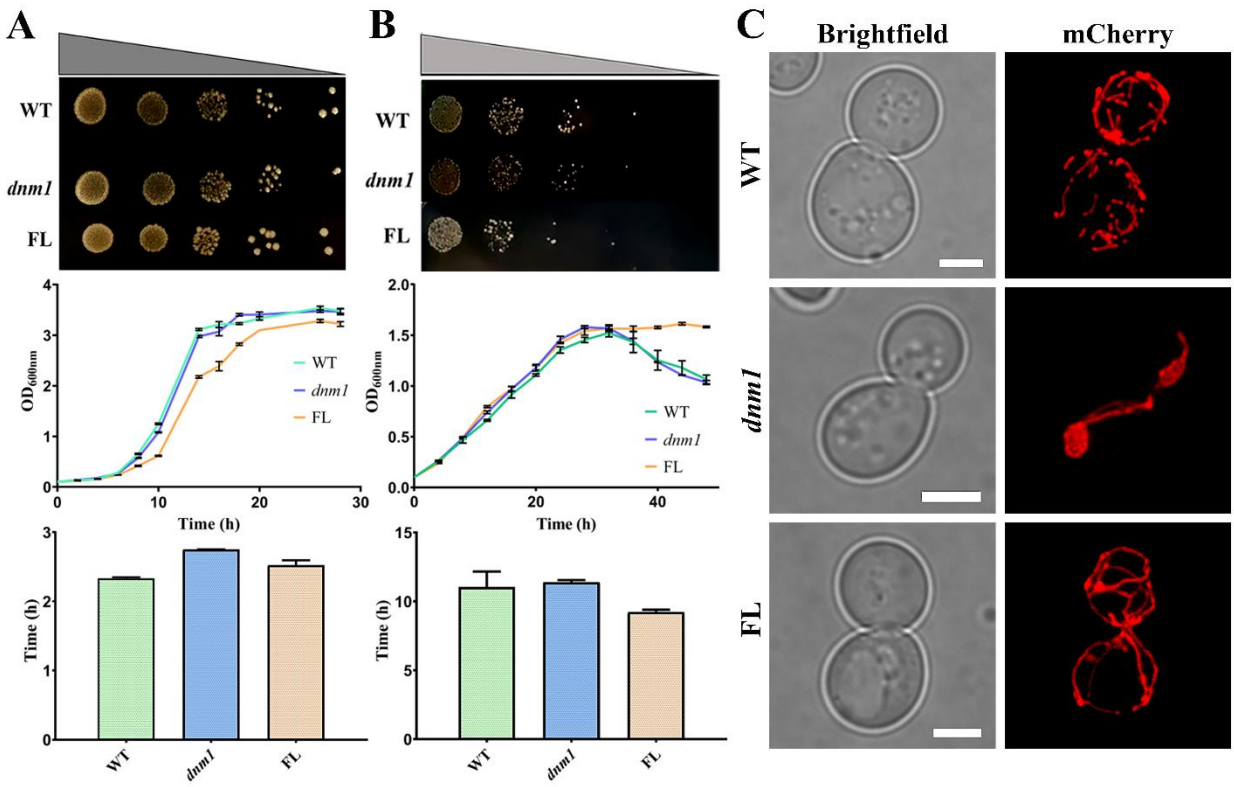

Fig. 3.2 Assessment of growth and mitochondrial morphology of cells expressing FL-Dnm1-GFP. Growth analysis of WT, *dnm1* and *dnm1* cells expressing FL-Dnm1-GFP under different carbon sources by drop serial-dilution assay and growth curve are represented. **(A)** and **(B)** represents culture conditions comprising glucose (YND) and glycerol (YNG), respectively. Tenfold successive dilutions of log phase cultures were spotted onto YND or YNG plates and incubated at 30 °C for 3 days and 7 days, respectively. For growth kinetics, cells were grown in liquid YND or YNG medium (Start OD_{600}: 0.1) at 30 °C. Samples were taken at different time intervals and OD_{600} was measured. Bar graphs represent the doubling time (h) of WT, *dnm*1 and FL grown in YND or YNG medium. Error bars indicate ± SEM from two independent experiments. **(C)** Mitochondrial morphology of WT, *dnm1* and FL is visualized using preCOX4-mCherry. Maximum intensity projections of the z-axis are used to depict the images. WT depicts cells expressing endogenous Dnm1, *dnm1* indicates complete absence of Dnm1 protein, and FL represents *dnm1* cells expressing FL-Dnm1-GFP. Scale bar - 5 μm.

3.2.2 FL-Dnm1-GFP shuttles between the cytosol and mitochondria

Dnm1-GFP is visualized as distinct dynamic puncta in cells [94, 95, 266]. A similar phenotype of FL-Dnm1-GFP, when expressed in *dnm1* cells, was also observed in our experimental conditions (Fig. 3.3.A). The number of GFP puncta was quantified in cells fixed using formaldehyde, followed by microscopy analysis. Discrete GFP spots of variable sizes were observed in these cells, which typically ranged from 2 to 7 puncta/cell (Fig. 3.3.A). Further, to analyze if FL-Dnm1-GFP localized to mitochondria, z-sections of the cells were analyzed for co-localization of Dnm1-GFP with preCOX4-mCherry. Consistent with previous studies, our data

also show that a fraction of the FL-Dnm1-GFP puncta in a cell colocalizes with the mitochondrial marker (Fig. 3.3.B) [94].

An intriguing feature of Dnm1 puncta *in vivo* is their dynamic nature, with a small number of puncta displaying rapid movement [94, 95, 113]. This dynamic nature of FL-Dnm1-GFP was analyzed in this study by time-lapse imaging and the particle tracker plugin of ImageJ. Dnm1-GFP puncta were tracked in several cells, and several puncta in each cell were also tracked. A representative image of such tracking is shown in Fig 3.3.C. Extensive movement of the tracked puncta (arrow) in both the X and Y directions was observed, highlighting the dynamic nature of the protein (Fig. 3.3.C).

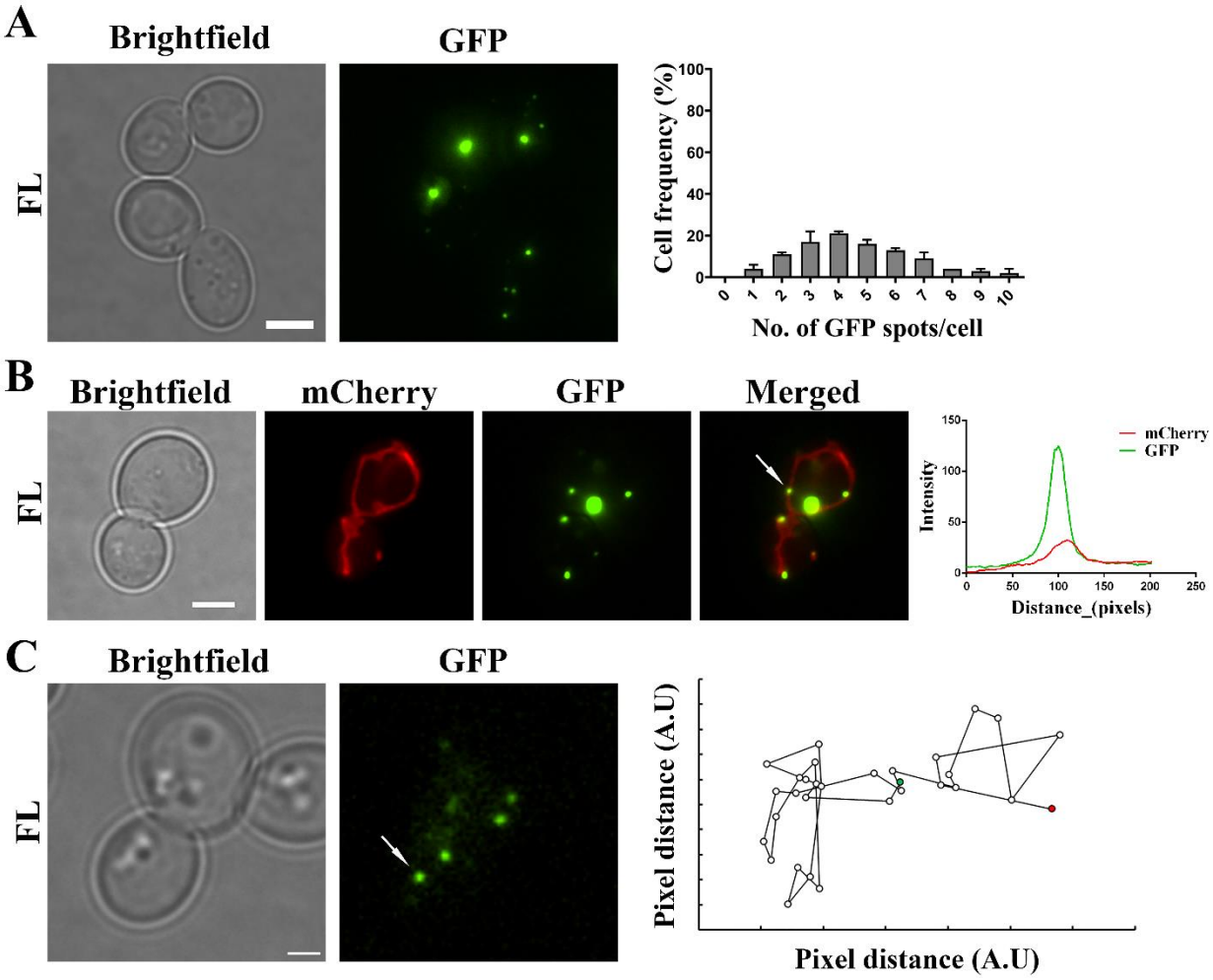

Fig. 3.3 FL-Dnm1-GFP is dynamic and shuttles between cytosol and mitochondria.
(A) *dnm1* cells expressing FL-Dnm1-GFP were analysed by fluorescence microscopy. Dnm1-GFP was visualized as distinct puncta of various sizes. Maximum intensity projection over the Z-axis was analyzed. Bar graphs represent the quantitative analysis of the number of Dnm1-GFP puncta/cell counted from randomly chosen Z-merged

fluorescence images. Error bars are obtained from two sets of independent biological replicates (50 cells in each) and are displayed as mean ± SEM. **(B)** Representative fluorescence image (single z plane) of cells expressing FL-Dnm1-GFP and preCOX4-mCherry. Randomly selected FL-Dnm1-GFP puncta (white arrow) were evaluated for co-localization with mitochondrial marker, and the extent of co-localization is also depicted as a line profile generated using ImageJ. **(C)** Time-lapse images of cells expressing FL-Dnm1-GFP were captured for 1 min. A single 0.28-µm section at the start of the imaging is shown. The arrow points to the Dnm1-GFP puncta that is tracked using the ImageJ plugin particle tracker. White circles indicate the recorded position of the puncta at each time point. Green and red circles indicate the start and end time of tracking. Scale bar - 5 µm.

3.2.3 Dnm1-His-HA retains its secondary structure *in vitro*

For *in vitro* studies, a plasmid expressing Dnm1 tagged with His-HA at the C-terminus and under the control of a galactose promoter was utilized (pRBA031). To ensure that the introduction of this tag does not interfere with the protein's functionality, pRBA031 was transformed into *dnm1* cells, and the mitochondrial morphology was examined. The mitochondrial phenotype of *dnm1* cells was effectively restored by pRBA031, indicating that Dnm1-His-HA fusion is functional *in vivo* (Fig. 3.4.A).

Dnm1 was expressed in the native host and subsequently purified by affinity chromatography to obtain insights into its mechanistic and structural properties. This approach facilitated the production of Dnm1 in its natural conformation, enabling accurate acquisition of data. *S. cerevisiae* cells containing pRBA031 were precultured in YND and shifted to raffinose-containing media (YNR). Following this, Dnm1 expression was induced by the addition of galactose (YPGal) to the YNR culture. Cells were cultured for another 6 h in the presence of YPGal. Protein expression was confirmed by western blotting of the whole cell lysate using the α-HA antibody (Fig. 3.4.B). Subsequently, Dnm1-His-HA was purified from the whole cell lysate by immobilized metal ion affinity chromatography (IMAC). The successful purification of Dnm1 was confirmed by both SDS-PAGE and western blotting using an α-HA antibody (Fig. 3.4.C). The purified protein was further confirmed using mass spectrometry analysis. A sequence coverage of 35% was obtained for Dnm1 (Fig. 3.4.D).

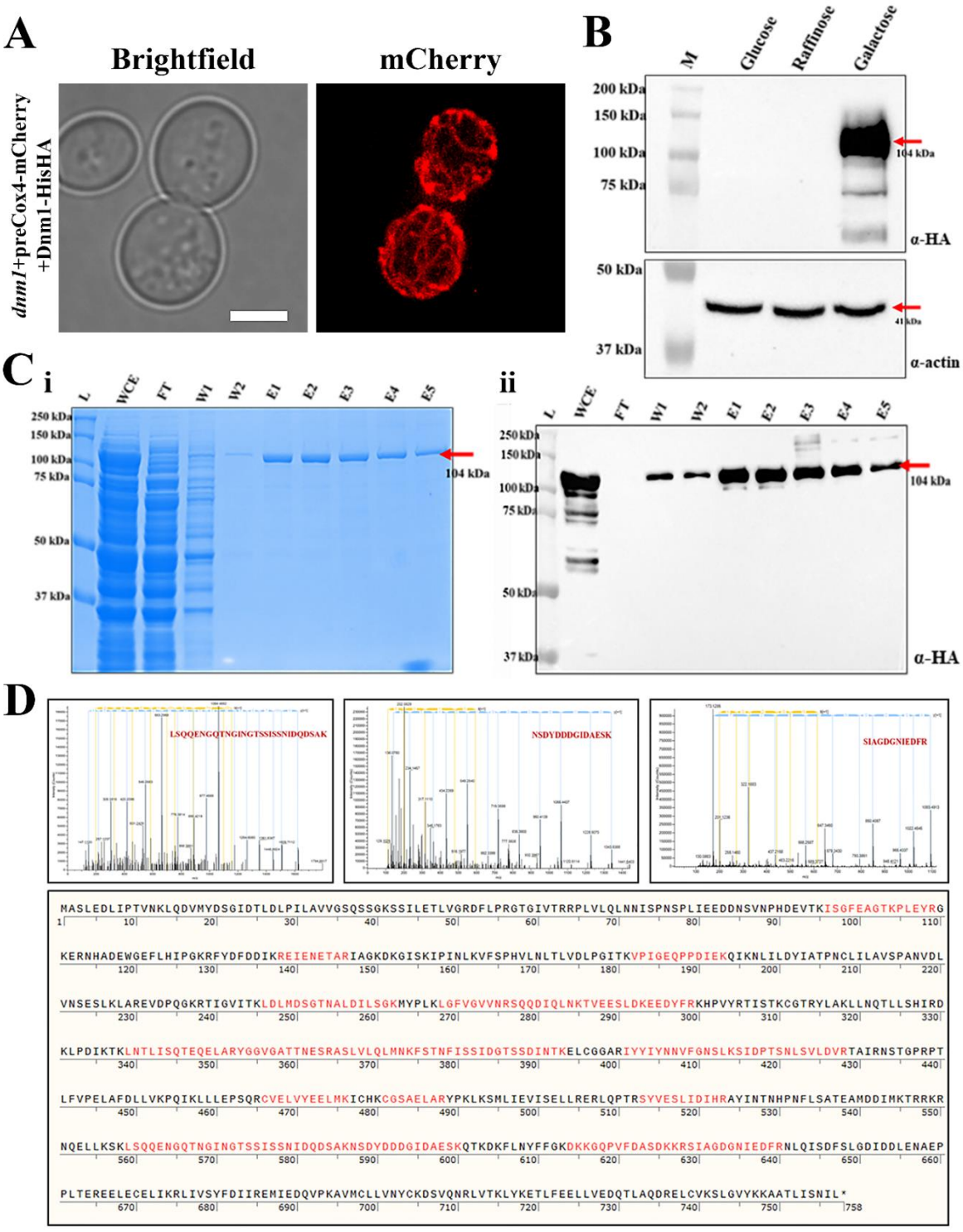

Fig. 3.4 Expression, purification, and mass spectrometry analysis of Dnm1-His-HA. (A) Mitochondrial morphology of *dnm1* cells expressing Dnm1-His-HA. preCOX4-mCherry was used to visualize mitochondrial morphology. Scale bar - 5 µm. **(B)** Cells expressing Dnm1-His-HA were cultured in YND and YNR media prior to induction by the addition of YPGal. The whole cell lysate was analyzed to confirm the expression of Dnm1 by western blotting using α-HA antibody (red arrow). A band of approximately 104 kDa was observed (M.W. of Dnm1 and His-HA tag is ≈ 85 kDa and 19 kDa, respectively). M represents the molecular weight marker. **(C)** represents affinity purification under native conditions. (i) Coomassie-stained SDS PAGE of the purification and (ii) western blotting using α-HA antibody is depicted. L – ladder, WCE – whole cell extract, FT – flow through, W – wash, E –

elute. **(D)** Representative MS/MS spectrum of purified Dnm1. Sequences highlighted in red represent peptide fragments of Dnm1 detected in MS/MS.

The structure of Dnm1 has not been reported in the literature to date. However, the structure of the human homolog DRP1 has been reported [73]. The purified protein was subjected to desalting and analyzed using far-UV CD spectroscopy to obtain hints of its secondary structure. The CD spectrum provides insights into the composition of the secondary structure of the protein, such as α-helices, β-sheets, turns, and random coils, based on the magnitude and distinct shape of the spectra [267, 268]. The far-UV CD spectra confirmed that the purified protein retained its secondary structure. Notably, two negative peaks were observed in the range of 220.5-221.5 nm and 208.5-209.5 nm, while a positive peak was observed in the range of 196.5-198 nm, indicating a α-helical structure (Fig. 3.5.A) predominantly. The sequence of Dnm1 was also analyzed using PSIPRED, a widely used bioinformatics tool for predicting the secondary structure of proteins [269]. This tool utilizes a combination of position-specific scoring matrices (PSSMs) and a machine learning algorithm to make accurate predictions about the secondary structure elements of a given protein sequence [269]. According to PSIPRED analysis, approximately 50.5% of the Dnm1 residues were predicted to form helices, while approximately 43% were predicted to form coils. In contrast, only 6.3% of the residues were predicted to form sheets (Fig. 3.5.B).

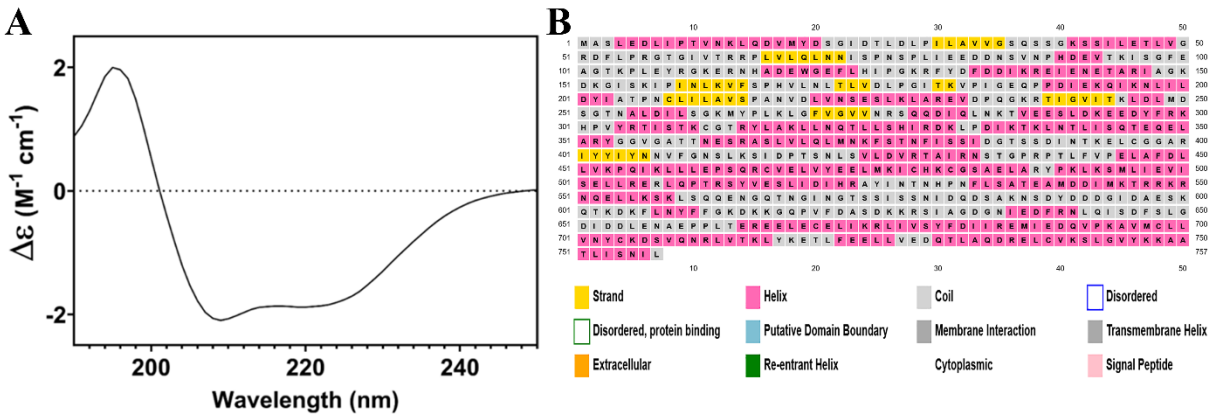

Fig. 3.5 Secondary structure determination of Dnm1. (A) The purified WT Dnm1-His-HA protein was subjected to a desalting column pre-calibrated with 20 mM phosphate buffer. The desalted protein eluted (0.25 mg/mL) in phosphate buffer was then analysed via far-UV CD spectroscopy. The data obtained are represented as Δε (M^{-1} cm^{-1}) vs wavelength (nm). **(B)** The PSIPRED algorithm was employed to predict the secondary structure elements of Dnm1. The predicted secondary structure includes helices (pink), strands (yellow), and coils (grey).

3.3 Discussion

The aim of this study was to investigate the structural and functional properties of Dnm1 fusion proteins. We used a combination of molecular, biochemical, and biophysical approaches to study these aspects. To visualize the localization of Dnm1 in cells, we generated the C-terminal fusion protein FL-Dnm1-GFP (Fig. 3.1.A). In literature, both C and N-terminal tagged Dnm1 fusion proteins are reported [94, 95, 99, 104, 270]. As mentioned earlier, the GTPase domain is at the N-terminus of the protein and hence, we resorted to the C-terminal fusion. This fusion protein was expressed in *S. cerevisiae dnm1* cells, and its localization was assessed using fluorescence microscopy and western blotting (Fig. 3.1.B). We observed that FL-Dnm1-GFP was expressed as multiple distinct green puncta consistent with the previous reports [94, 104]. Time-lapse imaging analysis revealed that Dnm1 is dynamic in nature, with some puncta displaying rapid movement. Also consistent with previous observations, we found that the majority of Dnm1 puncta are localized to mitochondria, as evident from the co-localization of FL-Dnm1-GFP with the mitochondrial marker preCOX4-mCherry (Fig. 3.3) [271].

Tagging a protein may sometimes result in impairment of its endogenous function. This emphasizes the importance of assessing the functional properties of the fusion protein. This evaluation is crucial to prevent any adverse effects on the protein's intended biological activity [272]. In this study, recombinant FL-Dnm1-GFP successfully restored the collapsed mitochondrial morphology of *dnm1* cells to a reticular phenotype, resembling cells expressing endogenous Dnm1 (Fig. 3.2.C). This finding suggests that FL-Dnm1-GFP was functional *in vivo*. Furthermore, overexpression of a protein may disrupt normal cell growth by burdening cellular machinery, affecting protein production and folding, leading to cellular stress and compromised

functions. The overexpressed protein may also interact with other cellular components and pathways, interfering with signaling cascades and essential protein-protein interactions, resulting in abnormal cellular responses and growth patterns. Additionally, overexpression can deplete critical cellular resources, such as energy and metabolites, necessary for normal cell division and metabolism [273]. We investigated the effect of FL-Dnm1-GFP expression on cell growth. When cultured in YND, the growth of *dnm1* cells expressing FL-Dnm1-GFP was similar to WT cells, indicating that the presence of the fusion protein did not significantly affect growth under these conditions (Fig. 3.2.A). However, when cells were cultured in YNG, the overall growth rate was slower for all strains compared to the YND medium. However, there were no notable differences in doubling time among WT, *dnm1*, and FL cells in YNG, signifying that overexpression did not affect cell growth (Fig. 3.2.B).

To gain insights into the structural properties of Dnm1, we used the C-terminal His-HA tagged Dnm1. Importantly; we observed that the addition of the tag did not affect the function of the protein, as Dnm1-His-HA was able to successfully restore the mitochondrial morphology in *dnm1* cells, similar to both endogenous Dnm1 and FL-Dnm1-GFP protein (Fig. 3.4.A). Furthermore, we used a native host for protein expression and purified the protein to obtain it in its natural conformation. Most *in vitro* studies using purified Dnm1 have expressed the protein in bacterial expression systems [100, 263, 274]. This may not be the most suitable way, as certain eukaryotic modifications that influence the protein structure and function may be missed. Dnm1-His-HA was successfully expressed and purified using affinity chromatography, resulting in approximately 1 mg of protein from 1g wet weight of cells (Fig. 3.4.B and 3.4.C). The presence of Dnm1 in the purified eluate was confirmed using MS analysis. MS accurately determined the mass of peptides generated through enzymatic digestion by analyzing their mass-to-charge ratio (Fig. 3.2.D). These peptide masses were compared to a protein sequence database, leading to the successful identification and confirmation of the Dnm1 sequence. Further, we employed far-UV

CD spectroscopy to gain insights into the secondary structure of the purified Dnm1-His-HA protein. The analysis of the far-UV CD spectra indicated that the purified protein maintained its characteristic secondary structure conformation, predominantly composed of α-helices (Fig. 3.5.A). This observation aligns with the results of the PSIPRED analysis, providing additional support to the CD data (Fig. 3.5.B).

It is interesting to note that Dnm1 undergoes repetitive assembly and disassembly on the target membrane. This process involves protein targeting to the membrane, GTP binding and hydrolysis, ultimately resulting in the remodelling of membrane curvature followed by fission and dislodging of the protein from the membrane. Several questions in this entire life cycle of Dnm1, from cytosol back to cytosol, are yet to be answered. What is the oligomeric status of the protein in all the intermediate steps? When and to which oligomeric state is GTP bound? Are there protein or lipid interactions specific at each step? Future experiments using the fusion proteins generated in this study will enable us to address some of these questions.

Chapter 4

Insights into the role of the conserved GTPase domain residues T62 and S277 in yeast Dnm1

Abstract

Mitochondrial division is a highly regulated process. The master regulator of this process is the multi-domain, conserved protein called Dnm1 in yeast. In this study, we systematically analyzed two residues, T62 and S277, reported to be putatively phosphorylated in the GTPase domain of the protein. These residues lie in the G2 and G5 motifs of the GTPase domain. Both residues are important for the function of the protein, as evident from *in vivo* and *in vitro* analysis of the non-phosphorylatable and phosphomimetic variants. Dnm1$^{T62A/D}$ and Dnm1$^{S277A/D}$ showed differences with respect to the protein localization and puncta dynamics *in vivo*, albeit both were non-functional as assessed by mitochondrial morphology and GTPase activity. Overall, the secondary structure of the protein variants was unaltered, but local conformational changes were observed. Interestingly, both Dnm1$^{T62A/D}$ and Dnm1$^{S277A/D}$ exhibited dominant-negative behavior when expressed in cells containing endogenous Dnm1. To our knowledge, we report for the first time a single residue (S277) change that does not alter the localization of Dnm1 but makes it non-functional in a dominant-negative manner. Intriguingly, the two residues analyzed in this study are present in the same domain but exhibit variable effects when mutated to alanine or aspartic acid.

This chapter is published as

Banerjee R, Mukherjee A, Adhikary A, Hussain S, Sharma S, Ali E, Nagotu S. Insights into the role of the conserved GTPase domain residues T62 and S277 in yeast Dnm1. **International Journal of Biological Macromolecules, 2023**.
DOI: https://doi.org/10.1016/j.ijbiomac.2023.127381

4.1 Introduction

The biogenesis of organelles has been an interesting topic for decades now. One such organelle that is essential in all eukaryotes is the mitochondrion. Regulation of mitochondrial dynamics by fission and fusion has been studied in various model organisms [275]. This process is extremely conserved and requires homologs of the dynamin-related proteins [86, 87, 260-262]. Dynamin-related protein 1 (Dnm1 in yeast and DRP1 in humans) is a large GTPase whose role in mitochondrial fission is now unequivocally accepted [81, 86, 87, 103, 116, 263]. It is a multi-domain protein that comprises an N-terminal GTP binding domain, a middle domain, a variable domain (B-insert), and a C-terminal GTPase effector domain (GED) [99, 100]. Interestingly, interacting partners of this protein required for its recruitment and association with the outer mitochondrial membrane (OMM) are variable in different organisms [88, 89, 93, 94, 98, 120, 139].

Yeast *Saccharomyces cerevisiae* is an immensely useful model organism for the study of organelle dynamics as this is a very conserved process. Dnm1-mediated mitochondrial fission is extensively studied in this model organism and has paved the way to understanding the molecular organization and function of the protein. The life cycle of Dnm1 unfolds in the cytosol, where it most likely exists as a dimer [104]. The process of targeting the protein to the membrane is not completely clear. However, a role for Fis1, a tail-anchored OMM protein, has been reported in the recruitment of Dnm1 [88, 89]. Additionally, two WD40 repeat adapter proteins, Mdv1/Caf4, that interact with Fis1 and Dnm1 are also a part of the fission complex at the OMM [92-94]. Lack of any of these proteins results in hampered mitochondrial division, albeit to a variable extent [89, 106, 276]. Electron microscopy studies have reported that Dnm1 forms large oligomers/helical structures at the OMM, with a radius similar to that of the mitochondrial girth [111, 116, 263]. These large oligomers are formed as a result of self-assembly and GTP binding of the protein [94, 111, 274]. The binding of GTP to the G-domain of the protein alters its

conformation and subsequently results in membrane constriction and fission [99, 116]. A role for endoplasmic reticulum (ER) in the spatial regulation of mitochondrial fission has also been reported. Contact sites between ER and mitochondria mark sites of the preconstriction on the OMM required for fission [20, 114]. Following fission, Dnm1 most likely dislodges itself from the membrane and is released into the cytosol. Thus highlighting the very dynamic nature of the protein in terms of its oligomeric status and sub-cellular localization [108]. Further, Dnm1 also interacts with other proteins such as Num1, Mdm36 and Srv2 (actin-binding protein) and aids in anchoring mitochondria to the cell cortex and regulates the organelle morphology and division [95, 96, 109]. Interestingly, a recent study reported the role of an intermembrane space protein, Mdi1, in the Dnm1-mediated mitochondrial division [277]. The authors propose that Mdi1 aids in Dnm1-mediated division by distorting the membrane from the inside of the organelle.

Remarkably, the structure and function of Dnm1 are highly conserved in all studied model organisms, including the human homolog DRP1. DRP1 is known to be regulated via post-translational modifications (PTM) such as phosphorylation, nitrosylation, ubiquitination and sumoylation [141, 143, 145, 147, 148, 151]. Such modifications regulate the response of cells to both intracellular and extracellular signals for the change of mitochondrial form and function. Phosphorylation of DRP1 at S616 and S637 has been extensively studied with respect to its activity [141, 143, 278]. Several kinases, such as PKA, FAK, ERK1/2, AKAP1, and TBK1, can phosphorylate DRP1 under various conditions [141, 143, 279-281]. Interestingly, no such modifications have been experimentally identified in *S. cerevisiae* Dnm1. DRP1 S616 is conserved in *S. cerevisiae* and a Threonine is present in the place of S637. On the other hand, Mehta and colleagues have reported that fission yeast lacks the S616 phosphorylation site, but S637 is conserved in this organism [282]. *Cyanidioschyzon merolae* is a red alga that has a single mitochondrion whose division requires Cm Dnm1. Recent studies have identified T139, a residue in the GTPase domain in Cm Dnm1, as an important site for phosphorylation by the Aurora

kinase [261]. The authors also report no role for this phosphorylation in the intracellular localization of the protein.

In this study, we aimed to identify residues important for the structure-function of *S. cerevisiae* Dnm1, which are also listed as putatively phosphorylated sites in the literature. Upon literature search and selection based on conservation, we chose five putative sites to analyze in this study. Using a holistic approach encompassing various methodologies, we have tried to understand the role of selected amino acid residues in the structure and function of the protein. Our data highlight the importance of two residues in the G2 and G5 motifs of the GTPase domain that affect the function of the protein both *in vivo* and *in vitro*.

4.2 Results and Discussion

4.2.1 Investigation of the phosphorylation status of *S. cerevisiae* Dnm1

Regulation of various dynamin-related proteins via phosphorylation has been previously reported [54, 141, 143, 145, 261, 283]. The importance of this modification in the function of DRP1 has been emphasized in earlier studies [70, 284]. Interestingly, there are no such studies on *S. cerevisiae* Dnm1. Data in Saccharomyces Genome Database (SGD: https://www.yeastgenome.org/) report 16 phosphorylation sites in Dnm1 compiled from various global phosphoproteome studies (Table 4.1) [214-219]. However, experimental verification of these sites has not been performed. In this study, we aimed to determine if Dnm1 undergoes phosphorylation in *S. cerevisiae* and if this modification is important for its function. To unravel this, we have taken two approaches: one is the expression and purification of the protein from *S. cerevisiae* and the identification of phosphorylation by mass spectrometry (MS). The second is to analyze the list of putative sites from SGD.

Dnm1 tagged with His-HA at the C-terminus was expressed under the GAL promoter in *S. cerevisiae* cells grown in galactose media and purified with the help of immobilized metal ion chromatography and subsequently analyzed by MS (Fig. 3.4C, 3.4D). Surprisingly, our MS

analysis was unable to identify any phosphorylated residues in contrast to the results obtained from the global phosphoproteome analysis (Fig. 3.4D). The purified protein was also resolved using a phos-tag SDS-PAGE and conventional SDS-PAGE and no mobility shift was observed upon treatment with calf intestinal alkaline phosphatase (CIAP) (Fig. 4.1A, 4.1B). We were unable to identify phosphorylation of the protein from our experimental setup, which may have been missed due to the dynamic nature of the modification, culture conditions, physiological state of the cells, and other experimental conditions. Hence, we resorted to the second approach of analyzing the putative sites obtained from SGD.

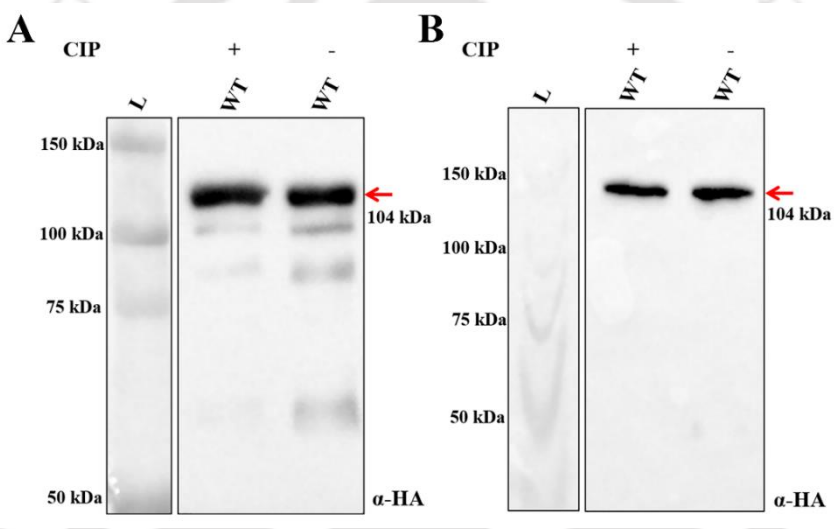

Fig. 4.1 Phos-tag gel analysis of Dnm1.
Purified WT Dnm1 was treated with CIAP and subjected to both **(A)** conventional and **(B)** 10 µM phos-tag SDS-PAGE followed by immunoblotting with α-HA antibody. The red arrow indicates Dnm1-His-HA band (104 kDa).

We analyzed the reported sites carefully and chose six out of the sixteen reported sites based on the following criteria (i) conserved residues across different yeast species, (ii) conserved sites with reported human DRP1 sites and (iii) number of times a site was reported in the literature. The selected residues are: T58, T62, S277, S575, S624, S629. All the selected residues were modified to either non-phosphorylatable alanine (A) or phosphomimetic aspartic acid (D) through SDM (Fig. 4.2). However, we were unable to mutate the T58 residue to either A or D

after multiple trials and continued with the other five residues (Fig. 4.3A, 4.3B, Table 4.1). The mutations were generated using the plasmid pRBA005, which has FL-*DNM1* fused to GFP. The confirmation of all *DNM1* variants was accomplished through restriction digestion using specific enzymes followed by DNA sequencing analysis (Fig. 4.2).

Table 4.1 Putative Dnm1 phosphorylation sites reported in SGD are mentioned in column 1. The selected residues in this study are italicized. Column 2 represents comparison of these reported residues of *Sc* Dnm1 with other yeast species (*Schizosaccharomyces pombe, Yarrowia lypolytica, Hansenula polymorpha, Candida albicans*). Column 3 shows corresponding residues found in DRP1.

***Sc* Dnm1 residue**	**Alignment with other yeast Dnm1**	**Corresponding residue in DRP1 (isoform 1)**	**References**
T62	Conserved	T59	[214]
S277	Conserved	T248	[214, 215]
S575	Conserved except in *H. polymorpha*	E554	[214, 216]
S624	S/L/T/P/-	S616	[214]
S629	S/L/T/P/-	Not aligned	[214-219]
T58	Conserved	T55	[214]
S77	S/T/D/E	D73	[214, 215]
T47	T in *S. cerevisiae*, N in all others	S44	[214]
S578	S/D/Q	G557	[214, 216]
S599	S/T/E/H/N	V581	[214]
S326	S/N/H	H295	[214]
S366	S/I/T/A/G	A331	[214]
S588	S/V/A/G/E	V570	[214, 215, 217]
S584	S/Q/H	S563	[214, 215]
S645	-/T/-/S	Not aligned	[217]
S648	-/-/-/T	Not aligned	[217]

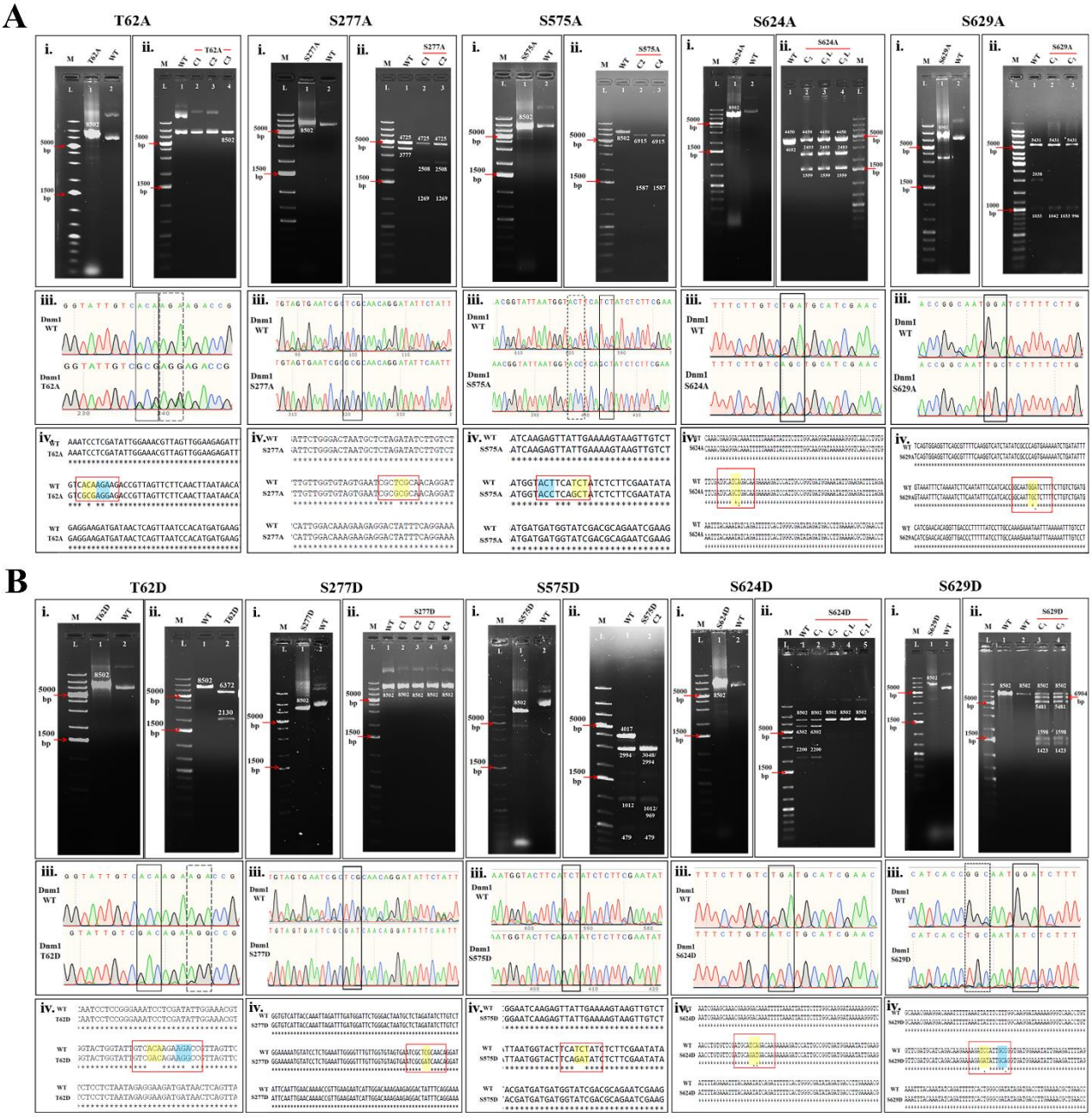

Fig. 4.2 Generation of Dnm1-GFP variants by SDM.
(A) and **(B)** represents SDM-mediated change of selected residues (T62, S277, S575, S624, S629) to either A or D variant, respectively. (i) agarose gel image depicting two-stage PCR product of template pRBA005 with respective primers required for the desired mutation. (ii) represents unique restriction digestion profiles of respective mutants compared to WT. (iii) represents further confirmation of the mutations with DNA sequencing analysis. Solid line boxes represent the key nucleotide changes for the intended mutations, while the dotted boxes represent nucleotide changes without changing the amino acid to create a unique restriction site for mutant screening. (iv) represents the sequence alignment of WT and mutants. The region of interest is marked with red outline. Key nucleotide mismatches that change the amino acid to A/D are highlighted in yellow. Blue highlighted regions show nucleotide changes that produce a unique restriction site for mutant screening without changing the amino acid.

4.2.2 Effect of Dnm1 variants on cell growth and protein expression

dnm1 cells expressing FL-Dnm1 and its variants were spotted onto selective fermentable (YND) and non-fermentable (YNG) plates by drop serial dilution assay to study the effect on cell growth (Fig. 4.3C, 4.3D). Expression of Dnm1 variants did not show any significant change in growth as compared to FL-expressing cells in YND (Fig. 4.3C). Interestingly, S624 that corresponds to the extensively studied S616 in DRP1 when mutated to A showed reduced growth in YNG compared to FL (Fig. 4.3D). No significant change in the growth of cells expressing other variants of Dnm1 was observed (Fig. 4.3C, 4.3D). Protein levels in exponentially growing cells cultured in YND were assessed by western blotting using α-GFP (Fig. 4.3E). Protein levels were quantified and are displayed as a fold change with respect to FL (Fig. 4.3E). Dnm1 T62A, S575A, and S624A/D levels were observed to be lower than FL by ~35% (Fig. 4.3E). On the other hand, S629D expression was reduced by ~26% when compared to FL (Fig. 4.3E). However, no significant difference was observed in the expression of T62D, S277A/D, S575D and S629A when compared to FL (Fig. 4.3E). Earlier studies have also reported DRP1 mutations resulting in disease conditions that are associated with reduced levels of the protein [191, 193].

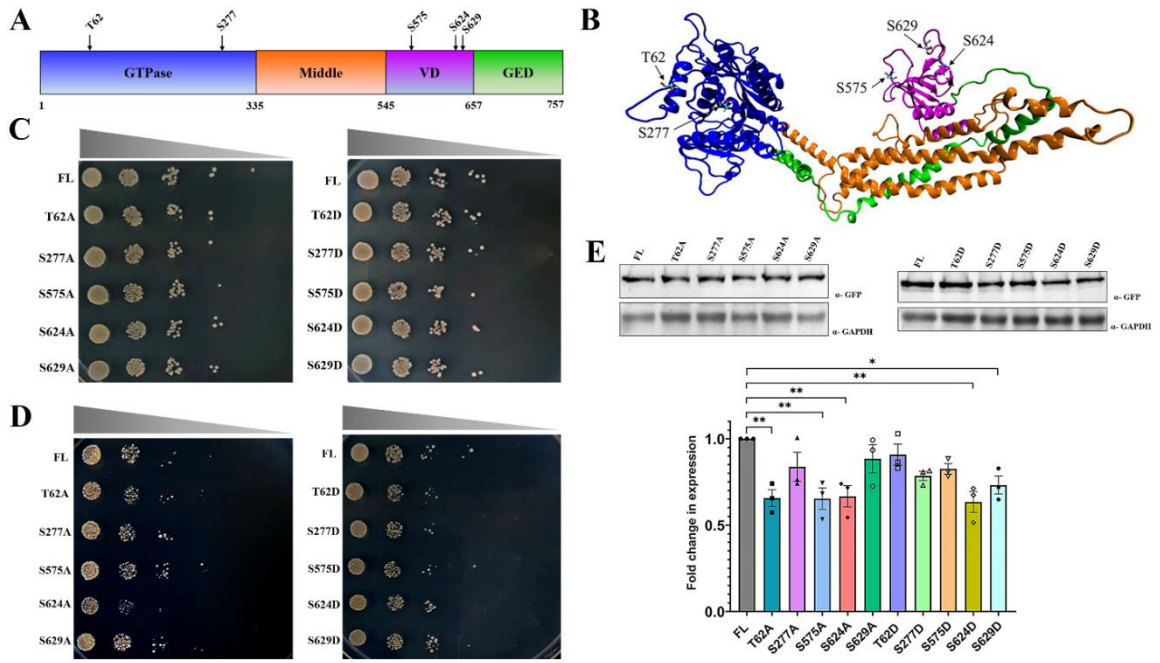

Fig. 4.3 Dnm1 residues selected for this study and the effect of mutations on cell growth and protein expression. (A) Schematic representing various domains of Dnm1: GTPase, middle, V domain (VD) containing B-insert and GED. The location of the residues selected for this study is depicted. (B) Representation of homology modeled structure of Dnm1 generated using Modeller program. Positions of the mutated residues are indicated. (C) and (D) represent growth analysis of *dnm1* cells expressing Dnm1-GFP variants under different carbon sources using drop serial dilution. Tenfold successive dilutions of log phase cultures were spotted onto (C) YND and (D) YNG plates and incubated in 30 °C for 3 days and 7 days, respectively. (E) Whole-cell lysates of *dnm1* cells expressing FL and variants of Dnm1-GFP equivalent to 3 OD_{600} were separated by SDS-PAGE and were subsequently detected using α-GFP antibody at 112 kDa. Band density was normalized to loading control (GAPDH) and compared to FL. Error bars indicate SEM obtained from 3 independent biological replicates. A one-way ANOVA with Dunnett's multiple comparison test was used to determine the importance of the difference between Dnm1 variants and cells expressing FL-Dnm1-GFP.

4.2.3 Dnm1 S624 corresponding to DRP1 S616 does not regulate the function of the protein

Mitochondria of *S. cerevisiae* cells expressing a functional Dnm1 display a characteristic reticular morphology signifying homeostasis between fission and fusion (Fig. 4.4) [86]. A complete lack of Dnm1 or mutations in specific residues that regulate the structure and function result in collapsed mitochondrial morphology in yeast (Fig. 4.4) [81, 86]. To evaluate if any of the above mutants affect the Dnm1-mediated mitochondrial division, we assessed the ability of the variants to rescue the mitochondrial morphology in *dnm1* cells. preCOX4-mCherry was used to mark the mitochondria in cells expressing FL and variants of Dnm1-GFP (Fig. 4.4) [271]. Cells were examined under a fluorescence microscope and graded for mitochondrial morphologies (reticular/branched, tubular, collapsed/fallen, and fragmented). When expressed in *dnm1* cells, FL-Dnm1-GFP almost fully recovered the WT reticular shape of mitochondria (Fig. 4.5A, 4.5B).

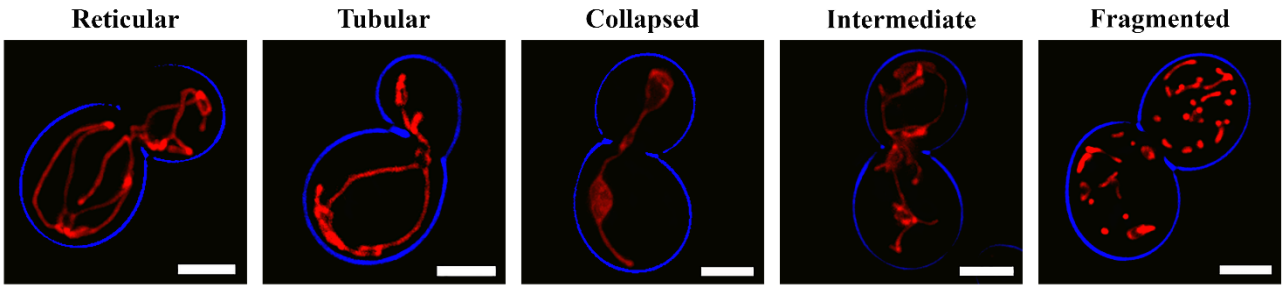

Fig. 4.4 Fluorescence images depicting various mitochondrial morphology phenotypes observed in *S. cerevisiae* cells and classified in this study. Mitochondria are visualized using preCOX4-mCherry. Blue line represents the cell boundary. Scale bar - 5 µm.

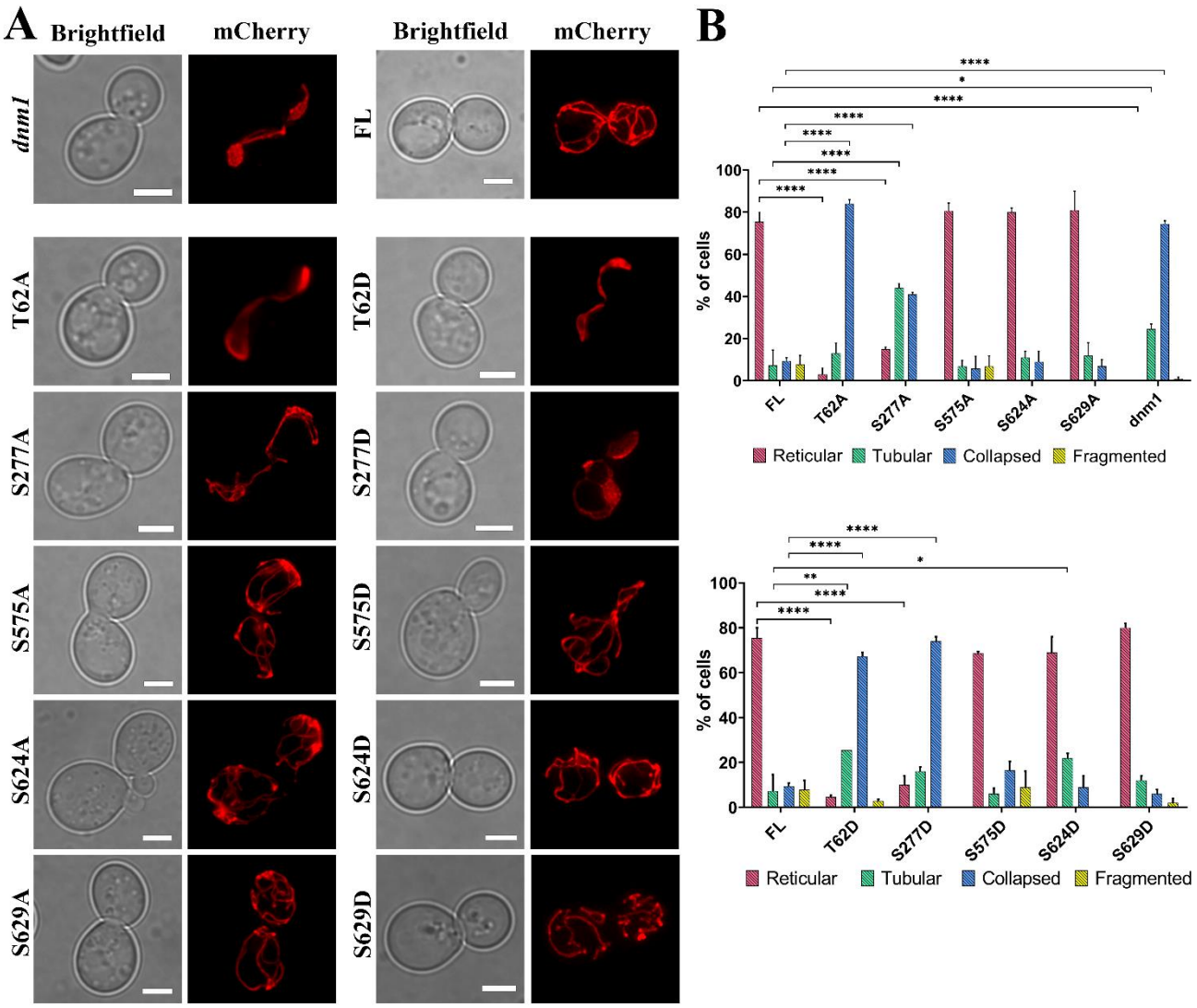

Fig. 4.5 Dnm1 T62 and S277 mutants exhibit defective mitochondrial fission.
(A) Mitochondrial morphology in *dnm1* cells upon the expression of FL and variants of Dnm1-GFP. preCOX4-mCherry was used as a marker to visualize mitochondria. Maximum intensity projections of the z-axis are used to depict the images. Scale bar - 5 µm. (B) Cells were grouped into four mitochondrial morphology phenotypes for quantification: reticular, tubular, collapsed and fragmented. Quantification was conducted on two sets of independent biological replicates, with 50 cells counted from each experiment. A two-way ANOVA with Dunnett's multiple comparison was used to evaluate the significance of the difference observed in cells expressing FL and variants of Dnm1-GFP. Error bars displayed are mean ± SEM.

Interestingly, most cells expressing either S624A/D variants exhibited reticulate mitochondrial morphology indicative of functional Dnm1. This is remarkably different when compared to the homologous residue in DRP1 (S616), which is crucial for the function and localization of the protein to mitochondria [54, 143, 278, 285]. A significant increase in tubular

morphology (≈ 22 %) when compared to FL (<10 %) was observed upon expression of S624D (Fig. 4.5A, 4.5B). FL-Dnm1-GFP was visualized as distinct dynamic punctate structures that are primarily localized to the cytosol and OMM marked with preCOX4-mCherry as reported earlier (Fig. 4.6A, 4.6B) [94]. In order to investigate whether the S624A/D variants exhibit altered Dnm1 localization, z-sections of these cells were examined for colocalization of Dnm1-GFP with preCOX4-mCherry (Fig. 4.6A, 4.6B). Dnm1$^{S624A/D}$ showed similar mitochondrial localization as visualized in FL-expressing cells (Fig. 4.6C, 4.6D).

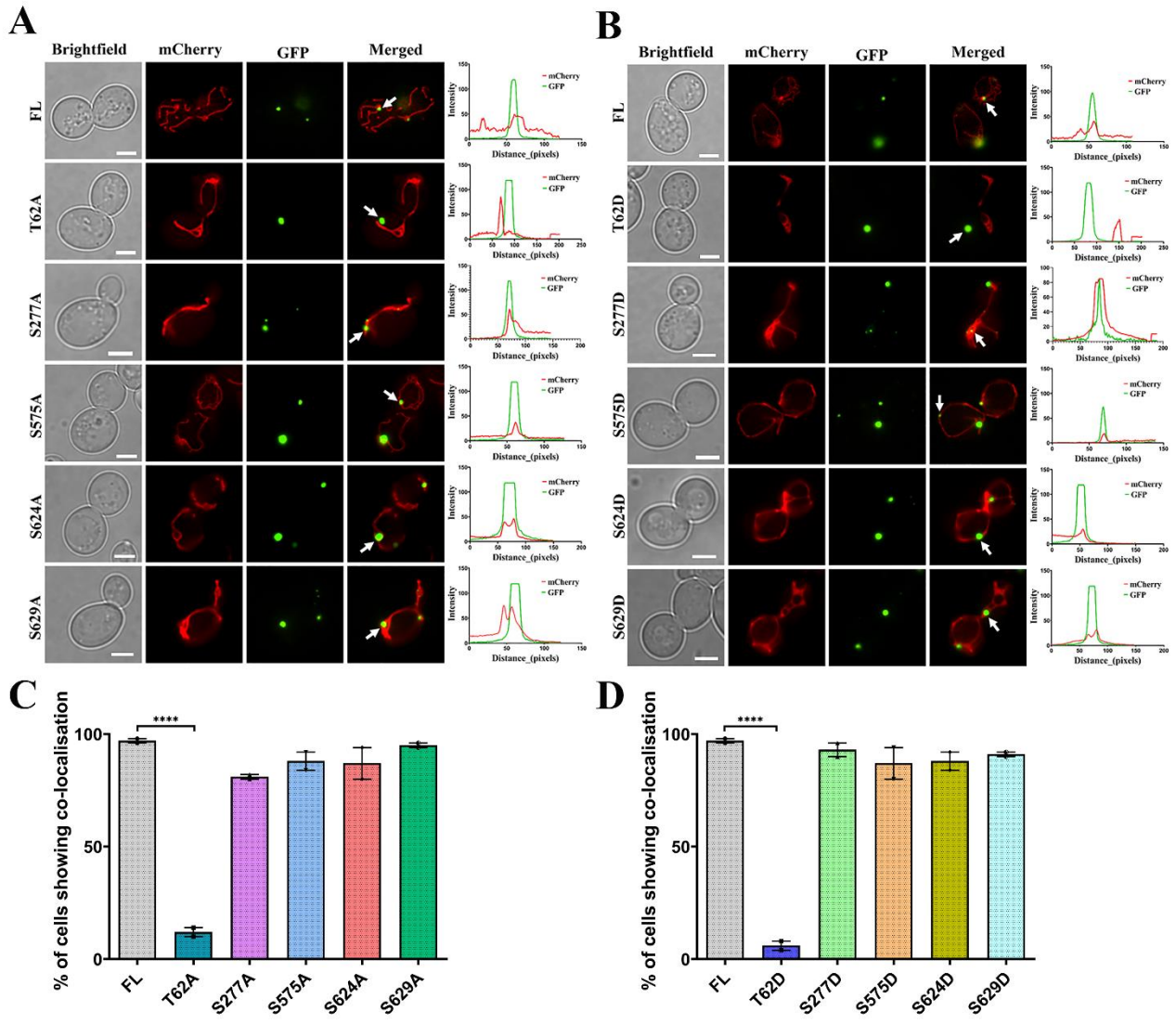

Fig. 4.6 Altered localization of Dnm1 was observed in T62A/D variants.
Representative fluorescence image (single z plane) of *dnm1* cells expressing Dnm1 variants and preCOX4-mCherry is depicted. Panel A represents 'A' variants and panel B represents 'D' variants. Randomly selected Dnm1-GFP puncta (white arrow) were evaluated for colocalization with mitochondrial marker and the extent of colocalization is also depicted as a line profile generated in ImageJ. Scale bar - 5 µm. (C and D) The extent of colocalization of

Dnm1-GFP with the mitochondrial marker was assessed by quantitative analysis. Statistical analysis was performed using a one-way ANOVA with Dunnett's multiple comparison test. Error bars are obtained from two sets of independent biological replicates (50 cells in each) and are displayed as mean ± SEM.

4.2.4 Dnm1 T62 and S277 reside in important GTP binding motifs and mutation in these conserved residues blocks protein function *in vivo*

Members of the dynamin superfamily have a characteristic large GTPase domain of around 300 amino acids, which sets them apart from other signalling GTPases [71, 286]. The GTPase domain of most dynamin superfamily members comprises five important GTP-binding motifs: G1 or P-loop (phosphate-binding loop) consisting of the highly conserved sequence GXQSXGKSSXLE, switch I with the central T62 in Dnm1 (DRP1 T59) as G2 element, switch II containing G3 element DLPG, G4 containing a conserved TKLD and a dynamin specific G5 or G-cap motif comprising GXXNRS^{277}Q (Fig 4.7A, 4.7B) [182]. These motifs are conserved among Dnm1 of different yeast species and human DRP1 (Fig. 4.7A). Earlier studies in yeast Dnm1 have analysed three residues in the G1 to G5 motifs [86, 94]. K41 in the G1 motif, when substituted with A showed loss of GTPase activity *in vitro* and, interestingly, when combined with WT Dnm1, stimulated the activity of the WT protein *in vitro* [94]. S42, when changed to N resulted in the loss of GTPase activity and the protein did not localize to the mitochondria *in vivo* [94]. On the other hand, T62, when replaced with D/F resulted in loss of GTPase activity *in vitro* and, when changed to A failed to rescue the *dnm1* mitochondrial phenotype *in vivo* [86, 94].

Interestingly, two of the predicted phosphorylation residues selected in this study, T62 and S277 are present in the conserved G2 and G5 motifs of the GTPase domain. In our study, we characterized the earlier reported T62 in detail and also, for the first time, characterized S277 residue in G5. The zoomed-in structure of the WT protein near T62 and S277 residues depicting key residues and hydrogen bonds in a vicinity of 20 Å is shown in Fig. 4.7C. Interactions via hydrogen bonds between the residue pairs, G50:E46, K137:F53, N160:L123 and R63:I154 were noticed. Interestingly, when these sites were changed to either A or D (T62A/D, S277A/D) the

protein was non-functional *in vivo* and a significant reduction in the number of cells exhibiting reticulate phenotype of mitochondria was observed (Fig. 4.5A, 4.5B). More than 85% of these cells exhibited collapsed and tubular phenotypes that represent defects in fission as observed in *dnm1* cells (Fig. 4.5A, 4.5B). On the other hand, cells expressing the B-insert variants, S575A/D and S629A/D, did not show any significant alteration in the mitochondrial morphology and resembled *dnm1* cells complemented with FL protein (Fig. 4.5A, 4.5B). It is to be noted that S629 is the most reported site to undergo phosphorylation in SGD, reported in six independent studies [214-219]. However, no change in mitochondrial morphology upon changing it to A/D was observed (Fig. 4.5A, 4.5B).

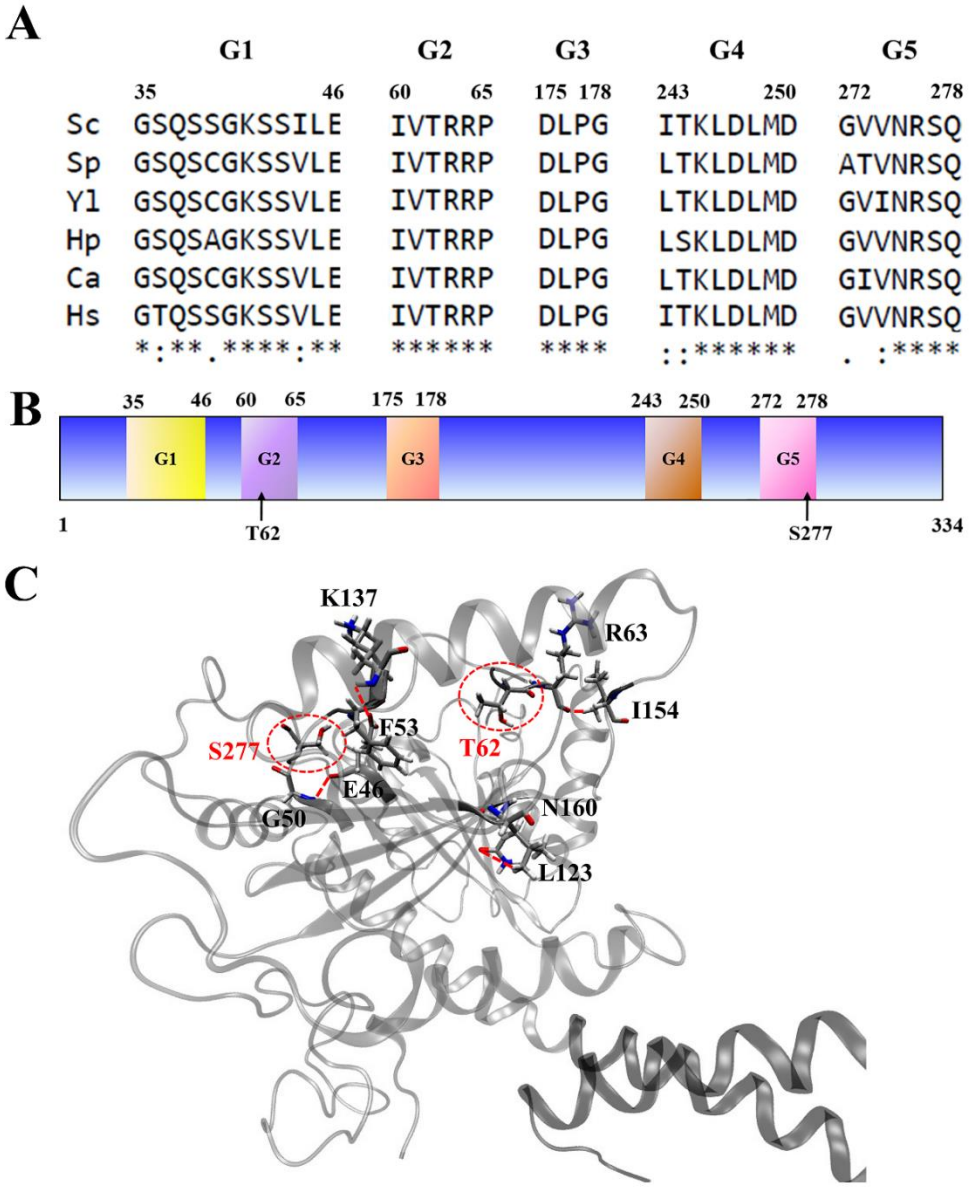

Fig. 4.7 T62 and S277 reside in the conserved G2 and G5 motifs of the GTPase domain.
(A) Sequence alignment comparing the five important motifs required for GTP binding of Dnm1 of different species. *Sc: Saccharomyces cerevisiae, Sp: Schizosaccharomyces pombe, Yl: Yarrowia lypolytica, Hp: Hansenula polymorpha, Ca: Candida albicans, Hs: Homo sapiens.* (B) The conserved T62 and S277 residues investigated in this study are located in the G2 and G5 motifs of the Dnm1 GTPase domain, respectively. (C) The zoomed-in view of the snapshots of WT Dnm1 structure highlighting T62 and S277 (marked with the red circle). The red dashed line represents the four key interactions in the analyzed 20 Å radii.

4.2.5 Dnm1$^{T62A/D}$ and Dnm1$^{S277A/D}$ exhibit variable puncta phenotype and localization

Dnm1-GFP characteristically forms distinct dynamic punctate structures that can be visualized in the cytosol and on mitochondria [94]. Typically, the puncta in cells expressing FL-Dnm1-GFP ranged in number from 2 to 7 puncta/cell (Fig. 4.8A, 4.8B). However, S277A/D depicted a reduced average number of puncta/cell. In both these variants, 2-4 distinct GFP puncta/cell were prevalently observed (Fig. 4.8A, 4.8B). Interestingly, only one puncta/cell was present in over 90% of the T62A/D expressing cells. These puncta were also structurally larger than those observed in FL and in the S277 variant (Fig. 4.8A, 4.8B). This is consistent with earlier studies that identified T62D/F as a significant aberrant structure that may result in dead-end aggregates [94]. Dnm1$^{T62A/D}$ and Dnm1$^{S277A/D}$ displayed differences in their *in vivo* localization pattern despite exhibiting indistinguishable non-functional behavior *in vivo*. Upon analysis of the colocalization of T62A/D variants, the large aberrant cytosolic structures did not associate with mitochondria (Fig. 4.6A, 4.6B). However, the localization of these aberrant structures reported in earlier studies was not the same (cytosolic and mitochondrial), presumably because different parental strains were used [94, 287]. Surprisingly, on the other hand, the S277A/D variants were observed to colocalize with mitochondrial-targeted mCherry similar to the FL protein, suggesting no influence of the change in the amino acid on the localization of the protein (Fig. 4.6A, 4.6B). Interestingly, all the B-insert variants (S575A, S575D, S624A, S624D, S629A, S629D) tagged to GFP showed a similar pattern of mitochondrial localization as the FL protein (Fig. 4.6A, 4.6B). Quantitative analysis of the colocalization is represented in Fig. 4.6C and 4.6D.

Owing to the altered phenotype of mitochondrial morphology, Dnm1 puncta number and localization, T62A/D and S277A/D were chosen for further analysis.

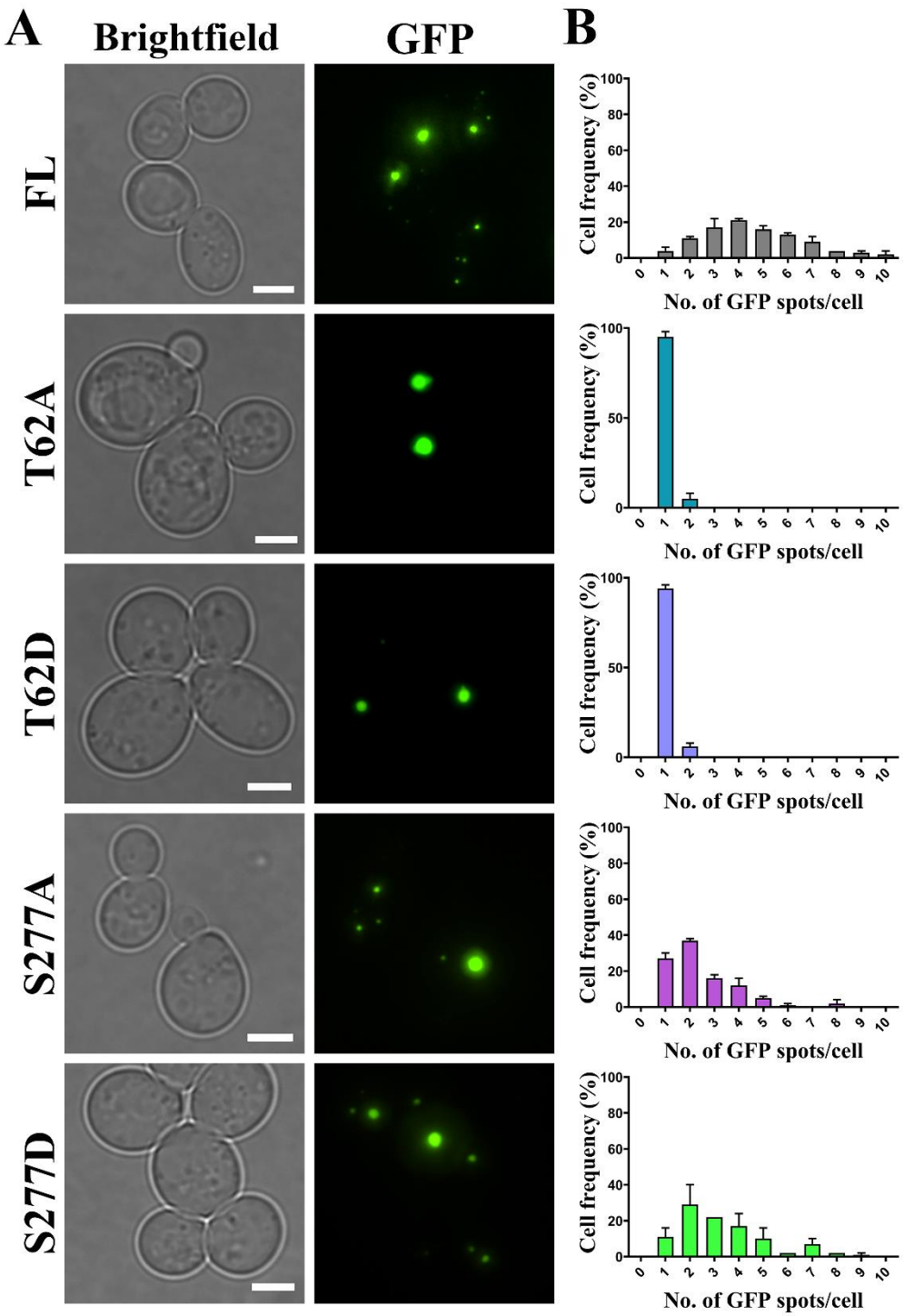

Fig. 4.8 GFP puncta phenotype is altered in Dnm1 variants. **(A)** Representative fluorescence images of *dnm1* cells expressing FL, T62A/D and S277A/D Dnm1-GFP variants. Dnm1-GFP was visualized as distinct puncta of various sizes. Maximum intensity projection over the z-axis were analyzed. Scale bar - 5 µm. **(B)** Bar graphs represent the quantitative analysis of the number of Dnm1-GFP puncta/cell counted from randomly chosen z-merged

fluorescence images. Error bars are obtained from two sets of independent biological replicates (50 cells in each) and are displayed as mean ± SEM.

4.2.6 Dnm1$^{T62A/D}$ and Dnm1$^{S277A/D}$ do not exhibit altered secondary structure and oligomerization but show reduced GTPase activity *in vitro*

In vivo, various structural forms (monomer, dimer, oligomer) of Dnm1 have been reported and hence, the protein's structure-function interdependence is crucial for regulating mitochondrial morphology. To investigate the structural aspects, a C-terminal His-HA tagged Dnm1 under the control of the galactose promoter was used (pRBA031). This plasmid was able to rescue the *dnm1* mitochondrial phenotype, suggesting that the plasmid is functional *in vivo* (Fig. 4.9). T62A/D and S277A/D mutations were generated using pRBA031 as a template resulting in plasmids pRBA032, pRBA033, pRBA034, pRBA035 (Fig. 4.10; Table 2.2). Protein expression of all variants was similar to that of WT (Fig. 4.11A). WT, T62A/D and S277A/D variants were purified to homogeneity and were analyzed by far-UV CD spectroscopy as described in materials and methods (Fig. 4.11B, 4.11C, 4.11D). Interestingly, the far-UV CD spectra of all Dnm1 variants were similar to that obtained for the WT protein, suggesting that the mutations did not alter the overall secondary structure significantly (Fig. 4.11D). Two negative peaks were obtained typically in the range of 220.5-221.5 nm and 208.5 - 209.5 nm, whereas the positive peak appeared in the range of 196.5-198 nm in all samples suggesting a predominant α-helical structure (Fig. 4.11D). The minor difference observed in the helical structures of the mutants is insignificant and is attributed to the minor differences in protein concentrations.

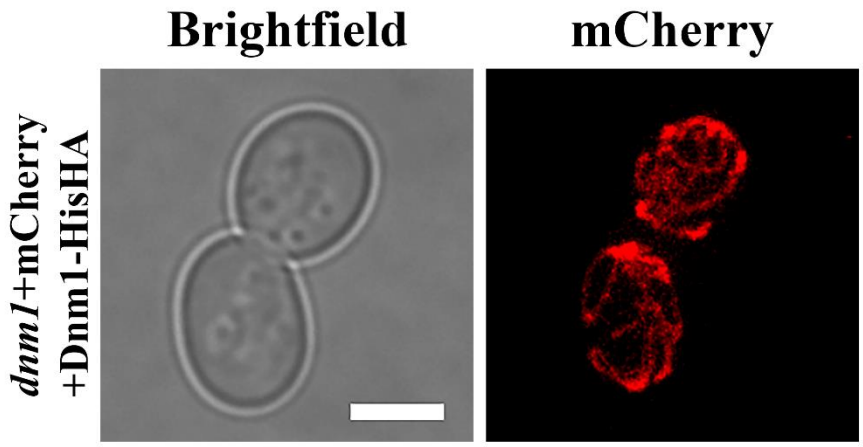

Fig. 4.9 C-terminal His-HA tagged Dnm1 is functional *in vivo*
Mitochondrial morphology of *dnm1* cells expressing both preCOX4-mCherry and galactose-induced Dnm1-His-HA visualized using fluorescence microscopy. Scale bar - 5 µm.

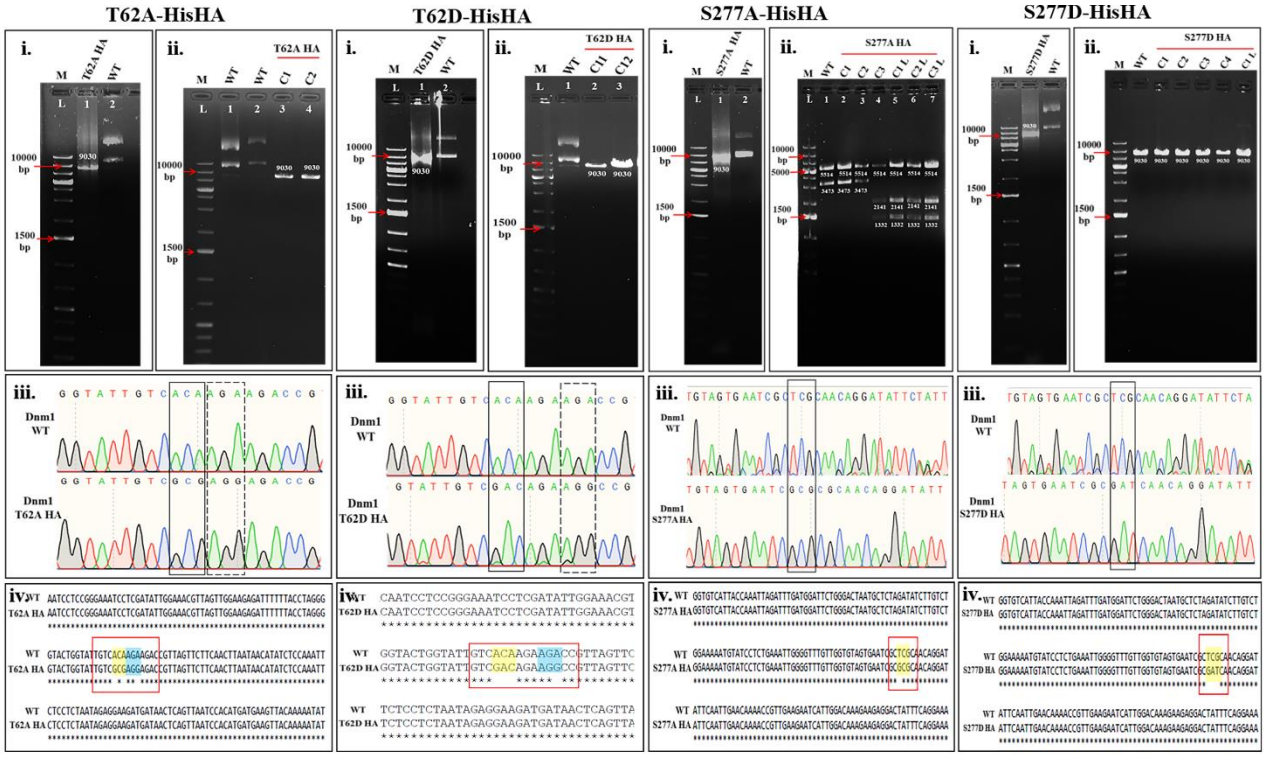

Fig. 4.10 Generation of Dnm1-His-HA variants by SDM. SDM-mediated generation of C-terminal His-HA tagged Dnm1 T62A, T62D, S277A and S277D, respectively is shown. (i) represents two stage PCR product of template pRBA031 with respective primer pairs required for the desired mutations. (ii) represents unique restriction digestion profiles of respective mutants compared to WT. (iii) represents further confirmation of the mutations with DNA sequencing analysis. Solid line boxes represent the key nucleotide changes for the intended mutations, while the dotted boxes represent nucleotide changes without changing the amino acid to create a unique restriction site for mutant screening. (iv) represents the sequence alignment of WT and mutants. The region of interest is marked with red outline. Key nucleotide mismatches that change the amino acid to A/D are highlighted in yellow. Blue highlighted regions show nucleotide changes that produce a unique restriction site for mutant screening without changing the amino acid.

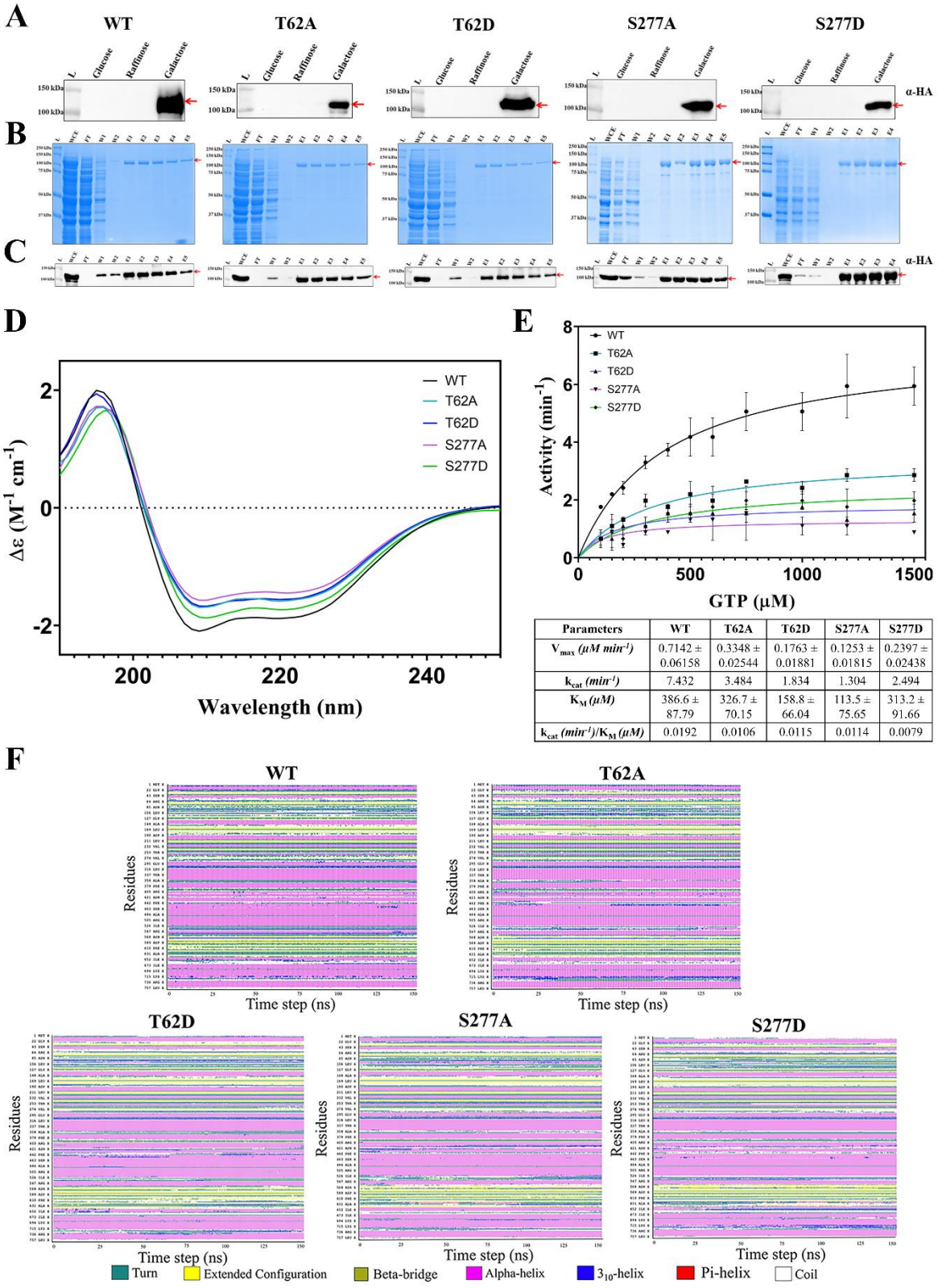

Parameters	WT	T62A	T62D	S277A	S277D
V_{max} *(μM min⁻¹)*	0.7142 ± 0.06158	0.3348 ± 0.02544	0.1763 ± 0.01881	0.1253 ± 0.01815	0.2397 ± 0.02438
k_{cat} *(min⁻¹)*	7.432	3.484	1.834	1.304	2.494
K_M *(μM)*	386.6 ± 87.79	326.7 ± 70.15	158.8 ± 66.04	113.5 ± 75.65	313.2 ± 91.66
k_{cat} *(min⁻¹)*/K_M *(μM)*	0.0192	0.0106	0.0115	0.0114	0.0079

Fig. 4.11 Dnm1$^{T62A/D}$ and Dnm1$^{S277A/D}$ do not exhibit altered overall secondary structure but show reduced GTPase activity *in vitro*. Cells expressing WT and mutant Dnm1 were cultured in YND and YNR media prior to induction by the addition of galactose. (A) represents the analysis of the whole cell lysates to confirm expression of the Dnm1 by western blotting using α-HA antibody (red arrow at 104 kDa). (B) and (C) represent affinity

purification under native conditions. Coomassie-stained SDS-PAGE of the purification and western blotting using α-HA antibody is depicted (red arrow at 104 kDa). L – ladder, WCE – whole cell extract, FT – flow through, W – wash, E – eluate. (D) Far-UV CD spectra of 0.25 mg/mL WT, T62A, T62D, S277A and S277D variants. Δε for each sample was calculated. (E) GTP hydrolysis by purified WT and Dnm1 protein variants. Dnm1 GTPase activity was determined using an enzyme-coupled assay by monitoring NADH depletion, which was subsequently translated to activity (min^{-1}). Data from two independent biological replicates were fit to a Michaelis-Menten model. Kinetic parameters V_{max}, k_{cat}, K_M and k_{cat}/K_M are shown. (F) Calculated secondary structure analysis of WT and mutants for 150 ns MD trajectories using timeline plugin in VMD. Timeline creates 2D box plot (time vs. structural residues) that shows detailed structural events of an entire system over an entire MD trajectory. The structural elements are shown in colored boxes below the secondary structure map.

Dynamin-related proteins, including yeast Dnm1, form higher-order oligomeric structures [94, 120, 131, 263, 283, 288]. To analyze if Dnm1 variants can also form higher-order structures, WT, T62A/D, and S277A/D were separately resolved by size exclusion chromatography (SEC) and native polyacrylamide gel electrophoresis (Native PAGE). WT Dnm1 yielded one large peak and two minor peaks in SEC, corresponding to higher, moderate, and lower-order oligomers, respectively, as reported earlier (Fig. 4.12A) [122]. S277A/D variants showed a similar SEC profile as the WT (Fig. 4.12A). However, T62 variants mostly lacked minor peaks in SEC, suggesting a prevalence of higher-order Dnm1 species (Fig. 4.12A). This observation aligns with the GFP puncta phenotype in T62A/D variants, where smaller dynamic spots in FL-Dnm1 cells were absent (Fig. 4.8, Fig. 4.12A). Although the exact molecular weights of the eluted proteins could not be determined from SEC, the presence of higher-order structures eluting as a prominent peak was evident. However, we cannot comment on the nature of these higher-order structures in WT and Dnm1 variants if these are functional or non-functional structures. Additionally, Native PAGE profiles of WT and S227A/D were similar, whereas T62A/D showed minor differences in band intensities for higher-order oligomers (Fig. 4.12B). The data from the above experiments suggests that Dnm1 variants do not exhibit significant defects in oligomerization and formation of higher-order structures.

Interestingly, both these variants are non-functional *in vivo* despite forming higher-order structures *in vitro*, prompting us to speculate that these structures are non-functional at different levels and may be different in their inter-molecular interactions, thereby affecting GTP

hydrolysis. In order to assess this, we analyzed the *in vitro* GTPase activity with increasing amounts of GTP to determine the V_{max}, K_M and k_{cat}. We observed that at the physiological salt concentration (150 mM NaCl) all variants exhibited significantly reduced GTPase activity (up to 1.5 mM of GTP) in contrast to WT (Fig. 4.11E). V_{max}, K_M, k_{cat}, k_{cat}/K_M values obtained for the WT and Dnm1 variants are shown in Fig. 4.11E.

If T62 and S277 undergo phosphorylation, it is interesting to note that both A/D variants exhibit the same mitochondrial phenotype, suggesting that the modification is dynamic and spatiotemporally regulated. Phosphorylation of these residues may affect GTP recruitment to Dnm1 and subsequent GTP hydrolysis. It will be interesting to analyze if these variants are not only hampered in GTP hydrolysis (as shown above) but also its binding. A role for phosphorylated residues in GTP binding and its hydrolysis has been reported for Rab and Ras GTPase in earlier studies [289, 290].

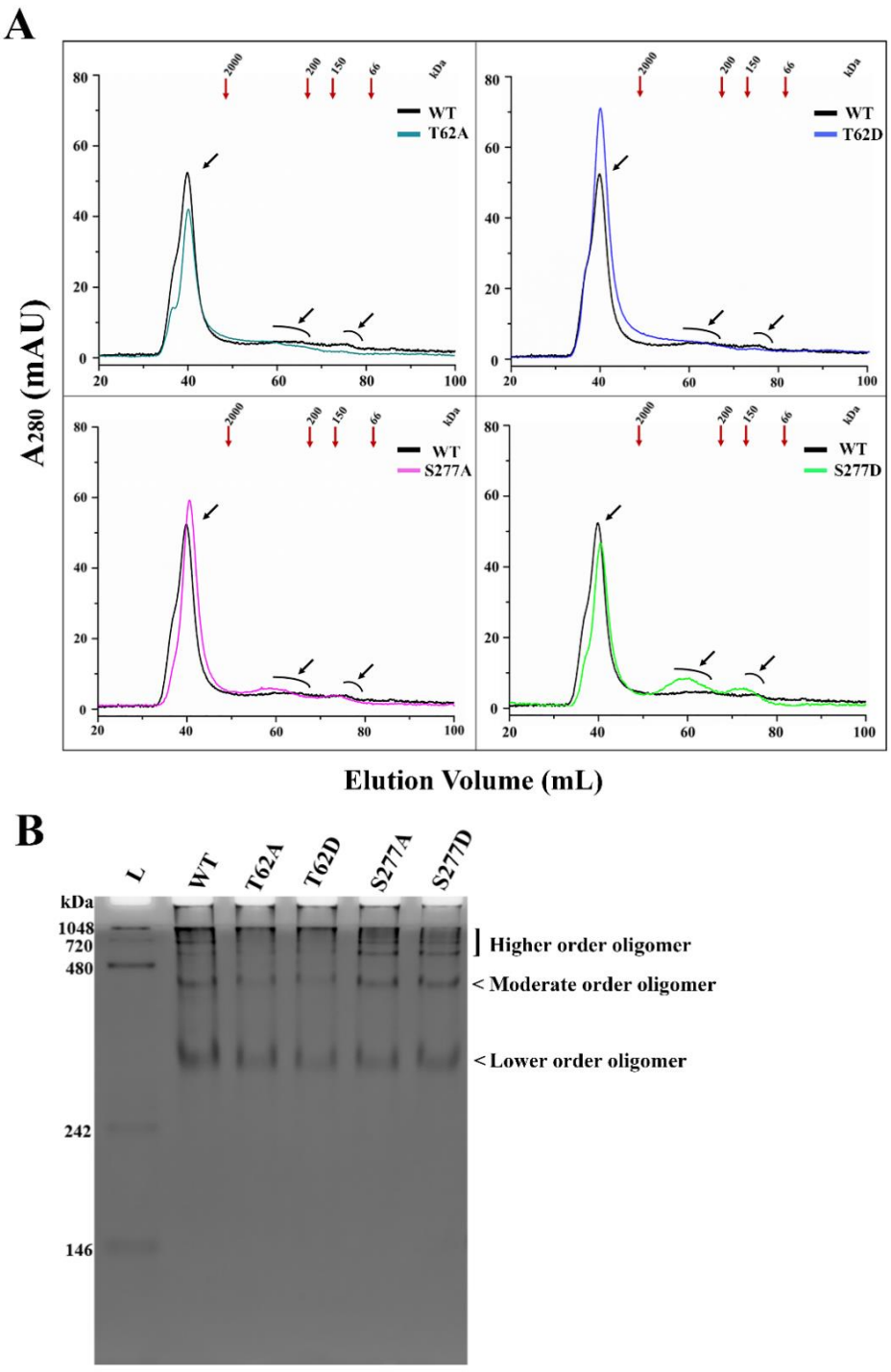

Fig. 4.12 Dnm1 variants can form higher-order structures.
(A) The oligomeric forms of WT and variants of Dnm1 were characterized by SEC using HiLoad™ 16/600 Superdex™ 200 pg column. The elution profiles of standard molecular weight protein markers are indicated with inverted arrows on top of the chromatogram. The molecular weight standard protein markers in kiloDalton (kDa) include (Blue Dextran, 2000 kDa, β-Amylase, 200 kDa; Alcohol dehydrogenase 150 kDa; Albumin, 66 kDa). WT and S277A/D mutant variant waere primarily eluted as 1 large peak (>2000 kDa; black arrow) and 2 minor broad peaks (200-1000 kDa and 80-150 kDa, respectively; black arrow with arch). Dnm1 T62A/D mutants predominantly showed only 1 large peak (>2000 kDa) with little or no minor peaks. (B) Native PAGE differentiated higher, moderate, and lower-order multimeric Dnm1 self-assembly units in WT and variants. L – ladder.

4.2.7 Computational studies to understand the dynamics of Dnm1$^{T62A/D}$ and Dnm1$^{S277A/D}$

Earlier studies have reported the use of computational structural analysis and machine learning to understand the structure-function relationship of dynamin-like proteins [263, 291]. To understand the effect observed due to mutations in the GTPase domain, the dynamics of the protein (WT, T62A/D and S277A/D variants) was analyzed using MD trajectories and compared. The RMSD plots for all five trajectories are shown in Fig. 4.13. Interestingly, despite the mutation sites being present in the GTPase domain, no significant fluctuations in the RMSD of this domain were observed. The RMSD fluctuations for the GTPase domain were quite small throughout the simulation for WT and T62A/D. However, certain conformational changes were observed at 100 ns in the S277A and the RMSD value obtained was higher for the GTPase domain in S277D as compared to other Dnm1 variants (Fig. 4.13). Furthermore, quite large fluctuations were observed in the GED in WT and T62D. On the other hand, in T62A and S277A, large fluctuations were observed for the B-insert. A high deviation in RMSD was seen in the B-insert of S277A at 120 ns (Fig. 4.13). Earlier studies have reported that intramolecular interactions between GTP binding and GED of Dnm1 are crucial for the function of the protein. A role for B-insert in the interaction of Dnm1 with its interacting partner Mdv1 has been shown [99, 204]. Loss of such intra-molecular interactions and altered interaction with proteins at the mitochondrial membrane upon mutating T62 and S277 can be envisaged. The fluctuations of individual amino acid residues were also analyzed and quantified with the RMSF. The protein Cα atoms were considered for the calculations of the RMSF values (Fig. 4.14). Large fluctuations were seen in the B-insert of the T62D (Fig. 4.14). The RMS fluctuations in the WT are the lowest compared to all the variants in the B-insert (Fig. 4.14). The fluctuation in the Rg as a function of time for WT and Dnm1 variants was estimated to determine the compactness of the protein. The average Rg value in the range of 36.60 to 47.19Å was obtained for all the cases (Fig. 4.15). The decrease in Rg value for S277A signify overall compactness of the protein (Fig. 4.15).

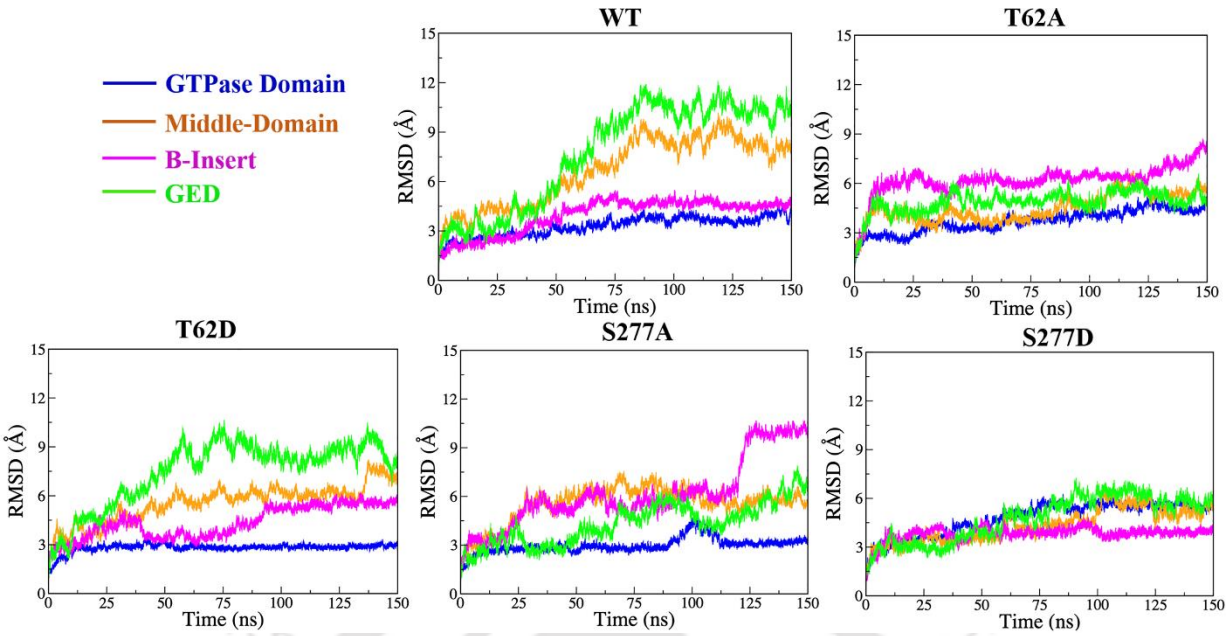

Fig. 4.13 Calculated RMSD for the WT and mutant structures of Dnm1 for 150 ns of simulated trajectory. High fluctuations were observed in the GED in WT, T62D and S277D. However, the B-insert showed large fluctuations in T62A and S277A. The GTPase domain shows very small RMSD fluctuation in all cases except S277D.

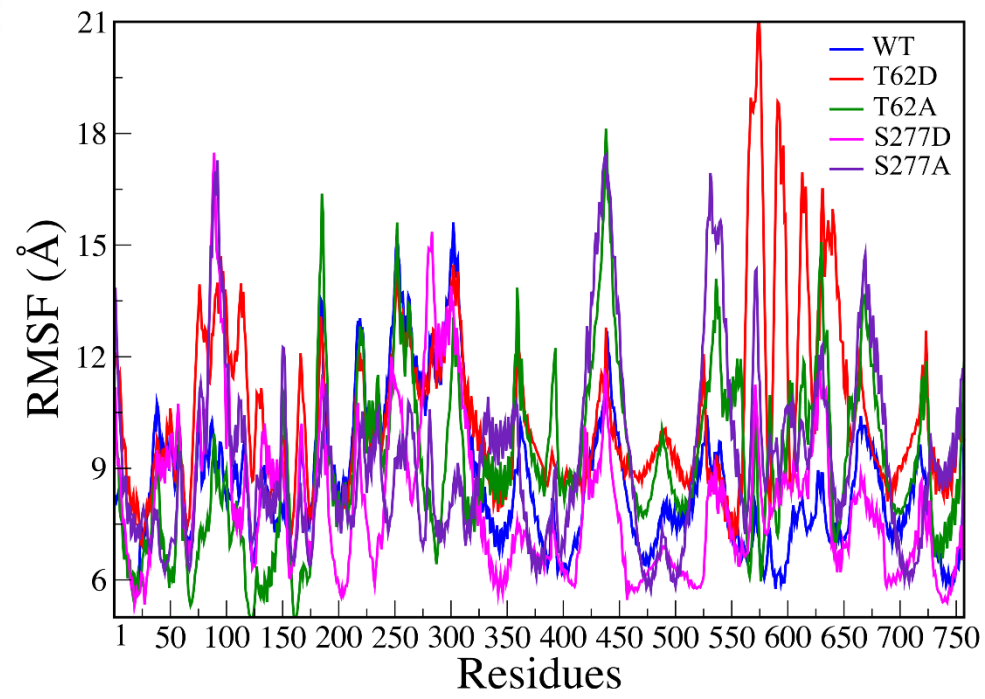

Fig. 4.14 Calculated RMSF of WT and variants of Dnm1. T62D mutation results in increase in the individual residue fluctuation around B-insert.

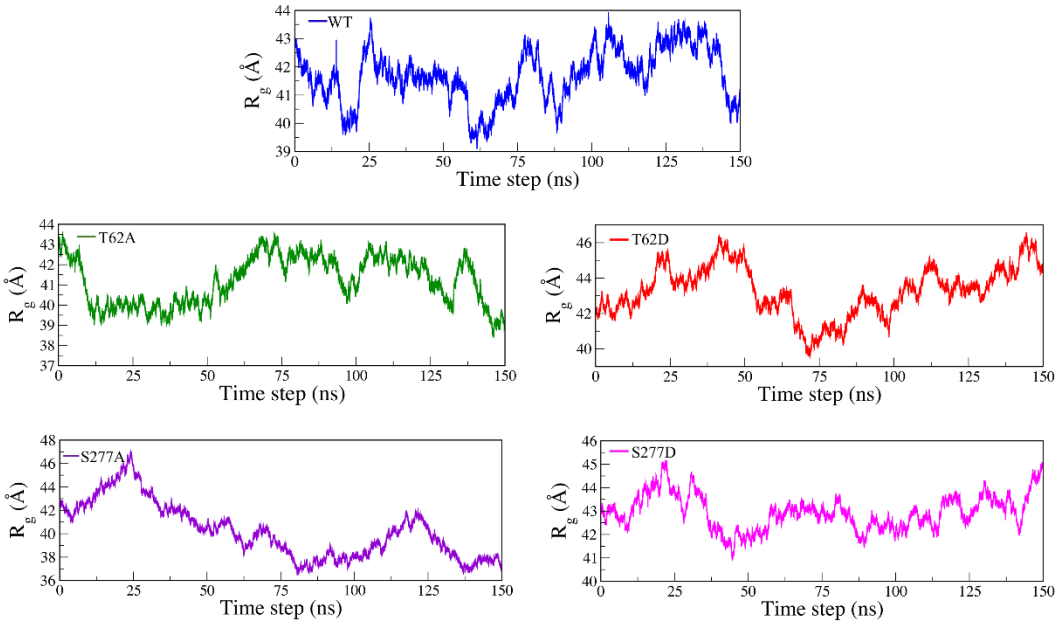

Fig. 4.15 Calculated Rg for the WT and mutants to compare the structural compactness of the protein. The Rg value was observed to change over the time in each case. The average Rg value was in the range of 36.60 to 47.19Å for all cases. In S277A, the Rg value was observed to be higher initially. However, over time it decreases, which reveals increased compactness of the protein.

Timeline plugin in VMD software was used to further confirm our CD result and to observe if Dnm1$^{T62A/D}$ and Dnm1$^{S277A/D}$ exhibit any changes in the secondary structure. This provides detailed information about the secondary structure all through the simulation. As shown, the secondary structure content was stably maintained by all residues in the WT and Dnm1 variants, and no significant variation in the overall secondary structure of WT and Dnm1 variants was observed, similar to as observed in our CD data (Fig. 4.11D, 4.11F; Table 4.2). Analysis of secondary structure using DSSP also suggests a predominant α-helical structure of the WT and Dnm1 variants (Table 4.2). However, upon comparing the dynamics of the WT and variant structures, local changes in the secondary structures, especially in the orientation, were observed (Fig. 4.16A). Changes in the local interaction network in response to T62A mutation include the loss of hydrogen bond interaction between R63:I154 (Figure 4.16A; Table 4.3). The other three hydrogen bond interactions i.e., G50:E46, K137:F53 and N160:L123 were intact as observed in WT (Figure 4.16A; Table 4.3). This loss of hydrogen bond interaction resulted in an

altered orientation of the loop region (residues P105 to E118; A148 to P158; P183 to I203 and S277 to V287). The residues 86-100 formed coils in WT and in the presence of mutation, formed α-helical structure. A similar loss of hydrogen bond interaction between R63:I154 was also observed upon T62D mutation (Fig. 4.16A; Table 4.3). However, the structural orientation was less altered in T62D. The loss of hydrogen bond interaction (R63:I154) resulted in a tilt in the helix conformation (residues M1- G22) and altered orientation of the helix-loop (V49 to Q278). In S277A and S277D, no loss of hydrogen bonds was observed (Table 4.3). Conversion of the coil to the helix in the residues K95 to Y108 and change in the orientation of the loop-helix (R276 to H301 and G185 to Q194) were observed in S277A. Changes in the loop orientation were observed in S277D (residues E107 to D117 and Q278 to V287) as highlighted in Fig. 4.16A. Further, no new interactions were observed in any of the Dnm1 variants.

The importance of residues in G2 and G5 motifs in DRP1 for intramolecular interactions was reported in earlier studies. The switch I residue T59 (the equivalent of Dnm1 T62) is important for the placement of the catalytic water molecule and Mg^{2+} coordination to facilitate the enzyme's mechanochemical energy conversion [182, 292]. The same may be envisaged for Dnm1. X-ray structure analysis of DRP1 using a GTP analog showed that the G5 motif functions as a rigid guanosyl binding pocket and characteristically binds to the substrate in a lock-and-key manner [182]. The adjacent residues to the DRP1 S248 (corresponding Dnm1 S277) in the G5 motif, R and N, were reported to stabilize ribose 2′-OH and N7 of the aromatic ring via interaction with water molecule, respectively [182].

For a deeper understanding of long-range interaction patterns, DCCM was performed by computing all the Pearson cross-correlation coefficients for the backbone Cα atoms of all the residues. The DCCM maps for the WT, T62A/D and S277A/D variants are graphically presented in Fig. 4.16B. Strongly correlated motions between specific residues are depicted in cyan and strongly anti-correlated motions are depicted in pink. The DCCM analysis reveals that the

atomistic motions are strongly correlated in WT as compared to the mutants. A correlation pattern was found between residues 1 to 350 in T62D. However, this correlation pattern was completely disrupted between the residues 350 to 700 (Fig. 4.16B). Similar pattern was also observed in S277A. However, the residues were both correlated and anti-correlated in this variant. Mostly, non-correlation of the residues was found in T62A (Fig. 4.16B). These results suggest that the mutations change the DCCM pattern of the residues and break the interdomain correlation in the proteins, suggesting mutation-driven changes. Interestingly, we observed that the mutations affect the atomistic motion of the residues far from the mutated site and exhibit an overall impact on the residue fluctuation of different domains (Fig. 4.16B).

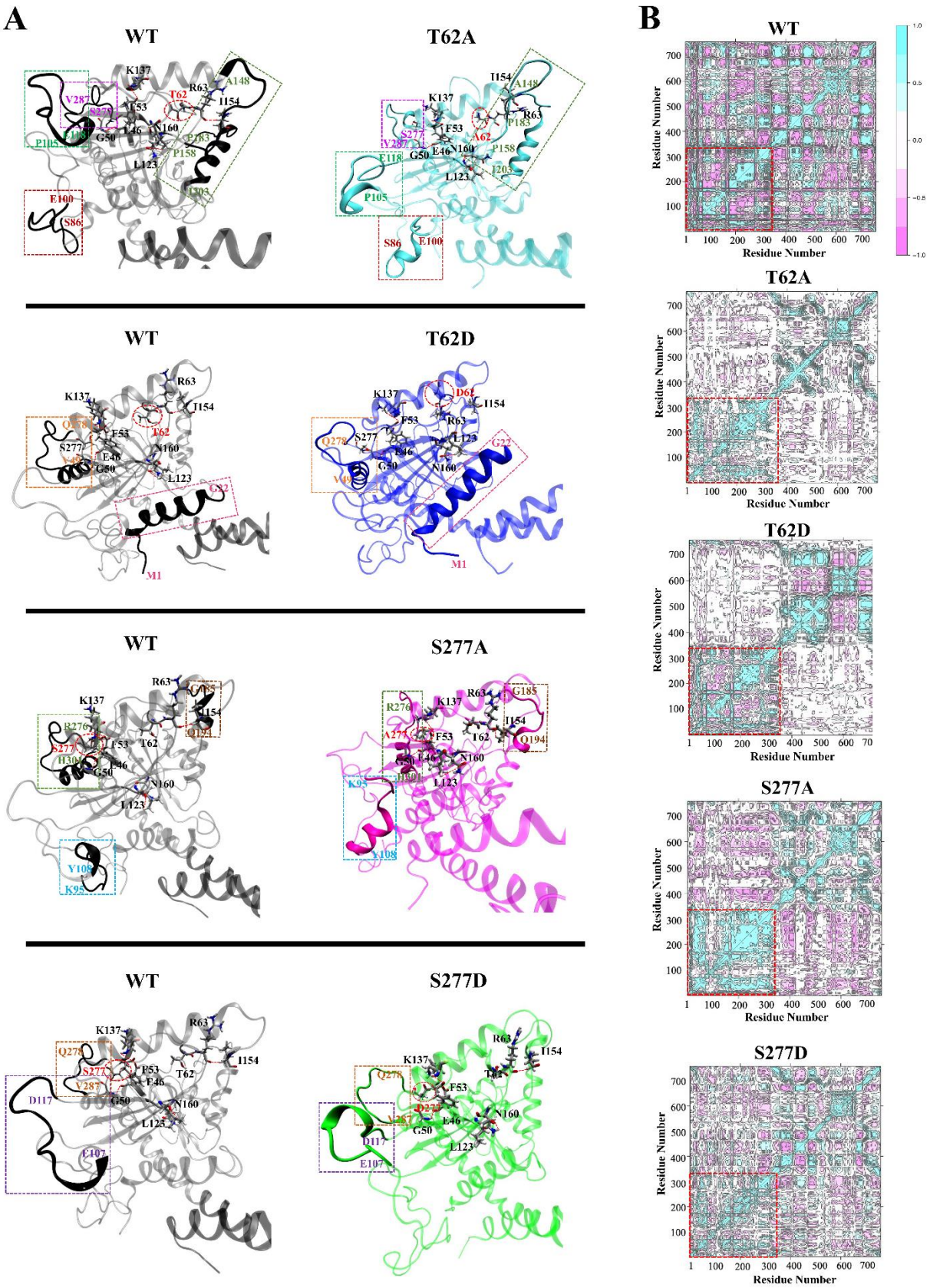

Fig. 4.16 MD simulation analysis of WT, Dnm1$^{T62A/D}$ and Dnm1$^{S277A/D}$
(A) Comparison of the structure of WT and variants of Dnm1 around the mutation site. The red dashed line highlights the key interactions and the residue is marked with a red circle. The mutant structures are compared with the WT and specific changes are highlighted and marked with different dashed boxes. (B) The DCCM of WT and variants obtained from the entire production dynamics are represented. The red-dotted region indicates the mutated domain (residues 1 to 334). The extent of correlated and anti-correlated motion are color coded as cyan-positive correlation, magenta-anti-correlation and white-non-correlation.

Table 4.2 Secondary structure content (in %) of Dnm1 WT, Dnm1$^{T62A/D}$ and Dnm1$^{S277A/D}$

Label	WT	T62A	T62D	S277A	S277D
Alpha-Helix (H)	41.1	44.8	43.3	43.91	42.0
3_{10}-Helix (G)	3.8	5.8	3.3	4.2	4.6
Pi-helix (I)	0.0	0.0	0.0	0.0	0.0
Extended-strand (E)	10.8	9.6	9.6	9.1	10.4
Beta-bridge (B)	0.7	1.6	0.9	0.8	1.7
Turn (T)	12.3	11.0	13.6	13.5	11.4
Bend (S)	12.8	9.6	11.1	10.5	10.8
Coil (C)	18.5	17.6	15.1	18.0	19.0

Table 4.3 Key interatomic distances (in Å) around the mutation sites of Dnm1 (averaged over the MD trajectories). Distances are averaged for 150 ns of MD and standard deviation is given as error after ±.

SI. No	Residue-pairs	WT	T62A	T62D	S277A	S277D
1	G50:E46	2.79 ± 0.44	3.28 ± 0.78	3.26 ± 0.93	3.11 ± 0.07	3.31 ± 0.72
2	K137:F53	3.10 ± 0.31	2.91 ± 0.11	3.74 ± 0.87	2.89 ± 0.19	3.14 ± 0.47
3	N160:L123	3.34 ± 0.82	2.88 ± 0.19	3.57 ± 0.73	3.93 ± 0.84	2.86 ± 0.67
4	R63:I154	2.51 ± 0.09	-	-	3.05 ± 0.21	2.85 ± 0.63

4.2.8 Dnm1$^{T62A/D}$ and Dnm1$^{S277A/D}$ exhibit dominant-negative effects *in vivo*

Earlier studies by Naylor and colleagues showed that T62D/F variants exhibited a dominant-negative effect in the *in vitro* GTPase activity assay in the presence of WT protein [94]. To analyze if GFP-tagged T62A/D and S277A/D variants in this study also exhibit similar effects, we expressed them in cells containing endogenous Dnm1. In contrast to the reticulate mitochondrial morphology observed in cells expressing only endogenous Dnm1, a significant change in mitochondrial phenotype was observed upon the expression of GFP-tagged T62A/D and S277D variants. More than 90% of cells had tubular and/or collapsed phenotype similar to that observed in *dnm1* cells (Fig. 4.17A, 4.17B). Interestingly, upon the expression of S277A variant, 62% of cells depicted problems in mitochondrial fission and an intermediate phenotype between WT and *dnm1* was observed in almost 30% of cells (Fig. 4.17A, 4.17B). This phenotype observed could be most likely due to the rendering of the endogenous Dnm1 non-functional by the expressed variant. It can be envisaged that the oligomeric form of the protein required for the division of mitochondria may be formed by a combination of monomers of endogenous and mutant Dnm1. This may result in the formation of non-functional higher-order structures.

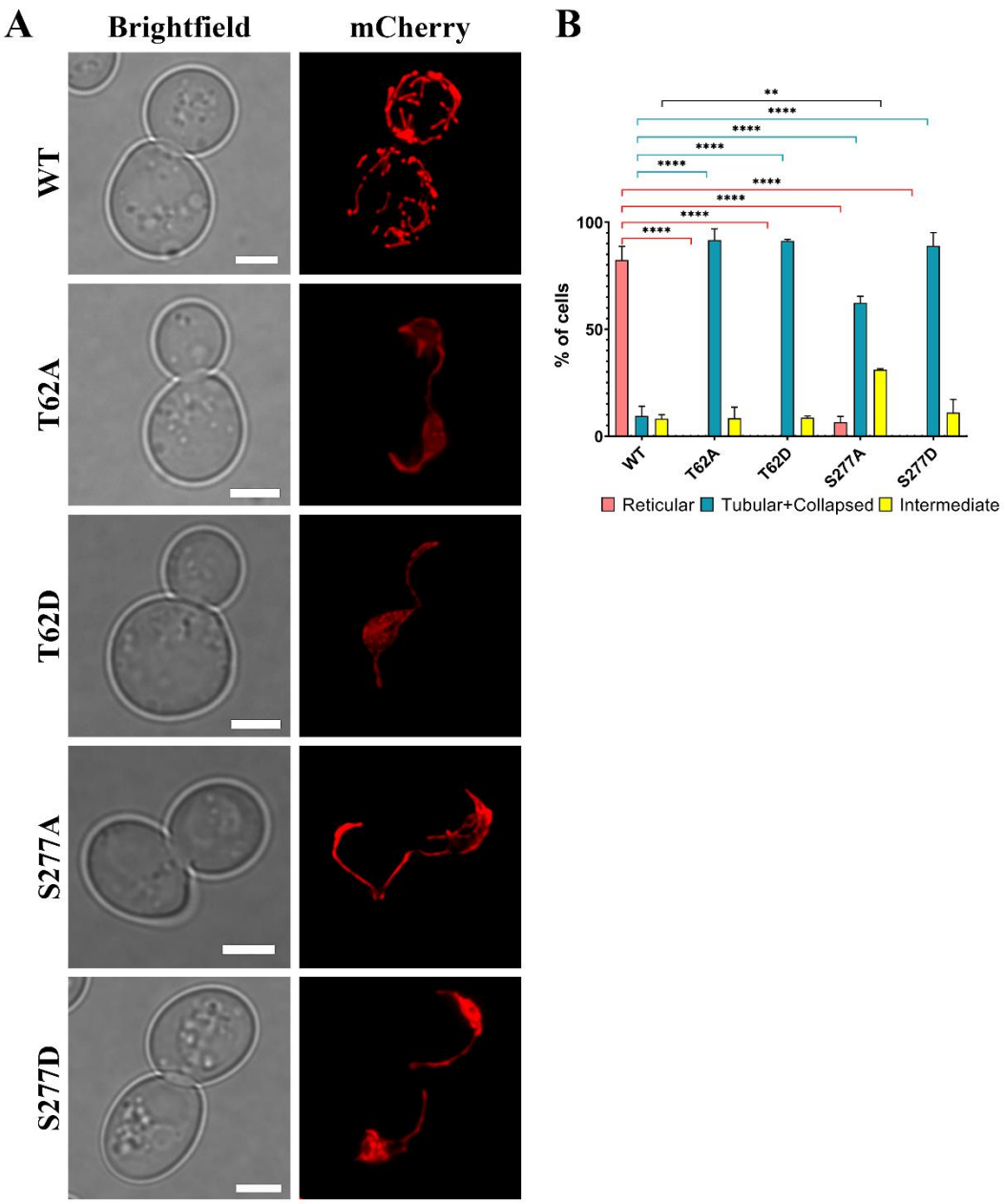

Fig. 4.17 T62 and S277 variants exhibit a dominant-negative phenotype.
(A) Mitochondrial morphology in WT cells upon the expression of Dnm1-GFP variants (T62A, T62D, S277A and S277D). Mitochondria are marked using preCOX4-mCherry. Maximum intensity projections of the z-axis are used to depict the images. Scale bar - 5 µm. (B) Quantification was conducted on two sets of independent biological replicates, with 50 cells counted from each experiment. A two-way ANOVA with Dunnett's multiple comparison was used to evaluate the significance of the difference observed in Dnm1 variants with WT. Error bars displayed are mean ± SEM.

4.3 Conclusion

In this study, we identified T62 and S277 as residues important for both *in vivo* and *in vitro* function of Dnm1. Cells expressing Dnm1$^{T62A/D}$ and Dnm1$^{S277A/D}$ showed mitochondrial morphology predominantly similar to *dnm1* cells. An interesting difference between T62 and S277 variants was the number of puncta and their localization. Dnm1$^{T62A/D}$ formed large puncta that did not colocalize with the mitochondrial marker in our study. Dnm1$^{S277A/D}$ GFP puncta, though localized to mitochondria, were non-functional, resulting in *dnm1*-like morphology. Not only the *in vivo* experiments but also the *in vitro* GTPase activity assay also revealed a significant reduction in the activity of T62A/D and S277A/D variants. Biochemical data show that both T62A/D and S277A/D mostly retain their secondary structure and are able to form higher-ordered structures *in vitro*. MD simulation and computational analysis show altered atomistic motion of residues situated farther away from the mutation site. Also, an increase in the overall compactness of the protein was observed in S277A. Large fluctuations in RMSD in other domains (GED and B-insert) of the protein have also been identified, suggesting altered intra-molecular interactions upon mutation of the residues located in the GTPase domain. The dominant-negative effect of the mutations suggests that the mutant protein interacts with the WT protein and renders it non-functional, which is evident from the observed mitochondrial phenotype. At this stage, we are unable to say if these residues (both T62 and S277) undergo phosphorylation and if the effect observed is due to the altered phosphorylation status of the protein in the variants or the change in the structure and interactions of the protein that may result due to aminoacyl substitution. Albeit, both scenarios highlight the importance of these residues for the function of the protein.

Recently, Bauer and colleagues studied disease-causing mutations in various domains of DRP1 [220]. The authors reported variable effects of two mutations in the GTPase domain on the structure-function of the protein. Indeed, our data also shows variation in the phenotype

observed with respect to protein puncta and localization to mitochondria in both T62A/D and S277A/D variants signifying the different effects caused due to mutations in the same domain. Interestingly, a recent study has reported a mutation of DRP1 T59 to N that resulted in adult encephalopathy due to hampered mitochondrial and peroxisomal fission [191]. This residue corresponds to yeast Dnm1 T62 studied in this manuscript. The authors also report reduced levels of DRP1 and suggest a role for PTM in the function of the protein. Our study reports similar observations in the yeast model and further evaluates the role of this residue in protein structure and function. Additionally, the conserved nature of these proteins from yeast to humans is highlighted and is a significant contribution of our study.

Chapter 5

Mimicking human DRP1 disease-causing mutations in yeast Dnm1 reveals altered mitochondrial dynamics

Abstract

The dynamin-related protein 1 (DRP1) and its homologs in various eukaryotes are essential to maintain mitochondrial morphology and regulate mitochondrial division. Several mutations in different domains of DRP1 have been reported, which result in debilitating conditions. Four such disease-causing mutations of the middle domain of DRP1 were mimicked in the yeast dynamin-related GTPase (Dnm1) and were characterized in this study. Mitochondrial morphology and protein function were observed to be altered to a variable extent in cells expressing the mutated variants of Dnm1. Several aspects related to the protein such as punctate formation, localization to mitochondria, dynamic behavior and structure were analyzed by microscopy, biochemical studies and molecular dynamics simulations. Significant effects on the protein structure and function were observed in cells expressing A430D and G397D mutations. Overall, our data provide insight into the molecular and cellular alterations resulting from middle domain mutations in Dnm1.

This chapter is published as

Banerjee R, Kumar A, Satpati P, Nagotu S. Mimicking human Drp1 disease-causing mutations in yeast Dnm1 reveals altered mitochondrial dynamics. Mitochondrion. 2021 Jul 1;59: 283-95. DOI: https://doi.org/10.1016/j.mito.2021.06.009

5.1 Introduction

Compartmentalization of cellular contents into functional units called organelles is an essential feature of eukaryotic cells. One of the most critical organelles of a cell is the mitochondrion, which harbors TCA cycle and oxidative phosphorylation machinery for energy production. Biosynthesis of cellular building blocks such as nucleotides and amino acids along with Ca^{2+} ion buffering also requires active mitochondria [15, 256]. A role for mitochondria in maintaining cellular redox balance and apoptotic pathway of cell death is also reported [257, 258]. Interestingly, mitochondrial shape and dynamics have been reported to have a profound role on the abovementioned functions. Mitochondria are dynamic in nature whose morphology is maintained by a continuous process of division and fusion [259]. Several proteins involved in these processes have been identified and these are conserved across eukaryotic organisms [108]. Mitochondrial fission in mammals is dependent on the GTPase DRP1 (Dynamin related protein 1) that belongs to the family of dynamin-related proteins [87]. The N-terminal GTP-binding domain, middle domain, variable domain containing B insert, and C-terminal GTPase effector domain (GED) constitute the protein [73, 108]. DRP1 exists as soluble dimers and tetramers in the cytosol and shuttles between the cytosol and the mitochondrial surface [293]. Extensive studies on the mechanism of action of DRP1 have revealed that it forms helical oligomers that wrap around the mitochondrial outer membrane and subsequently utilize GTP hydrolysis activity leading to membrane fission [87, 294]. Specific receptors and interacting proteins (Mff, MiD49/51, and human Fis1) function together with DRP1 in this process [90, 97, 98].

As mentioned earlier an intricate relationship between mitochondrial function and dynamics has been reported and is an important aspect of investigation in several human diseases such as neurodegeneration [147, 155, 295-297]. Interestingly, loss of DRP1 also triggered genome instability and initiated DNA damage response [117]. Several mutations in DRP1 have been identified to date that resulted in various disease conditions [183, 187, 188, 194-197, 199].

These mutations have been identified in various domains of the protein. However, the most number of mutations are reported in the middle domain of DRP1. A role for the middle domain in dimerization, tetramerisation and formation of higher ordered oligomers has been reported [288, 293, 298].

Homolog of DRP1 is called Dnm1 in yeast and Drp3A/B in plants [103, 108, 262]. A number of recruitment factors such as Fis1, Mdv1 and/or Caf4 are required for the association of Dnm1 to the mitochondrial membrane [88, 93, 94]. A role for these proteins in peroxisome division in various model organisms has also been reported [299-302]. As the yeast Dnm1 is highly conserved with DRP1, structural and functional analysis performed using Dnm1 as a model mostly holds true for DRP1. To better understand the role of the DRP1 middle domain mutations in disease pathology, we have constructed the equivalent yeast Dnm1 mutations and analyzed structural and functional alterations. The mutations chosen to study are R438C (equivalent to DRP1-R403C resulting in epileptic encephalopathy), C481F (equivalent to DRP1-C446F leading to infantile parkinsonism), G397D (equivalent to DRP1-G362D observed in refractory epilepsy) and A430D (equivalent to DRP1-A395D that results in a lethal defect) [194, 195, 197, 199]. Though some of these mutations were analyzed earlier for effect on organelle morphology, the aspects related to the protein localization, distribution, function and structure have not been reported. In this study, we aim to address these questions using biochemical methods, microscopy and molecular dynamics (MD) simulations.

5.2 Results

5.2.1 Generation of orthologous disease mutation in Dnm1

DRP1 and its homologs belong to a highly conserved protein family that regulate mitochondrial structure in various organisms. Four DRP1 mutations known to cause disease conditions in humans were introduced into equivalent residues of the *S. cerevisiae DNM1* by SDM. The mutations of Dnm1, equivalent to the disease causing mutations of DRP1 studied in this work are R438C, C481F, G397D and A430D [194, 195, 197, 199]. The sequence alignment of the relevant region of DRP1 and Dnm1 is depicted in Fig. 5.1.A and shows that the residues mutated in the disease conditions are conserved in yeast Dnm1 (residues in red colour) (Fig. 5.1A). A schematic that depicts the domain structure of Dnm1 and the 3D structure of Dnm1 obtained using the webtool Phyre2 are depicted in Fig. 5.1B and C, respectively. The position of the mutations is indicated in these figures and it can be noted that all the four studied mutations lie in the highly conserved middle domain of the protein (Fig. 5.1B & 5.1C). The mutant variants were generated using the plasmid pRBA005 that contains FL-Dnm1 fused to GFP. Restriction digestion and sequencing analysis confirmed the successful generation of the mutant variants (Fig. 5.2).

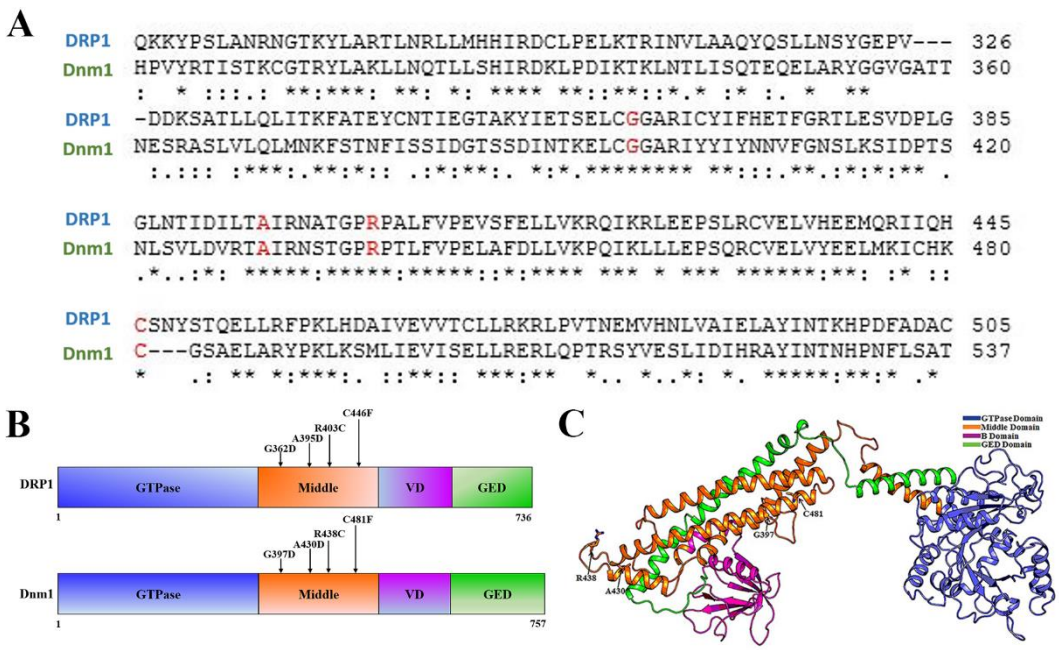

Fig. 5.1 Mimicking orthologous disease-causing human DRP1 mutations in *S. cerevisiae* Dnm1. (A) Sequence alignment of middle domain region of human DRP1 (Uniprot ID: O00429) and *S. cerevisiae* Dnm1 (SGD ID: YLL001W) depicting the position of amino acids selected for this study. **(B)** Schematic showing domain architecture of DRP1 (736 aa) and Dnm1 (757 aa) and corresponding positions of mutations. **(C)** Structure of yeast Dnm1 generated using Phyre2 and the positions of the mutagenized residues in Dnm1 are depicted.

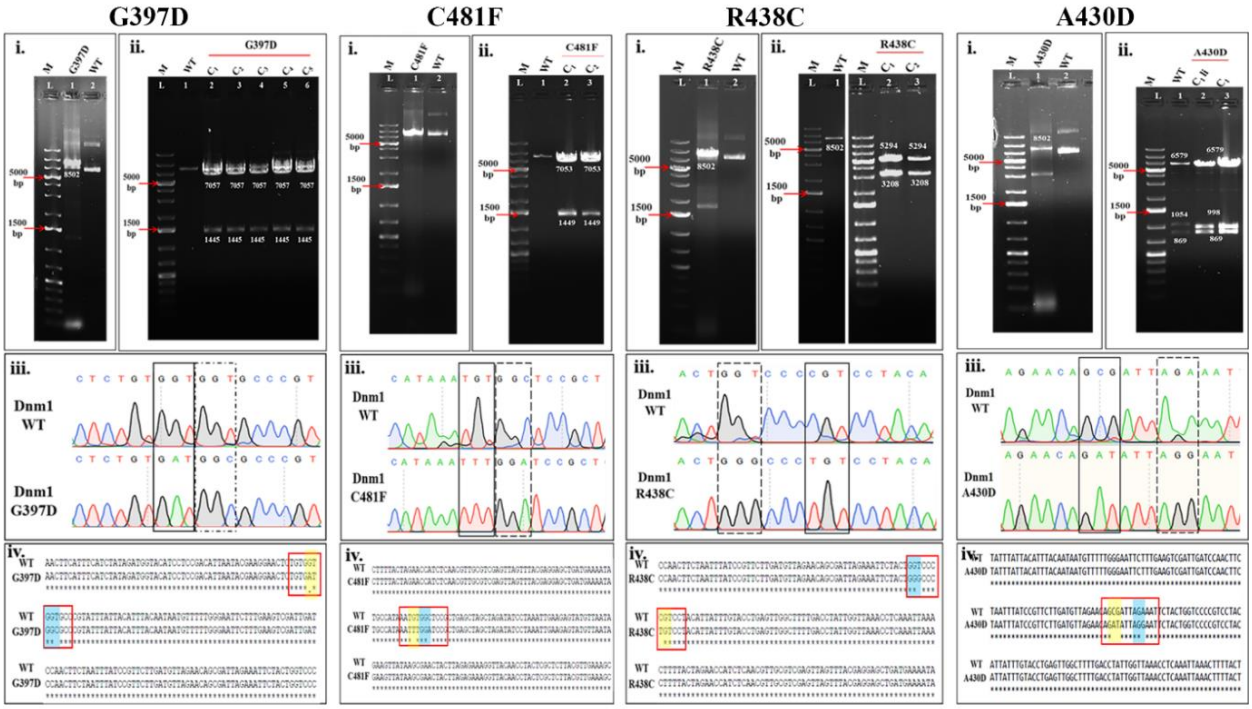

Fig. 5.2 Construction of Dnm1-GFP variants G397D, C481F, R438C and A430D respectively by SDM. **(i)** Agarose gel image depicting two stage PCR product of template pRBA005 with respective primers required for the desired mutation (Table 2.4). **(ii)** Represents unique restriction digestion profiles of respective mutants compared to WT (Table 2.4). **(iii)** represents further confirmation of the mutations with DNA sequencing analysis. Solid line boxes represent the key nucleotide changes for the intended mutations, while the dotted boxes represent nucleotide changes without changing the amino acid to create a unique restriction site for mutant screening. **(iv)** represents sequence alignment of WT and mutants. Region of interest is marked with red outline. Key nucleotide mismatches that changes the amino acid are highlighted in yellow. Blue highlighted regions show nucleotide changes that produce a unique restriction site for mutant screening without changing the amino acid.

5.2.2 Effect of Dnm1 mutations on cell growth and protein expression

The mutated *DNM1* variants were generated in a yeast expression plasmid (pRBA005) in which *DNM1* was expressed under the control of met25 promoter and was fused to GFP at its C-terminus. The plasmids were subsequently transformed into yeast cells lacking the endogenous Dnm1 (*dnm1*). To determine the effect of expression of mutated variants on cell growth, *dnm1* cells carrying the plasmids were both spotted onto selective (glucose) plates by drop serial dilution and cultured in liquid medium containing glucose (YND medium) (Fig. 5.3A, 5.3B,

5.3C). Interestingly, neither deletion of *DNM1* nor the expression of the mutant variants R438C, C481F and A430D resulted in a significant difference in growth as compared to WT and FL (Fig. 5.3A, 5.3B, 5.3.C). However, among all the variants, G397D exhibited slower growth with a doubling time of 3.98 h (Fig. 5.3B). In general, *S. cerevisiae* cells exhibited slower growth when glycerol was used as the sole carbon source compared to glucose medium as reported earlier [264] (Fig. 5.3D, 5.3E, 5.3F). Interestingly, G397D grew very slowly also on glycerol (YNG) liquid medium, suggesting a possible functional loss of mitochondria (Fig. 5.3D, 5.3E). Similarly, no growth was observed on spotting these cells on plates containing glycerol as carbon source (Fig. 5.3F). To understand if the mutations alter protein expression, levels of Dnm1 from exponentially growing and stationary cells were determined by western blotting using α-GFP (Fig. 5.4A, 5.4C). The expression of WT and mutant variants was quantified and is represented as a fold change in expression (Fig. 5.4B, 5.4D). In the log phase, expression of the mutant variants was not significantly different to cells expressing FL-Dnm1-GFP (Fig. 5.4A, 5.4B). However, in stationary cells, the levels of the G397D variant was significantly reduced (Fig. 5.4C, 5.4D). Equal loading of the samples was confirmed using α-actin.

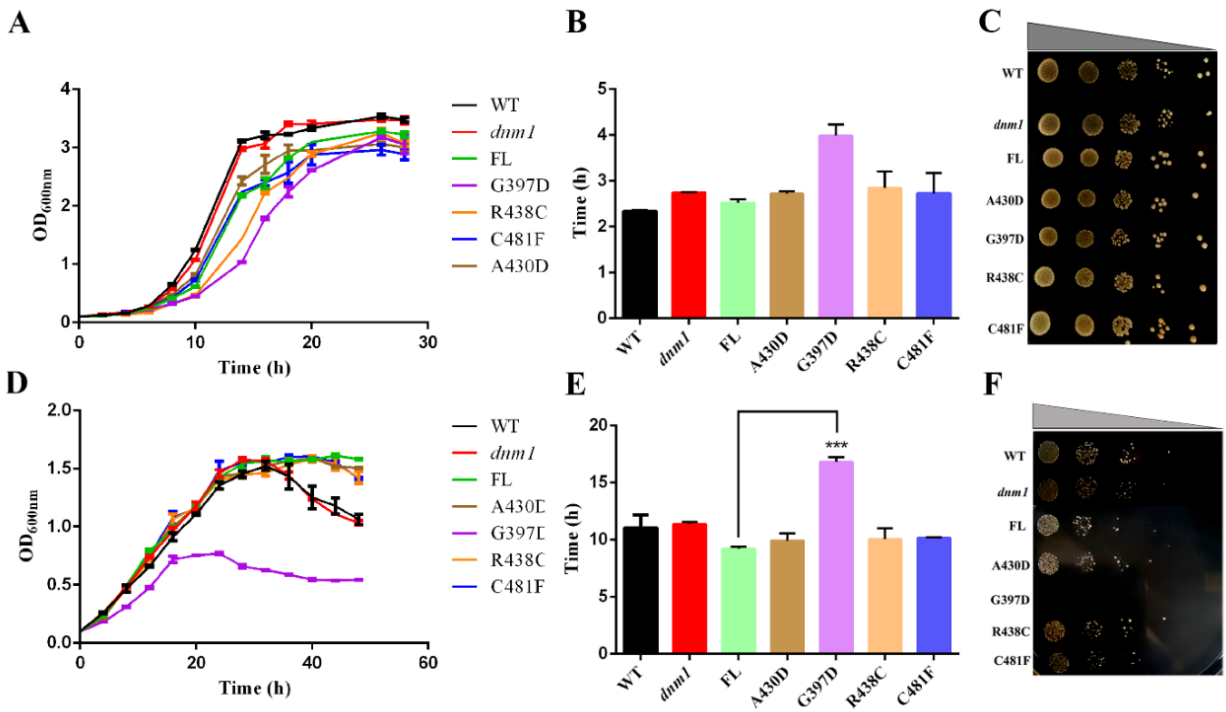

Fig. 5.3 Growth of different Dnm1 mutant variants. Growth analysis by growth curve and drop serial-dilution assay of WT, *dnm1* and *dnm1* cells expressing FL-Dnm1-GFP and mutant variants (A430D, G397D, R438C, C481F). Cells were grown in liquid YND **(A)** or YNG medium **(D)** (Start OD_{600}: 0.1) at 30 °C. Samples were taken at different time intervals and OD_{600} was measured. Error bars indicate SEM from two independent experiments. Doubling time (h) of WT, *dnm1* and *dnm1* cells expressing FL-Dnm1-GFP and different Dnm1 mutations grown on YND **(B)** or YNG **(E)** medium. Tenfold serial dilutions of log phase cultures were spotted onto YND **(C)** and YNG **(F)** plates and were incubated for 3 days and 7 days respectively in 30 °C.

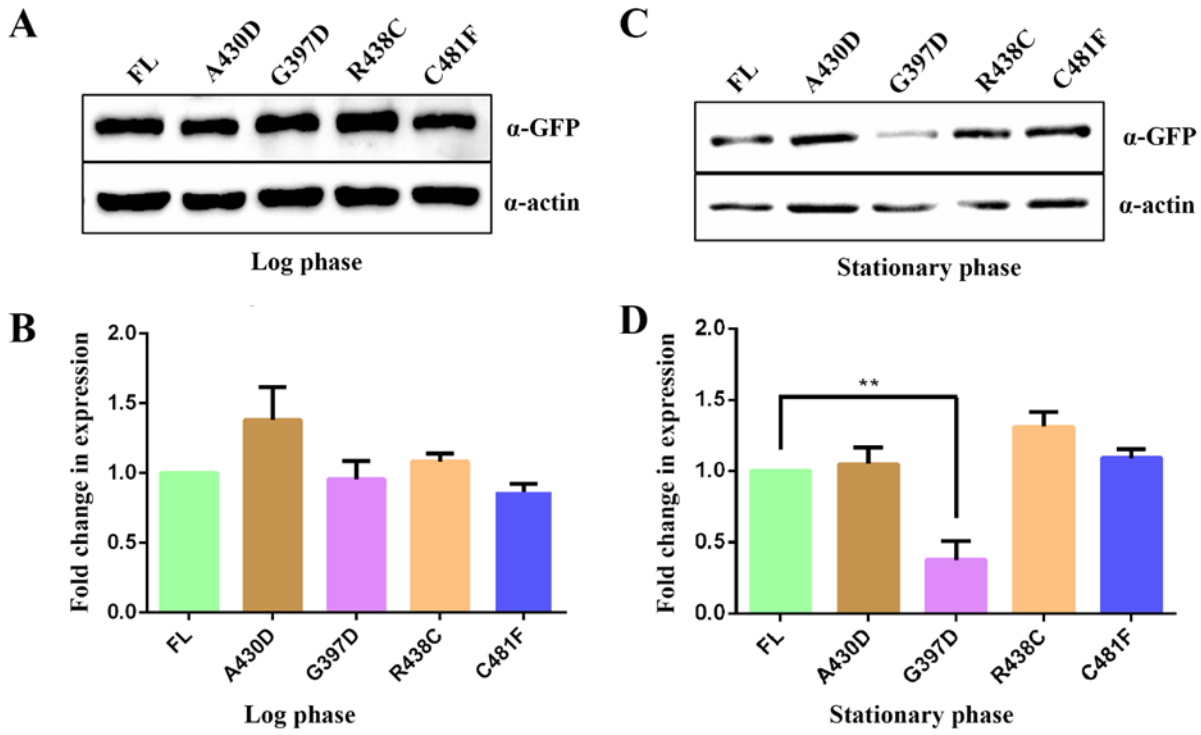

Fig. 5.4 Expression of different Dnm1 mutant variants. Whole cell lysates from YND grown log phase **(A)** and stationary phase cultures **(C)** equivalent to 3 OD_{600} units were separated by SDS-PAGE and immunoblotted with α-GFP antibody. Quantitative analysis of the Dnm1-GFP immunoblots in both log **(B)** and stationary phase **(D)** were normalised with actin (loading control) and represented as bar diagrams. Error bars indicate SEM obtained from 3 independent experiments. A one-way ANOVA was used with Dunnett's multiple comparison test to assess significance of difference in Dnm1 mutant variants with cells expressing FL-Dnm1-GFP. **$p < 0.01$.

5.2.3 Dnm1^{A430D} mutation leads to aberrant mitochondrial morphology

To determine whether the disease-causing mutations alter the function of Dnm1, cells expressing FL-Dnm1-GFP and mutated variants grown in YND medium were analyzed for mitochondrial morphology using the plasmid pHS12 that expresses preCOX4-mCherry to mark mitochondria [271]. Cells were visualized under a fluorescence microscope and scored for various morphologies (reticular/ branched, tubular, collapsed/fallen and fragmented) of mitochondria. The FL-Dnm1-GFP, when expressed in *dnm1* cells, completely restored the WT

reticular morphology of mitochondria (Fig. 5.5A, 5.5B). The mutant proteins were able to rescue the mitochondrial fission defect of *dnm1* cells to a variable extent. C481F restored the morphology of mitochondria similar to the FL protein, with most cells (80%) exhibiting reticular mitochondrial phenotype (similar to that in WT cells) (Fig. 5.5A, 5.5B). A small increase in the collapsed mitochondrial phenotype was observed in this mutant. However, this was not statistically significant when compared to the FL expressing cells. R438C and G397D could partially rescue *dnm1* mitochondrial morphology and exhibited intermediate phenotype with nearly 60% and 50% cells harboring WT like reticular mitochondria, respectively (Fig. 5.5A, 5.5B). These mutants also had an increased number of cells with tubular and/or collapsed mitochondria (morphology typical for *dnm1* cells), indicating a partial loss of Dnm1 function (Fig. 5.5A, 5.5B). However, approximately 18% of the cells expressing Dnm1G397D-GFP mutation also showed fragmented mitochondria (Fig. 5.5B). Of all the studied mutants, A430D was not capable of rescuing *dnm1* mitochondrial morphology, indicating a loss of function of Dnm1. The majority of the A430D cells (70%) exhibited collapsed mitochondria like that in *dnm1* cells (Fig. 5.5A, 5.5B). Morphology of mitochondria in cells grown on glycerol as carbon source (YNG medium) was also evaluated (Fig. 5.6). Cells expressing FL-Dnm1-GFP showed extensive reticulate like mitochondria and cells expressing A430D depicted fallen/ tubular mitochondrial morphology. G397D on the other hand exhibited fragmented mitochondria in most of the cells. Cells expressing R438C variant exhibited a mixed phenotype of reticulate and tubular mitochondria. C481F expressing cells depicted mitochondrial morphology similar to FL-Dnm1-GFP expressing cells with most cells having reticulate mitochondria (Fig. 5.6).

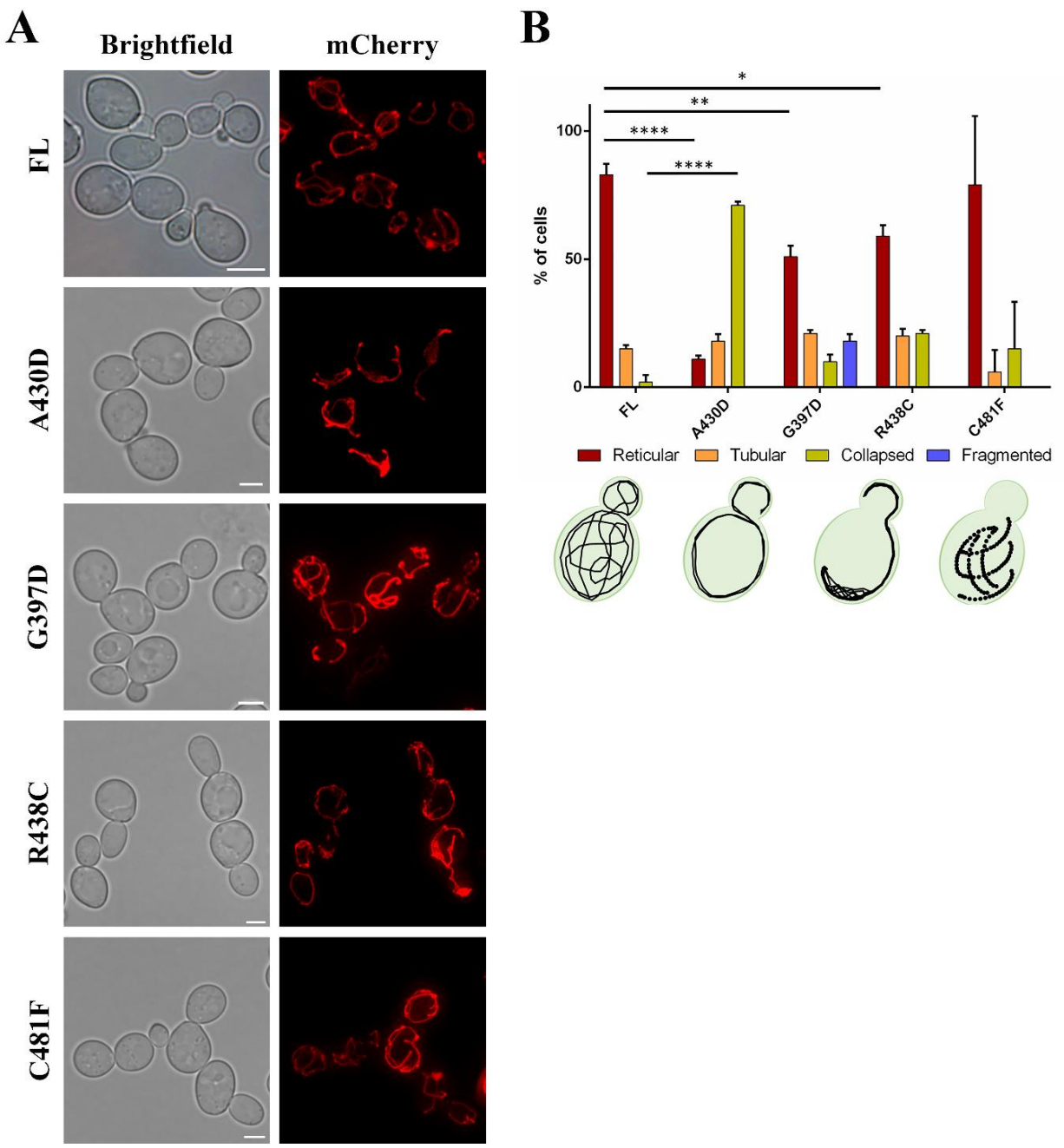

Fig. 5.5 A430D mutant shows defective mitochondrial fission. (A) Mitochondrial morphology in *dnm1* cells upon expression of FL-Dnm1-GFP and mutant variants (A430D, G397D, R438C and C481F) grown in YND medium. Mitochondria were labelled with mitochondrial membrane targeted preCOX4-mCherry. Scale bar represents 5 µm. **(B)** For quantification of mitochondrial morphology cells were differentiated into four categories of mitochondrial morphology *i.e.* reticular, tubular, meshwork and/or fragmented. Quantification was performed in two sets of data and 50 cells were counted from each experiment. Error bar indicates SEM. Schematic images represent the classified mitochondrial morphology. A two-way ANOVA with Dunnett's multiple comparison was used to assess the significance of difference observed in mutant variants with cells expressing FL-Dnm1-GFP. *$p < 0.05$, **$p < 0.01$, ***$p < 0.001$, ****$p < 0.0001$.

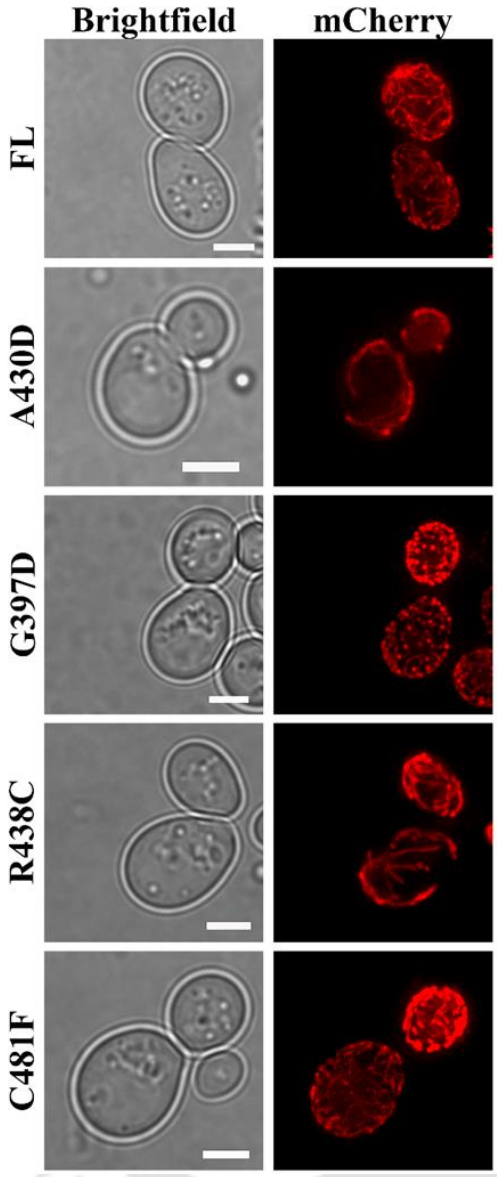

Fig. 5.6 Mitochondrial morphology in *dnm1* cells upon expression of FL and different mutant variants (A430D, G397D, R438C and C481F) grown in YNG medium. Mitochondria were labelled with mitochondrial membrane targeted preCOX4-mCherry. Scale bar represents 5 µm.

5.2.4 Mutated variants of Dnm1 show altered localization and dynamics

Dnm1-GFP is visualized as distinct dynamic puncta in cells [94, 95, 266]. A similar phenotype of FL-Dnm1-GFP, when expressed in *dnm1* cells was also observed in our experimental conditions (Fig. 5.7A). Discrete GFP spots of variable sizes were observed in these cells. The change of the mitochondrial morphology in *dnm1* cells from collapsed to reticulate upon expression of FL-Dnm1-GFP confirms that the fusion protein is functional. Similarly, all the mutant variants were analyzed for expression and distribution of the protein. To quantify the

number of GFP puncta, cells were fixed using formaldehyde, followed by microscopy analysis. The phenotype and distribution of Dnm1-GFP puncta in R438C and C481F variants was similar to that of FL-Dnm1-GFP (Fig. 5.7A, 5.7B). Discrete GFP puncta were observed in these cells which ranged between 2 and 7. A substantial reduction in the number of puncta was observed in the mutant variant G397D with most cells showing only 1 punctum/cell (Fig. 5.7A, 5.7B). Interestingly A430D, on the other hand, exhibited cytosolic distribution of GFP in a large fraction of cells (≈30%, Fig. 5.7A, 5.7B). However, cells with many discrete small puncta were also visible, albeit to a lesser extent (Fig. 5.7A, 5.7B).

To further explore the possibility of altered sub-cellular distribution of the protein upon expression of mutant variants, we examined protein levels in the cytosolic and organellar fractions (Fig. 5.7C). Quantitative analysis showed that larger fraction of FL-Dnm1-GFP is in the cytosol and not tightly associated with the mitochondria. A similar distribution was also observed in mutants A430D, R438C and C481F respectively. Interestingly, G397D cells showed an increased amount of Dnm1 in the organellar fraction compared to the supernatant suggesting a tighter association of the protein with mitochondria (Fig. 5.7D).

Further, to analyze if the mutated variants of the protein can still localize to mitochondria, z-sections of the cells were analyzed for co-localization of Dnm1-GFP with preCOX4-mCherry (Fig. 5.8A). As mentioned in 5.2.4, Dnm1-GFP is visualized as puncta in cells, which are variable in size and number. Interestingly Dnm1 puncta still localized to mitochondria in G397D, R438C and C481F cells (Fig. 5.8A). As mentioned above in 5.2.4, most of the cells of A430D exhibited cytosolic Dnm1, and hence in these cells, no co-localization was observed (Fig. 5.8A). However, in cells where small puncta of Dnm1 were visualized, localization to mitochondria was observed (Fig. 5.8A). Co-localization of a single puncta (marked by an arrow) in all mutant variants is also depicted as a line graph using intensity profiles obtained from ImageJ (Fig. 5.8A). The quantification data (Fig. 5.8B) was obtained from two independent experiments by scoring 50

cells where at least one Dnm1-GFP puncta was localized to mitochondria. A430D cells with only cytosolic GFP fluorescence were not taken into account for this quantification. As seen in Fig. 5.8B, the percentage of cells showing co-localization of Dnm1-GFP with mitochondrial marker did not vary in cells expressing mutant variants or FL-Dnm1-GFP.

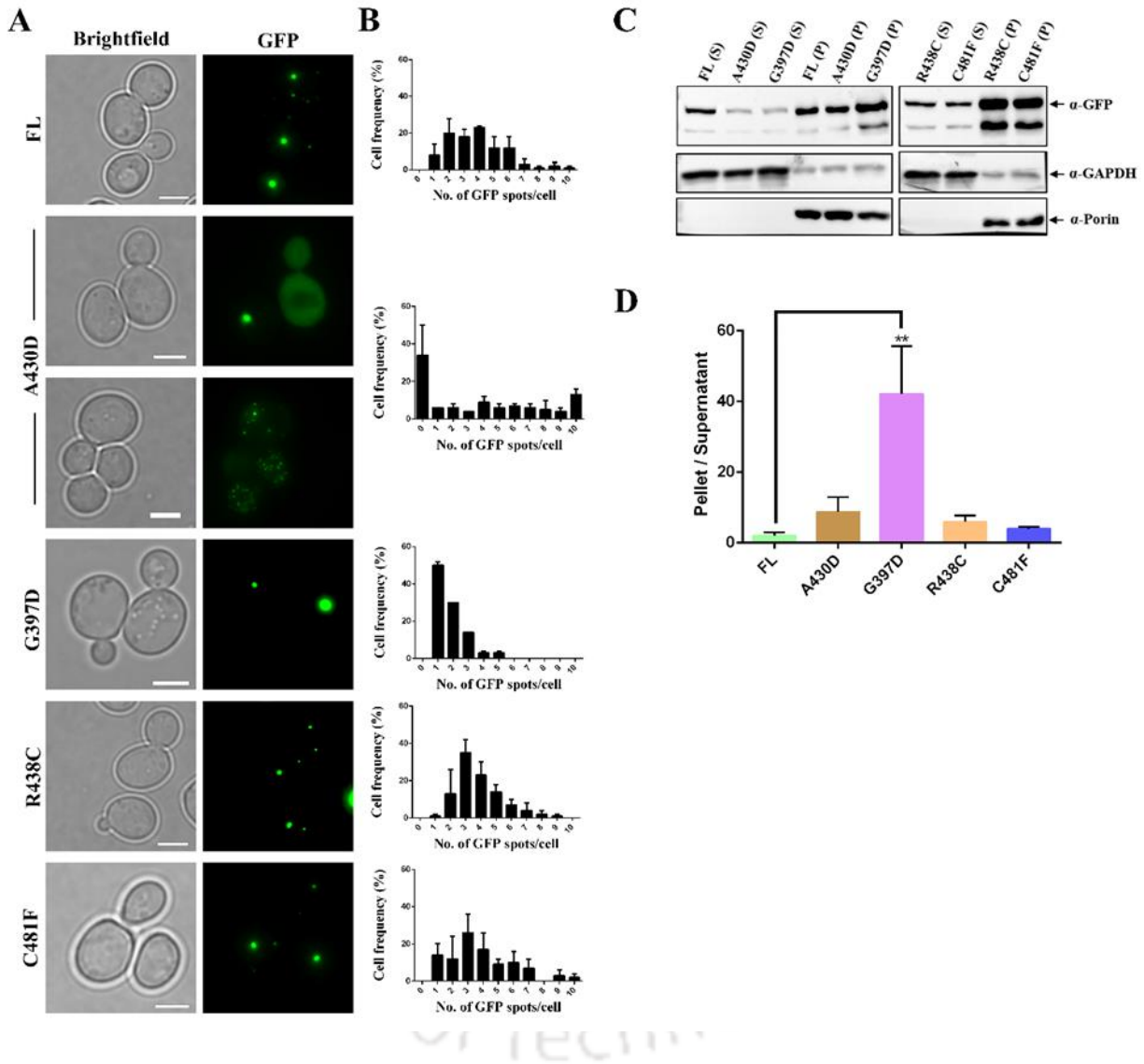

Fig. 5.7 Dnm1-GFP puncta number and distribution varies in different mutants. (A) Fluorescence microscopy images of *dnm1* cells expressing FL-Dnm1-GFP and mutant variants (A430D, G397D, R438C, C481F). Dnm1-GFP was either visualized as distinct puncta or as diffused cytosolic fluorescence. Scale bar represents 5 µm. **(B)** Quantification of Dnm1-GFP puncta in FL and mutant variants corresponding to those in A is shown. Fluorescence spots were counted from randomly taken fluorescence microscopy images (z-projection merge). Quantification was done from two independent experiments taking 50 cells into account. Error bar indicates SEM. **(C)** Dnm1-GFP distribution pattern in cytosolic (S) and mitochondrial fraction (P) was evaluated by immunoblotting. Cytosolic and mitochondrial protein was normalised with GAPDH (cytosolic marker) and porin (mitochondrial marker), respectively. **(D)** Quantitative analysis of immunoblots are represented as bar diagrams. Error bars indicate SEM obtained from 3 independent experiments. A one-way ANOVA was used with Dunnett's multiple comparison test to assess significance of difference in Dnm1 mutant variants with cells expressing FL-Dnm1-GFP. **$p < 0.01$.

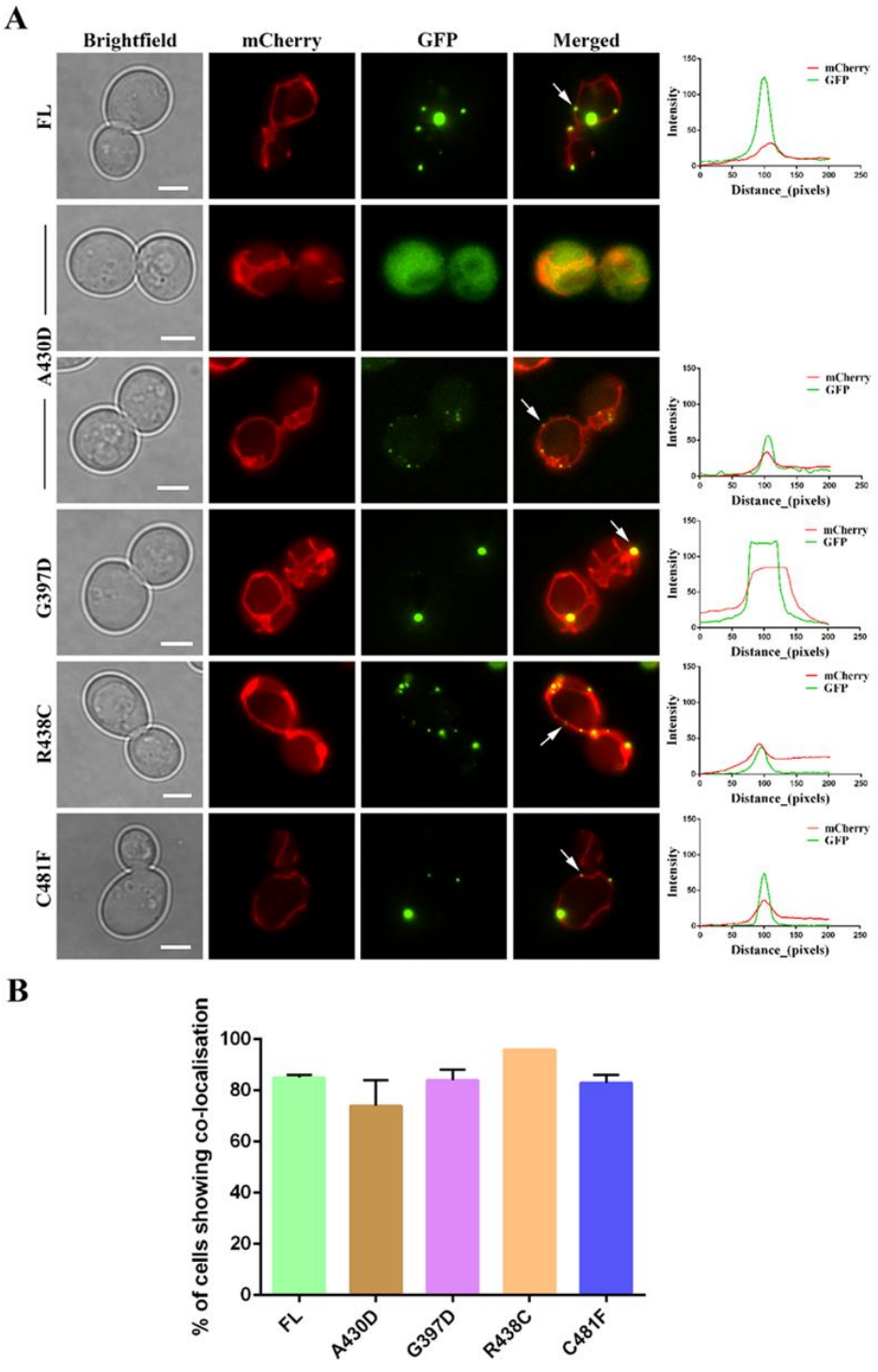

Fig. 5.8 Dnm1-GFP puncta depicted altered localization in A430D variant. (A) *dnm1* cells expressing different Dnm1-GFP mutations and mitochondria targeted preCOX4-mCherry were imaged by fluorescence microscopy for co-localisation analysis. Randomly selected (white arrows) Dnm1-GFP puncta were assessed for their association with mitochondria and represented as line profile generated using ImageJ. Scale bar represents 5 µm. **(B)** Percentage of cells that showed mitochondrial localization of at least one Dnm1-GFP puncta are represented as a bar graph. Error bar indicates SEM from two independent experiments (50 cells in each).

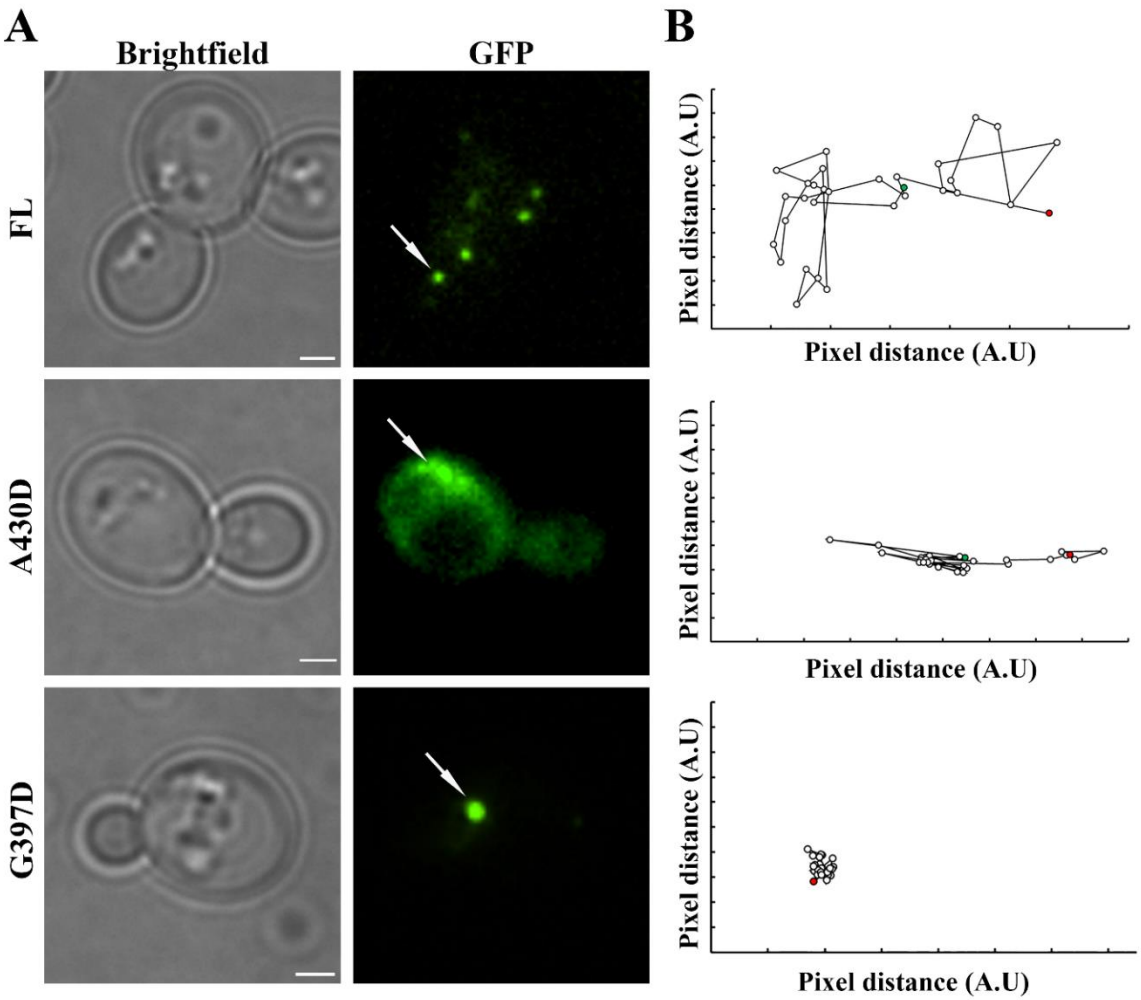

Fig. 5.9 Altered dynamic behaviour of Dnm1-GFP mutant variants. (A) Time-lapse images of cells expressing FL-Dnm1-GFP, A430D and G397D variants were captured for 1 min. A single 0.28-µm section at the start of the imaging is shown. Arrows point to the Dnm1-GFP puncta that is tracked. All the movies are available as supplementary data. **(B)** Movement of Dnm1-GFP puncta from images in A are tracked using the ImageJ plugin particle tracker. White spots indicate the recorded position of the puncta at each time point. Green and red spots indicate start and end time of tracking.

Another interesting feature of Dnm1 puncta observed in cells is their dynamic nature [94, 266]. WT protein was reported to be dynamic in nature with few puncta that exhibit rapid movement [95]. As G397D and A430D mutant variants showed significant alteration in Dnm1 puncta phenotype and number, these mutations along with FL-Dnm1-GFP were further analyzed for the dynamic nature of the protein by time-lapse imaging. Several cells were analyzed for tracking Dnm1-GFP puncta and a representative image of such a tracking is shown in Fig. 5.9. The puncta that was tracked using ImageJ is marked by an arrow (Fig. 5.9A). The tracks of

movement of the selected puncta are shown in Fig. 5.9B. As depicted, FL-Dnm1-GFP exhibited the most dynamic behavior with extensive movement in both X and Y directions. The small puncta in A430D cells exhibited restricted movement and the punctate structure in G397D cells was almost immobile.

5.2.5 A430D exhibits a dominant-negative effect

The DRP1 mutations exerted a heterozygous dominant-negative effect in the patients i.e. mutant alleles showed interference with the function of the WT DRP1 allele [194, 195, 197, 199]. To analyze if the dominant-negative effect can also be observed in yeast cells, all the mutant variants were expressed in WT cells that also expresses endogenous Dnm1. The WT mitochondrial morphology in most cells is reticular and branched and this did not alter significantly with the expression of plasmid encoded Dnm1 (Fig. 5.10A, 5.10B). In contrast, A430D mutant showed the most drastic change in mitochondrial morphology where 65% of the cells showed collapsed and 25% of the cells exhibited tubular mitochondrial phenotype (Fig. 5.10A, 5.10B). This was the most significant dominant-negative allele. Approximately 35% of the R438C expressing cells showed either tubular or collapsed mitochondria, indicating a moderate interference of this particular mutation on the endogenously expressed WT functional Dnm1 (Fig. 5.10A, 5.10B). However, mutants G397D and C481F had almost no effect on Dnm1-WT function as both mutants showed more than 80% cells with reticular and branched mitochondrial morphology (Fig. 5.10A, 5.10B).

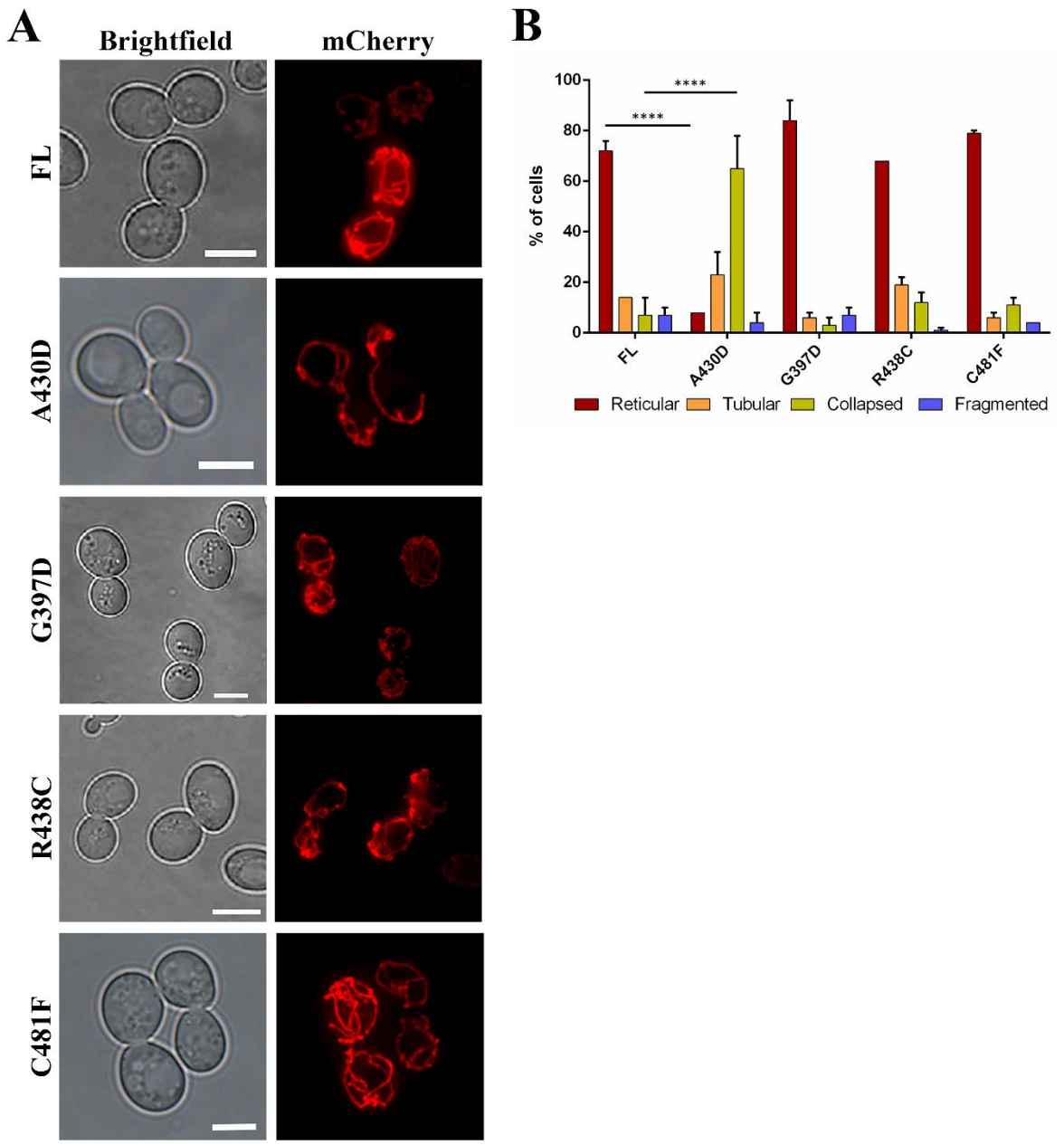

Fig. 5.10 Expression of Dnm1 mutant variants in WT yeast cells for assessment of dominant-negative effects. (A) Mitochondrial morphology in WT yeast upon expression of different Dnm1 mutant variants (A430D, G397D, R438C and C481F). Scale bar represents 5 µm. **(B)** The graph represents quantification of mitochondrial morphology in WT yeast cells expressing mitochondrial membrane targeted preCOX4-mCherry and mutant variants of Dnm1. Error bar indicates SEM of two independent experiments. A two-way ANOVA with Dunnett's multiple comparison was used to assess the significance of difference observed in mutant variants with cells expressing FL-Dnm1-GFP. ****$p < 0.0001$.

5.2.6 MD simulation of mutated variants of Dnm1

Recently, machine learning was used to investigate the role of Dnm1 in mitochondrial fission [263]. The computational structural analysis suggested that mutation in the GTPase domain (e.g, G43S and K206N) results in impaired nucleotide-binding [291]. The link between

the structure and dynamics of Dnm1 protein is not completely understood. MD simulation can be a useful tool in understanding the structure-dynamics relationship of Dnm1. To understand the effects of mutations in the middle domain on the local structure and dynamics of Dnm1, we first built the 3D structure of Dnm1 using homology modelling and the resulting structure was subjected to MD simulations for the first time. Results indicate that A430D mutation exerts pronounced effect in altering the local structure and dynamics.

Root mean square deviation (RMSD) of the protein-heavy atoms of Dnm1 relative to the homology modelled structure was estimated and is given in Fig. 5.11. Small RMSD of < 3.4 Å indicates that the MD structures are very similar to the starting template homology structure. The region around residue 430 shows the highest structural deviation relative to the starting template structure. Plateau of RMSD vs time plot confirm structural convergence.

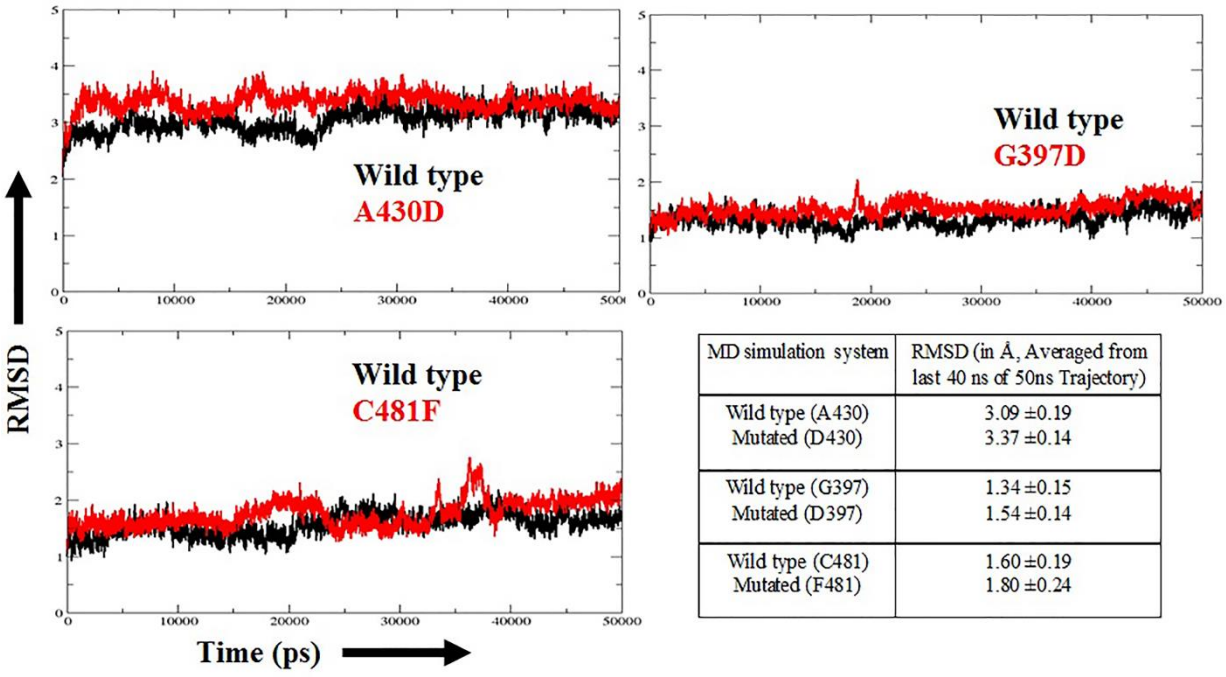

MD simulation system	RMSD (in Å, Averaged from last 40 ns of 50ns Trajectory)
Wild type (A430)	3.09 ±0.19
Mutated (D430)	3.37 ±0.14
Wild type (G397)	1.34 ±0.15
Mutated (D397)	1.54 ±0.14
Wild type (C481)	1.60 ±0.19
Mutated (F481)	1.80 ±0.24

Fig. 5.11 Root mean square deviation (RMSD in Å) vs time (in ps) plot. RMSD was estimated relative to the starting structure (homology modelled Dnm1). Average RMSD was estimated from the last 40 ns of trajectory. Standard deviation is reported after ±.

Root-mean-square fluctuations (RMSF) is a popular choice to measure the flexibility of biomolecule during an MD trajectory. RMSF was estimated along the MD trajectory and averaged for every amino acid residue. Comparison of RMSF between WT and mutant Dnm1 indicates that (1) local flexibility is severely altered in response to A430D mutation (see residue 417–423, and 436–449, Fig. 5.12A). Note, flexibility increases in the residue 417–423 region and decreases in residue 436–449 region upon A430D mutation. (2) G397D and C481F mutations are less significant in altering protein flexibility (Fig. 5.13).

A430D mutation results in a conformational change of helix-loop region (residue 421–443, Fig. 5.12B) and alters the local intra-protein interaction network around the mutation site (Fig. 5.12B). The appearance of polar side-chain upon A430→D430 mutation in the hydrophobic patch (consist of V427, I431, and V443) of Dnm1 is energetically unfavorable and induces the conformation change by exposing the D430 side-chain to solvents and fine-tune the intra-protein interaction network (Fig. 5.12B, Table 5.1). A430D mutation results in the formation of hydrogen bonding network involving R438 (side-chain) and T435 (backbone), disrupting T419 (side-chain) and P418 residues. Hence, A430D mutation results in a decrease and increase in the flexibility in the region containing R438 and T419 respectively (Fig. 5.12A). Conformation change of the helix-loop region (residue 421–443) is a robust feature observed in the MD simulations (Fig. 5.12B). R428 and R432 form salt-bridge with E667 and E669, respectively in the A430D mutant (Fig. 5.12B), whereas WT Dnm1 shows R428:E666 and R432:E667 salt-bridges.

Comparison of the WT and G397D mutant structures reveals a noticeable change in the loop (residue 384–397) orientation (Fig. 5.14A). The change in local interaction network in response to G397D mutation includes (1) formation of salt bridge interaction between D397 and K480, and (2) loss of two backbone hydrogen bonds (i.e, R400:C396, I401:G397) (Fig. 5.14A, Table 5.1). Loss of backbone interactions leads to the altered orientation of the loop (residue

384–397).

Structural integrity was preserved and least altered in C481F mutant relative to its analogue (WT). The bulky phenyl side-chain of F481 in the mutant is adjusted in the hydrophobic patch by disrupting C481-N378 interaction (Fig. 5.14B).

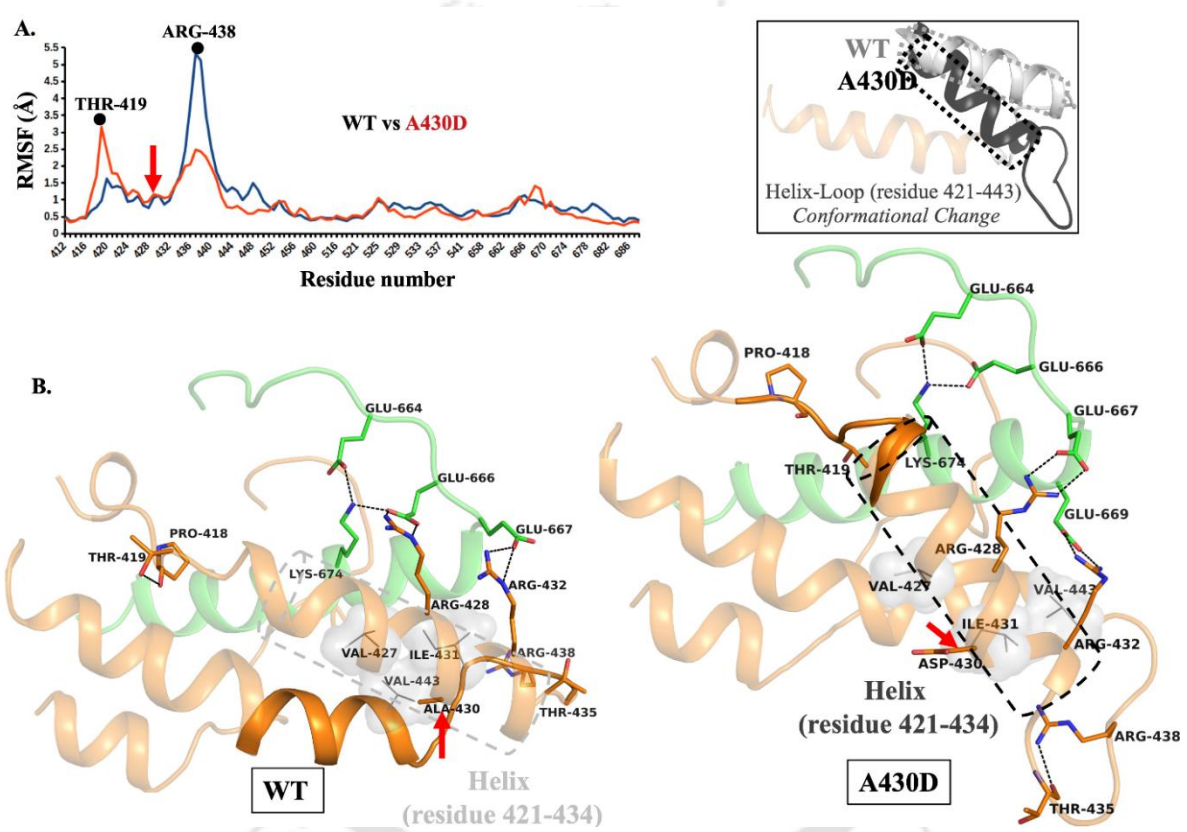

Fig. 5.12 (A) MD trajectory averaged residue-wise RMSF of protein-heavy atoms. A430D mutation results in increase and decrease of flexibility around T419 and R438 residues. **(B)** MD structure of WT and mutant (A430D) around the mutation site. Hydrophobic pocket in the vicinity of the residue 430 is denoted by grey surface. Key interactions are highlighted by the broken line and the location of mutation is marked with red arrow. Helix-loop conformation change as a result of A430D mutation is highlighted within the black-box.

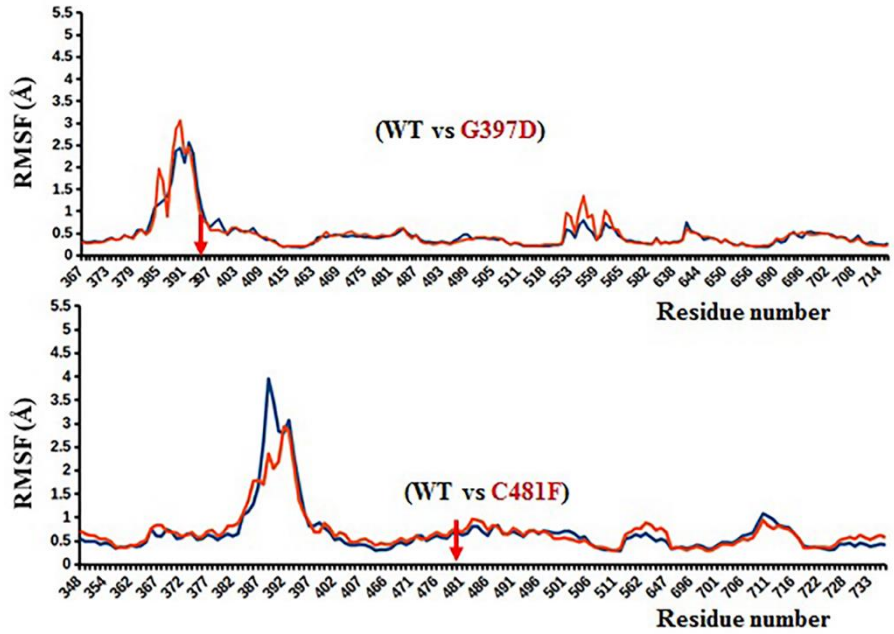

Fig. 5.13 Residue-wise RMSF of protein-heavy atoms: WT vs G397D (upper panel), WT vs C481F (lower panel). RMSF was estimated by averaging over last 25 ns of 50 ns trajectory. Location of mutation is marked with red arrow.

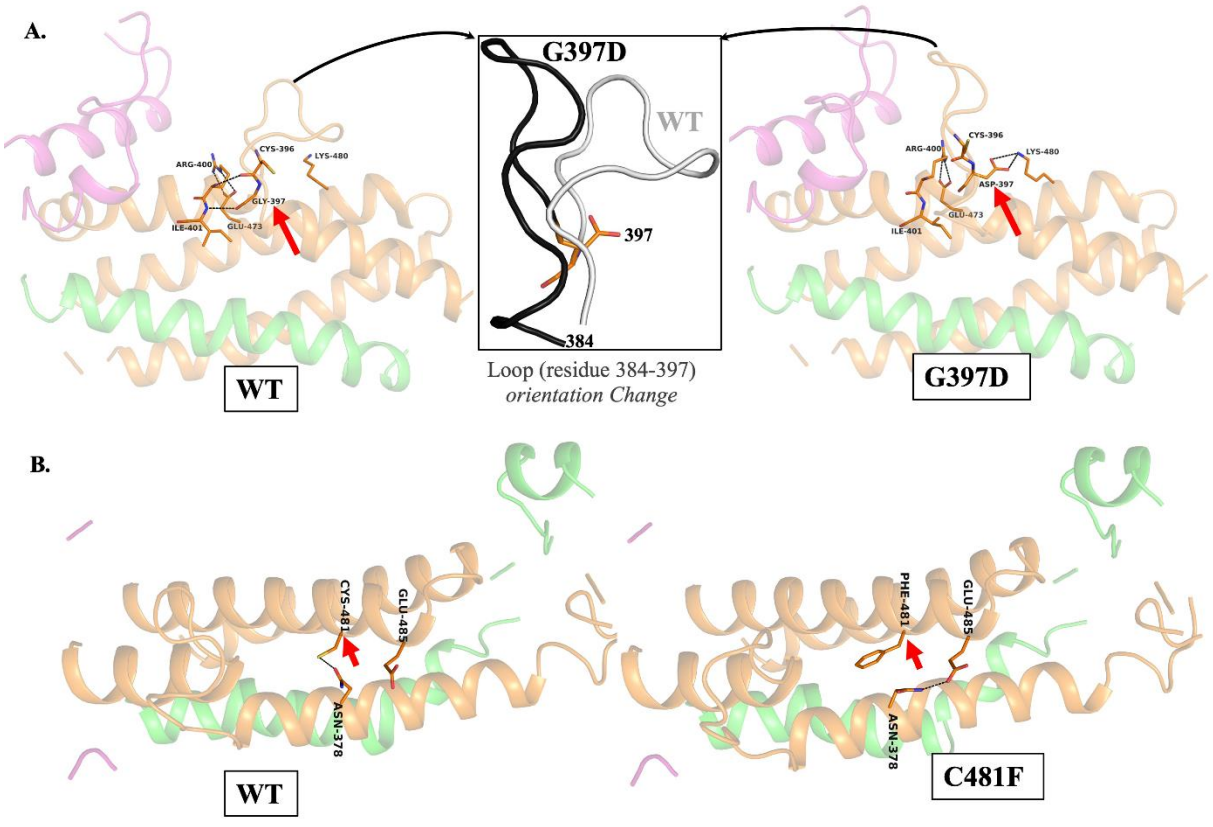

Fig. 5.14 Structural comparison of WT and mutant variants. (A) WT vs G397D mutant. Significant change in loop (residue 384–397) orientation as a result of G397D mutation is highlighted within the black-box. **(B)** WT vs C481F. Key interactions are highlighted by the broken line and the location of mutation is marked with red arrow.

Solvent accessible surface area (SASA) of a biomolecule is a geometric measure of the surface area that is accessible to a solvent. SASA plays a key role in biomolecular association (binding affinity). Estimation of SASA from the MD trajectories suggests no significant change in SASA in response to mutations (Table 5.2). A small increase in SASA in case of C481F mutation is due to the larger size of F side-chain. Secondary structural content (helix, sheet and loop region) was also well conserved during MD simulations for both WT and mutant variants of Dnm1 (Fig. 5.13).

R438 is located in the loop region of the middle domain of modelled WT Dnm1 (Fig. 5.1C). R438 is not involved in interactions with any other protein residues of Dnm1 monomer and exposes its side-chain to the water. Hence, R438C mutation is unlikely to alter the secondary structural feature of the protein. Thus, we have not performed simulations with R438C mutant. It can be argued that R438C mutation might hinder the dimer/higher-order structure or disrupt interaction with other interacting partners. The lack of high resolution experimental structural data certainly limits the computational analysis. Furthermore, our MD simulations is not appropriate to address the importance of bio-molecular cross talk involving multiple bio-macromolecular partners including Dnm1; nevertheless, the results provide atomic insights into the structural and dynamical aspects of monomeric Dnm1 in response to mutations (A430D, G397D, and C481F).

Table 5.1 Key interatomic distances (in Å) around the mutation sites of Dnm1 (averaged over the MD trajectories) WT (3rd column) and its mutant analogue (4th column). Distances are averaged over last 25 ns of 50 ns MD and standard deviation is given as error after ±. Heavy atom distances more than 3.4 Å are not reported.

SI. No	Residue pairs	WT (Distances in Å)	A430D (Distances in Å)
1	K674: E664	3.29 ± 0.78	2.77 ± 0.12
2	K674: E666	2.68 ± 0.09	2.87 ± 0.43
3	E666: R428	2.73 ± 0.12 2.74 ± 0.13	- -
5	E667: R432	2.98 ± 0.54 3.50 ± 0.43	- -
7	E667: R428	- -	2.95 ± 0.47 2.91 ± 0.44
8	E669: R432	-	2.69 ± 0.09 2.73 ± 0.11
9	T419: P418 (main-chain/O)	2.68 ± 0.93	-
10	R428: T435 (main-chain/O)	-	2.90 ± 0.21
SI. No	**Residue pairs**	**WT (Distances in Å)**	**G397D (Distances in Å)**
1	R400: E473	2.80 ± 0.17 2.76 ± 0.15	2.96 ± 0.36 2.96 ± 0.31
2	R400 (main-chain/N): C396 (main-chain/O)	3.31 ± 0.20	-
3	I401 (main-chain/N): G397 (main-chain/O)	2.76 ± 0.15	-
4	D397: K480	- -	2.90 ± 0.32 2.99 ± 0.44

Table 5.2 Trajectory averaged (from last 25 ns of 50 ns production dynamics) SASA and secondary structural elements for WT and mutant Dnm1. Standard deviation is given after ±.

MD simulation system	SASA (in nm²)	Secondary structural content (in %)		
		Helix	Sheet	Loop
WT (A430)	82.39 ±1.37	47.7	-	52.3
Mutated (D430)	82.22 ±1.31	47.7	-	52.3
WT (G397)	121.16 ±1.54	65.1	01.1	33.8
Mutated (D397)	120.55 ±1.46	69.3	01.1	29.7
WT (C481)	119.84 ±1.57	65.4	-	34.6
Mutated (F481)	124.34 ±1.89	66.7	-	33.6

5.3 Discussion

DRP1 is the central protein that regulates mitochondrial fission. It is conserved across eukaryotes and the yeast orthologue is called Dnm1. DRP1/Dnm1 belongs to the family of dynamin-like GTPase proteins whose mechanism of action is proposed to be similar to that of classical dynamins with a difference in their membrane association [303]. The role of distinct domains of the protein in its function has been extensively studied. Earlier studies have analyzed various pathogenic mutations of DRP1 and their corresponding Dnm1 variants such as K41A, G385D, G35A, A430G, R438C, C466Y for mitochondrial morphology in yeast [189]. In this study, we have chosen four additional pathogenic mutations and investigated the mitochondrial morphology and studied in detail the effect of the chosen mutations on protein structure and function. The four Dnm1 mutations mimicking equivalent DRP1 mutations that cause disease conditions in humans were generated and expressed in yeast. All the chosen mutations in this study are mapped to the middle domain of the protein. Fluorescence microscopy and western blotting confirms that all the mutant variants of the protein were expressed in yeast cells.

DRP1^{G362D} mutation resulted in hyperfused mitochondria in patient cells [195]. In our study, expression of G397D (DRP1^{G362D}) (neutral non-polar glycine to acidic polar aspartic acid) was reduced in stationary cells when compared to the FL-Dnm1 and other mutant variants. Further, we also observed reduced number of Dnm1 puncta in these cells which were also larger in size. These puncta also differed in their dynamic nature and were observed to be very static, unlike the WT protein. Strikingly, cells expressing this mutation had reduced growth on glycerol signifying loss of mitochondrial function. Additionally, these cells depicted highly fragmented mitochondria on glycerol unlike WT cells. Fragmentation of mitochondria in these cells could be as a result of accumulation of reactive oxygen species which in turn could be due to dysfunctional mitochondria. Our observation that the cytosolic fraction of the protein is reduced in cells expressing G397D and also that the puncta are immobile suggests that this mutation most

likely does not interfere with the localization of the protein to the mitochondria but may hamper the disassociation of the protein from the organelle. Computer simulations of G397D mutant of the monomeric Dnm1 reveals a striking change in the orientation of a loop region (residue 384–397, Fig. 5.14A). This conformational change of the loop might hamper the formation of higher order structure resulting in functional loss. Earlier studies have reported a lack of association of DRP1^{G362D} variant with its anchor Mid49. Interestingly, cryo EM studies of this variant showed that DRP1 formed only closed ring-like structures which differed from the tubules and rings formed by the WT protein. Also the WT rings were dynamic and disassembled in the presence of GTP unlike the mutant [131].

The mutation that showed the greatest effect on mitochondrial morphology and protein function was the A430D. This is equivalent to the DRP1^{A395D} mutation that was reported in a patient who exhibited abnormal brain development and survived only 37 days of birth. The patient fibroblasts exhibited aberrant mitochondrial and peroxisome morphology [194]. This mutation also showed problems with higher order assembly and enhanced monomeric species of the protein were observed using size exclusion chromatography [122]. Very interestingly, A430D resulted in the loss of punctate phenotype of Dnm1 with most cells expressing cytosolic fluorescence. However, a fraction of cells expressing A430D also exhibited numerous small puncta albeit which showed reduced dynamic behavior when compared to WT protein. A similar cytosolic distribution of the protein was earlier reported for another middle domain mutation G385D which was also reported to be non-functional and exhibited aberrant mitochondrial morphology [104, 189]. In our study, A430D also exhibited the most robust dominant-negative phenotype when expressed in WT cells and interfered with the function of the WT protein. MD simulations suggest that A430D mutation induces a conformational change of a helix-loop region (Fig. 5.12B) and severely alters the local flexibility (Fig. 5.12A) relative to WT monomeric Dnm1 and corroborates the experimental observations.

The C481F (neutral slightly polar cysteine to neutral nonpolar phenylalanine) and R438C (basic polar arginine to neutral slightly polar cysteine) mutations had a more subtle effect on the overall function of Dnm1. Approximately, 40% of cells in R438C showed fallen or tubular morphology similar to *dnm1* cells. Similar data was earlier reported in MEF cells harboring $DRP1^{R403C}$ mutation [199]. The number of Dnm1 puncta, localization and the dynamic behavior of the protein in cells expressing R403C was similar to that of WT protein. R438C in our study showed a milder dominant-negative effect in yeast which is in line with an earlier report [189]. Yeast cells expressing C481F did not show any marked difference in mitochondrial morphology, localization and dynamics of the protein. In contrary, patient cells expressing C446F exhibited hampered mitochondrial fission and reduced expression of the protein [197].

Overall, we have shown that mutations at equivalent sites of Dnm1 can be used to model fundamental aspects of DRP1 function. Interestingly, not all studied disease mutations exhibited a dominant-negative effect as reported in disease conditions. We therefore, cannot exclude that yeast do not fully recapitulate the complexity of the diseased conditions though much of our understanding of mitochondrial function comes from studies in *S. cerevisiae*. Interestingly, though all the studied mutations are mapped to the middle domain of the protein, the extent of effect caused by these on mitochondrial structure, structure and function of the protein is very diverse. This further highlights important residues/ regions in the middle domain of the protein needed to maintain optimum structure and function. Our data suggests that detailed study of individual mutations is necessary to understand the molecular alterations in disease mimicking conditions. However, as mitochondria have a key role in several essential cellular functions, the diseases caused due to alterations in this organelle are also not only very diverse but challenging to study.

Chapter 6

Conclusion and Future perspectives

6.1 Conclusion

The important feature that differentiates eukaryotic and prokaryotic cells is the presence of membrane-bound structures in the former. Hence, eukaryotic cells rely on extensive membrane dynamics. Most of these membranes undergo constant remodelling, fission and fusion to maintain the organelle shape and form. This shape and form are ultimately linked to the function of the sub-cellular structures. Several cellular functions, such as secretion, organelle biogenesis, autophagy, and cell division, rely on this ability of membranes [304, 305]. Membrane remodelling, fission and fusion are regulated by several proteins [27, 306, 307]. The large GTPase protein family that comprises dynamins and related proteins constitutes an important group of such proteins [71, 308]. The importance of dynamin-related proteins in organelle biogenesis has been accepted for a long time and is also reported in several model organisms [86, 87, 260, 261, 275, 300].

One such organelle that is dependent on the dynamin-related proteins for the fission and fusion of its membrane is the mitochondria [68, 71, 309]. Interestingly, the proteins required for mitochondrial fission are conserved across all eukaryotic organisms, and so is the central regulator, the GTPase Dnm1 (DRP1 in mammals), which is essential for mitochondrial fission [71, 310]. In yeast, the transmembrane protein Fis1 recruits Dnm1 with the assistance of adaptor proteins Mdv1 or Caf4 [88, 92, 93, 103, 107]. Subsequently, Dnm1 forms oligomers on the mitochondrial membrane, which encircles the fission site and eventually divides the membrane by its GTPase activity [111]. The ER-mediated constriction marks the fission site on the mitochondria and a role for cytoskeletal elements in this has also been proposed [20, 136, 311].

Most studies concerning yeast Dnm1 have utilized microscopy and biochemical approaches as the major tool, to characterize the role of the protein in mitochondrial fission. Residues in various domains of the protein have been reported to be essential for the function

of the protein [94, 99, 104, 263]. Mutations not only in the GTPase domain of the protein but also in the other domains are reported that lead to the loss of function of the protein [99, 104]. This emphasizes the importance of inter-molecular interactions that form large oligomers involving different domains [94, 99, 111, 274]. On the other hand, it is noteworthy that extensive literature is available on the regulation of human DRP1 by various post-translational modifications (PTMs) in different cell types [141, 143, 145, 147, 148, 151]. Among these, the regulation of DRP1 activity via phosphorylation has been extensively studied [141, 143, 145]. Very few studies have reported such regulation in other model organisms [261, 282]. Several global proteome studies have reported sites that can undergo phosphorylation in *Saccharomyces cerevisiae*. However, it is unknown if this phosphorylation has any role in regulating the protein's structure and function. Interestingly, recent study has identified phosphorylation of *C. merolae* Dnm1 at T139. However, the authors reported that this modification had no role in the localization of the protein [261].

The research pertaining to organelles has garnered attention in recent times, especially with the emergence of studies reporting organelle dysfunction in disease conditions. Dysfunctional mitochondria and especially lack of regulation of fission (i.e. both excessive fission and lack of fission) are associated with various pathological conditions in humans [41, 155, 312]. The altered PTM status of DRP1 is a major contributor to this lack of regulation of mitochondrial fission [143, 147, 284, 313]. Not only PTM, but several studies have linked specific mutations in DRP1 to disease conditions in humans [187, 193, 194, 197]. Given the high degree of conservation between Dnm1 and DRP1, structural and functional analysis conducted using Dnm1 as a model largely applies to DRP1. Thus, to further understand the regulation of Dnm1-mediated mitochondrial fission a two-sided approach was used. The first is to decipher and characterize phosphorylation-mediated regulation of Dnm1 and the second is to gain insights into disease-causing DRP1 mutations using Dnm1 as a model.

To achieve the above objectives, we started off with the construction of two Dnm1 fusion proteins, Dnm1-GFP and Dnm1-His-HA. Both the fusion proteins were functional as they complemented cells lacking Dnm1 and restored the defective mitochondrial morphology. The fusion proteins also enabled us to study the expression, localization and function of Dnm1 *in vivo* and *in vitro*. The secondary structure of the purified protein was determined to be predominantly α-helical. These fusion proteins were subsequently used for determining the effect of selected residues on the structure and function of the protein. To dig deeper into the regulation of Dnm1 by phosphorylation, five putative residues (T62, S277, S575, S624, S629) conserved across species and reported by global phosphoproteome studies were analyzed. We identified T62 and S277 two residues in the GTPase domain, as important for both *in vivo* and *in vitro* function of Dnm1. Cells expressing mutant variants Dnm1T62A/D and Dnm1S277A/D showed mitochondrial morphology predominantly similar to *dnm1* cells (Fig. 4.5). However, T62A/D and S277A/D mutant variants differed in the number of GFP-puncta in the cells and their localization. We report for the first time a residue in the GTPase domain, S277 which when mutated to either A/D still localized to the mitochondria, retained its secondary structure but was non-functional. Not only the *in vivo* experiments but also the *in vitro* GTPase activity assay revealed a significant reduction in the activity of T62A/D and S277A/D variants (Fig. 4.11E). T62A/D and S277A/D are able to form higher-ordered structures *in vitro*, which are most likely non-functional (Fig. 4.12). MD simulation and computational analysis revealed altered atomistic motion of residues far from the mutation site (Fig. 4.16B), increased protein compactness in S277A (Fig. 4.15), and large RMSD fluctuations in GED and B-insert domains (Fig. 4.13), suggesting altered intramolecular interactions upon mutation of GTPase domain residues (Fig. 4.16A).

The mutations exhibited a dominant-negative effect, suggesting that the mutant protein interacts with the WT protein and renders it non-functional (Fig. 4.17). At this stage, we are

unable to say if these residues (both T62 and S277) undergo phosphorylation and if the effect observed is due to the altered phosphorylation status of the protein in the variants or the change in the structure and interactions of the protein that may result due to aminoacyl substitution. However, both scenarios highlight the importance of these residues for the function of the protein.

In this study, we also further mimicked four disease-causing mutations of the middle domain of human DRP1 in yeast Dnm1. Altered mitochondrial morphology similar to as in *dnm1* cells was observed in A430D. Protein expression, localization and dynamics were analyzed and have been found to be affected in these cells. The reduced cytosolic fraction and presence of immobile puncta in cells expressing G397D variant suggested that this mutation does not affect the localization of Dnm1 to mitochondria but may hinder its disassociation from the organelle (Fig. 5.7, Fig. 5.8). MD simulations of the G397D variant revealed a significant conformational change in a loop region, potentially disrupting higher-order structural formation and causing functional loss (Fig. 5.14). A430D mutation, on the other hand, resulted in a completely different phenotype of Dnm1-GFP, unlike all other mutant variants analyzed in this thesis. Cells expressing A430D displayed cytosolic fluorescence and Dnm1 puncta was not visible in most cells (Fig. 5.7). A430D also showed a strong dominant-negative effect when expressed in WT cells similar to T62A/D and S277A/D variants (Fig. 5.10). MD simulations suggested that A430D induced a conformational change in a helix-loop region, severely affecting local flexibility compared to the WT monomeric Dnm1, consistent with experimental findings (Fig. 5.12). The R438C and C481F mutations showed milder effects on mitochondrial morphology and protein function.

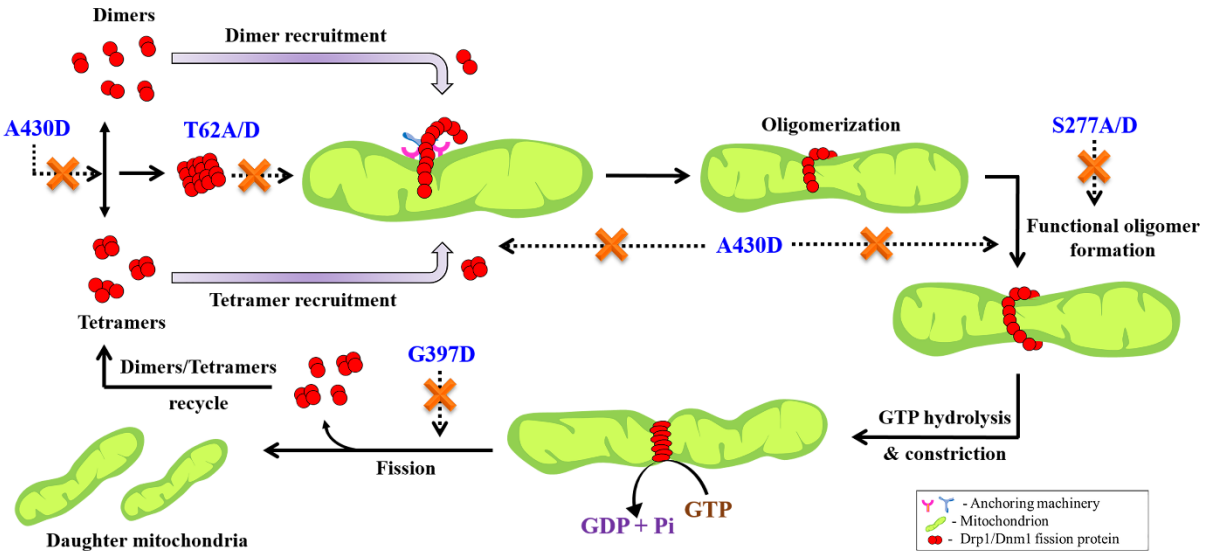

Fig. 6.1. Schematic representing the life cycle of Dnm1 and its role in mitochondrial fission. From the results obtained in our study, the mutant variants are most likely affected at different stages of the lifecycle of Dnm1. The cytosolic fluorescence observed in most A430D expressing cells indicate that the dimer-tetramer interconversion in the cytosol may be dysregulated in these cells. On the other hand, very small and weak fluorescent spots were observed in some cells, posing a question of their functional oligomeric status on the OMM. T62A/D mutations most likely hinder the recruitment of Dnm1 to the OMM. S277A/D though localized to OMM, may impede the formation of functional oligomers. Lastly, G397D mutation most likely hampers the release of Dnm1 oligomers from the OMM.

In a nutshell, in this study we have analysed nine residues, out of which two are in the GTPase domain, four in the middle domain and three are in the variable domain of the protein. Interesting phenotypic changes were observed upon mutating four residues, T62, S277, G397D, and A430D. The lifecycle of Dnm1 from the cytosol back to cytosol has been described in the earlier chapters. From the different phenotypes observed in our study and their detailed analysis, we hypothesize and indicate the role of the four residues in various stages of the life cycle of Dnm1 (Fig. 6.1). We propose that A430D variants are most likely arrested at the dimer (or monomer) stage that in turn also effects the dimer-tetramer stoichiometry in the cytosol and their recruitment to the OMM. Interestingly, small and faint Dnm1 puncta on the OMM were observed in some of these cells suggesting dysregulated higher-order structure formation. T62A/D, on the other hand, may form oligomers in the cytosol but are not recruited to the OMM (Fig. 6.1). S277A/D are recruited to the OMM but are unable to form functional higher-

order structures (Fig. 6.1). Lastly, G397D is also recruited to the OMM but is unable to disassociate from the OMM, an important step in the life cycle (Fig. 6.1). In summary, these findings highlight the diverse effects of mutations on Dnm1 and emphasize the importance of studying individual mutations to understand the structure-function relationship of the protein.

6.2 Future perspectives

- Our data highlights the significance of two residues (T62 and S277) in the G2 and G5 motifs of the GTPase domain that affect the function of the protein both *in vivo* and *in vitro*. We could not detect the phosphorylation of these residues in the conditions used in this study. The contribution of this modification to the phenotypes observed needs to be assessed.
- However, it cannot be ruled out that the changes are purely due to structural alterations. For this, X-ray crystallography or Cryo-EM structure of the purified protein can be determined to pinpoint the exact structural changes.
- Interestingly, some recent literature on other proteins, such as Ras and Rab, suggests a link between the phosphorylation of residues in the GTPase domain and GTP hydrolysis. It can be determined if this is also true in the case of Dnm1.
- Altered local structure and localization phenotype upon mutating key residues have been observed in this study. This also suggests altered interactions with the interacting partners of Dnm1 and should be analyzed.
- In our study, we propose two types of higher-order structures of Dnm1, functional and non-functional. It is intriguing as to how these two can be distinguished.
- The cytosolic fluorescence observed in A430D is a very interesting phenotype observed for Dnm1, which is otherwise always seen as dynamic puncta. Dnm1 is also reported to exist as dimers in the cytosol. Hence, the observed phenotype in A430D variant needs further characterization.

- We have also reported that the mutations resulted in dominant-negative effects when expressed in WT cells. How this is exactly achieved needs to be investigated.
- Several new mutations have been reported after our study was initiated [190-193]. It is important to study different mutations in detail to link the structural alterations with the observed defects in function.
- The exact regions of G1/G2/G3/G4/G5 in yeast Dnm1 are not identified. The effect of each region on GTP-binding and GTP hydrolysis needs to be understood.
- Finally, we have also observed some variation with respect to the importance of residues in human and yeast proteins. For instance, S616 is extensively phosphorylated and crucial for the function in human DRP1. On the other hand, the corresponding residue in yeast S624 is not indispensable for the function of Dnm1. Initial studies suggest that phosphorylation of Dnm1 may not be as essential in both budding yeast and fission yeast as in human DRP1. Is there an evolutionary significance for such a mechanism of regulation in higher eukaryotes? This needs to be addressed.
- Given the significance of mitochondria in cellular processes, diseases associated with mitochondrial alterations are diverse and challenging to study. Studying the role of Dnm1 in different model organisms will also provide comprehensive insights into mitochondrial dysfunction-related disorders. Ultimately, understanding the precise molecular mechanisms that regulate the function of Dnm1 and DRP1 can also open avenues that can be used as a therapeutic approach in treating disease conditions where altered mitochondrial fission is a major contributor to the disease pathology.

Bibliography

1. Ernster L, Schatz G: **Mitochondria: a historical review.** *The Journal of cell biology* 1981, **91:**227s-255s.
2. Ploumi C, Daskalaki I, Tavernarakis N: **Mitochondrial biogenesis and clearance: a balancing act.** *The FEBS Journal* 2017, **284:**183-195.
3. McBride HM, Neuspiel M, Wasiak S: **Mitochondria: more than just a powerhouse.** *Current Biology* 2006, **16:**R551-R560.
4. Brand M, Orr A, Perevoshchikova I, Quinlan C: **The role of mitochondrial function and cellular bioenergetics in ageing and disease.** *British Journal of Dermatology* 2013, **169:**1-8.
5. Murphy E, Ardehali H, Balaban RS, DiLisa F, Dorn GW, Kitsis RN, Otsu K, Ping P, Rizzuto R, Sack MN, Wallace D: **Mitochondrial function, biology, and role in disease: a scientific statement from the American Heart Association.** *Circulation research* 2016, **118:**1960-1991.
6. Rossmann MP, Dubois SM, Agarwal S, Zon LI: **Mitochondrial function in development and disease.** *Disease Models & Mechanisms* 2021, **14:**dmm048912.
7. Kowallik KV, Martin WF: **The origin of symbiogenesis: An annotated English translation of Mereschkowsky's 1910 paper on the theory of two plasma lineages.** *Biosystems* 2021, **199:**104281.
8. Gray MW, Burger G, Lang BF: **Mitochondrial evolution.** *Science* 1999, **283:**1476-1481.
9. Gray MW: **Mitochondrial evolution.** *Cold Spring Harbor perspectives in biology* 2012, **4:**a011403.
10. Roger AJ, Muñoz-Gómez SA, Kamikawa R: **The origin and diversification of mitochondria.** *Current Biology* 2017, **27:**R1177-R1192.
11. Malina C, Larsson C, Nielsen J: **Yeast mitochondria: an overview of mitochondrial biology and the potential of mitochondrial systems biology.** *FEMS yeast research* 2018, **18:**foy040.
12. Richard P: **The rhythm of yeast.** *FEMS microbiology reviews* 2003, **27:**547-557.
13. Hagman A, Piškur J: **A study on the fundamental mechanism and the evolutionary driving forces behind aerobic fermentation in yeast.** 2015, **10:**e0116942.
14. Alan L, Scorrano L: **Shaping fuel utilization by mitochondria.** *Current Biology* 2022, **32:**R618-R623.
15. Spinelli JB, Haigis MC: **The multifaceted contributions of mitochondria to cellular metabolism.** *Nature cell biology* 2018, **20:**745-754.
16. McCommis KS, Finck BN: **Mitochondrial pyruvate transport: a historical perspective and future research directions.** *Biochemical journal* 2015, **466:**443-454.
17. Protasoni M, Zeviani M: **Mitochondrial structure and bioenergetics in normal and disease conditions.** *International journal of molecular sciences* 2021, **22:**586.
18. Joubert F, Puff N: **Mitochondrial cristae architecture and functions: lessons from minimal model systems.** *Membranes* 2021, **11:**465.
19. Muñoz JP, Basei FL, Rojas ML, Galvis D, Zorzano A: **Mechanisms of Modulation of Mitochondrial Architecture.** *Biomolecules* 2023, **13:**1225.
20. Friedman JR, Lackner LL, West M, DiBenedetto JR, Nunnari J, Voeltz GK: **ER tubules mark sites of mitochondrial division.** *Science* 2011, **334:**358-362.
21. Schrader M, Godinho LF, Costello JL, Islinger M: **The different facets of organelle interplay—an overview of organelle interactions.** *Frontiers in cell and developmental biology* 2015, **3:**56.
22. Xia M, Zhang Y, Jin K, Lu Z, Zeng Z, Xiong W: **Communication between mitochondria and other organelles: a brand-new perspective on mitochondria in cancer.** *Cell & Bioscience* 2019, **9:**1-19.

23. Newby ZE, O'Connell Iii J, Robles-Colmenares Y, Khademi S, Miercke LJ, Stroud RM: **Crystal structure of the aquaglyceroporin PfAQP from the malarial parasite Plasmodium falciparum.** *Nature structural & molecular biology* 2008, **15:**619-625.
24. Varughese JT, Buchanan SK, Pitt AS: **The role of voltage-dependent anion channel in mitochondrial dysfunction and human disease.** *Cells* 2021, **10:**1737.
25. Palade GE: **An electron microscope study of the mitochondrial structure.** *Journal of Histochemistry & Cytochemistry* 1953, **1:**188-211.
26. Wolf DM, Segawa M, Kondadi AK, Anand R, Bailey ST, Reichert AS, van der Bliek AM, Shackelford DB, Liesa M, Shirihai OS: **Individual cristae within the same mitochondrion display different membrane potentials and are functionally independent.** *The EMBO journal* 2019, **38:**e101056.
27. Giacomello M, Pyakurel A, Glytsou C, Scorrano L: **The cell biology of mitochondrial membrane dynamics.** *Nature reviews Molecular cell biology* 2020, **21:**204-224.
28. Paumard P, Vaillier J, Coulary B, Schaeffer J, Soubannier V, Mueller DM, Brèthes D, Di Rago J-P, Velours J: **The ATP synthase is involved in generating mitochondrial cristae morphology.** *The EMBO journal* 2002, **21:**221-230.
29. Frazier AE, Chacinska A, Truscott KN, Guiard B, Pfanner N, Rehling P: **Mitochondria use different mechanisms for transport of multispanning membrane proteins through the intermembrane space.** *Molecular and cellular biology* 2003, **23:**7818-7828.
30. Lee W-K, Thévenod F: **A role for mitochondrial aquaporins in cellular life-and-death decisions?** *American Journal of Physiology-Cell Physiology* 2006, **291:**C195-C202.
31. Kühlbrandt W: **Structure and function of mitochondrial membrane protein complexes.** *BMC biology* 2015, **13:**1-11.
32. Colina-Tenorio L, Horten P, Pfanner N, Rampelt H: **Shaping the mitochondrial inner membrane in health and disease.** *Journal of Internal Medicine* 2020, **287:**645-664.
33. Edwards R, Eaglesfield R, Tokatlidis K: **The mitochondrial intermembrane space: The most constricted mitochondrial sub-compartment with the largest variety of protein import pathways.** *Open biology* 2021, **11:**210002.
34. Herrmann JM, Riemer J: **The intermembrane space of mitochondria.** *Antioxidants & redox signaling* 2010, **13:**1341-1358.
35. Martínez-Reyes I, Chandel NS: **Mitochondrial TCA cycle metabolites control physiology and disease.** *Nature communications* 2020, **11:**102.
36. Zhelev Z, Aoki I, Lazarova D, Vlaykova T, Higashi T, Bakalova R: **A "weird" mitochondrial fatty acid oxidation as a metabolic "secret" of cancer.** *Oxidative Medicine and Cellular Longevity* 2022, **2022**.
37. Langkjær RB, Casaregola S, Ussery D, Gaillardin C, Piškur J: **Sequence analysis of three mitochondrial DNA molecules reveals interesting differences among Saccharomyces yeasts.** *Nucleic acids research* 2003, **31:**3081-3091.
38. Vafai SB, Mootha VK: **Mitochondrial disorders as windows into an ancient organelle.** *Nature* 2012, **491:**374-383.
39. Green A, Hossain T, Eckmann DM: **Mitochondrial dynamics involves molecular and mechanical events in motility, fusion and fission.** *Frontiers in cell and developmental biology* 2022, **10:**1010232.
40. Chan DC: **Mitochondrial dynamics and its involvement in disease.** *Annual Review of Pathology: Mechanisms of Disease* 2020, **15:**235-259.
41. Yapa NM, Lisnyak V, Reljic B, Ryan MT: **Mitochondrial dynamics in health and disease.** *FEBS letters* 2021, **595:**1184-1204.

42. Van der Bliek AM, Shen Q, Kawajiri S: **Mechanisms of mitochondrial fission and fusion.** *Cold Spring Harbor perspectives in biology* 2013, **5:**a011072.
43. Altmann K, Frank M, Neumann D, Jakobs S, Westermann B: **The class V myosin motor protein, Myo2, plays a major role in mitochondrial motility in Saccharomyces cerevisiae.** *The Journal of cell biology* 2008, **181:**119-130.
44. Fung TS, Chakrabarti R, Higgs HN: **The multiple links between actin and mitochondria.** *Nature reviews Molecular cell biology* 2023**:**1-17.
45. Ren L, Chen X, Chen X, Li J, Cheng B, Xia J: **Mitochondrial dynamics: fission and fusion in fate determination of mesenchymal stem cells.** *Frontiers in Cell and Developmental Biology* 2020, **8:**580070.
46. Liu YJ, McIntyre RL, Janssens GE, Houtkooper RH: **Mitochondrial fission and fusion: A dynamic role in aging and potential target for age-related disease.** *Mechanisms of ageing and development* 2020, **186:**111212.
47. Chen H, Vermulst M, Wang YE, Chomyn A, Prolla TA, McCaffery JM, Chan DC: **Mitochondrial fusion is required for mtDNA stability in skeletal muscle and tolerance of mtDNA mutations.** *Cell* 2010, **141:**280-289.
48. Chen H, Chomyn A, Chan DC: **Disruption of fusion results in mitochondrial heterogeneity and dysfunction.** *Journal of Biological Chemistry* 2005, **280:**26185-26192.
49. Merz S, Westermann B: **Genome-wide deletion mutant analysis reveals genes required for respiratory growth, mitochondrial genome maintenance and mitochondrial protein synthesis in Saccharomyces cerevisiae.** *Genome biology* 2009, **10:**1-18.
50. Silva Ramos E, Motori E, Brüser C, Kühl I, Yeroslaviz A, Ruzzenente B, Kauppila JH, Busch JD, Hultenby K, Habermann BH, Jakobs S: **Mitochondrial fusion is required for regulation of mitochondrial DNA replication.** *PLoS genetics* 2019, **15:**e1008085.
51. Chen H, McCaffery JM, Chan DC: **Mitochondrial fusion protects against neurodegeneration in the cerebellum.** *Cell* 2007, **130:**548-562.
52. Ishihara T, Ban-Ishihara R, Maeda M, Matsunaga Y, Ichimura A, Kyogoku S, Aoki H, Katada S, Nakada K, Nomura M, Mizushima N: **Dynamics of mitochondrial DNA nucleoids regulated by mitochondrial fission is essential for maintenance of homogeneously active mitochondria during neonatal heart development.** *Molecular and cellular biology* 2015, **35:**211-223.
53. Westermann B: **Mitochondrial inheritance in yeast.** *Biochimica et Biophysica Acta (BBA)-Bioenergetics* 2014, **1837:**1039-1046.
54. Taguchi N, Ishihara N, Jofuku A, Oka T, Mihara K: **Mitotic phosphorylation of dynamin-related GTPase Drp1 participates in mitochondrial fission.** *Journal of Biological Chemistry* 2007, **282:**11521-11529.
55. Twig G, Elorza A, Molina AJ, Mohamed H, Wikstrom JD, Walzer G, Stiles L, Haigh SE, Katz S, Las G, Alroy J: **Fission and selective fusion govern mitochondrial segregation and elimination by autophagy.** *The EMBO journal* 2008, **27:**433-446.
56. Innokentev A, Kanki T: **Mitophagy in yeast: Molecular mechanism and regulation.** *Cells* 2021, **10:**3569.
57. Mao K, Klionsky DJ: **Participation of mitochondrial fission during mitophagy.** vol. 12. pp. 3131-3132: Taylor & Francis; 2013:3131-3132.
58. Mao K, Wang K, Liu X, Klionsky DJ: **The scaffold protein Atg11 recruits fission machinery to drive selective mitochondria degradation by autophagy.** *Developmental cell* 2013, **26:**9-18.
59. Kageyama Y, Hoshijima M, Seo K, Bedja D, Sysa-Shah P, Andrabi SA, Chen W, Höke A, Dawson VL, Dawson TM, Gabrielson K: **Parkin-independent mitophagy requires**

Drp1 and maintains the integrity of mammalian heart and brain. *The EMBO journal* 2014, **33:**2798-2813.

60. Ikeda Y, Shirakabe A, Maejima Y, Zhai P, Sciarretta S, Toli J, Nomura M, Mihara K, Egashira K, Ohishi M, Abdellatif M: **Endogenous Drp1 mediates mitochondrial autophagy and protects the heart against energy stress.** *Circulation research* 2015, **116:**264-278.
61. Kanki T, Furukawa K, Yamashita S-i: **Mitophagy in yeast: Molecular mechanisms and physiological role.** *Biochimica et Biophysica Acta (BBA)-Molecular Cell Research* 2015, **1853:**2756-2765.
62. Abeliovich H, Zarei M, Rigbolt KT, Youle RJ, Dengjel J: **Involvement of mitochondrial dynamics in the segregation of mitochondrial matrix proteins during stationary phase mitophagy.** *Nature communications* 2013, **4:**2789.
63. Mendl N, Occhipinti A, Müller M, Wild P, Dikic I, Reichert AS: **Mitophagy in yeast is independent of mitochondrial fission and requires the stress response gene WHI2.** *Journal of cell science* 2011, **124:**1339-1350.
64. Chipuk J, Bouchier-Hayes L, Green D: **Mitochondrial outer membrane permeabilization during apoptosis: the innocent bystander scenario.** *Cell Death & Differentiation* 2006, **13:**1396-1402.
65. Fannjiang Y, Cheng W-C, Lee SJ, Qi B, Pevsner J, McCaffery JM, Hill RB, Basañez G, Hardwick JM: **Mitochondrial fission proteins regulate programmed cell death in yeast.** *Genes & development* 2004, **18:**2785-2797.
66. Frank S, Gaume B, Bergmann-Leitner ES, Leitner WW, Robert EG, Catez F, Smith CL, Youle RJ: **The role of dynamin-related protein 1, a mediator of mitochondrial fission, in apoptosis.** *Developmental cell* 2001, **1:**515-525.
67. Jenner A, Peña-Blanco A, Salvador-Gallego R, Ugarte-Uribe B, Zollo C, Ganief T, Bierlmeier J, Mund M, Lee JE, Ries J, D S: **DRP1 interacts directly with BAX to induce its activation and apoptosis.** *The EMBO journal* 2022, **41:**e108587.
68. Westermann B: **Mitochondrial fusion and fission in cell life and death.** *Nature reviews Molecular cell biology* 2010, **11:**872-884.
69. Ferguson SM, De Camilli P: **Dynamin, a membrane-remodelling GTPase.** *Nature reviews Molecular cell biology* 2012, **13:**75-88.
70. Kar UP, Dey H, Rahaman A: **Regulation of dynamin family proteins by post-translational modifications.** *Journal of biosciences* 2017, **42:**333-344.
71. Ramachandran R, Schmid SL: **The dynamin superfamily.** *Current Biology* 2018, **28:**R411-R416.
72. Lu B, Kennedy B, Clinton RW, Wang EJ, McHugh D, Stepanyants N, Macdonald PJ, Mears JA, Qi X, Ramachandran R: **Steric interference from intrinsically disordered regions controls dynamin-related protein 1 self-assembly during mitochondrial fission.** *Scientific reports* 2018, **8:**1-21.
73. Fröhlich C, Grabiger S, Schwefel D, Faelber K, Rosenbaum E, Mears J, Rocks O, Daumke O: **Structural insights into oligomerization and mitochondrial remodelling of dynamin 1-like protein.** *The EMBO journal* 2013, **32:**1280-1292.
74. Rapaport D, Brunner M, Neupert W, Westermann B: **Fzo1p is a mitochondrial outer membrane protein essential for the biogenesis of functional mitochondria in Saccharomyces cerevisiae.** *Journal of Biological Chemistry* 1998, **273:**20150-20155.
75. Hermann GJ, Thatcher JW, Mills JP, Hales KG, Fuller MT, Nunnari J, Shaw JM: **Mitochondrial fusion in yeast requires the transmembrane GTPase Fzo1p.** *The Journal of cell biology* 1998, **143:**359-373.
76. Sesaki H, Jensen RE: **UGO1 encodes an outer membrane protein required for mitochondrial fusion.** *The Journal of cell biology* 2001, **152:**1123-1134.

77. Sesaki H, Jensen RE: **Ugo1p links the Fzo1p and Mgm1p GTPases for mitochondrial fusion.** *Journal of Biological Chemistry* 2004, **279:**28298-28303.
78. Hoppins S, Horner J, Song C, McCaffery JM, Nunnari J: **Mitochondrial outer and inner membrane fusion requires a modified carrier protein.** *Journal of Cell Biology* 2009, **184:**569-581.
79. Meeusen S, DeVay R, Block J, Cassidy-Stone A, Wayson S, McCaffery JM, Nunnari J: **Mitochondrial inner-membrane fusion and crista maintenance requires the dynamin-related GTPase Mgm1.** *Cell* 2006, **127:**383-395.
80. Wong ED, Wagner JA, Gorsich SW, McCaffery JM, Shaw JM, Nunnari J: **The dynamin-related GTPase, Mgm1p, is an intermembrane space protein required for maintenance of fusion competent mitochondria.** *The Journal of cell biology* 2000, **151:**341-352.
81. Sesaki H, Jensen RE: **Division versus Fusion: Dnm1p and Fzo1p Antagonistically Regulate Mitochondrial Shape.** *Journal of Cell Biology* 1999, **147:**699-706.
82. Chen H, Detmer SA, Ewald AJ, Griffin EE, Fraser SE, Chan DC: **Mitofusins Mfn1 and Mfn2 coordinately regulate mitochondrial fusion and are essential for embryonic development.** *The Journal of cell biology* 2003, **160:**189-200.
83. Olichon A, Baricault L, Gas N, Guillou E, Valette A, Belenguer P, Lenaers G: **Loss of OPA1 perturbates the mitochondrial inner membrane structure and integrity, leading to cytochrome c release and apoptosis.** *Journal of Biological Chemistry* 2003, **278:**7743-7746.
84. Cipolat S, de Brito OM, Dal Zilio B, Scorrano L: **OPA1 requires mitofusin 1 to promote mitochondrial fusion.** *Proceedings of the National Academy of Sciences* 2004, **101:**15927-15932.
85. Ge Y, Shi X, Boopathy S, McDonald J, Smith AW, Chao LH: **Two forms of Opa1 cooperate to complete fusion of the mitochondrial inner-membrane.** *Elife* 2020, **9:**e50973.
86. Otsuga D, Keegan BR, Brisch E, Thatcher JW, Hermann GJ, Bleazard W, Shaw JM: **The dynamin-related GTPase, Dnm1p, controls mitochondrial morphology in yeast.** *The Journal of cell biology* 1998, **143:**333-349.
87. Smirnova E, Griparic L, Shurland D-L, Van Der Bliek AM: **Dynamin-related protein Drp1 is required for mitochondrial division in mammalian cells.** *Molecular biology of the cell* 2001, **12:**2245-2256.
88. Mozdy A, McCaffery J, Shaw J: **Dnm1p GTPase-mediated mitochondrial fission is a multi-step process requiring the novel integral membrane component Fis1p.** *The Journal of cell biology* 2000, **151:**367-380.
89. Zhang Y, Chan DC: **Structural basis for recruitment of mitochondrial fission complexes by Fis1.** *Proceedings of the National Academy of Sciences* 2007, **104:**18526-18530.
90. James DI, Parone PA, Mattenberger Y, Martinou J-C: **hFis1, a novel component of the mammalian mitochondrial fission machinery.** *Journal of Biological Chemistry* 2003, **278:**36373-36379.
91. Tieu Q, Nunnari J: **Mdv1p is a WD repeat protein that interacts with the dynamin-related GTPase, Dnm1p, to trigger mitochondrial division.** *The Journal of cell biology* 2000, **151:**353-366.
92. Tieu Q, Okreglak V, Naylor K, Nunnari J: **The WD repeat protein, Mdv1p, functions as a molecular adaptor by interacting with Dnm1p and Fis1p during mitochondrial fission.** *Journal of Cell Biology* 2002, **158:**445-452.

93. Griffin EE, Graumann J, Chan DC: **The WD40 protein Caf4p is a component of the mitochondrial fission machinery and recruits Dnm1p to mitochondria.** *The Journal of cell biology* 2005, **170:**237-248.
94. Naylor K, Ingerman E, Okreglak V, Marino M, Hinshaw JE, Nunnari J: **Mdv1 interacts with assembled dnm1 to promote mitochondrial division.** *Journal of Biological Chemistry* 2006, **281:**2177-2183.
95. Cerveny KL, Studer SL, Jensen RE, Sesaki H: **Yeast mitochondrial division and distribution require the cortical num1 protein.** *Developmental cell* 2007, **12:**363-375.
96. Hammermeister M, Schödel K, Westermann B: **Mdm36 is a mitochondrial fission-promoting protein in Saccharomyces cerevisiae.** *Molecular biology of the cell* 2010, **21:**2443-2452.
97. Otera H, Wang C, Cleland MM, Setoguchi K, Yokota S, Youle RJ, Mihara K: **Mff is an essential factor for mitochondrial recruitment of Drp1 during mitochondrial fission in mammalian cells.** *Journal of Cell Biology* 2010, **191:**1141-1158.
98. Palmer CS, Osellame LD, Laine D, Koutsopoulos OS, Frazier AE, Ryan MT: **MiD49 and MiD51, new components of the mitochondrial fission machinery.** *EMBO reports* 2011, **12:**565-573.
99. Bui HT, Karren MA, Bhar D, Shaw JM: **A novel motif in the yeast mitochondrial dynamin Dnm1 is essential for adaptor binding and membrane recruitment.** *Journal of Cell Biology* 2012, **199:**613-622.
100. Wells RC, Picton LK, Williams SC, Tan FJ, Hill RB: **Direct binding of the dynamin-like GTPase, Dnm1, to mitochondrial dynamics protein Fis1 is negatively regulated by the Fis1 N-terminal arm.** *Journal of Biological Chemistry* 2007, **282:**33769-33775.
101. Gammie AE, Kurihara LJ, Vallee RB, Rose MD: **DNM1, a dynamin-related gene, participates in endosomal trafficking in yeast.** *The Journal of cell biology* 1995, **130:**553-566.
102. Van Der Bliek AM: **Functional diversity in the dynamin family.** *Trends in cell biology* 1999, **9:**96-102.
103. Bleazard W, McCaffery JM, King EJ, Bale S, Mozdy A, Tieu Q, Nunnari J, Shaw JM: **The dynamin-related GTPase Dnm1 regulates mitochondrial fission in yeast.** *Nature cell biology* 1999, **1:**298-304.
104. Bhar D, Karren MA, Babst M, Shaw JM: **Dimeric Dnm1-G385D interacts with Mdv1 on mitochondria and can be stimulated to assemble into fission complexes containing Mdv1 and Fis1.** *Journal of Biological Chemistry* 2006, **281:**17312-17320.
105. Lackner LL, Horner JS, Nunnari J: **Mechanistic analysis of a dynamin effector.** *Science* 2009, **325:**874-877.
106. Guo Q, Koirala S, Perkins EM, McCaffery JM, Shaw JM: **The mitochondrial fission adaptors Caf4 and Mdv1 are not functionally equivalent.** *PloS one* 2012, **7:**e53523.
107. Schauss AC, Bewersdorf Jr, Jakobs S: **Fis1p and Caf4p, but not Mdv1p, determine the polar localization of Dnm1p clusters on the mitochondrial surface.** *Journal of cell science* 2006, **119:**3098-3106.
108. Elgass K, Pakay J, Ryan MT, Palmer CS: **Recent advances into the understanding of mitochondrial fission.** *Biochimica et Biophysica Acta (BBA) - Molecular Cell Research* 2013, **1833:**150-161.
109. Chen Y-C, Cheng T-H, Lin W-L, Chen C-L, Yang WY, Blackstone C, Chang C-R: **Srv2 is a pro-fission factor that modulates yeast mitochondrial morphology and respiration by regulating actin assembly.** *iScience* 2019, **11:**305-317.

110. Roux A, Uyhazi K, Frost A, De Camilli P: **GTP-dependent twisting of dynamin implicates constriction and tension in membrane fission.** *Nature* 2006, **441:**528-531.
111. Ingerman E, Perkins EM, Marino M, Mears JA, McCaffery JM, Hinshaw JE, Nunnari J: **Dnm1 forms spirals that are structurally tailored to fit mitochondria.** *The Journal of cell biology* 2005, **170:**1021-1027.
112. Jakobs S, Martini N, Schauss AC, Egner A, Westermann B, Hell SW: **Spatial and temporal dynamics of budding yeast mitochondria lacking the division component Fis1p.** *Journal of cell science* 2003, **116:**2005-2014.
113. Legesse-Miller A, Massol RH, Kirchhausen T: **Constriction and Dnm1p recruitment are distinct processes in mitochondrial fission.** *Molecular biology of the cell* 2003, **14:**1953-1963.
114. Abrisch RG, Gumbin SC, Wisniewski BT, Lackner LL, Voeltz GK: **Fission and fusion machineries converge at ER contact sites to regulate mitochondrial morphology.** *Journal of Cell Biology* 2020, **219**.
115. Bui HT, Shaw JM: **Dynamin assembly strategies and adaptor proteins in mitochondrial fission.** *Current Biology* 2013, **23:**R891-R899.
116. Mears JA, Lackner LL, Fang S, Ingerman E, Nunnari J, Hinshaw JE: **Conformational changes in Dnm1 support a contractile mechanism for mitochondrial fission.** *Nature structural & molecular biology* 2011, **18:**20-26.
117. Hu C, Huang Y, Li L: **Drp1-dependent mitochondrial fission plays critical roles in physiological and pathological progresses in mammals.** *International journal of molecular sciences* 2017, **18:**144.
118. Rosdah AA, Smiles WJ, Oakhill JS, Scott JW, Langendorf CG, Delbridge LM, Holien JK, Lim SY: **New perspectives on the role of Drp1 isoforms in regulating mitochondrial pathophysiology.** *Pharmacology & Therapeutics* 2020**:**107594.
119. Strack S, Wilson TJ, Cribbs JT: **Cyclin-dependent kinases regulate splice-specific targeting of dynamin-related protein 1 to microtubules.** *Journal of Cell Biology* 2013, **201:**1037-1051.
120. Liu R, Chan DC: **The mitochondrial fission receptor Mff selectively recruits oligomerized Drp1.** *Molecular biology of the cell* 2015, **26:**4466-4477.
121. Yu R, Lendahl U, Nistér M, Zhao J: **Regulation of mammalian mitochondrial dynamics: opportunities and challenges.** *Frontiers in Endocrinology* 2020, **11:**374.
122. Chang C-R, Manlandro CM, Arnoult D, Stadler J, Posey AE, Hill RB, Blackstone C: **A lethal de novo mutation in the middle domain of the dynamin-related GTPase Drp1 impairs higher order assembly and mitochondrial division.** *Journal of Biological Chemistry* 2010, **285:**32494-32503.
123. Kornfeld OS, Qvit N, Haileselassie B, Shamloo M, Bernardi P, Mochly-Rosen D: **Interaction of mitochondrial fission factor with dynamin related protein 1 governs physiological mitochondrial function in vivo.** *Scientific reports* 2018, **8:**14034.
124. Lee Y-j, Jeong S-Y, Karbowski M, Smith CL, Youle RJ: **Roles of the mammalian mitochondrial fission and fusion mediators Fis1, Drp1, and Opa1 in apoptosis.** *Molecular biology of the cell* 2004, **15:**5001-5011.
125. Zhao J, Liu T, Jin S, Wang X, Qu M, Uhlén P, Tomilin N, Shupliakov O, Lendahl U, Nistér M: **Human MIEF1 recruits Drp1 to mitochondrial outer membranes and promotes mitochondrial fusion rather than fission.** *The EMBO journal* 2011, **30:**2762-2778.
126. Shen Q, Yamano K, Head BP, Kawajiri S, Cheung JT, Wang C, Cho J-H, Hattori N, Youle RJ, van der Bliek AM: **Mutations in Fis1 disrupt orderly disposal of defective mitochondria.** *Molecular biology of the cell* 2014, **25:**145-159.

127. Joshi AU, Saw NL, Shamloo M, Mochly-Rosen D: **Drp1/Fis1 interaction mediates mitochondrial dysfunction, bioenergetic failure and cognitive decline in Alzheimer's disease.** *Oncotarget* 2018, **9:**6128.
128. Xian H, Yang Q, Xiao L, Shen H-M, Liou Y-C: **STX17 dynamically regulated by Fis1 induces mitophagy via hierarchical macroautophagic mechanism.** *Nature communications* 2019, **10:**2059.
129. Losón OC, Meng S, Ngo H, Liu R, Kaiser JT, Chan DC: **Crystal structure and functional analysis of MiD49, a receptor for the mitochondrial fission protein Drp1.** *Protein Science* 2015, **24:**386-394.
130. Losón OC, Liu R, Rome ME, Meng S, Kaiser JT, Shan S-o, Chan DC: **The mitochondrial fission receptor MiD51 requires ADP as a cofactor.** *Structure* 2014, **22:**367-377.
131. Kalia R, Wang RY-R, Yusuf A, Thomas PV, Agard DA, Shaw JM, Frost A: **Structural basis of mitochondrial receptor binding and constriction by DRP1.** *Nature* 2018, **558:**401-405.
132. Cho HM, Ryu JR, Jo Y, Seo TW, Choi YN, Kim JH, Chung JM, Cho B, Kang HC, Yu S-W, Yoo S: **Drp1-Zip1 interaction regulates mitochondrial quality surveillance system.** *Molecular Cell* 2019, **73:**364-376. e368.
133. Francy CA, Clinton RW, Fröhlich C, Murphy C, Mears JA: **Cryo-EM studies of Drp1 reveal cardiolipin interactions that activate the helical oligomer.** *Scientific reports* 2017, **7:**1-12.
134. Bustillo-Zabalbeitia I, Montessuit S, Raemy E, Basañez G, Terrones O, Martinou J-C: **Specific interaction with cardiolipin triggers functional activation of dynamin-related protein 1.** *PloS one* 2014, **9:**e102738.
135. Ji W-k, Hatch AL, Merrill RA, Strack S, Higgs HN: **Actin filaments target the oligomeric maturation of the dynamin GTPase Drp1 to mitochondrial fission sites.** *Elife* 2015, **4:**e11553.
136. Prudent J, McBride HM: **Mitochondrial dynamics: ER actin tightens the Drp1 noose.** *Current Biology* 2016, **26:**R207-R209.
137. Hatch AL, Ji W-K, Merrill RA, Strack S, Higgs HN: **Actin filaments as dynamic reservoirs for Drp1 recruitment.** *Molecular biology of the cell* 2016, **27:**3109-3121.
138. Rehklau K, Hoffmann L, Gurniak CB, Ott M, Witke W, Scorrano L, Culmsee C, Rust MB: **Cofilin1-dependent actin dynamics control DRP1-mediated mitochondrial fission.** *Cell death & disease* 2017, **8:**e3063-e3063.
139. Losón OC, Song Z, Chen H, Chan DC: **Fis1, Mff, MiD49, and MiD51 mediate Drp1 recruitment in mitochondrial fission.** *Molecular biology of the cell* 2013, **24:**659-667.
140. Jin J-y, Wei X-x, Zhi X-l, Wang X-h, Meng D: **Drp1-dependent mitochondrial fission in cardiovascular disease.** *Acta Pharmacologica Sinica* 2020**:**1-10.
141. Chang C-R, Blackstone C: **Cyclic AMP-dependent protein kinase phosphorylation of Drp1 regulates its GTPase activity and mitochondrial morphology.** *Journal of Biological Chemistry* 2007, **282:**21583-21587.
142. Cereghetti G, Stangherlin A, De Brito OM, Chang C, Blackstone C, Bernardi P, Scorrano L: **Dephosphorylation by calcineurin regulates translocation of Drp1 to mitochondria.** *Proceedings of the National Academy of Sciences* 2008, **105:**15803-15808.
143. Kashatus JA, Nascimento A, Myers LJ, Sher A, Byrne FL, Hoehn KL, Counter CM, Kashatus DF: **Erk2 phosphorylation of Drp1 promotes mitochondrial fission and MAPK-driven tumor growth.** *Molecular Cell* 2015, **57:**537-551.

144. Ko SH, Choi GE, Oh JY, Lee HJ, Kim JS, Chae CW, Choi D, Han HJ: **Succinate promotes stem cell migration through the GPR91-dependent regulation of DRP1-mediated mitochondrial fission.** *Scientific reports* 2017, **7:**12582.
145. Chou C-H, Lin C-C, Yang M-C, Wei C-C, Liao H-D, Lin R-C, Tu W-Y, Kao T-C, Hsu C-M, Cheng J-T, Hong Y-R: **GSK3beta-mediated Drp1 phosphorylation induced elongated mitochondrial morphology against oxidative stress.** *PloS one* 2012, **7:**e49112.
146. Zhou L, Zhang Q, Zhang P, Sun L, Peng C, Yuan Z, Cheng J: **c-Abl-mediated Drp1 phosphorylation promotes oxidative stress-induced mitochondrial fragmentation and neuronal cell death.** *Cell death & disease* 2017, **8:**e3117-e3117.
147. Cho D-H, Nakamura T, Fang J, Cieplak P, Godzik A, Gu Z, Lipton SA: **S-nitrosylation of Drp1 mediates β-amyloid-related mitochondrial fission and neuronal injury.** *Science* 2009, **324:**102-105.
148. Figueroa-Romero C, Iñiguez-Lluhí JA, Stadler J, Chang C-R, Arnoult D, Keller PJ, Hong Y, Blackstone C, Feldman EL: **SUMOylation of the mitochondrial fission protein Drp1 occurs at multiple nonconsensus sites within the B domain and is linked to its activity cycle.** *The FASEB Journal* 2009, **23:**3917.
149. Yamada S, Sato A, Ishihara N, Akiyama H, Sakakibara S-i: **Drp1 SUMO/deSUMOylation by Senp5 isoforms influences ER tubulation and mitochondrial dynamics to regulate brain development.** *iScience* 2021, **24**.
150. Guo C, Hildick KL, Luo J, Dearden L, Wilkinson KA, Henley JM: **SENP3-mediated deSUMOylation of dynamin-related protein 1 promotes cell death following ischaemia.** *The EMBO journal* 2013, **32:**1514-1528.
151. Karbowski M, Neutzner A, Youle RJ: **The mitochondrial E3 ubiquitin ligase MARCH5 is required for Drp1 dependent mitochondrial division.** *The Journal of cell biology* 2007, **178:**71-84.
152. Wang H, Song P, Du L, Tian W, Yue W, Liu M, Li D, Wang B, Zhu Y, Cao C: **Parkin ubiquitinates Drp1 for proteasome-dependent degradation: implication of dysregulated mitochondrial dynamics in Parkinson disease.** *Journal of Biological Chemistry* 2011, **286:**11649-11658.
153. Shi L, Liu J, Peng Y, Zhang J, Dai X, Zhang S, Wang Y, Liu J, Long J: **Deubiquitinase OTUD6A promotes proliferation of cancer cells via regulating Drp1 stability and mitochondrial fission.** *Molecular oncology* 2020, **14:**3169-3183.
154. Khacho M, Slack RS: **Mitochondrial dynamics in the regulation of neurogenesis: from development to the adult brain.** *Developmental Dynamics* 2018, **247:**47-53.
155. Serasinghe MN, Chipuk JE: **Mitochondrial fission in human diseases.** *Pharmacology of Mitochondria* 2016**:**159-188.
156. Park SJ, Bae J-E, Jo DS, Kim JB, Park NY, Fang J, Jung Y-K, Jo DG, Cho D-H: **Increased O-GlcNAcylation of Drp1 by amyloid-beta promotes mitochondrial fission and dysfunction in neuronal cells.** *Molecular Brain* 2021, **14:**1-3.
157. Kandimalla R, Reddy PH: **Multiple faces of dynamin-related protein 1 and its role in Alzheimer's disease pathogenesis.** *Biochimica et Biophysica Acta (BBA)-Molecular Basis of Disease* 2016, **1862:**814-828.
158. Yan J, Liu X-H, Han M-Z, Wang Y-M, Sun X-L, Yu N, Li T, Su B, Chen Z-Y: **Blockage of GSK3β-mediated Drp1 phosphorylation provides neuroprotection in neuronal and mouse models of Alzheimer's disease.** *Neurobiology of aging* 2015, **36:**211-227.
159. Zhang X, Wang R, Hu D, Sun X, Fujioka H, Lundberg K, Chan ER, Wang Q, Xu R, Flanagan ME: **Oligodendroglial glycolytic stress triggers inflammasome activation and neuropathology in Alzheimer's disease.** *Science advances* 2020, **6:**eabb8680.

160. Portz P, Lee MK: **Changes in Drp1 Function and Mitochondrial Morphology Are Associated with the α-Synuclein Pathology in a Transgenic Mouse Model of Parkinson's Disease.** *Cells* 2021, **10:**885.
161. Dagda RK, Cherra III SJ, Kulich SM, Tandon A, Park D, Chu CT: **Loss of PINK1 function promotes mitophagy through effects on oxidative stress and mitochondrial fission.** *Journal of Biological Chemistry* 2009, **284:**13843-13855.
162. Feng S-T, Wang Z-Z, Yuan Y-H, Wang X-L, Sun H-M, Chen N-H, Zhang Y: **Dynamin-related protein 1: a protein critical for mitochondrial fission, mitophagy, and neuronal death in Parkinson's disease.** *Pharmacological research* 2020, **151:**104553.
163. Cui M, Tang X, Christian WV, Yoon Y, Tieu K: **Perturbations in mitochondrial dynamics induced by human mutant PINK1 can be rescued by the mitochondrial division inhibitor mdivi-1.** *Journal of Biological Chemistry* 2010, **285:**11740-11752.
164. Qi X, Qvit N, Su Y-C, Mochly-Rosen D: **A novel Drp1 inhibitor diminishes aberrant mitochondrial fission and neurotoxicity.** *Journal of cell science* 2013, **126:**789-802.
165. Solesio ME, Prime TA, Logan A, Murphy MP, del Mar Arroyo-Jimenez M, Jordán J, Galindo MF: **The mitochondria-targeted anti-oxidant MitoQ reduces aspects of mitochondrial fission in the 6-OHDA cell model of Parkinson's disease.** *Biochimica et Biophysica Acta (BBA)-Molecular Basis of Disease* 2013, **1832:**174-182.
166. Wang X, Yan MH, Fujioka H, Liu J, Wilson-Delfosse A, Chen SG, Perry G, Casadesus G, Zhu X: **LRRK2 regulates mitochondrial dynamics and function through direct interaction with DLP1.** *Human molecular genetics* 2012, **21:**1931-1944.
167. Prudent J, Zunino R, Sugiura A, Mattie S, Shore GC, McBride HM: **MAPL SUMOylation of Drp1 stabilizes an ER/mitochondrial platform required for cell death.** *Molecular Cell* 2015, **59:**941-955.
168. Zhang Q, Hu C, Huang J, Liu W, Lai W, Leng F, Tang Q, Liu Y, Wang Q, Zhou M: **ROCK1 induces dopaminergic nerve cell apoptosis via the activation of Drp1-mediated aberrant mitochondrial fission in Parkinson's disease.** *Experimental & molecular medicine* 2019, **51:**1-13.
169. Zheng J, Winderickx J, Franssens V, Liu B: **A mitochondria-associated oxidative stress perspective on Huntington's disease.** *Frontiers in molecular neuroscience* 2018, **11:**329.
170. Haun F, Nakamura T, Shiu AD, Cho D-H, Tsunemi T, Holland EA, La Spada AR, Lipton SA: **S-nitrosylation of dynamin-related protein 1 mediates mutant huntingtin-induced mitochondrial fragmentation and neuronal injury in Huntington's disease.** *Antioxidants & redox signaling* 2013, **19:**1173-1184.
171. Lima AR, Santos L, Correia M, Soares P, Sobrinho-Simões M, Melo M, Máximo V: **Dynamin-related protein 1 at the crossroads of cancer.** *Genes* 2018, **9:**115.
172. Liu Z, Sun Y, Tan S, Liu L, Hu S, Huo H, Li M, Cui Q, Yu M: **Nutrient deprivation-related OXPHOS/glycolysis interconversion via HIF-1α/C-MYC pathway in U251 cells.** *Tumor Biology* 2016, **37:**6661-6671.
173. Zhan L, Cao H, Wang G, Lyu Y, Sun X, An J, Wu Z, Huang Q, Liu B, Xing J: **Drp1-mediated mitochondrial fission promotes cell proliferation through crosstalk of p53 and NF-κB pathways in hepatocellular carcinoma.** *Oncotarget* 2016, **7:**65001.
174. Parker DJ, Iyer A, Shah S, Moran A, Hjelmeland AB, Basu MK, Liu R, Mitra K: **A new mitochondrial pool of cyclin E, regulated by Drp1, is linked to cell-density-dependent cell proliferation.** *Journal of cell science* 2015, **128:**4171-4182.
175. Rehman J, Zhang HJ, Toth PT, Zhang Y, Marsboom G, Hong Z, Salgia R, Husain AN, Wietholt C, Archer SL: **Inhibition of mitochondrial fission prevents cell cycle progression in lung cancer.** *The FASEB Journal* 2012, **26:**2175-2186.

176. Xu S, Wang P, Zhang H, Gong G, Cortes NG, Zhu W, Yoon Y, Tian R, Wang W: **CaMKII induces permeability transition through Drp1 phosphorylation during chronic β-AR stimulation.** *Nature communications* 2016, **7:**1-13.
177. Maneechote C, Palee S, Chattipakorn SC, Chattipakorn N: **Roles of mitochondrial dynamics modulators in cardiac ischaemia/reperfusion injury.** *Journal of cellular and molecular medicine* 2017, **21:**2643-2653.
178. Hasan P, Saotome M, Ikoma T, Iguchi K, Kawasaki H, Iwashita T, Hayashi H, Maekawa Y: **Mitochondrial fission protein, dynamin-related protein 1, contributes to the promotion of hypertensive cardiac hypertrophy and fibrosis in Dahl-salt sensitive rats.** *Journal of molecular and cellular cardiology* 2018, **121:**103-106.
179. Macdonald PJ, Francy CA, Stepanyants N, Lehman L, Baglio A, Mears JA, Qi X, Ramachandran R: **Distinct splice variants of dynamin-related protein 1 differentially utilize mitochondrial fission factor as an effector of cooperative GTPase activity.** *The Journal of biological chemistry* 2016, **291:**493.
180. Yoon G, Malam Z, Paton T, Marshall CR, Hyatt E, Ivakine Z, Scherer SW, Lee K-S, Hawkins C, Cohn RD: **Lethal disorder of mitochondrial fission caused by mutations in DNM1L.** *The Journal of pediatrics* 2016, **171:**313-316. e312.
181. Nasca A, Legati A, Baruffini E, Nolli C, Moroni I, Ardissone A, Goffrini P, Ghezzi D: **Biallelic mutations in DNM1L are associated with a slowly progressive infantile encephalopathy.** *Human mutation* 2016, **37:**898-903.
182. Wenger J, Klinglmayr E, Fröhlich C, Eibl C, Gimeno A, Hessenberger M, Puehringer S, Daumke O, Goettig P: **Functional mapping of human dynamin-1-like GTPase domain based on x-ray structure analyses.** *PloS one* 2013, **8:**e71835.
183. Gerber S, Charif M, Chevrollier A, Chaumette T, Angebault C, Kane MS, Paris A, Alban J, Quiles M, Delettre C, Guy L: **Mutations in DNM1L, as in OPA1, result in dominant optic atrophy despite opposite effects on mitochondrial fusion and fission.** *Brain* 2017, **140:**2586-2596.
184. Song Z, Ghochani M, McCaffery JM, Frey TG, Chan DC: **Mitofusins and OPA1 mediate sequential steps in mitochondrial membrane fusion.** *Molecular biology of the cell* 2009, **20:**3525-3532.
185. Hogarth KA, Costford SR, Yoon G, Sondheimer N, Maynes JT: **DNM1L variant alters baseline mitochondrial function and response to stress in a patient with severe neurological dysfunction.** *Biochemical genetics* 2018, **56:**56-77.
186. Jendrach M, Mai S, Pohl S, Vöth M, Bereiter-Hahn J: **Short-and long-term alterations of mitochondrial morphology, dynamics and mtDNA after transient oxidative stress.** *Mitochondrion* 2008, **8:**293-304.
187. Verrigni D, Di Nottia M, Ardissone A, Baruffini E, Nasca A, Legati A, Bellacchio E, Fagiolari G, Martinelli D, Fusco L, Bertini E: **Clinical-genetic features and peculiar muscle histopathology in infantile DNM1L-related mitochondrial epileptic encephalopathy.** *Human mutation* 2019, **40:**601-618.
188. Longo F, Benedetti S, Zambon AA, Sora MGN, Di Resta C, De Ritis D, Quattrini A, Maltecca F, Ferrari M, Previtali SC: **Impaired turnover of hyperfused mitochondria in severe axonal neuropathy due to a novel DRP1 mutation.** *Human molecular genetics* 2020, **29:**177-188.
189. Whitley BN, Lam C, Cui H, Haude K, Bai R, Escobar L, Hamilton A, Brady L, Tarnopolsky MA, Dengle L: **Aberrant Drp1-mediated mitochondrial division presents in humans with variable outcomes.** *Human molecular genetics* 2018, **27:**3710-3719.

190. Keller N, Paketci C, Edem P, Thiele H, Yis U, Wirth B, Karakaya M: **De novo DNM1L variant presenting with severe muscular atrophy, dystonia and sensory neuropathy.** *European Journal of Medical Genetics* 2021, **64:**104134.
191. Lhuissier C, Wagner BE, Vincent A, Garraux G, Hougrand O, Van Coster R, Benoit V, Karadurmus D, Lenaers G, Gueguen N, et al: **Case report: Thirty-year progression of an EMPF1 encephalopathy due to defective mitochondrial and peroxisomal fission caused by a novel de novo heterozygous DNM1L variant.** *Frontiers in neurology* 2022, **13:**937885.
192. Wei Y, Qian M: **Case report: a novel de novo mutation in DNM1L presenting with developmental delay, ataxia, and peripheral neuropathy.** *Frontiers in Pediatrics* 2021, **9:**604105.
193. Nolden KA, Egner JM, Collier JJ, Russell OM, Alston CL, Harwig MC, Widlansky ME, Sasorith S, Barbosa IA, Douglas AG, et al: **Novel DNM1L variants impair mitochondrial dynamics through divergent mechanisms.** *Life Science Alliance* 2022, **5**.
194. Waterham HR, Koster J, van Roermund CW, Mooyer PA, Wanders RJ, Leonard JV: **A lethal defect of mitochondrial and peroxisomal fission.** *New England Journal of Medicine* 2007, **356:**1736-1741.
195. Vanstone JR, Smith AM, McBride S, Naas T, Holcik M, Antoun G, Harper M-E, Michaud J, Sell E, Chakraborty P, Matthew AL: **DNM1L-related mitochondrial fission defect presenting as refractory epilepsy.** *European Journal of Human Genetics* 2016, **24:**1084-1088.
196. Sheffer R, Douiev L, Edvardson S, Shaag A, Tamimi K, Soiferman D, Meiner V, Saada A: **Postnatal microcephaly and pain insensitivity due to a de novo heterozygous DNM1L mutation causing impaired mitochondrial fission and function.** *American Journal of Medical Genetics Part A* 2016, **170:**1603-1607.
197. Diez H, Cortès-Saladelafont E, Ormazabal A, Marmiese AF, Armstrong J, Matalonga L, Bravo M, Briones P, Emperador S, Montoya J, Àngels G-C: **Severe infantile parkinsonism because of a de novo mutation on DLP1 mitochondrial-peroxisomal protein.** *Movement Disorders* 2017, **32:**1108-1110.
198. Cho B, Choi SY, Cho HM, Kim HJ, Sun W: **Physiological and pathological significance of dynamin-related protein 1 (drp1)-dependent mitochondrial fission in the nervous system.** *Experimental neurobiology* 2013, **22:**149.
199. Fahrner JA, Liu R, Perry MS, Klein J, Chan DC: **A novel de novo dominant-negative mutation in DNM1L impairs mitochondrial fission and presents as childhood epileptic encephalopathy.** *American Journal of Medical Genetics Part A* 2016, **170:**2002-2011.
200. Zaha K, Matsumoto H, Itoh M, Saitsu H, Kato K, Kato M, Ogata S, Murayama K, Kishita Y, Mizuno Y: **DNM1L-related encephalopathy in infancy with Leigh syndrome-like phenotype and suppression-burst.** *Clinical genetics* 2016, **90:**472-474.
201. Chao Y-H, Robak LA, Xia F, Koenig MK, Adesina A, Bacino CA, Scaglia F, Bellen HJ, Wangler MF: **Missense variants in the middle domain of DNM1L in cases of infantile encephalopathy alter peroxisomes and mitochondria when assayed in Drosophila.** *Human molecular genetics* 2016, **25:**1846-1856.
202. Mew NA, Loewenstein JB, Kadom N, Lichter-Konecki U, Gropman AL, Martin JM, Vanderver A: **MRI features of 4 female patients with pyruvate dehydrogenase E1 alpha deficiency.** *Pediatric neurology* 2011, **45:**57-59.

203. Vandeleur D, Chen CV, Huang EJ, Connolly AJ, Sanchez H, Moon-Grady AJ: **Novel and lethal case of cardiac involvement in DNM1L mitochondrial encephalopathy.** *American Journal of Medical Genetics Part A* 2019, **179:**2486-2489.
204. Zhu P-P, Patterson A, Stadler J, Seeburg DP, Sheng M, Blackstone C: **Intra-and intermolecular domain interactions of the C-terminal GTPase effector domain of the multimeric dynamin-like GTPase Drp1.** *Journal of Biological Chemistry* 2004, **279:**35967-35974.
205. Batzir NA, Bhagwat PK, Eble TN, Liu P, Eng CM, Elsea SH, Robak LA, Scaglia F, Goldman AM, Dhar SU: **De novo missense variant in the GTPase effector domain (GED) of DNM1L leads to static encephalopathy and seizures.** *Molecular Case Studies* 2019, **5:**a003673.
206. Resnick MA, Cox BS: **Yeast as an honorary mammal.** *Mutation Research/Fundamental and Molecular Mechanisms of Mutagenesis* 2000, **451:**1-11.
207. Goffeau A, Barrell BG, Bussey H, Davis RW, Dujon B, Feldmann H, Galibert F, Hoheisel JD, Jacq C, Johnston M, Louis E: **Life with 6000 genes.** *Science* 1996, **274:**546-567.
208. Venter JC, Smith HO, Adams MD: **The sequence of the human genome.** *Clinical chemistry* 2015, **61:**1207-1208.
209. Bassett DE, Boguski MS, Hieter P: **Yeast genes and human disease.** *Nature* 1996, **379:**589-590.
210. Lasserre J-P, Dautant A, Aiyar RS, Kucharczyk R, Glatigny A, Tribouillard-Tanvier Db, Rytka J, Blondel M, Skoczen N, Reynier P, Pitayu L: **Yeast as a system for modelling mitochondrial disease mechanisms and discovering therapies.** *Disease Models & Mechanisms* 2015, **8:**509-526.
211. Rinaldi T, Dallabona C, Ferrero I, Frontali L, Bolotin-Fukuhara M: **Mitochondrial diseases and the role of the yeast models.** *FEMS yeast research* 2010, **10:**1006-1022.
212. Boonekamp FJ, Knibbe E, Vieira-Lara MA, Wijsman M, Luttik MA, Van Eunen K, Den Ridder M, Bron R, Suarez AMA, Van Rijn P, Wolters J: **Full humanization of the glycolytic pathway in Saccharomyces cerevisiae.** *Cell reports* 2022, **39**.
213. Kachroo AH, Vandeloo M, Greco BM, Abdullah M: **Humanized yeast to model human biology, disease and evolution.** *Disease Models & Mechanisms* 2022, **15:**dmm049309.
214. Lanz MC, Yugandhar K, Gupta S, Sanford EJ, Faça VM, Vega S, Joiner AM, Fromme JC, Yu H, Smolka MB: **In-depth and 3-dimensional exploration of the budding yeast phosphoproteome.** *EMBO reports* 2021, **22:**e51121.
215. Holt LJ, Tuch BB, Villén J, Johnson AD, Gygi SP, Morgan DO: **Global analysis of Cdk1 substrate phosphorylation sites provides insights into evolution.** *Science* 2009, **325:**1682-1686.
216. Swaney DL, Beltrao P, Starita L, Guo A, Rush J, Fields S, Krogan NJ, Villén J: **Global analysis of phosphorylation and ubiquitylation cross-talk in protein degradation.** *Nature methods* 2013, **10:**676-682.
217. Zhou X, Li W, Liu Y, Amon A: **Cross-compartment signal propagation in the mitotic exit network.** *Elife* 2021, **10:**e63645.
218. Albuquerque CP, Smolka MB, Payne SH, Bafna V, Eng J, Zhou H: **A multidimensional chromatography technology for in-depth phosphoproteome analysis.** *Molecular & Cellular Proteomics* 2008, **7:**1389-1396.
219. Soulard A, Cremonesi A, Moes S, Schütz F, Jenö P, Hall MN: **The rapamycin-sensitive phosphoproteome reveals that TOR controls protein kinase A toward some but not all substrates.** *Molecular biology of the cell* 2010, **21:**3475-3486.

220. Bauer BL, Rochon K, Liu J, Ramachandran R, Mears JA: **Disease-associated mutations in Drp1 have fundamentally different effects on the mitochondrial fission machinery.** *Biophysical Journal* 2023, **122:**482a.
221. Gerik KJ, Gary SL, Burgers PM: **Overproduction and affinity purification of Saccharomyces cerevisiae replication factor C.** *Journal of Biological Chemistry* 1997, **272:**1256-1262.
222. Gietz RD, Woods RA: **Transformation of yeast by lithium acetate/single-stranded carrier DNA/polyethylene glycol method.** In *Methods in enzymology. Volume* 350: Elsevier; 2002: 87-96
223. Wang W, Malcolm BA: **Two-stage PCR protocol allowing introduction of multiple mutations, deletions and insertions using QuikChangeTM site-directed mutagenesis.** *Biotechniques* 1999, **26:**680-682.
224. Deori NM, Infant T, Sundaravadivelu PK, Thummer RP, Nagotu S: **Pex30 undergoes phosphorylation and regulates peroxisome number in Saccharomyces cerevisiae.** *Molecular Genetics and Genomics* 2022, **297:**573-590.
225. Gao B, Zhu S: **A Fungal Defensin Targets the SARS− CoV− 2 Spike Receptor− Binding Domain.** *Journal of Fungi* 2021, **7:**553.
226. Olsen JV, de Godoy LM, Li G, Macek B, Mortensen P, Pesch R, Makarov A, Lange O, Horning S, Mann M: **Parts per million mass accuracy on an Orbitrap mass spectrometer via lock mass injection into a C-trap.** *Molecular & Cellular Proteomics* 2005, **4:**2010-2021.
227. Kinoshita E, Kinoshita-Kikuta E, Koike T: **Separation and detection of large phosphoproteins using Phos-tag SDS-PAGE.** *Nature protocols* 2009, **4:**1513-1521.
228. Ingerman E, Nunnari J: **A continuous, regenerative coupled GTPase assay for dynamin-related proteins.** *Methods in enzymology* 2005, **404:**611-619.
229. Hussain MS, Kumar M: **Assembly of Cas7 subunits of Leptospira on the mature crRNA of CRISPR-Cas IB is modulated by divalent ions.** *Gene* 2022, **818:**146244.
230. Diekert K, de Kroon AI, Kispal G, Lill R: **Isolation and subfractionation of mitochondria from the yeast Saccharomyces cerevisiae.** *Methods in cell biology* 2001, **65:**37-51.
231. Baerends RJ, Faber KN, Kram AM, Kiel JA, van der Klei IJ, Veenhuis MJJoBC: **A Stretch of Positively Charged Amino Acids at the N Terminus ofHansenula polymorpha Pex3p Is Involved in Incorporation of the Protein into the Peroxisomal Membrane.** *Journal of Biological Chemistry* 2000, **275:**9986-9995.
232. Lowry OHJJbC: **Protein measurement with the Folin phenol resgent.** *Journal of Biological Chemistry* 1951, **193:**265-275.
233. Kruger N: **The Bradford method for protein quantitation.** *The protein protocols handbook springer* 2009**:**17-24.
234. Kelley LA, Mezulis S, Yates CM, Wass MN, Sternberg MJ: **The Phyre2 web portal for protein modelling, prediction and analysis.** *Nature protocols* 2015, **10:**845-858.
235. Bisht A, Sharma M, Sharma S, Ali ME, Panda JJ: **Carrier-free self-built aspirin nanorods as anti-aggregation agents towards alpha-crystallin-derived peptide aggregates: potential implications in non-invasive cataract therapy.** *Journal of Materials Chemistry B* 2019, **7:**6945-6954.
236. Kour A, Sharma S, Dube T, Bisht A, Sharma M, Mishra J, Ali ME, Panda JJ: **l-3, 4-Dihydroxyphenylalanine templated anisotropic gold nano/micro-roses as potential disrupters/inhibitors of α-crystallin protein and its gleaned model peptide aggregates.** *International Journal of Biological Macromolecules* 2020, **163:**2374-2391.

237. Faelber K, Posor Y, Gao S, Held M, Roske Y, Schulze D, Haucke V, Noé F, Daumke O: **Crystal structure of nucleotide-free dynamin.** *Nature* 2011, **477:**556-560.
238. Reubold TF, Faelber K, Plattner N, Posor Y, Ketel K, Curth U, Schlegel J, Anand R, Manstein DJ, Noé F, et al: **Crystal structure of the dynamin tetramer.** *Nature* 2015, **525:**404-408.
239. Ford MG, Jenni S, Nunnari J: **The crystal structure of dynamin.** *Nature* 2011, **477:**561-566.
240. DeLano WL: **Pymol: An open-source molecular graphics tool.** *Newsl Protein Crystallogr* 2002, **40:**82-92.
241. Sharma S, Ali ME: **How do the mutations in Pf K13 protein promote anti-malarial drug resistance?** *Journal of Biomolecular Structure and Dynamics* 2022**:**1-10.
242. Bhatt A, Ali ME: **Understanding the role of R266K mutation in cystathionine β-synthase (CBS) enzyme: an in silico study.** *Journal of Biomolecular Structure and Dynamics* 2022, **40:**12690-12698.
243. Maier JA, Martinez C, Kasavajhala K, Wickstrom L, Hauser KE, Simmerling C: **ff14SB: improving the accuracy of protein side chain and backbone parameters from ff99SB.** *Journal of chemical theory and computation* 2015, **11:**3696-3713.
244. Nelson MT, Humphrey W, Gursoy A, Dalke A, Kalé LV, Skeel RD, Schulten K: **NAMD: a parallel, object-oriented molecular dynamics program.** *The International Journal of Supercomputer Applications and High Performance Computing* 1996, **10:**251-268.
245. Mark P, Nilsson L: **Structure and dynamics of the TIP3P, SPC, and SPC/E water models at 298 K.** *The Journal of Physical Chemistry A* 2001, **105:**9954-9960.
246. Darden T, York D, Pedersen L: **Particle mesh Ewald: An N· log (N) method for Ewald sums in large systems.** *The Journal of chemical physics* 1993, **98:**10089-10092.
247. Goga N, Rzepiela A, De Vries A, Marrink S, Berendsen H: **Efficient algorithms for Langevin and DPD dynamics.** *Journal of chemical theory and computation* 2012, **8:**3637-3649.
248. Humphrey W, Dalke A, Schulten K: **VMD: visual molecular dynamics.** *Journal of molecular graphics* 1996, **14:**33-38.
249. Grant BJ, Rodrigues AP, ElSawy KM, McCammon JA, Caves LS: **Bio3d: an R package for the comparative analysis of protein structures.** *Bioinformatics* 2006, **22:**2695-2696.
250. Allen MP, Tildesley DJ: *Computer simulation of liquids*. Oxford university press; 2017.
251. Feller SE, Zhang Y, Pastor RW, Brooks BR: **Constant pressure molecular dynamics simulation: the Langevin piston method.** *The Journal of chemical physics* 1995, **103:**4613-4621.
252. MacKerell Jr AD, Bashford D, Bellott M, Dunbrack Jr RL, Evanseck JD, Field MJ, Fischer S, Gao J, Guo H, Ha S, Karplus M: **All-atom empirical potential for molecular modelling and dynamics studies of proteins.** *The journal of physical chemistry B* 1998, **102:**3586-3616.
253. Jorgensen WL, Chandrasekhar J, Madura JD, Impey RW, Klein ML: **Comparison of simple potential functions for simulating liquid water.** *The Journal of chemical physics* 1983, **79:**926-935.
254. Brooks BR, Brooks III CL, Mackerell Jr AD, Nilsson L, Petrella RJ, Roux B, Won Y, Archontis G, Bartels C, Boresch S, Karplus M: **CHARMM: the biomolecular simulation program.** *Journal of computational chemistry* 2009, **30:**1545-1614.
255. Phillips JC, Braun R, Wang W, Gumbart J, Tajkhorshid E, Villa E, Chipot C, Skeel RD, Kale L, Schulten K: **Scalable molecular dynamics with NAMD.** *Journal of computational chemistry* 2005, **26:**1781-1802.

256. Walsh C, Barrow S, Voronina S, Chvanov M, Petersen OH, Tepikin A: **Modulation of calcium signalling by mitochondria.** *Biochimica et Biophysica Acta (BBA)-Bioenergetics* 2009, **1787:**1374-1382.
257. Addabbo F, Montagnani M, Goligorsky MS: **Mitochondria and reactive oxygen species.** *Hypertension* 2009, **53:**885-892.
258. Jeong S-Y, Seol D-W: **The role of mitochondria in apoptosis.** *BMB reports* 2008, **41:**11-22.
259. Berman S, Pineda FJ, Hardwick JM: **Mitochondrial fission and fusion dynamics: the long and short of it.** *Cell Death & Differentiation* 2008, **15:**1147-1152.
260. Melatti C, Pieperhoff M, Lemgruber L, Pohl E, Sheiner L, Meissner M: **A unique dynamin-related protein is essential for mitochondrial fission in Toxoplasma gondii.** *PLoS Pathogens* 2019, **15:**e1007512.
261. Kato S, Okamura E, Matsunaga TM, Nakayama M, Kawanishi Y, Ichinose T, Iwane AH, Sakamoto T, Imoto Y, Ohnuma M, Matsunaga S: **Cyanidioschyzon merolae aurora kinase phosphorylates evolutionarily conserved sites on its target to regulate mitochondrial division.** *Communications Biology* 2019, **2:**477.
262. Fujimoto M, Arimura Si, Mano S, Kondo M, Saito C, Ueda T, Nakazono M, Nakano A, Nishimura M, Tsutsumi N: **Arabidopsis dynamin-related proteins DRP3A and DRP3B are functionally redundant in mitochondrial fission, but have distinct roles in peroxisomal fission.** *The Plant Journal* 2009, **58:**388-400.
263. Lee MW, Lee EY, Lai GH, Kennedy NW, Posey AE, Xian W, Ferguson AL, Hill RB, Wong GC: **Molecular motor Dnm1 synergistically induces membrane curvature to facilitate mitochondrial fission.** *ACS central science* 2017, **3:**1156-1167.
264. Olivares-Marin IK, González-Hernández JC, Regalado-Gonzalez C, Madrigal-Perez LA: **Saccharomyces cerevisiae exponential growth kinetics in batch culture to analyze respiratory and fermentative metabolism.** *JoVE (Journal of Visualized Experiments)* 2018**:**e58192.
265. Magrì A, Di Rosa MC, Tomasello MF, Guarino F, Reina S, Messina A, De Pinto V: **Overexpression of human SOD1 in VDAC1-less yeast restores mitochondrial functionality modulating beta-barrel outer membrane protein genes.** *Biochimica et Biophysica Acta (BBA)-Bioenergetics* 2016, **1857:**789-798.
266. Jensen RE, Aiken Hobbs AE, Cerveny KL, Sesaki H: **Yeast mitochondrial dynamics: fusion, division, segregation, and shape.** *Microscopy research and technique* 2000, **51:**573-583.
267. Kelly SM, Jess TJ, Price NC: **How to study proteins by circular dichroism.** *Biochimica et Biophysica Acta (BBA)-Proteins and Proteomics* 2005, **1751:**119-139.
268. Greenfield NJ: **Using circular dichroism spectra to estimate protein secondary structure.** *Nature protocols* 2006, **1:**2876-2890.
269. McGuffin LJ, Bryson K, Jones DT: **The PSIPRED protein structure prediction server.** *Bioinformatics* 2000, **16:**404-405.
270. Koirala S, Guo Q, Kalia R, Bui HT, Eckert DM, Frost A, Shaw JM: **Interchangeable adaptors regulate mitochondrial dynamin assembly for membrane scission.** *Proceedings of the National Academy of Sciences* 2013, **110:**E1342-E1351.
271. Vowinckel J, Hartl J, Butler R, Ralser M: **MitoLoc: A method for the simultaneous quantification of mitochondrial network morphology and membrane potential in single cells.** *Mitochondrion* 2015, **24:**77-86.
272. Zordan RE, Beliveau BJ, Trow JA, Craig NL, Cormack BP: **Avoiding the ends: internal epitope tagging of proteins using transposon Tn7.** *Genetics* 2015, **200:**47-58.

273. Li Z, Rinas U: **Recombinant protein production associated growth inhibition results mainly from transcription and not from translation.** *Microbial cell factories* 2020, **19:**1-11.
274. Fukushima NH, Brisch E, Keegan BR, Bleazard W, Shaw JM: **The GTPase effector domain sequence of the Dnm1p GTPase regulates self-assembly and controls a rate-limiting step in mitochondrial fission.** *Molecular biology of the cell* 2001, **12:**2756-2766.
275. Westermann B: **Mitochondrial dynamics in model organisms: what yeasts, worms and flies have taught us about fusion and fission of mitochondria.** In *seminars in cell & developmental biology*. Elsevier; 2010: 542-549.
276. Zhang Z, Sliter DA, Bleck CK, Ding S: **Fis1 deficiencies differentially affect mitochondrial quality in skeletal muscle.** *Mitochondrion* 2019, **49:**217-226.
277. Connor OM, Matta SK, Friedman JR: **An intermembrane space protein facilitates completion of mitochondrial division in yeast.** *bioRxiv* 2023**:**2023.2003. 2031.535139.
278. Han H, Tan J, Wang R, Wan H, He Y, Yan X, Guo J, Gao Q, Li J, Shang S, Zhang Z: **PINK 1 phosphorylates Drp1S616 to regulate mitophagy-independent mitochondrial dynamics.** *EMBO reports* 2020, **21:**e48686.
279. Chang YW, Song ZH, Chen CC: **FAK regulates cardiomyocyte mitochondrial fission and function through Drp1.** *The FEBS Journal* 2022, **289:**1897-1910.
280. Chen S, Liu S, Wang J, Wu Q, Wang A, Guan H, Zhang Q, Zhang D, Wang X, Song H, Xu P: **TBK1-mediated DRP1 targeting confers nucleic acid sensing to reprogram mitochondrial dynamics and physiology.** *Molecular Cell* 2020, **80:**810-827. e817.
281. Ansari M, Novak K, Haqqi T: **ERK1/2-mediated activation of DRP1 regulates mitochondrial dynamics and apoptosis in chondrocytes.** *Osteoarthritis and Cartilage* 2022, **30:**315-328.
282. Mehta K, Chacko LA, Chug MK, Jhunjhunwala S, Ananthanarayanan V: **Association of mitochondria with microtubules inhibits mitochondrial fission by precluding assembly of the fission protein Dnm1.** *Journal of Biological Chemistry* 2019, **294:**3385-3396.
283. Smaczynska-de Rooij II, Marklew CJ, Allwood EG, Palmer SE, Booth WI, Mishra R, Goldberg MW, Ayscough KR: **Phosphorylation regulates the endocytic function of the yeast dynamin-related protein Vps1.** *Molecular and cellular biology* 2016, **36:**742-755.
284. Ji Y, Zhou H, Yang CY, Li J: **Post-Translational Modification of Drp1 is a Promising Target for Treating Cardiovascular Diseases.** *Cardiovascular Innovations and Applications* 2023, **8**.
285. Gao Q, Tian R, Han H, Slone J, Wang C, Ke X, Zhang T, Li X, He Y, Liao P, Zhang Z: **PINK1-mediated Drp1S616 phosphorylation modulates synaptic development and plasticity via promoting mitochondrial fission.** *Signal Transduction and Targeted Therapy* 2022, **7:**103.
286. Ford MG, Chappie J: **The structural biology of the dynamin-related proteins: New insights into a diverse, multitalented family.** *Traffic* 2019, **20:**717-740.
287. Cerveny KL, Jensen RE: **The WD-repeats of Net2p interact with Dnm1p and Fis1p to regulate division of mitochondria.** *Molecular biology of the cell* 2003, **14:**4126-4139.
288. Basu K, Lajoie D, Aumentado-Armstrong T, Chen J, Koning RI, Bossy B, Bostina M, Sik A, Bossy-Wetzel E, Rouiller I: **Molecular mechanism of DRP1 assembly studied in vitro by cryo-electron microscopy.** *PloS one* 2017, **12:**e0179397.

289. Jeong GR, Jang E-H, Bae JR, Jun S, Kang HC, Park C-H, Shin J-H, Yamamoto Y, Tanaka-Yamamoto K, Dawson VL, Lee BD: **Dysregulated phosphorylation of Rab GTPases by LRRK2 induces neurodegeneration.** *Molecular neurodegeneration* 2018, **13:**1-17.
290. Bunda S, Heir P, Srikumar T, Cook JD, Burrell K, Kano Y, Lee JE, Zadeh G, Raught B, Ohh M: **Src promotes GTPase activity of Ras via tyrosine 32 phosphorylation.** *Proceedings of the National Academy of Sciences* 2014, **111:**E3785-E3794.
291. Nakashima M, Kouga T, Lourenço CM, Shiina M, Goto T, Tsurusaki Y, Miyatake S, Miyake N, Saitsu H, Ogata K, Matsumoto N: **De novo DNM1 mutations in two cases of epileptic encephalopathy.** *Epilepsia* 2016, **57:**e18-e23.
292. Song BD, Leonard M, Schmid SL: **Dynamin GTPase domain mutants that differentially affect GTP binding, GTP hydrolysis, and clathrin-mediated endocytosis.** *Journal of Biological Chemistry* 2004, **279:**40431-40436.
293. Sesaki H, Adachi Y, Kageyama Y, Itoh K, Iijima M: **In vivo functions of Drp1: lessons learned from yeast genetics and mouse knockouts.** *Biochimica et Biophysica Acta (BBA)-Molecular Basis of Disease* 2014, **1842:**1179-1185.
294. Francy CA, Alvarez FJ, Zhou L, Ramachandran R, Mears JA: **The mechanoenzymatic core of dynamin-related protein 1 comprises the minimal machinery required for membrane constriction.** *The Journal of biological chemistry* 2015, **290:**11692.
295. Alexiou A, Nizami B, Khan FI, Soursou G, Vairaktarakis C, Chatzichronis S, Tsiamis V, Manztavinos V, Yarla NS, Ashraf GM: **Mitochondrial dynamics and proteins related to neurodegenerative diseases.** *Current Protein and Peptide Science* 2018, **19:**850-857.
296. Narendra D, Tanaka A, Suen D-F, Youle RJ: **Parkin-induced mitophagy in the pathogenesis of Parkinson disease.** *Autophagy* 2009, **5:**706-708.
297. Shirendeb UP, Calkins MJ, Manczak M, Anekonda V, Dufour B, McBride JL, Mao P, Reddy PH: **Mutant huntingtin's interaction with mitochondrial protein Drp1 impairs mitochondrial biogenesis and causes defective axonal transport and synaptic degeneration in Huntington's disease.** *Human molecular genetics* 2012, **21:**406-420.
298. Michalska B, Duszyński J, Szymański J: **Mechanism of mitochondrial fission-structure and function of Drp1 protein.** *Postepy biochemii* 2016, **62:**127-137.
299. Koch A, Thiemann M, Grabenbauer M, Yoon Y, McNiven MA, Schrader M: **Dynamin-like protein 1 is involved in peroxisomal fission.** *Journal of Biological Chemistry* 2003, **278:**8597-8605.
300. Kuravi K, Nagotu S, Krikken AM, Sjollema K, Deckers M, Erdmann R, Veenhuis M, Van Der Klei IJ: **Dynamin-related proteins Vps1p and Dnm1p control peroxisome abundance in Saccharomyces cerevisiae.** *Journal of cell science* 2006, **119:**3994-4001.
301. Nagotu S, Saraya R, Otzen M, Veenhuis M, van der Klei IJ: **Peroxisome proliferation in Hansenula polymorpha requires Dnm1p which mediates fission but not de novo formation.** *Biochimica et Biophysica Acta (BBA)-Molecular Cell Research* 2008, **1783:**760-769.
302. Schrader M, Costello JL, Godinho LF, Azadi AS, Islinger M: **Proliferation and fission of peroxisomes—an update.** *Biochimica et Biophysica Acta (BBA)-Molecular Cell Research* 2016, **1863:**971-983.
303. Williams M, Kim K: **From membranes to organelles: emerging roles for dynamin-like proteins in diverse cellular processes.** *European journal of cell biology* 2014, **93:**267-277.

304. Stefan CJ, Trimble WS, Grinstein S, Drin G, Reinisch K, De Camilli P, Cohen S, Valm AM, Lippincott-Schwartz J, Levine TP, McBride HM: **Membrane dynamics and organelle biogenesis—lipid pipelines and vesicular carriers.** *BMC biology* 2017, **15:**1-24.
305. Carlton JG, Jones H, Eggert US: **Membrane and organelle dynamics during cell division.** *Nature reviews Molecular cell biology* 2020, **21:**151-166.
306. Varkey J, Langen R: **Membrane remodelling by amyloidogenic and non-amyloidogenic proteins studied by EPR.** *Journal of magnetic resonance* 2017, **280:**127-139.
307. Sabouny R, Shutt TE: **Reciprocal regulation of mitochondrial fission and fusion.** *Trends in biochemical sciences* 2020, **45:**564-577.
308. Praefcke GJ, McMahon HT: **The dynamin superfamily: universal membrane tubulation and fission molecules?** *Nature reviews Molecular cell biology* 2004, **5:**133-147.
309. Shaw JM, Nunnari J: **Mitochondrial dynamics and division in budding yeast.** *Trends in cell biology* 2002, **12:**178-184.
310. Westermann B: **Molecular machinery of mitochondrial fusion and fission.** *Journal of Biological Chemistry* 2008, **283:**13501-13505.
311. Friedman JR, Webster BM, Mastronarde DN, Verhey KJ, Voeltz GK: **ER sliding dynamics and ER–mitochondrial contacts occur on acetylated microtubules.** *Journal of Cell Biology* 2010, **190:**363-375.
312. Chen W, Zhao H, Li Y: **Mitochondrial dynamics in health and disease: mechanisms and potential targets.** *Signal Transduction and Targeted Therapy* 2023, **8:**333.
313. Qi Z, Huang Z, Xie F, Chen L: **Dynamin-related protein 1: a critical protein in the pathogenesis of neural system dysfunctions and neurodegenerative diseases.** *Journal of cellular physiology* 2019, **234:**10032-10046.

List of Publications, Conferences & Workshops attended

Publications from Ph. D thesis

- **Banerjee R**, Mukherjee A, Adhikary A, Hussain S, Sharma S, Ali E, Nagotu S. Insights into the role of the conserved GTPase domain residues T62 and S277 in yeast Dnm1. **International Journal of Biological Macromolecules, 2023**, DOI: https://doi.org/10.1016/j.ijbiomac.2023.127381
- **Banerjee R**, Mukherjee A, Nagotu S. Mitochondrial dynamics and its impact on human health and diseases: inside the DRP1 blackbox. **Journal of Molecular Medicine, 2022** Jan 1:1-21. DOI: 10.1007/s00109-021-02150-7
- **Banerjee R**, Kumar A, Satpati P, Nagotu S. Mimicking human Drp1 disease-causing mutations in yeast Dnm1 reveals altered mitochondrial dynamics. **Mitochondrion, 2021** Jul 1;59: 283-95. DOI: https://doi.org/10.1016/j.mito.2021.06.009

Publications from collaborative research

- Adhikary A, Mukherjee A, **Banerjee R**, Nagotu S. DRP1: At the crossroads of dysregulated mitochondrial dynamics and altered cell signaling in cancer cells. **American Chemical Society, Omega. 2023**. DOI: https://pubs.acs.org/doi/10.1021/acsomega.3c06547
- **Banerjee R,** Joshi N, Nagotu S. Cell organelles and yeast longevity: an intertwined regulation. **Current Genetics**, **2020** Feb;66(1):15-41. DOI: https://doi.org/10.1007/s00294-019-01035-0
- **Banerjee R*,** Deb R*****, Roy K*****, Chatterjee S, Nagotu S. Uptake and intracellular fate of nona-arginine peptide in yeast. **Biopolymer, Peptide Science**.e24101. **2018** * Equal contribution. DOI: https://doi.org/10.1002/pep2.24101
- Deori NM*****, Deb R*****, **Banerjee R***, Nagotu S. Yeast: A Multifaceted Eukaryotic Microbe and Its Biotechnological Applications. Advances in Microbial Biotechnology **2018** Aug 31 (pp. 191-224). **Apple Academic Press**. * Equal contribution. DOI: https://doi.org/10.1201/9781351248914-7

Conferences and workshops attended

- **Banerjee R,** Kumar A, Satpati P, Nagotu S. Mimicking human Drp1 disease-causing mutations in yeast Dnm1 reveals altered mitochondrial dynamics. **44th AICB - 2022, University of Kashmir, September 2022.**
- **Banerjee R,** Kumar A, Satpati P, Nagotu S. Mimicking human Drp1 disease-causing mutations in yeast Dnm1 reveals altered mitochondrial dynamics. **MICON 2022, Advances in microbiology.**
- **Banerjee R,** Kumar A, Satpati P, Nagotu S. Mimicking human Drp1 disease-causing mutations in yeast Dnm1 reveals altered mitochondrial dynamics. **3rd National Biomedical Research Competition, December 2021.**
- **Banerjee R,** Nagotu S. To gain insights into the Drp1 related disorders through analysis of equivalent orthologous mutations in budding yeast Dnm1. **11th ICBYFF, UOH Hyderabad, 2020.**
- **Banerjee R,** Nagotu S. To gain insights into the function of yeast Dnm1 in organelle biology and cellular ageing**. Research Conclave, IIT Guwahati, 2019.**
- **Banerjee R,** Deb R, Roy K, Chatterjee S, Nagotu S. Uptake and intracellular fate of nona-arginine peptide in yeast. **Research Conclave, IIT Guwahati, 2018.**
- **Banerjee R,** Deb R, Roy K, Chatterjee S, Nagotu S. Uptake and intracellular fate of nona-arginine peptide in yeast. **10th conference on yeast biology, JNU, New Delhi, 2018.**
- **20th Indo-US flow cytometry symposium cum workshop** on "Applications of flow cytometry in Biotechnology"